



HAL
open science

Study and improvement of non-aqueous Lithium-Air batteries via the development of a silicon-based anode

Florent Lepoivre

► **To cite this version:**

Florent Lepoivre. Study and improvement of non-aqueous Lithium-Air batteries via the development of a silicon-based anode. Material chemistry. Université Pierre et Marie Curie - Paris VI, 2016. English. NNT : 2016PA066326 . tel-01474849

HAL Id: tel-01474849

<https://theses.hal.science/tel-01474849>

Submitted on 23 Feb 2017

HAL is a multi-disciplinary open access archive for the deposit and dissemination of scientific research documents, whether they are published or not. The documents may come from teaching and research institutions in France or abroad, or from public or private research centers.

L'archive ouverte pluridisciplinaire **HAL**, est destinée au dépôt et à la diffusion de documents scientifiques de niveau recherche, publiés ou non, émanant des établissements d'enseignement et de recherche français ou étrangers, des laboratoires publics ou privés.

Université Pierre et Marie Curie

ED 397 – Chimie et physico-chimie des matériaux

Chaire de Chimie du Solide et Énergie – Collège de France

Study and improvement of non-aqueous Lithium-Air batteries via the development of a silicon-based anode

By Florent Lepoivre

PhD thesis in Chemistry

Directed by Dominique Larcher and Jean-Marie Tarascon

Presented and defended in public on November 15th, 2016

In front of the jury:

Dr. Fanny Bardé	Senior scientist, Toyota Motor Europe	Referee
Prof. Clare P. Grey	Group leader, University of Cambridge	Referee
Dr. Natacha Krins	Associate professor, UPMC - Sorbonne University	Examiner
Dr. Olivier Fontaine	Associate professor, University of Montpellier	Examiner
Dr. Alexis Grimaud	CNRS researcher, Collège de France, Paris	Invited
Prof. Dominique Larcher	Professor, LRCS, Amiens	Director
Prof. Jean-Marie Tarascon	Professor, Collège de France, Paris	Director



Except where otherwise noted, this work is licensed under
<http://creativecommons.org/licenses/by-nc-nd/3.0/>

Université Pierre et Marie Curie

ED 397 – Chimie et physico-chimie des matériaux

Chaire de Chimie du Solide et Énergie – Collège de France

Etude et amélioration des batteries Lithium-Air via l'optimisation de l'électrode négative avec des alliages de silicium

Par Florent Lepoivre

Thèse de Doctorat en Chimie

Dirigée par Dominique Larcher et Jean-Marie Tarascon

Présentée et soutenue publiquement le 15 Novembre 2016

Devant un jury composé de :

Dr. Fanny Bardé	Senior scientist, Toyota Motor Europe	Rapporteur
Prof. Clare P. Grey	Group leader, University of Cambridge	Rapporteur
Dr. Natacha Krins	Maître de conférences, UPMC - Sorbonne Universités	Examinateur
Dr. Olivier Fontaine	Maître de conférences, Université de Montpellier	Examinateur
Dr. Alexis Grimaud	Chargé de recherche CNRS, Collège de France, Paris	Invité
Prof. Dominique Larcher	Professeur, LRCS, Amiens	Directeur
Prof. Jean-Marie Tarascon	Professeur, Collège de France, Paris	Directeur



Except where otherwise noted, this work is licensed under
<http://creativecommons.org/licenses/by-nc-nd/3.0/>

A mes grands-parents,

Gisèle Lepoivre

Micheline Martin

Jacques Lepoivre

Maurice Martin

Remerciements / Acknowledgements :

Je souhaiterais dédier les premières pages de ce manuscrit aux personnes que j'ai côtoyées et/ou rencontrées durant mon doctorat, grâce auxquelles j'ai pu profiter pleinement de ces trois années, tant au niveau professionnel que personnel.

First, I would like to express my sincere gratitude to the referees and examiners of my PhD committee Fanny Bardé, Clare P. Grey, Natacha Krins and Olivier Fontaine for their interest in my work and their insightful comments.

Je souhaite aussi remercier très chaleureusement mes encadrants de thèse, qui ont su accompagner et aiguiller mon travail habilement, tout en me laissant mener le navire où je le souhaitais. J'ai ainsi pu donner libre cours à mon imagination et à ma créativité. Il en résulte un travail vraiment personnel et qui, je l'espère, sera utile au laboratoire pour de nombreuses années. Merci à Jean-Marie Tarascon pour son inestimable aide scientifique, sa bienveillance et son accompagnement tout au long de la thèse. Sa fascination et sa curiosité pour les Sciences sont une formidable source d'inspiration et de motivation. Merci aussi pour le cadre de travail exceptionnel qu'il a réussi à créer dans son nouveau laboratoire au Collège de France, à la fois convivial et stimulant. De la même manière, je souhaite remercier Dominique Larcher, qui, depuis la Picardie, m'a fait bénéficier de son immense savoir (et de sa culture !) et m'a guidé dans ma quête de réversibilité des alliages de silicium. J'en apprenais davantage à chacune de nos discussions et ce fut un réel plaisir de travailler ensemble. Moins loin que la Picardie, je souhaite exprimer ma sincère gratitude à Alexis Grimaud qui m'a activement soutenu et aidé dès son arrivée au laboratoire. Que ce soit sur le fond (contenu scientifique, expériences pertinentes...) ou sur la forme (présentation des résultats, rédaction...), son aide m'a été très précieuse.

Si je garde un excellent souvenir de la thèse, c'est aussi et surtout grâce à la bonne ambiance dans le laboratoire. Pour cela, je remercie du fond du cœur tous mes collègues, et en particulier mes co-bureaux. Merci Laura (aka Doctor Lander) pour ces trois ans passés « dos à dos » qui m'ont permis de te connaître et ont fait naître une véritable amitié. Malgré des différences apparentes, nous étions au fond sur la même longueur d'onde, et j'ai vraiment apprécié notre cohabitation aussi improbable que parfaitement adaptée. Merci de m'avoir fait sentir incroyablement intelligent (*cf* nos discussions sur l'informatique), et merci de m'avoir aidé à ne pas oublier qu'en réalité je ne savais rien (*cf* nos discussions sur l'art photographique par exemple...). Malheureusement, cette ignorance s'étend à d'autres domaines tels que celui des affinements Rietveld ; une honte lorsqu'on a passé trois ans au

côté de Gwenaëlle Rouse. Désolé Gwen de ne pas m'être laissé convaincre par cette science que tu chéris tant, ce fut tout de même un plaisir de partager ce bureau avec toi ! Merci pour ton aide, ta bonne humeur, et tous les bons moments passés en ta compagnie ; J'espère sincèrement que nous resterons en contact dans le futur.

Thanks to all my other colleagues in Collège de France from whom I learnt a lot and who made the everyday life so pleasant at and outside of the lab. Chin, Sathiya, Eric and Prakash were like my big brothers/sisters who helped me to get started with the science of swageloks; Thanks to Wei and Lukas, and good luck struggling with Metal-Air batteries; Thanks to the "new" PhD student, Arnaud, Quentin, Gaurav, Paul, who managed to keep such a good atmosphere in the lab; Thanks to the Chinese Crew, Meiling, Wei again, Leiting, Biao, Yin, Guochun, Chunzhen, for teaching me a piece of your Chinese culture and traditions; Thanks to the other post-docs and permanent members, Vanessa, Romain, Matthieu, Ignacio, Alexis again and Daniel for sharing your experience, for your help in the lab and for your precious advice. Finally, I'd like to thank my "A-team"-mate and friend, Florian (aka Doctor Strauss), for the fun we had during these three years and the joy on your face when you said "party time!" =).

At this point I want to thank all the collaborators and colleagues from LRCS, the Li-Air Task Force, and Chimie ParisTech – M. Courty, B. Mirvaux, A. Demortière, C. Chazel, C. Colin, A. Charbonnier, A. Franco, F. Favier, P. G. Bruce, L. Johnson, J. Scoyer, E. Nanini-Maury, G. Van Staen and all the others – for their precious help and fruitful discussions. I would like to address a special thanks to Chunmei Li, Amina Toudjine and Vincent Giordani for sharing with me all their technics and secrets regarding Li-Air and Silicon batteries, and for always answering my numerous (and annoying) questions. Merci aussi aux différents services du Collège de France (atelier de physique/mécanique, menuiserie, plomberie, DSI...) pour leur aide technique qui a grandement facilité l'installation du nouveau laboratoire et leurs services tout au long de ces trois années. Enfin, je voudrais remercier Philippe Barbox pour son accueil dans son laboratoire durant les premières semaines de ma thèse, et plus généralement pour sa bienveillance à mon égard depuis ma scolarité à Chimie Paris.

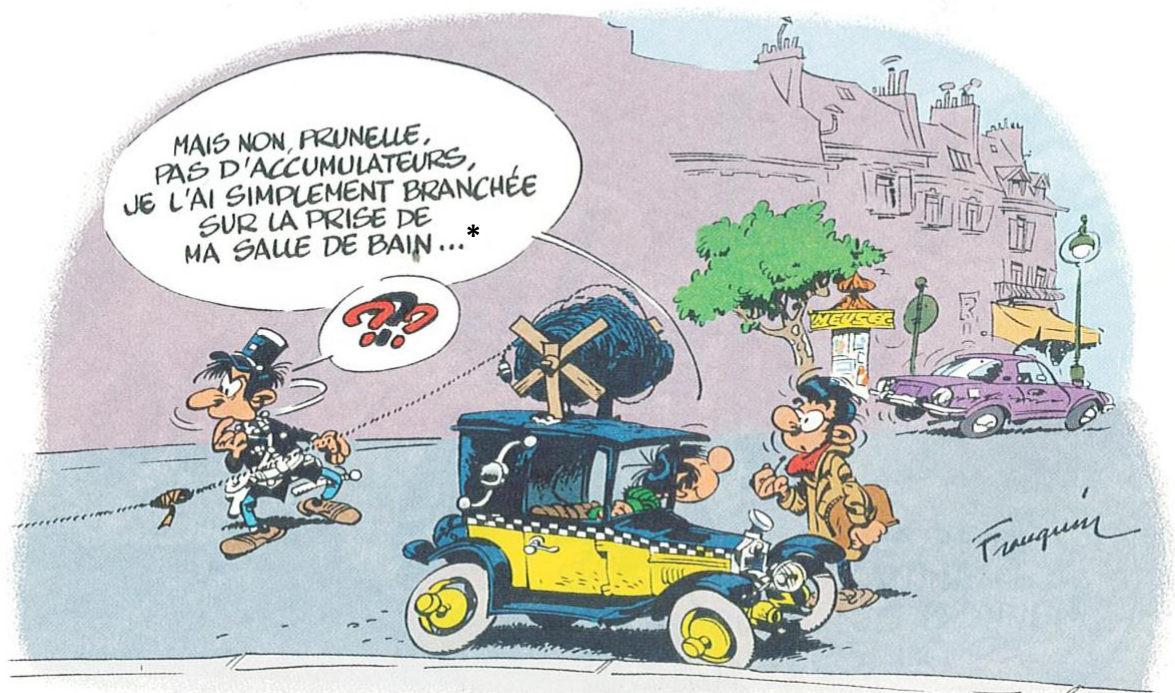
Ces trois ans au Collège de France furent aussi pour moi l'occasion de m'investir dans plusieurs associations afin de réaliser d'autres projets tout aussi formateurs que la thèse en elle-même. Merci à l'association Doc'Up et au festival les Chercheurs font leur Cinéma de m'avoir permis de réaliser le court métrage « L'homme qui murmurait aux oreilles des batteries ». Ce fut un réel plaisir de produire ce film et d'en parler devant des lycéens, et par la suite de faire vivre ce projet aux côtés de Fanny, Marie-Pauline, Aline, Quentin, Clément et Jean-David, ainsi que tous les autres organisateurs et réalisateurs qui ont pris part à

l'aventure. D'autre part, un grand merci à l'association des Chadocs et surtout à Véro, Chayma et Davide pour l'organisation d'événements au Collège de France ; pouvoir m'approprier et investir ce lieu mythique avec vous fut très grisant, notre équipe va bien me manquer !

Je souhaiterais maintenant remercier tous les amis qui m'ont soutenu pendant ces trois ans, qui furent compréhensifs durant mes absences et qui m'ont bien aidé à décompresser. Je pense bien entendu aux personnes rencontrées durant la thèse et dans les associations citées plus haut et au Collège de France – j'ai adoré traîner au milieu des lasers des labos de physique et me déguiser en biologiste –, mais aussi aux amis rencontrés durant mes études et ceux de plus longue date. Merci aux amis de Chimie Paris, entre-autre aux doctorants de la promo 2013 (ceux de la Montagne Ste Geneviève, du plateau de Saclay, de province, et au doctorant avorté), à mes chers collègues délégués de promo (officiels et officieux), et à tous mes acolytes de danse, de badminton et de soirée. Merci aux locataires permanents et éphémères de la rue du Sahel pour leur soutien, leur renfort graphique et artistique, et l'aide à la conception de la cellule XRD. Merci aux amis du Lycée Saint Louis avec qui je suis resté en contact et ceux que j'ai eu la chance de retrouver plus récemment. Merci aux amis du lycée Jacques Amyot pour ces moments de détente autour d'un feu dans les champs et pour les barbecues melunais estivaux. Merci enfin à l'équipe loossoise pour ces week-end chaleureux passés ensemble à déguster les produits locaux.

Pour finir, je souhaiterais remercier mes parents, qui ont su éveiller ma curiosité pour les Sciences et la Nature, qui m'ont encouragé durant toute ma scolarité, et qui m'ont soutenu et se sont montrés très compréhensifs durant les périodes plus intenses. Merci aussi à mes frères dont j'admire les multiples talents et qui depuis Paris, la Seine-et-Marne et le Cantal, m'ont accompagné, chacun à leur façon, tout au long de mon parcours. Plus généralement, j'ai une pensée pour toute ma famille que je remercie du fond du cœur pour leur infaillible soutien.

Gaston Lagaffe, genius inventor of the first « Plug-in » electric car...



* :

“No, no Prunelle,
no batteries,
I simply plugged it
in the wall plug of
my bathroom...”

Abstract:

Supplying the world energy demand while reducing the greenhouse gases emissions is one of the biggest challenges of the 21st century; this requires the development of efficient energy storage devices enabling the utilization of renewable energies. Among them, Lithium-Air batteries are very attractive due to their high theoretical energy density – 10 times that of the current Li-ion batteries – but their development is hindered by the complexity of the chemistry at play.

In order to understand such chemistry, we designed a new electrochemical test cell that integrates a pressure sensor, thereby enabling an accurate *in operando* monitoring of the pressure changes during charge/discharge with high reproducibility and sensitivity. Its use is demonstrated by quantifying the parasitic reactions in Li-O₂ cells for various electrolytes frequently encountered in the literature. Through this comparative study, we are able to observe the phenomena currently limiting the performances of Li-O₂ batteries after a long cycling (> 1000 h), such as parasitic reactions and the instability of the Li anode.

To address the later issue, Li was replaced by a prelithiated silicon electrode made of Si particles oxidized in surface. We demonstrated the feasibility of enhancing both their capacity and cycle life *via* a pre-formatting treatment that triggers the reduction of their SiO₂ coating by liberating pure Si metal. The full Li_xSi-O₂ cells using such treated electrodes exhibit performances competing with the best analogous systems reported in the literature (> 30 cycles; more than 400 h of cycling), but the development of practical prototypes still requires to improve the cycle-life.

Résumé :

Face aux défis du XXI^{ème} siècle concernant l'approvisionnement mondial en énergie et le réchauffement climatique, il est capital de développer des systèmes de stockage d'énergie efficaces et compétitifs. Parmi eux, la technologie Lithium-Air fait l'objet de nombreuses recherches car elle présente une densité d'énergie théorique dix fois supérieure à celle des batteries Li-ion actuellement utilisées, mais la complexité des réactions chimiques mises en jeu la cantonne au stade de la recherche.

Afin d'étudier de manière fiable et reproductible les batteries Li-Air, une nouvelle cellule de test électrochimique intégrant un capteur de pression a été développée. Elle permet d'estimer la quantité de réactions parasites associées à une configuration de batterie lors du cyclage à court et long terme (> 1000 h). Une étude comparative des différents électrolytes les plus utilisés a été réalisée, révélant la différence de comportement entre ces différentes espèces ainsi que l'instabilité de l'anode composée de lithium métallique.

Nous avons donc abordé le remplacement de l'anode de lithium par une électrode de silicium pré-lithié. En étudiant l'influence de différentes techniques de pré-lithiation sur des électrodes contenant des particules de Si oxydées en surface, un phénomène de réduction de SiO_2 en Si a été mis en évidence, apportant ainsi un gain substantiel en capacité. Les électrodes « activées » ont ensuite été utilisées en tant qu'anode dans les cellules complètes $\text{Li}_x\text{Si-O}_2$. Après optimisation, la durée de vie obtenue est supérieure à 400 h (> 30 cycles), ce qui est comparable à la littérature actuelle mais toutefois limité par la présence de réactions parasites.

General Introduction..... 1

I A world of energies..... 3

 I.1 Greenhouse gases & global warming..... 3

 I.2 Fossil fuels and energy 3

 I.3 Renewable energies and batteries..... 5

II Nowadays' batteries and their limitations..... 6

 II.1 Battery market 6

 II.2 The electrical vehicles 8

III Thesis outline..... 10

Chapter 1: State of the Art 13

I	Early days of batteries.....	15
I.1	From the frog pond to the salt pond.....	15
I.2	Some lithium batteries sound better than others	16
II	Current lithium battery technologies	17
II.1	Cathode materials	17
II.2	Anode materials	18
II.3	Electrolytes for Li batteries	20
III	Post-Li-ion battery technologies	22
III.1	Lithium-sulfur	23
III.2	Non-aqueous metal-air batteries.....	25
III.3	Aqueous Li-Air batteries.....	27
IV	Rechargeable Aprotic Li-O₂ batteries – Last 5 years’ news.....	29
IV.1	Basic components	29
IV.1.a	Negative electrode	29
IV.1.b	Positive electrode	32
IV.1.c	Electrolytes	36
IV.2	New trends	38
IV.2.a	Redox mediators.....	38
IV.2.b	Unified ORR mechanism	40
IV.3	Challenges and perspectives in non-aqueous Li-O ₂ batteries.....	41
V	Lithium-Silicon Alloys	42
V.1	Electrochemical behavior and structural changes	42
V.2	Limiting the impacts of volume expansions.....	44
V.2.a	Morphology of the particles	44
V.2.b	Composite electrodes.....	45
V.2.c	SEI and Electrolyte additives.....	45
V.2.d	SiO _x compounds.....	46
V.3	Prelithiation methods	48
V.4	Challenges and perspectives for lithium-silicon alloys	49
VI	Conclusions.....	50

Chapter 2: Experimental procedures and new design of the Li-O₂ test cell 53

I	Material preparation	55
I.1	Electrodes for Li-O ₂ batteries	55
I.1.a	Positive electrode	55
I.1.b	Negative electrode	56
I.2	Preparation of electrolytes	57
I.2.a	Electrolytes used in Li half-cells.....	57
I.2.b	Electrolytes in Li-O ₂ -type batteries.....	57
II	Battery testing.....	59
II.1	Testing cells for Li-ion type batteries	59
II.1.a	Two-electrode cells: Swagelok vs. Coin Cell	59
II.1.b	Three-electrode cell.....	60
II.2	Testing cells for Li-O ₂ batteries	61
II.2.a	Overview of common cells used in the literature	61
II.2.a.i	Rudimentary cells.....	61
II.2.a.ii	Metal-air dedicated cells.....	63
II.2.b	Cells formerly used in our laboratory	64
II.2.c	Cells for gas analysis	65
III	Design of the pressurized Li-O₂ test cell.....	67
III.1	Problematic	67
III.1.a	Gas evolution monitoring	68
III.1.b	Reproducibility.....	68
III.1.c	User-friendliness.....	69
III.2	Cell description.....	70
III.3	Pressure measurement	73
III.3.a	Sensor connection	73
III.3.b	Sensor calibration	74
III.4	Related equipment.....	76
III.4.a	Filling station	76
III.4.b	Temperature controlled chamber	77
IV	Figures of merit of the pressurized cell.....	79
IV.1	Stability.....	79
IV.2	Sensitivity	80
V	Conclusions.....	81

Chapter 3: Study of lithium-oxygen batteries using a pressurized electrochemical test cell 83

I	Prologue	85
I.1	Data interpretation	85
I.2	Added value of Pressurized Cells for studying Li-O ₂ batteries	86
II	Lithium Nitrate in N,N-Dimethylacetamide (DMA)	87
III	Tetraethyleneglycol dimethylether (TEGDME)	90
III.1	Electrochemical behavior	90
III.2	Identification of the parasitic reactions	92
III.2.a	Comparing DMA- and TEGDME-based systems by impedance spectroscopy	92
III.2.b	Parasitic reactions at the positive and negative electrodes	94
III.2.c	Mitigating parasitic reactions using redox mediators	96
IV	Influence of the glyme chain length	99
IV.1	DME vs. longer glymes	99
IV.2	Redox mediator in DME-based cells	101
V	Dimethyl Sulfoxide (DMSO)	102
V.1	Quantification of parasitic reactions	103
VI	Conclusions	107

Chapter 4: Development of Si composite electrodes as anode in $\text{Li}_x\text{Si-O}_2$ batteries..... 109

I	<i>Si composite electrode with good cycling performance</i>	111
I.1	Composite electrode preparation.....	111
I.2	Influence of the particle size on the cycling performances	113
I.3	Improving the cycling retention of M-Si-based electrodes.....	115
I.4	Improving the capacity of Si NP-based electrodes.....	116
II	<i>Influence of the pre-lithiation onto Si NP and their SiO_2 shell</i>	117
II.1	Electrochemical pre-lithiation techniques	117
II.2	Improved performances of prelithiated Si NP electrodes	119
II.2.a	Effect of a short-circuit and a plating sequence	119
II.2.b	Investigating the SiO_2 reduction process using a potentiostatic discharge.....	122
II.3	Reduction of pure silica.....	125
III	<i>Lithium-Air batteries using lithiated silicon as anode</i>	127
III.1	The Li_xSi electrodes within the context of Li-Air batteries.....	128
III.1.a	Electrode loading	128
III.1.b	Balancing Li losses	129
III.1.c	Prelithiation sequence.....	130
III.2	Recovering the Li_xSi electrode.....	130
III.2.a	Resting time after lithiation.....	130
III.2.b	Glass Fiber vs. Celgard-type separator	131
III.2.c	Washing process and cycling in a Li-O_2 electrolyte	132
III.3	Study of full $\text{Li}_x\text{Si-O}_2$ batteries	134
III.3.a	Experimental setup.....	134
III.3.b	$\text{Li}_x\text{Si-O}_2$ full cells using high capacity Si electrodes	135
III.3.c	$\text{Li}_x\text{Si-O}_2$ full cells using $p\text{-Li}_x\text{Si}$ electrodes.....	137
III.3.d	$\text{Li}_x\text{Si-O}_2$ full cells with limited depth of discharge	137
III.3.e	Improving the cycle-life of the Li_xSi anode with a physical protection.....	140
IV	<i>Conclusions</i>	143

General Conclusions..... 145

Bibliography.....**153**

Annexes.....**177**

GENERAL INTRODUCTION

I A world of energies

I.1 Greenhouse gases & global warming

The writing of this manuscript was finished a few days after China and the USA ratified their participation in the Paris Agreement on climate changeⁱ, which aims at reducing the impact of human activity in the climate change by holding the increase in the global average temperature to well below 2 °C above pre-industrial levels¹. The climate changes are influenced by many factors which can be natural (solar activity, volcanos, etc...) or anthropogenic (*i.e.* resulting from mankind activities), which relative impact on the average Earth temperature – quantified by their forcingⁱⁱ – is reported in Figure 1. This graph, which corroborates numerous work on climate change independently carried out by the ICPP^{2,3} or the NASA⁴ for instance, shows that the greenhouse gas (GhG) emissions are mainly responsible for the +1°C global temperature increase observed between 1901 and 2012³. In this context, the ratification of the COP21 pact by the Top 2 world polluters (China and the USA are together responsible for 42 % of the total GhG emissions) is a decisive step forward.

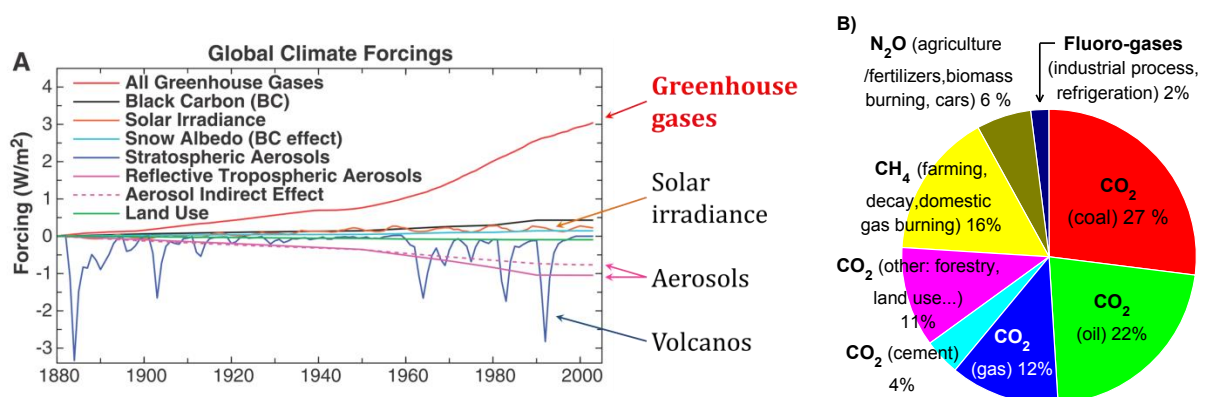


Figure 1: (A) Effect of various factors on the average Earth temperature responsible for the climate change⁵. (B) Global GhG emissions by gas and origin in 2014. Based on the 5th IPCC Report⁶, adapted from the US Environmental Protection Agency⁷ and the Global Carbon Project⁸.

I.2 Fossil fuels and energy

Most of the GhG comes from the combustion of fossil fuels such as coal, oil and gas, which transforms into CO₂ stored into the atmosphere for a hundred years (Figure 1B). Even

ⁱ The 2015 United Nations Climate Change Conference was the 21st session of the Conference of the Parties (COP21). It was held in Paris in December 2015 and resulted in the Paris Agreement which was signed by 190 countries so far (September 2016).

ⁱⁱ According to ref²: "The forcing is a measure of the influence a factor has in altering the balance of incoming and outgoing energy in the Earth-atmosphere system and is an index of the importance of the factor as a potential climate change mechanism. In the literature, the forcing values are for changes relative to preindustrial conditions defined at 1750 and are expressed in W/m²".

though the atmospheric greenhouse effect is known since 1824 (Fourier) and the impact of CO₂ onto the global warming was reported as early as 1869 (Arrhenius), the utilization of fossil fuels during and after the industrial revolution was justified by their outstanding energy density surpassing by far these of other traditional energy sources such as manpower or biomass (for instance, 20 cL of gasoline can provide as much energy as a man climbing up a 2 km high mountain with 30 kg on his back ⁱⁱⁱ).

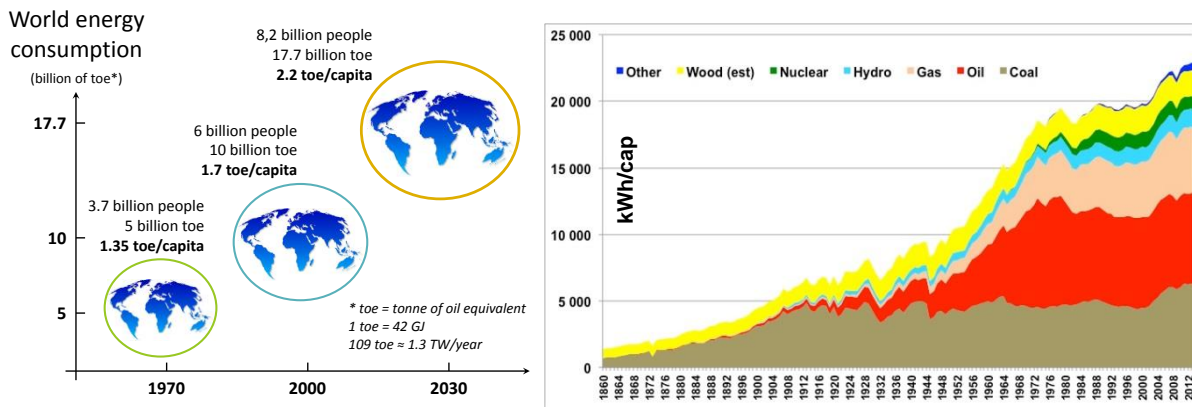


Figure 2: (a) Evolution and prevision of the world population and its energy consumption ⁹, adapted from the 2007 IEA “World Energy Outlook”. (b) Evolution of the average global (primary) energy consumption per capita (y-axis is in kWh/cap). Based on Shilling et al. 1977, BP Statistical Review 2015, Global Carbon Budget ¹⁰.

Nowadays, fossil fuels provide ~ 80 % of the energy produced in the world (Figure 2b), but the global energy supply is facing four challenges:

- i) the growth of the world population along with an increase of the average quality of life (Figure 2a), which could lead to a 30 % increase of the global energy consumption;
- ii) the rarefaction of the fossil fuels, which implies an increase of the extraction costs (drilling in deep water or frozen areas) and the commercialization of low quality products (tar sand, shale gas, etc...) extracted with questionable techniques;
- iii) the non-uniform distribution of the reserves on earth, which is at the origin of economical and geopolitical tensions. For instance, Venezuela – where 90 % of the foreign trade is based on oil exports ¹¹ – is currently facing a major crisis due to a sudden drop of oil prices in 2015 (- 55 % vs. 2014). The latter was purposely provoked by the largest OPEC producers to destabilize (with success (!)) the US shale gas industry and recover its market share ¹²;

ⁱⁱⁱ 1 L of gasoline contains ~ 10 kWh of energy, which can be converted into a mechanical energy with a yield of 20 to 40 % (i.e. 2 to 4 kWh/L). Based on the E=mgh equation, a man (70 kg) carrying 30 kg load during a climb of 2 km produces an energy of (70+30)*2000*9.81 ≈ 2 MJ ≡ 0.55 kWh. For comparison, a man digging a 1 m deep pit during 8 h at a rate of 1 spadeful (3 kg) every 5 seconds carries in 8 hours 17.3 tons of earth, which is equivalent to 0.05 kWh.

- iv) environmental and health issues: Aside from their involvement in the global warming, the combustion of fossil fuels – in thermal engines or power plants – is causing severe air pollution issues in densely populated areas. According to a World Bank Report ¹³, it was responsible for the death of 2.9 million people in 2013, which justifies – probably more than the will to limit the climate change, whose short-term effect is marginal – the recent political actions in favor of the reduction of fossil fuels utilization, such as in China.

I.3 Renewable energies and batteries

To address these challenges, it is crucial to reduce our dependency on fossil fuels by decreasing the global demand in energy and diversifying our power sources. Iceland for instance relies on fossil fuels only for transportation (15 % of its primary energy consumption), while the other 85 % are provided by geothermal energy and hydropower. Other countries which do not benefit from such natural resources have minimized their use of fossil fuel for producing electricity – representing $\sim 1/5$ of the global energy consumption ¹⁴ – in favor of the nuclear fission, but this technology suffers from environmental issues (radioactive wastes, nuclear disasters) and from the risk of proliferation.

To avoid these problems, it is necessary to develop the utilization of abundant and sustainable energy sources. Among them, renewable energies such as wind and solar power are very attractive as they are unlimited ^{iv} and available everywhere, but they suffer from intermittence and are diffuse which restricts their practical utilization. Their democratization nests in the development of energy storage technologies uncoupling the electricity production and its utilization, along with enabling a suitable integration within the electrical network. Similarly, efficient energy storage devices are also required to develop electrical vehicles over thermal ones ¹⁵, in order to reduce air pollution and CO₂ emissions related to transportation.

There are many ways to store energy according to its nature (electrical, thermal, chemical, mechanical, nuclear, etc..) and its final utilization. For both applications previously mentioned – mass storage and transportation –, chemical energy is a clever choice since it involves electron transfer, and so does electricity. The combination of these two fields gave birth to a whole chapter of the chemistry called “electrochemistry”, which includes all chemical reactions driven by or resulting from an electrical current flowing at a

^{iv} The sources are unlimited but their capture requires the utilization of limited materials, such as Silver (and Rare Earth) for solar panels, or Neodymium and Dysprosium for wind turbine magnets.

given potential. It enlists various technologies dedicated to energy storage, such as fuel cells, supercapacitors and batteries. Among them, rechargeable (secondary) batteries are actively studied worldwide due to their wide range of application (Figure 3) and their relatively high energy density.

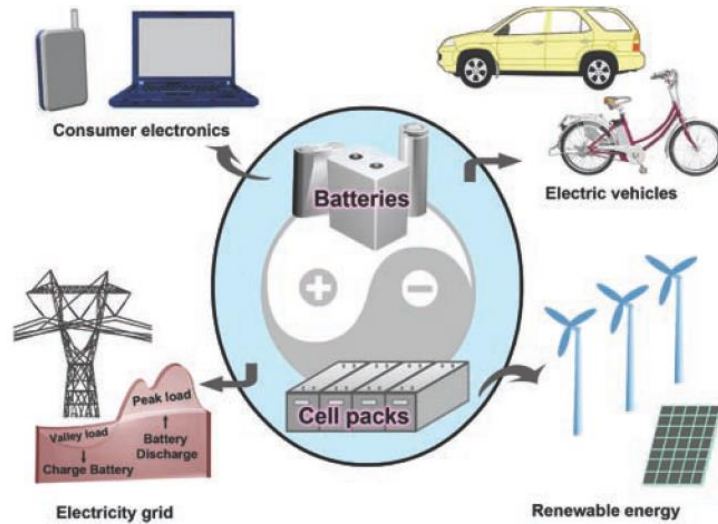


Figure 3: Representative applications for rechargeable batteries¹⁶.

II Nowadays' batteries and their limitations

II.1 Battery market

After a fast development at the beginning of the 21st century, the battery market nowadays represents 60 billion \$ (pack level, 2014) with an average growth of 5 % per year since 1990.

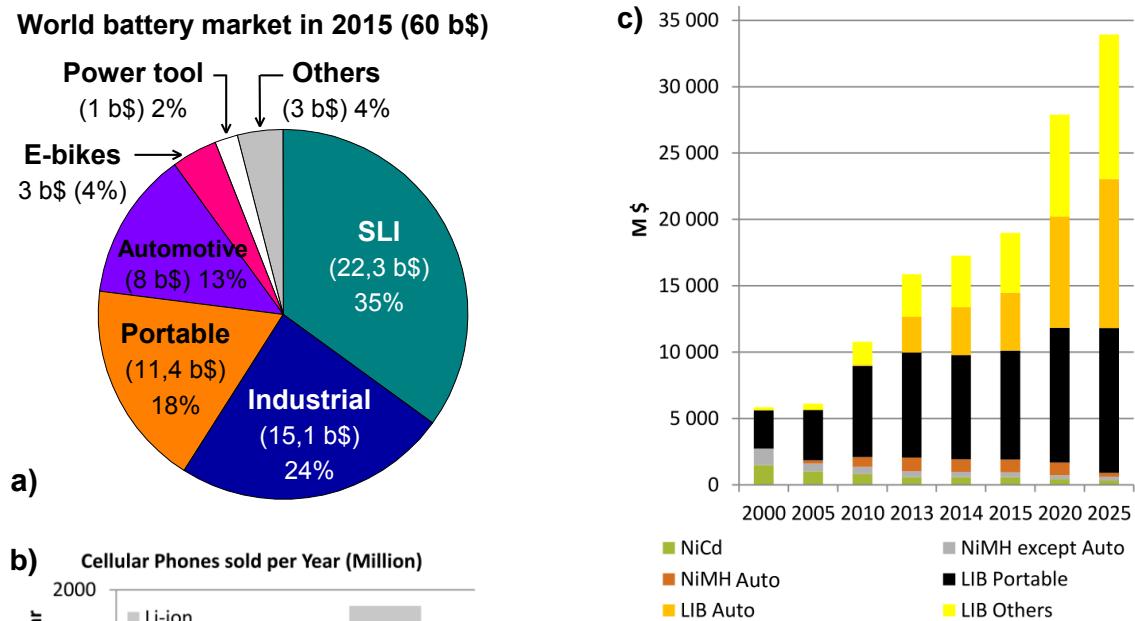


Figure 4: Market share of the worldwide rechargeable battery market in 2015¹⁷ (a); Evolution of the battery technology powering cellular phones between 2000 and 2014¹⁷ (b); Evolution of the NiCd, NiMH, and Li-ion battery market (cell level) between 2000 and 2014, and forecast up to 2025, including car applications ("Auto")¹⁷ (c).

The market is dominated by the Lead-Acid technology^v, used as start light and ignition batteries (SLI) in thermal engines and for mass storage at the industrial level, owing to its low cost and long cycle-life (Figure 4a). However, this technology is not suitable for portable applications in which the gravimetric and volumetric energy densities prevail above all. Over one decade, this segment has been conquered by the Li-ion technology^{vi}, which nowadays equips 100 % of the portable electronic devices such as cellular, laptops, tablets, cameras, and other handy terminals (Figure 4b). Owing to their good performances and relatively high gravimetric energy density, their use has been extended to automobile applications and Li-ion batteries are foreseen as the best solution to power electric vehicles in the near future when compared to the Ni-MH technology (Figure 4c). Their development is thus a great opportunity to reduce the air pollution and, provided that the electricity is produced by clean means, to minimize the carbon footprint related to transportation, alone responsible for 1/3 of the anthropogenic GhG emissions in developed countries¹⁸.

^v In 2015, the Lead-Acid technology represents 87 % of the capacity sold (350 MWh) for a total of 37 b\$ (57 % of the market share).

^{vi} The Li-ion technology represents 11 % (45 MWh) in term of capacity, for a market of 24 b\$ (37 %). The % values are given with respect to the worldwide rechargeable battery market in 2015.

II.2 The electrical vehicles

The market of hybrid and electrical vehicles shows a constant growth and is stimulated by massive investments (10-12 b\$ worldwide between 2011 and 2014) and a strong competition between the car manufacturers (Figure 5a). This led to the commercialization of 2.7 million of cars (including HEV, P-HEV and BEV^{vii}) worldwide in 2014, as compared to 0.9 million in 2010, while it could reach 4.6 to 6 million in 2020, corresponding to an estimated market of 70 b\$¹⁷.

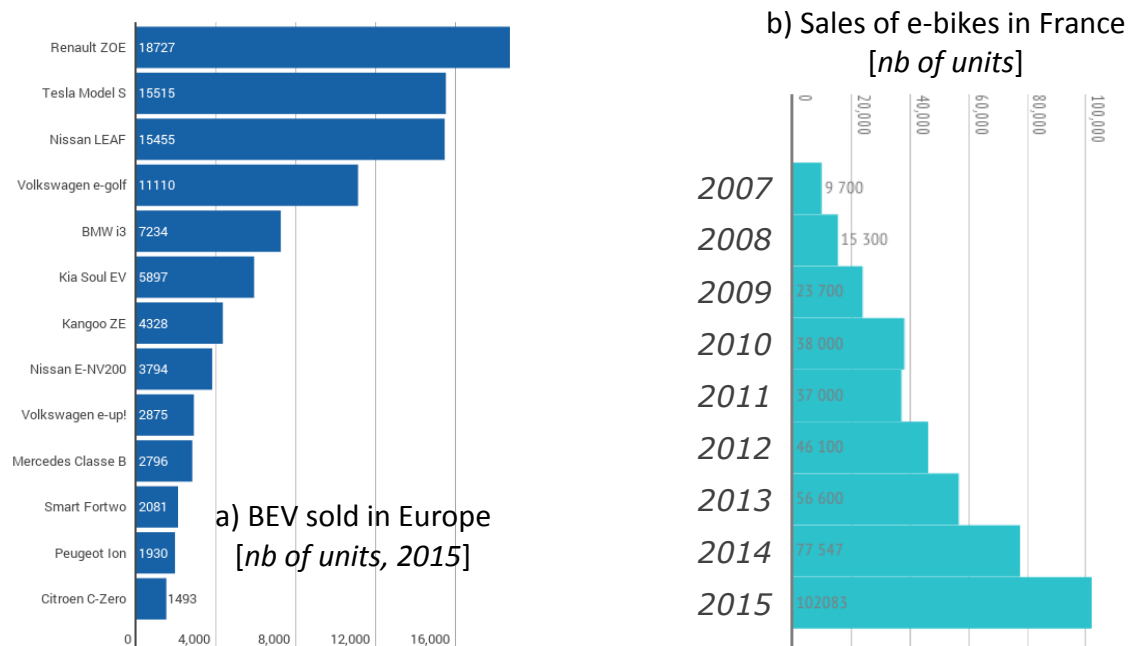


Figure 5: (a) Number of BEV sold in Europe as function of the manufacturer¹⁹. (b) Evolution of the number of electrical bikes sold in France²⁰.

The most significant environmental benefits come from the use of fully electrical vehicles (BEVs) which do not directly consume any fossil fuels^{viii}. Despite many advantages such as the driving comfort, the easier maintenance of the engine, and its low “fuel” cost (~ 1.5 €/100 km for an BEV in France vs. ~ 9 €/100 km for a thermal engine), the world market penetration is only 0.25 %^{25,26}. Their popularity is hindered by their relatively low driving range which rarely exceeds 200 km except for the most expensive ones (*e.g.* 500 km for the Tesla Model S (2012); ~ 70000 €). If this appears as a limitation when compared to

^{vii} HEV = Hybrid electrical vehicles, which includes both a thermal and an electrical engine. The battery provides an extra power during the acceleration but is only recharged during the deceleration. In contrast, the battery of a plug-in hybrid electrical vehicle (P-HEV) can be recharged using dedicated terminals. Battery electrical vehicles (BEV) are fully battery-powered (no thermal engine).

^{viii} The benefits of BEV utilization in term of GhG emissions are strongly correlated to the electricity generation mode. They are high in countries producing a low-carbon electricity such as Switzerland or France (only 2 %²¹ and 5 %²² of the electricity was produced using fossil fuels in 2014), but are less significant in China or USA where > 75 %²³ and 66 %²⁴ of the electricity come from fossil fuels.

gas-powered cars, it is actually suitable for most daily commute in developed countries such as France, where 78 % of car trips do not exceed 50 km²⁷. Thus, the further development of the EVs is nested in two strategies:

- The first one consists in developing the idea that the general (ecological) interest prevails over the individual comfort of possessing a car whose full range is only useful a few times per year. It is a matter of social acceptance which can be influenced by a committed political action. For instance, the market penetration of electrical vehicles is higher in areas enforcing strong regulations against air pollution (*e.g.* in Tokyo where diesel is forbidden) or in countries providing practical advantages to clean vehicles, such as Norway where 1 out of 7 new car sold in 2015 was a BEV. This type of actions is also an opportunity to reorganize our mobility scheme, so far based on the individual cars which are not used/parked 95 % of their life-time²⁸. Numerous cities have for instance developed bike-promoting plans, which may include a financial support to people replacing an old car by an electrical bike (e-bike). The latter is now considered as a viable alternative to cars for small journeys, as indicated by the constant sale increase which was multiplied by 10 between 2007 and 2015 (Figure 5b).
- The second strategy consists in improving the battery performances such as the energy densities (*i.e.* higher range) and the rate capability (*i.e.* faster charge), in concert with reducing their cost. This can be done by developing new electrode materials, which has focused countless research efforts from both the academic and the industrial Li-ion community in the last decades. Despite notable discoveries, this approach is intrinsically limited by the chemistry at play in Li-ion batteries, which involves a heavy cathodic active material (Figure 6).

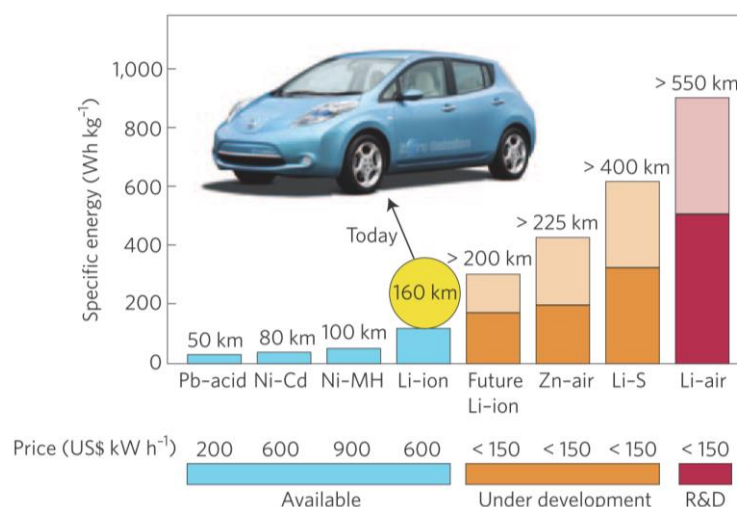


Figure 6: Practical specific energies for some rechargeable batteries, along with estimated driving distances and pack prices²⁹.

This thesis aims at overcoming these limitations by contributing to the development of an alternative battery technology called Lithium-Air (Li-Air) or Lithium-Oxygen (Li-O₂). These “breathing” batteries draw their energy from the electrochemical reaction between the lithium and the oxygen contained in the ambient air, which is absorbed into the battery during the charge and released during the discharge. Thanks to the light weight of the involved elements (Li, O) as compared to the Li-ion cathode, a significant increase of the gravimetric energy is expected. Nonetheless, the development of this technology is full of challenges owing to the high reactivity of the chemical species created during cycling. It is also necessary to improve the capacity of the negative electrode to match that of the positive. These two aspects were studied during this thesis, and the results obtained will be discussed as follow:

III Thesis outline

The **first chapter** will be focused in the journey taken by the battery technology to reach the current state of the art. A dedicated attention will be given to the Li-O₂ technology, in order to highlight the obstacles hindering its development and the possible solutions to overcome these limitations. We will also detail the efforts made for developing high capacity anode materials such as silicon, which is, in theory, a suitable anode material for Li-O₂ batteries.

In a **second chapter**, we will detail the experimental procedures for mounting Li-O₂ batteries prior to focus on the electrochemical cells used in the literature to study them, hence revealing the importance of considering the gas evolved during the cycling. Acknowledging the weaknesses of the cell hitherto used in our lab, we built a new testing device enabling to monitor the gas evolved in the battery while cycling. The design and figures of merit of this new cell will be discussed.

Our newly-designed cell was used for testing various Li-O₂ systems, whose performances will be reported in a **third chapter**. Thanks to accurate pressure measurements coupled with other electrochemical techniques, we were able to identify and quantify various phenomenon currently limiting the cycle-life of Li-O₂ batteries. Among them is the instability of lithium metal, hence calling for its replacement.

This will be the topic of the **fourth chapter**, in which high capacity Si electrodes were developed in view of being used as a lithium source in Li-O₂ batteries. In this purpose, our efforts were initially focused in mastering the Li-Si alloying process and investigate the

effect of a few pre-lithiation techniques which, in addition to lithiating the electrode, also tend to improve their overall performances. The results obtained with full $\text{Li}_x\text{Si-O}_2$ batteries will then be discussed.

The manuscript will be terminated by a **general conclusion** summarizing our findings, giving a few perspectives, and highlighting the contribution of this work to the lithium battery research community.

CHAPTER 1: STATE OF THE ART

I Early days of batteries

I.1 From the frog pond to the salt pond

All batteries are based on reduction-oxidation (Redox) reaction between two species happening simultaneously but at different potentials. One of the first “redox reaction” was reported in 1781 by Luigi Galvani (1737-1798) who noticed that the muscle of a frog’s leg would contract if connected to the spinal nerves by an “electrical circuit” composed of two different metals. Initially misunderstood by Galvani, this experiment was repeated by Alessandro Volta ³⁰ (1745-1827) who attributed this contraction to the electricity produced by connecting two metals soaked in a conductive liquid. He used the same concept to build the first primary battery in 1789, which consisted in a stacking of silver and zinc layers separated by a cloth wetted with a saline solution. This demonstration paved the road to other discoveries in the forthcoming years such as the constant current battery and the two-compartment-cell discovered by Antoine Becquerel (1788-1878) and John F. Daniell (1790-1845) in the early 1830’s, and the lead acid battery (1859) by Gaston Planté ³¹ (1834-1889). More than 150 years after its discovery, this latter technology still represents 87% (350 MWh/year) in volume and 57% (37 billion \$/year) in turnover in 2015 of the worldwide rechargeable battery market ¹⁷. New battery technologies based on Nickel were then developed during the 20th century: the nickel-cadmium ³² (Ni-Cd, 1899) which is still but rarely used nowadays due to toxicity issues, and the nickel metal hydride ^{33,34} (Ni-MH, 1970) which used to power the 1st generation of widely commercialized hybrid vehicles (Toyota Prius ³⁵, 1997). Both Ni-Cd and Ni-MH batteries, which were mostly used for portable applications, were progressively replaced by lithium batteries since the beginning of the 1990’s ³⁶. Indeed, lithium (mostly produced in salt ponds ³⁷ in South America) it is the most reducing element, which provides a high cell potential and thus a high energy density. Due to its strong reaction with water, its utilization came together with the development of organic electrolytes with a large stability window (x3 when compared to water) enabling high cell potentials, like 3.6 V for current Li-ion cells.

Nowadays, Li-ion batteries power every portable device and are closely associated to high technologies. However, Figure 7 shows that batteries energy densities only increased by a factor of ~ 5 in 200 years, which is much lower than those of electronics and often source of frustration for the consumer. These asymmetric developments can be explained by the fact that electronics – which is a physical matter dealing with pure elements – is only limited by the transistor size which decreases by a factor of 2 every 18 months ^{38,39} (Moore’s law), whereas batteries – which involves a chemical reaction with numerous components – require the discovery of new materials and the meticulous optimization of numerous

parameters to increase their performances⁴⁰. In the next section, we will present the current Li battery technologies in order to understand their limitations and the alternatives to go beyond.

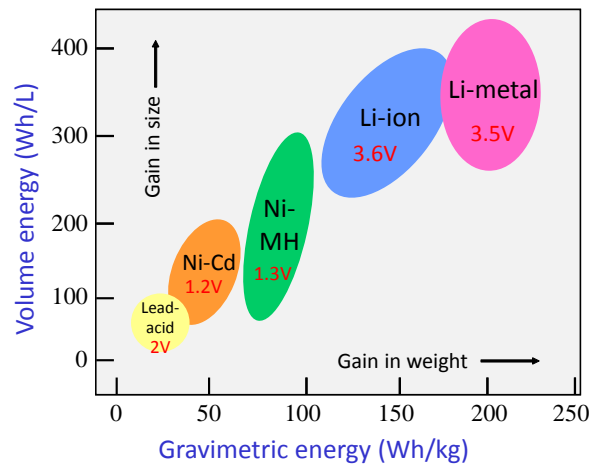


Figure 7: Different battery technologies and associated gravimetric and volumetric capacities (adapted from⁴¹).

I.2 Some lithium batteries sound better than others

The concept of intercalation compounds on which are based current Li batteries was established in the early 70's^{42,43} and used chalcogenides as positive electrode material. Early work of Rouxel⁴⁴ and Whittingham⁴⁵ on TiS_2 and MoS_2 led to the commercialization of the first lithium battery by Moli Energy in 1986 using MoS_2 and Li metal as positive and negative electrodes. Two million batteries were sold in NEC laptops and NTT cell phones (Japan) before being recalled in 1989 due to some accidents involving battery fires and explosions. It was due to the growth, after long cycling, of metallic lithium dendrites eventually shorting both sides of the battery through the separator⁴⁶, leading to an unstoppable thermal runaway. Two strategies were considered to prevent this situation, implying the replacement of either the electrolyte or the negative electrode. The first approach, whose concept was developed by Armand in the early 80's⁴⁷, consists in using a polymer electrolyte such as poly(ethylene oxide) (PEO) coupled with a lithium salt preventing dendrite growth. The main limitation, namely the low conductivity of the electrolyte, was overcome in practice by maintaining the battery at $\sim 70^\circ\text{C}$, temperature that does not prevent its use in commercial cars such as the Autolib' for instance⁴⁸ (Bolloré Group, 2011). The second approach consists in replacing the Li metal anode by another material, such as an insertion compound as demonstrated by Murphy and Scrosati in the late 70's^{49,50}. This concept – called “Rocking chair” owing to the Li ions swinging in between

both sides of the battery – led to the commercialization of the first Li-ion battery by Sony Corporation in 1991 in the Walkman⁵¹. Since then, the Li-ion technology has entirely conquered the market of portable electronics and started a harsh competition within industries and research laboratories for the discovery of the most competitive battery technology.

II Current lithium battery technologies

II.1 Cathode materials

In order to compensate the output voltage loss due to lithium metal replacement, the research field was focused on finding higher voltage cathode materials⁴⁰. This was done by moving from the chalcogenides to the oxides family owing to the higher ionicity of the metal-oxygen bond as compared to the metal-sulfur one¹⁵. Pioneering work was done in Bell Labs with the use of vanadium oxides (*e. g.* V_6O_{13})⁵². This work was then followed by Goodenough who introduced the Li_xMO_2 compounds ($M = Co$ or Ni)^{53,54}.

In 2014, one third of the commercial batteries sold in the world used $LiCoO_2$ as cathode materials, owing to its reversible capacity of 140 mAh/g. This capacity is far below the theoretical one of 275 mAh/g, owing to the difficulty to remove more than 0.5 Li^+ without damaging the crystalline structure. The latter can be practically stabilized by substituting the Co by other metallic cations, which led to the development of the Nickel-Cobalt-Aluminum⁵⁵ (NCA) and the Nickel-Manganese-Cobalt⁵⁶⁻⁵⁸ (NMC) phases, which nowadays represent respectively 10 % and 25 % of the battery market.

Pushing further this strategy, it is possible to substitute the metallic cations within the MO_2 layers by Li itself so as to obtain the so-called Li-rich NMC phase⁵⁹⁻⁶². These compounds exhibit a capacity as high as ~ 270 mAh/g, which sometimes even exceeds the theoretical one. This phenomenon was shown to be nested in the redox activity of the anions network within the structure⁶³⁻⁶⁷ (*i.e.* the oxide ions), which adds to the usual cationic redox process. In 2013, Sathiya *et al.* were able to demonstrate the reversibility of the anionic redox activity in the model compound Li_2RuO_3 ^{68,63}, which is accompanied by the formation of O-O dumbbells in the structure as observed later by McCalla *et al.*⁶⁹. Such discovery opens the door to new compounds where the redox activity is not only supported by the cations but also the anions, hence enabling significant increase in capacity of positive electrodes⁶⁶. Consequently, high capacity negative electrodes have to be developed so as to balance the Li-rich NMC as positive electrode.

II.2 Anode materials

After the first attempt to use Li metal as negative electrodes, the possibility of using graphite as an intercalation compound was investigated. Indeed, it was already used in other battery technologies^{70,71,72} and its ability to electrochemically react with lithium in a reversible way was reported as early as in the 70's^{73,74-76}. Lithium intercalation happens at around 0.09 V with a theoretical capacity of 372 mAh/g. However, the use of graphite as negative electrode was triggered by the development of the aforementioned layered transition metal oxides synthesized in their discharged (*i.e.* lithiated) state, therefore enabling the use of graphite without the need of prelithiation step⁷⁷⁻⁷⁹. Nowadays, it is still used in commercial batteries owing to its high reversibility, low volume expansion, and a relatively high capacity.

Nonetheless, other types of materials with much larger capacities exist and are studied as alternative anode materials⁸⁰. As illustrated in Figure 8, they can react with lithium according to three reactions: Insertion (like graphite), conversion and alloying.

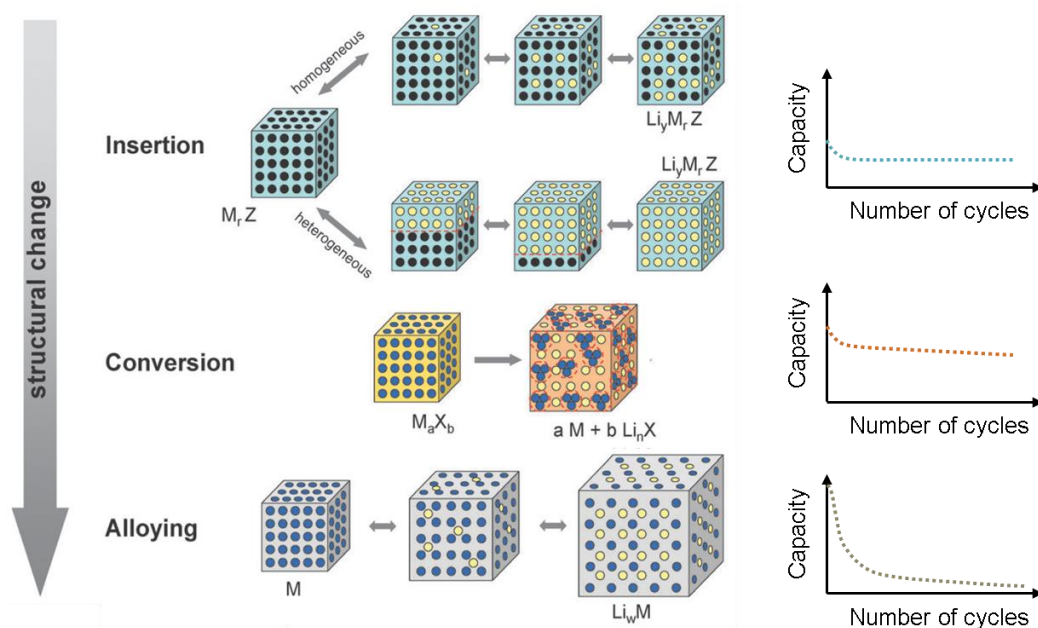


Figure 8: Schematic representation of anodic reaction types and associated cycling retention (adapted from⁸¹ and⁸²).

Intercalation compounds – example of them being the layered oxides used as cathode materials – possess a crystallographic structure into which sites are available for lithium ions to be reversibly inserted and extracted while preserving the structural framework. Aside graphite which intercalate Li^+ in between the graphitic planes, $\text{Li}_4\text{Ti}_5\text{O}_{12}$ ⁸³⁻⁸⁵ is used commercially owing to its well defined charge/discharge plateau and its high rate capability, while $\text{TiO}_2\text{-}\beta$ is still under study^{86,87}.

Conversion materials are a class of materials for which lithium reacts with the anionic ligand to form a new phase while the metal cation is reduced to the metallic oxidation state. Most conversion materials are oxides which form nanoclusters of metallic particles embedded inside a Li_2O matrix^{88,89}. The reversibility of such reactions is enabled by the small size of the reacting domains forming a high amount of interface in which ion diffusivity is enhanced. Usual conversion materials enlist oxides⁹⁰⁻⁹² (cobalt, iron...), phosphides (VP_2 ⁹³, Ni_3P ⁹⁴), nitrides (CrN ⁹⁵, GeN ⁹⁶...), fluorides⁹⁷, sulfides⁹⁸ or hydrides⁹⁹, but their practical utilization is limited by a high irreversibility of the first cycle and a too large polarization between charge and discharge.

Least but not least, some materials have the ability to alloy electrochemically with lithium at ambient temperature. Many Li-Metal binaries were explored from the early 70's, including Li-Al^{100,101}, Li-Si¹⁰²⁻¹⁰⁵, Li-Sn¹⁰⁶, Li-Bi¹⁰⁷, Li-Sb¹⁰⁸, Li-Ga¹⁰⁹, Li-Mg¹¹⁰, Li-B¹¹¹... However, despite numerous studies, these materials are still at the research stage due to an intrinsic limitation that was already pointed out by Dey *et al.* in 1971¹¹²: "...the alloying caused complete disintegration of the electrodes and the consequent loss of electronic contact". The poor mechanical behavior of alloyed electrodes arises from huge volume expansions upon lithiation, for instance + 280 % for $\text{Li}_{3.5}\text{Si}$, 244 % for $\text{Li}_{4.4}\text{Sn}$, 222 % for $\text{Li}_{4.5}\text{Pb}$ or 147 % for Li_3Sb when compared to the volume of the respective non-lithiated metals.

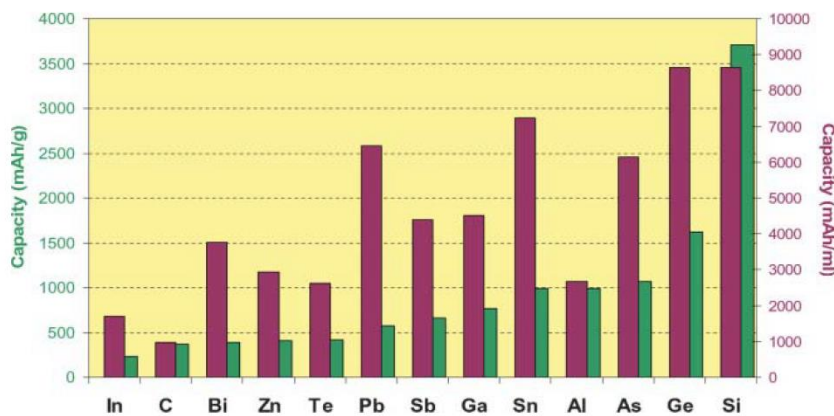


Figure 9: Charge/discharge capacities for selected Li-Metal alloys (as compared to C)⁸⁰.

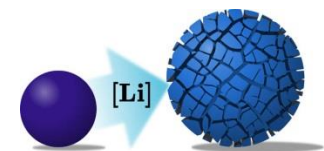


Figure 10: Schematic representation of particle swelling and cracking during the lithiation process¹¹³.

Aside from active material disconnection, the constant swelling and shrinking processes promote side reactions owing to the creation of fresh surface newly exposed to the electrolyte at each cycle. Since the alloying process happens at a potential lower than the electrochemical stability window of the electrolyte, the latter is reduced on the newly formed fresh surface to form the so-called solid electrolyte interphase (SEI) which largely reduces the capacity of such materials. Owing from the constant particle breathing process,

the SEI is constantly renewed upon cycling which leads to poor coulombic efficiency and rapid capacity fade in half and full cells ^{114,115}.

Several strategies have been employed to limit the capacity fading and improve the cycling retention. Among them, some have shown interesting improvements, such as:

- The realization of composite electrodes utilizing a suitable binder such as CarboxylMethylCellulose salts (CMC) ^{116,117} or Styrene Butadiene Rubber (SBR) ¹¹⁸ that embraces the particles swelling and compression,
- The addition to the electrode composition of a buffer compound which is able to accommodate the volume variations without cracking ^{119,120}. The buffer can take various forms, such as cleverly designed carbon particles ¹²¹ in the case of silicon, a binary alloy such as Cu_6Sn_5 , Ni_xSn , CoSn_2 ^{122,123}, etc. or an oxide such as SiO ¹²⁴,
- The control of the particles shape in order to expose stable facets and/or to limit their expansion ¹²⁵ or the use of nanoscale particles so as to alleviate the physical strains of the contractions/expansions ¹²⁶,
- The limitation of the depth of discharge so as to avoid the formation of highly lithiated alloys ¹²⁷.

Finally, significant improvements were reported when using electrolyte additives, such as vinylene carbonate (VC) ¹²⁸ or fluoroethylene carbonate (FEC) ^{129,130}, which improve the coulombic efficiency of the SEI formation as well as its robustness against large volume changes. The issues encountered when developing a novel anode material and especially the surface reactivity with the electrolyte shines the light on the crucial role played by the electrolyte's composition regarding battery performances, which will be described in the next session. Despite such an effort, the use of Si anode is still problematic and battery manufacturers are moving towards the commercial use of C/Si composites with only a 5 to 10 % content in Si only (Panasonic, etc..).

II.3 Electrolytes for Li batteries

The electrolyte is the third component of a battery which enables the internal transport of lithium ions between both electrodes. Its most critical features concern safety (thermal stability), cell rate capability (conductivity) and reactivity (electrochemical stability windows) ¹³¹. Commonly used electrolytes are *liquid electrolytes*, composed of a lithium salt dissolved in a liquid organic solvent. The most common electrolytes are a mix of carbonate species ¹³² such as Ethyl- (EC), Propyl- (PC), DiMethy- (DMC) or DiEthyl Carbonate (DEC) associated with LiTFSI (Bis(trifluoromethane)sulfonimide lithium salt) or

LiPF_6 ¹³³ (lithium hexafluorophosphate), at a concentration from 0.5 to 1 mol/L, giving a conductivity of around 1 mS/cm at room temperature^{131,133}. Aside organic ones, a few aqueous electrolytes have been proposed and the development of aqueous Li-ion cells is still continuing¹³⁴, despite the reactivity of such electrolytes towards Li which so far prevents their utilization in commercial Li-ion batteries.

In practical cells, electrolyte decomposes during the first cycle to form the SEI at the anode surface^{135,136}. This layer, which is vital for the proper cell functioning, prevents further electrolyte degradation later on cycling owing from its insulating character while ensuring a good Li^+ conduction from the electrolyte to the electrode¹³⁷. Interestingly, LiPF_6 also decomposes at the positive side on the surface of the current collector, which enables the utilization of Aluminum as collector¹³⁸. This fortuitous property explains the difficulty encountered by the research community to replace this salt.

Aside liquid electrolytes, much effort have been devoted to the development of *polymer electrolytes*, which consist of a polymeric gel such as polyethylene oxide (PEO) enabling the use of Li metal anode by preventing dendrite growth^{47,139,140}. The major challenge for this type of electrolytes is to achieve higher conductivity, which would enable their utilization at room temperature instead of 70 °C as currently employed. In order to tackle this issue and improve the mechanical properties of such gels, Bellcore's group has developed *plastic electrolytes* enabling the fabrication of plastic Li-ion batteries¹⁴¹ (PLiON). Such electrolyte is composed of a copolymer (PVDF-HFP) capable of trapping large amounts of liquid electrolytes within its amorphous domains, while the crystalline ones provide a good mechanical integrity. Owing to the easy manufacturing and high flexibility of both the plastic electrolyte and electrodes, such technology was at the source of significant advances in the battery field, especially at the packaging level.

Finally, in order to tackle the safety issues related to the use of liquid electrolytes, the development of *solid electrolytes* with sufficiently large conductivity is currently pursued for the development of all-solid states batteries but also micro-batteries¹⁴². Solid electrolytes are typically inorganic materials with remarkable crystallographic structures enabling relatively high diffusion of lithium atoms within the structure. Among them, the most interesting solid electrolytes are currently the garnets¹⁴³, NASICON type such as LAGP, perovskites such as LLTO, a brief description of the most important ones can be find in Table 1. The absence of any organic specie procures a better chemical and electrochemical stability which would enables high voltage applications. However, their practical utilization is still limited due to interfacial issues preventing long cycling, and electrochemical stability.

Name	Type	Typical composition	Ionic conductivity (S cm ⁻¹ , RT)	Stability with Li metal	Chemical stability
NASICON	glass ceramics	Li ₂ O-Al ₂ O ₃ -TiO ₂ -P ₂ O ₅	1.3 × 10 ⁻³	no	stable in air, mild acids and bases
NASICON	crystalline	Li _{1.3} Al _{0.3} Ti _{1.7} (PO ₄) ₃	bulk 3 × 10 ⁻³	no	stable in air
NASICON	crystalline	Li _{1.15} Y _{0.15} Zr _{1.85} (PO ₄) ₃	bulk 1.4 × 10 ⁻⁴	yes	stable in air
Garnet	crystalline	Li _{7-x} La ₃ Zr _{2-x} Ta _x O ₁₂	1 × 10 ⁻³	yes	stable in air, LiCl saturated water
Perovskite	crystalline	Li _{3x} La _{(2/3)-x} □ _{(1/3)-2x} TiO ₃	bulk 1.5 × 10 ⁻³	no	stable in air, water
LISICON	crystalline	Li ₁₄ ZnGe ₄ O ₁₆	1 × 10 ⁻⁶	no	not stable in air
Si wafer	single crystal	Si	6 × 10 ⁻⁷	no	stable in air, acids

Table 1: Summary of a few solid electrolytes and some of their properties ¹⁴⁴.

Interestingly, recent studies ¹⁴⁵⁻¹⁴⁷ report the use of solid electrolytes combined with liquid ones, hence enabling the presence of two (liquid) electrolytes in the same cell ¹⁴⁷. Although this idea comes from the past (*cf* the two-compartment cell of Antoine Becquerel in 1829), it was used to develop the batteries of the future (“beyond Li-ion” technologies).

As we’ve seen, many years of development have been required to develop the three main components of the Li-ion batteries, namely the cathode, the anode and the electrolyte. However, despite numerous developments and discoveries, the energy density of the current Li-ion batteries doesn’t exceed 200 Wh/kg and this energy density is not expected to exceed 300 Wh/kg within the next few years. Therefore, they will never cope with the need of very high energy density means required to bury the age of fossil fuels (*e.g.* gasoline energy density is ~ 10000 Wh/kg), hence calling for a game change through the development of new battery technologies. Furthermore, one battery technology cannot realistically meet all the requirements for applications such as portable electronic, electrical cars or grid storage and this situation is clearly favorable to the development of new battery technologies. Hence, this period calls for new concepts and the field is blooming of new ideas to go beyond Li-ion batteries. The next section is dedicated to a brief introduction to the emergent technologies with a special emphasis devoted to the Li-air technology – which is the object of this thesis – and its later development.

III Post-Li-ion battery technologies

Owing to the wide diversity of their chemistries, some post Li-ion battery technologies still require further research work at the fundamental level while other are at an advanced development stage. For instance, Na-ion and all solid state batteries clearly benefited from the development of Li-ion technologies and are on the verge to commercialization, as indicated by the production of Na-ion 18650 prototypes by the RS2E network in 2015 ¹⁴⁸. Likewise, Bosch announced the commercialization of all-solid state

battery by 2020 at half the price of current LiBs ¹⁴⁹, and Dyson is currently developing an electrical car powered by solid state batteries ^{150,151}. However, despite beneficial improvements regarding safety and energy density, solid state batteries will still suffer from the same limitations as Li-ion batteries owing to the heavy active material, especially at the positive side (*e.g.* LiCoO₂, LiMn₂O₄... ^{152,153}).

In order to overcome this limitation, a strategy is based on a chemical reaction instead of a redox one, in which Li⁺ reacts with the active material after its reduction at the cathode surface. Therefore, the capacity relies on the formation of a discharge product much lighter than host structure of Li-ion-type batteries. Based on this concept, two technologies are currently developed using respectively sulfur and oxygen as active material, which should provide a non-negligible boost of battery capacities (Figure 11 and Figure 12). Nonetheless, the potentiality of such technologies will never be accessible without a better fundamental understanding on the chemistry at play, as discussed in the next sections.

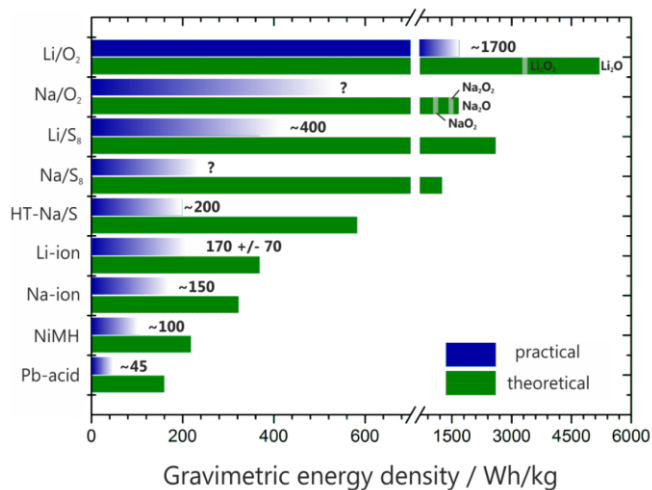


Figure 11: Theoretical and (estimated) practical energy densities of different rechargeable batteries. All values for practical energy densities refer to the cell level (except Pb-acid, 12 V (6 cells)) ¹⁵⁴.

III.1 Lithium-sulfur

In order to remove the heavy insertion cathode materials pertaining to the Li-ion batteries, one idea was to use the chemical reaction of lithium with a light solid that can be loaded into a porous conductive framework such as sulfur, which reacts with Li to form Li₂S in discharge. Despite promises, this technology is currently limited by mastering the reactivity of intermediary soluble polysulfides that tend to migrate and react at the anode

Chemistry	Discharge reaction	Cell voltage [V]	Theoretical energy density [W h kg ⁻¹]
Fuel cells	H ₂ + ½ O ₂ → H ₂ O	1.23	1100
Li/S	2 Li + S ⇌ Li ₂ S	2.1	2567
Zn/air	2 Zn + O ₂ → 2 ZnO	1.65	1084
Al/air	4 Al + 3 O ₂ + 6 H ₂ O → 4 Al(OH) ₃	2.71	8135
Na/air	4 Na + O ₂ ⇌ 2 Na ₂ O	1.95	1691
	2 Na + O ₂ ⇌ 2 Na ₂ O ₂	2.33	1605
	Na + O ₂ ⇌ NaO ₂	2.27	1108
Mg/air	2 Mg + O ₂ + 2 H ₂ O → 2 Mg(OH) ₂	3.1	6800
K/air	K + O ₂ ⇌ KO ₂	2.48	935
Li/air	2 Li + O ₂ ⇌ Li ₂ O ₂	2.96	3458

Figure 12: Various high capacity battery technologies and some of their characteristics ¹⁵⁵.

surface, resulting in a rapid capacity fading and to a practical capacity which is still far from the theoretical one of 1660 mAh/g_s.

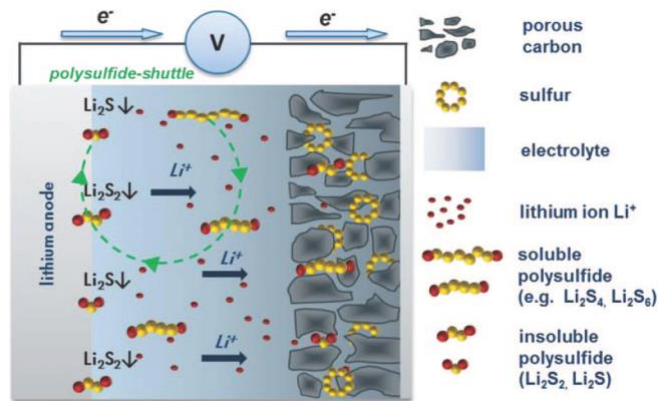


Figure 13: Schematic representation of a lithium-sulfur battery ¹⁵⁶.

Over the last decade, considerable efforts have been devoted to improve cycling performances by preventing the previously described shuttle mechanism ^{157,158}. Many strategies have been considered, such as the utilization of solid or polymer electrolytes as a physical barrier ¹⁵⁹, the encapsulation of sulfur species ¹⁶⁰⁻¹⁶², the utilization of an active material dissolved into the electrolyte called “catholyte” ¹⁶³, or the utilization of a pre-charged cathode (Li₂S instead of S) hence enabling using Li-free anode ^{145,164,165}, which overall gave mitigated results. Better performances were obtained using Ti₄O₇ as cathode material owing to its good electronic conduction and the intrinsic polarity of its surface, which chemically binds to the Li polysulfides hence preventing their migration ^{166,167}. More recently, some groups reported the use of “interlayer” added next to the separator to trap the soluble polysulfide ¹⁶⁸⁻¹⁷¹, which gives encouraging results at the expense of the mass of the battery. Another approach towards improved cycling consists in preventing lithium from reacting with dissolved species thanks to a protective layer. For instance, lithium nitrate (LiNO₃) has successfully been used as an electrolyte additive promoting the formation of a protecting SEI at the lithium surface, which greatly improved the cycle-life ¹⁷²⁻¹⁷⁴. Therefore, the most promising approach seems to be the containment of the polysulfides species at the cathode through the use of either a physical barrier or a chemical interaction with them.

III.2 Non-aqueous metal-air batteries

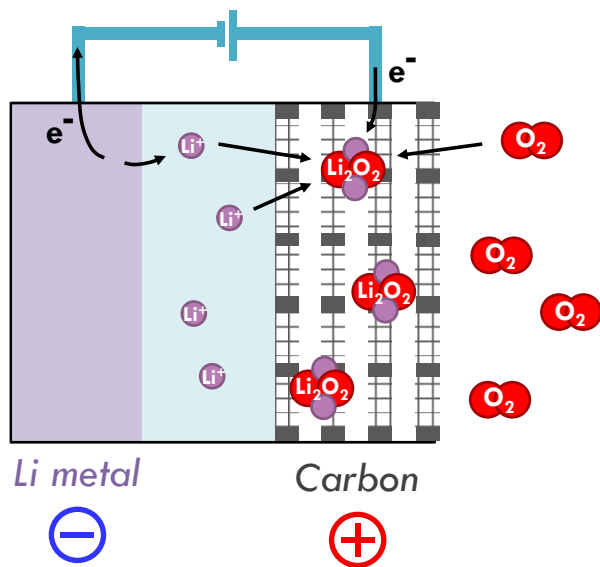


Figure 14: Schematic representation of a Li-O₂ battery.

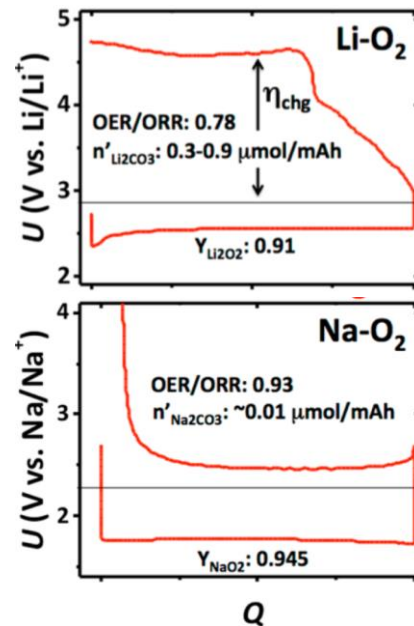
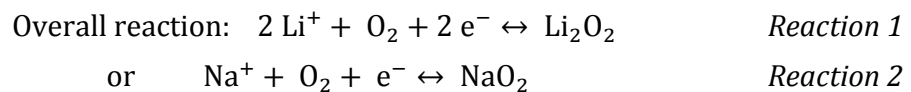


Figure 15: Voltage-Capacity profile curves of a Li-O₂ and Na-O₂ cell¹⁷⁵.



In contrast to Li-S, the Li-O₂ batteries and their sodium-based analogous (Na-O₂) use dissolved gaseous oxygen instead of solid sulfur as active materials to react with lithium/sodium upon discharge¹⁷⁶. The first rechargeable Li-O₂ battery was reported in 1996 by Abraham *et al.*¹⁷⁷ whereas Na-O₂ batteries were recently introduced by Hartmann *et al.* in 2012¹⁷⁸. In the next paragraphs, we will recall a few challenges common to most Metal-Air battery technologies, while the section IV of this chapter will be specifically dedicated to non-aqueous Li-O₂ batteries.

First, metal-air systems are very sensitive to impurities owing to the reactive nature of the alkali metals as well as reduced oxygen^{179,180}. In order to reduce the occurrence of parasitic reactions, the use of pure oxygen is hence required. Note that these cells should be designed as Metal-Oxygen (Li-O₂ or Na-O₂) batteries, even though “Metal-Air” (Li-Air or Na-Air) is frequently used and tolerated. This first point is to keep in mind when designing a practical cell and defining the actual capacity of such cells¹⁸¹.

Secondly, the capacity is obviously defined by the amount of available and dissolved oxygen into the electrolyte, which is largely governed by the physical properties of the

solvent and given by the Henry coefficient^{182,183}. Nonetheless, the solvents must also satisfy most restrictive criteria such as being aprotic, able to dissolve lithium salts and stable towards reactive species formed during cycling, which may be contradictory (*e.g.* the need of a polar solvent to solubilize the Li salt, while O₂ will be more easily dissolved in an apolar one). In practice, most candidates exhibit low O₂ solubility in the order of magnitude of a few mmol/L^{184,185}. Such a low concentration becomes an issue when i) other dissolved species can be competitively reduced, such as CO₂ which has a much higher dissolution coefficient, and ii) for practical applications, whose rate capability relies on high O₂ concentration. At a lab scale, the low concentration of dissolved O₂ does not seem to limit the performances of Li-O₂ batteries since Li₂O₂ is formed all along the electrode thickness, thus indicating a sufficient O₂ concentration deep inside the air electrode. On the contrary, this parameter seems more crucial for Na-O₂ batteries, for which NaO₂ formation occurs almost exclusively on the cathode area directly exposed to the gas¹⁸⁶.

The first step of the oxygen reduction reaction (ORR) is the reduction of O₂ dissolved into the electrolyte to form O₂⁻ (oxygen superoxide). Much effort has been devoted to understand its reactivity owing to its high oxidative power threatening every compound of the battery. In 2011, several groups have reported the instability of carbonate-based solvents in presence of superoxide, therefore preventing the use of the most common Li-ion electrolytes¹⁸⁷⁻¹⁸⁹. Many alternatives have been proposed over the last 5 years such as glymes, dimethyl sulfoxide (DMSO)^{190,191}, Acetonitrile¹⁹², N,N-Dimethylacetamide (DMA)^{193,194} etc... Despite numerous studies, the ideal solvent with perfect stability giving high concentration of dissolved oxygen has not been found yet.

Once the O₂⁻ superoxide is formed, it reacts with the alkaline metal cations to form the discharge product, such as lithium peroxide (Li₂O₂) or sodium superoxide (NaO₂) for Li- and Na-O₂ batteries, respectively. If their chemical nature is known, the parameters influencing their morphology are actively debated in the community¹⁹⁵⁻²⁰⁵. It has been shown that owing to the insulating character of Li₂O₂, the growth of a 5-10 nm thick film would eventually lead to the electrode passivation and therefore the death/stop of the cell²⁰³; thus the ongoing research towards developing high surface area cathodes. In parallel, many groups reported the growth of Li₂O₂ toroidal particles^{196,197,199,200} hence enabling higher capacity, but the factors promoting their formation are diverse (discharge rate²⁰⁰, the nature of the electrolyte^{204,206}, and impurities in the solvent^{201,202}...) and not consensually agreed upon. As for Na-O₂ batteries, many groups have reported the formation of micron-sized NaO₂ cubic particles when diglyme was used¹⁷⁸, but none was able to explain why such morphology was not found using other solvents.

A direct consequence of the search for the formation of large discharge product particles is that relatively large overpotential must be applied in charge to compensate for their low electronic conductivity ($\sim 10^{-13}$ S/cm²⁰⁷). Hence, mastering the charging process is also a challenging issue and poor faradic efficiencies are often encountered. Taking Li-O₂ batteries as example, the charge usually occurs around 3.8 to 4.5 V vs. Li⁺/Li⁰, which is 1 to 1.7 V above the discharge plateau, hence leading to a poor energy efficiency. Moreover, such high potential may favor the oxidation of the electrolyte and of the electrode which leads to poor cycle life. One solution, common in the Li-O₂ field, is to limit the discharge capacity (and so the size of the discharge product), but it is done at the price of the overall energy density.

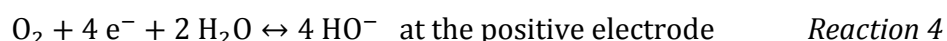
Finally, based on my own experience, the biggest challenge with laboratory Li-Air cells is their reproducibility. This was recently pointed out in a letter form Noked *et al.*²⁰⁸ which evidences major result discrepancies when changing minor parameters (e.g. cathode carbon loading). Such differences are reinforced by uneven protocols between different laboratories, such as electrode preparation and cell assembly. Additionally, the lack of universal electrochemical tests cells led to the development of various designs, which undoubtedly leads to incomparable results. In front of such remnant inconsistencies, many calls^{209,210} have encouraged researchers to be as accurate as possible, especially when detailing experimental protocols and calculating capacity values. In spite of these calls, numerous papers are still published without specifying absolute and relative capacity per surface area and per gram *of what*. Consequently, without suggesting any intellectual dishonesty from other researchers, one must at the student level adopt a critical state of mind when reading metal-air related literature.

Lastly, prior to focus more specifically on non-aqueous Li-O₂ batteries, we will give a brief overview of another Metal-Air technology which uses an aqueous instead of an organic electrolyte.

III.3 Aqueous Li-Air batteries

Bearing in mind all the challenges related to master the electrolyte properties for non-aqueous Li-O₂ batteries as well as their relatively poor cycling properties, the switch to aqueous Lithium-Air batteries has been considered. In contrary to non-aqueous ones, aqueous Li-Air batteries rely on the reaction of lithium ions with hydroxide anions in water so as to form lithium hydroxide in discharge (*cf Reactions 3 to 5*). In order to prevent such reaction from happening directly at the surface of the Li anode, the latter has to be protected

from the electrolyte. In 2007, Visco *et al.* was the first to cope with this issue by using a protective bilayer between the aqueous electrolyte and the lithium^{211,212}. The first layer is stable in presence of water, such as a ceramic glass like LISICON (Ohara Inc.); the second, stable in contact of lithium metal, can be either solid (Li₃N, LiPON), liquid (organic solvents), or polymeric. This Protected Lithium Anode (PLA) cell, which exhibits good stability up to 2 years²¹³, has helped in generating a renewed interest towards aqueous systems.



More recently, Stevens *et al.* (EDF, France) proposed an alternative design including a third electrode (called “evolution” electrode) separated from the regular air cathode by a physical membrane^{214,215} blocking all chemical species except anions (anionic membrane, *cf* Figure 16). During the discharge, O₂ is reduced at the air electrode into OH⁻ which migrates through the anionic membrane into the central compartment where it reacts with Li⁺ to form the final discharge product LiOH (Reaction 5). The membrane thus enables the formation of large amounts of LiOH outside of the air electrode’s compartment, hence protecting the latter from any pore clogging once the solubility limit of LiOH is reached. Accordingly, the charge does not occur at the air electrode – which is not in contact with LiOH – but at the evolution electrode located in the central compartment.

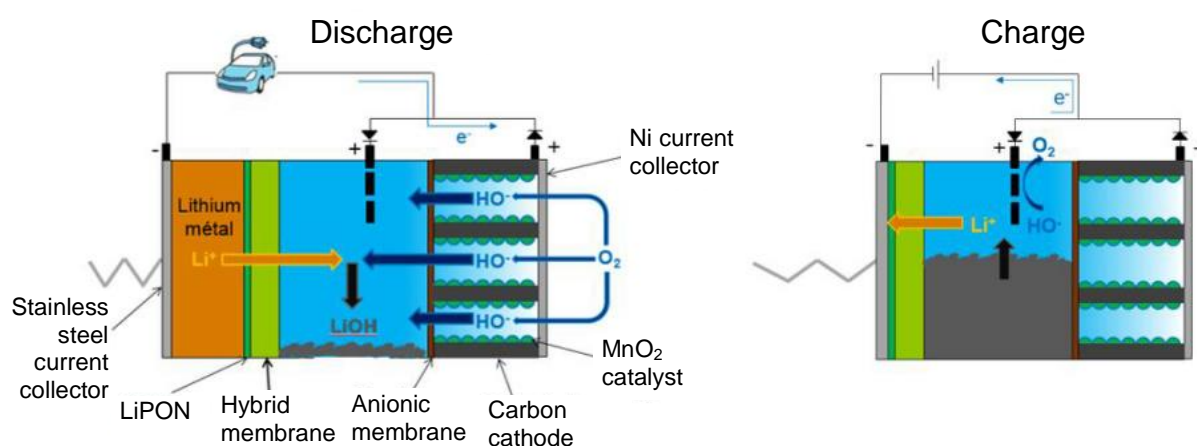


Figure 16: Schematic representation of an aqueous Li-O₂ battery in charge and discharge²¹⁶.

The anionic membrane, which is selectively permeable to hydroxide anions, prevents the potential formation of Li₂CO₃ and therefore enables cycling under ambient air (even contaminated with CO₂). Practical cells were able to cycle > 100 times over more than 1000 hours with an energy density of ~ 500 Wh/kg^{214,217,218} (with respect to the mass of the whole battery), which is about twice of today’s LiB. However, many challenges related to i)

the compatibility with other air components such as CO_2 ^{217,218}, ii) the full re-oxidation of LiOH and iii) the ceramic glass membrane fragility, remain before considering this technology as fully viable.

The group of rechargeable metal-air batteries also includes aqueous Na-O_2 ^{219,220} and organic K-O_2 batteries, which are both in early research stage. Other metal-air technologies have been reported in the literature such as Zinc-Air, Aluminum-Air and Magnesium-Air batteries (*cf* associated capacities in Figure 12), but are less relevant here since these are aqueous primary batteries.

Despite all the available metal air technologies, the non-aqueous Li-Air one remains one of the most attractive owing to its large capacity as well as potential of operation. Half way between Li-ion batteries and fuel cells, the development of this new chemistry is fundamentally challenging since it couples the issues associated to these two fields. On the negative side, one has to deal with the cyclability of the lithium metal electrode, the formation of a stable electrolyte interphase and the growth of lithium dendrites. As for the air electrode, the main issues concern oxygen solubility and diffusivity, the formation of a solid discharge product (as opposed to liquid water in fuel cell), and its proper oxidation possibly assisted by a catalyst or a redox mediator. Within the first 15 years of research, many strategies used to overcome these issues were inspired from the Li-ion field. Acknowledging the limited success of such approach, many groups went back to fundamental studies, bringing more understanding to this complex chemistry. The most relevant results and outcomes will now be discussed.

IV Rechargeable Aprotic Li-O₂ batteries – Last 5 years' news

Nowadays, classical lab-scale Li-O₂ batteries are composed of a carbon air electrode, a lithium metal anode, a non-carbonate based electrolyte and a pure oxygen reservoir (or flow). Yet, none of these compounds is fully satisfying all the criteria required for practical application, as discussed next.

IV.1 Basic components

IV.1.a Negative electrode

Owing to its low potential (-3.05 V vs. SHE) and high capacity (3860 mAh/g_{Li} and 2060 mAh/cm³), lithium metal is, in theory, an excellent electrode material. However, its

practical utilization in lithium batteries was a failure in term of safety ²²¹ leading to its total removal from commercial battery in the metallic state until the development of suitable polymer electrolytes. Controversially, Li metal is widely used in laboratory Li-O₂ batteries due to its simplicity of utilization and since it provides a large excess of lithium. However, the instability of Li metal in presence of oxygen has been reported in several studies as outlined below.

Argonne's group focused on parasitical reactions happening at the negative electrode in presence of O₂ using lithium triflate in tetraglyme (TEGDME) as electrolyte ²²². *In situ* XRD data (cf Figure 17) show the progressive formation and accumulation of LiOH and Li₂CO₃ over cycling, suggesting an electrolyte decomposition reaction.

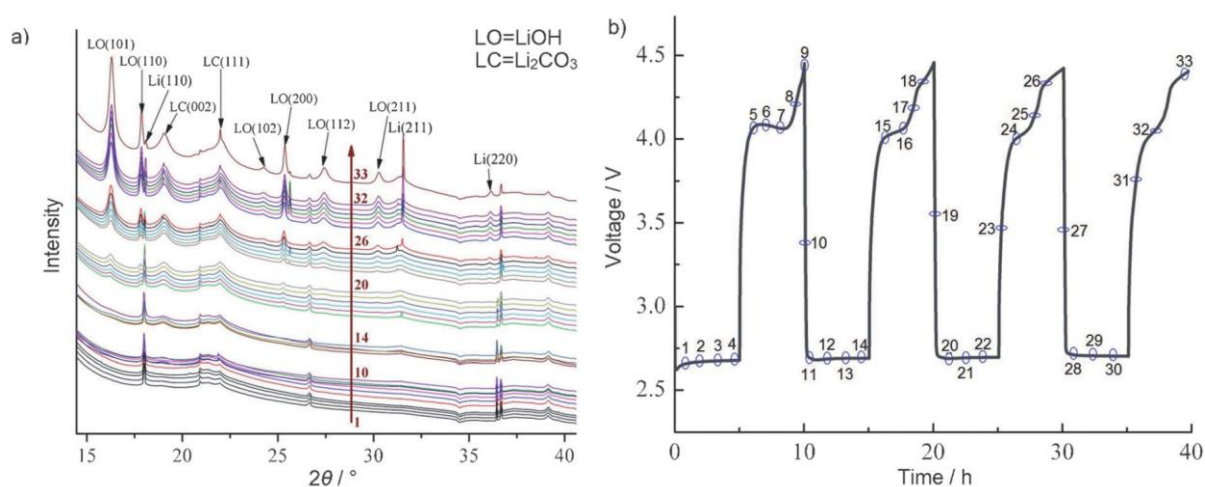


Figure 17: (a) *In situ* XRD patterns of Li the negative electrode showing LiOH formation during operation, and (b) corresponding voltage-time profile. The numbers on the XRD data correspond to those on voltage profile ²²².

They proposed a reaction mechanism based on DFT calculations, in which the etheral chain is deprotonated by an oxygen molecule in solution, eventually leading to formation of crystalline LiOH and Li₂CO₃. The continuous accumulation of LiOH in both charge and discharge conditions using the same electrolyte was later confirmed by Shui *et al.* ²²³ using a 3-dimensional micro-tomography technique coupled with *in situ* XRD. They observed a 140 μm thick LiOH layer in between the bulk Li and the electrolyte after 14 cycles. Even though the cell was still operating, they point out inevitable limitations in case of long-term cycling due to poor Li⁺ diffusion inside LiOH and total consumption of pure Li.

Such side reactions are visually observable in post-mortem analysis as reported by Abraham's ²²⁴ and Zaghbi's ²²⁵ groups. The former, by cycling a carbon/PVDF [8:1] air electrode in a 1M LiPF₆/TEGDME electrolyte for ~ 40 cycles, reported the formation of a dark-brown precipitate on the electrode surface (cf Figure 18). In contrast, Zaghbi and coworker attributed the coloration of metallic lithium to humidity (cf Figure 19), hence

highlighting the importance of eliminating trace amount of water infiltrated into the cell components.

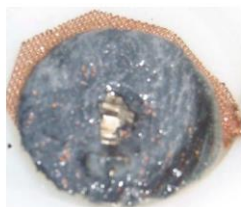


Figure 18. (Color online) Photograph of the Li anode surface after cycling.

Figure 18: Photograph of a Li negative electrode surface after cycling in a Li-O₂ battery with 1M LiPF₆ in TEGDME as electrolyte²²⁴.

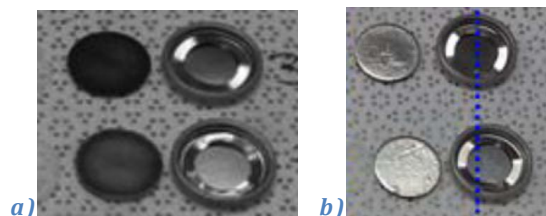


Figure 19: Photographs of Li electrode next to the disassembled coin-cell after cycling in a sealed O₂-filled box. In a), the box was placed in ambient atmosphere while in b) in was kept in the glovebox²²⁵.

In order to prevent the degradation of both Li electrode and electrolyte, two strategies were reported. The first one consists in covering the lithium anode by a solid electrolyte layer blocking the O₂ diffusion (*e.g.* LISICON)²²⁶. Despite its elegance, such concept is however practically limited owing to the brittleness, cost and weight of LISICON. On the other hand, Scrosati and coworkers proposed a Li-ion/O₂ cell based on prelithiated silicon anode instead of metallic lithium¹⁴⁶, and they obtained the electrochemical performances reported in Figure 20:

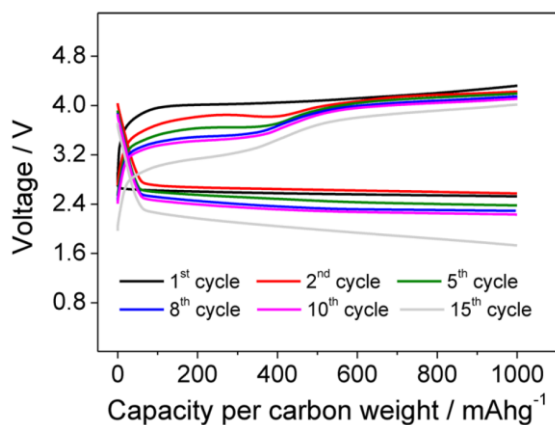


Figure 20: Voltage-Capacity profile of a lithiated-silicon/carbon - oxygen cell using LiOTf in TEGDME as electrolyte and a current of 200 mA/gc¹⁴⁶.

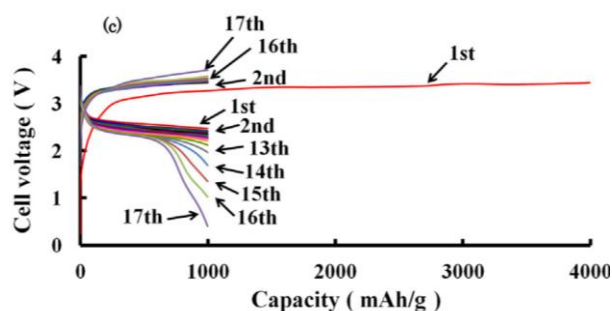


Figure 21: Voltage-Capacity profile of a hybrid Si/1M LiClO₄ in EC-DEC/LTAP/5MLiCl-1MLiOH/KB aprotic/organic Li-O₂ cell at a current of 0.33 mA/cm²¹⁴⁷.

XRD data shows the reversible formation of Li₂O₂ over cycling, which is yet limited to 15 cycles due to potential drop arising from the negative electrode. The authors suggest that despite the thick SEI layer formed during the prelithiation process presumably protecting the anode, the silicon electrode is slowly oxidized due to O₂ crossover.

Interestingly, the same approach was recently implemented into a hybrid Li-O₂ battery whose electrolytes, aqueous at the positive and organic at the negative, were

separated by a LATP ceramic glass membrane¹⁴⁷. As opposed to Scrosati's work, the rapid capacity fade cannot be here attributed to undesirable oxidation since the LATP interlayer prevents oxygen from crossing-over. Therefore, it was attributed to the silicon electrode itself which suffers from large volume changes and terrible mechanical behavior in absence of FEC.

It is worth noting that the utilization of silicon in "post Li-ion" systems had already been reported by Yang *et al.* in 2010¹⁶⁴ in a Li-S battery consisting of a Li₂S/mesoporous carbon composite cathode and a silicon nanowire anode. The initial capacity was around 500 mAh/g_{anode+cathode}, but a rapid capacity fade was observed due to parasitic reaction at both positive and negative sides. Two years later, Scrosati and coworkers introduced a few modifications to this system using (TEGDME)₄LiCF₃SO₃ as electrolyte and Hard-carbon spherule/sulfur as cathode, which gave limited cycle-life improvement (600, 300 and 150 mAh/g_s after 2, 20 and 100 cycles respectively)¹⁴⁵.

Overall, despite its frequent utilization as negative electrode in Li-O₂ batteries, Li metal still remains an issue that needs to be addressed for the following reasons: the formation of dendrite, the lack of interfacial control when using non-carbonated-based electrolyte and its high propensity towards oxidation. Unfortunately, no suitable alternative combining high capacity and stability towards oxygen has yet been developed, hence calling for more efforts on preventing O₂ crossover, protecting the anode, and/or replacing it. This later option will be developed in the 7th chapter of this manuscript.

IV.1.b Positive electrode

In Metal-Air technologies, the cathode is used as electron carrier and support for the discharge product growth. Owing to its lightness, abundance and high conductivity, carbon is wildly used in Li-O₂ cells. Moreover, its morphology (particles, nanowires, fibers, papers, gas diffusion layer...), surface area and porosity (see table in Figure 22) can be easily tuned, which makes it an ideal playground for researchers. However, many studies have demonstrated its instability in Li-O₂ batteries due to i) its reactivity with Li₂O₂ and ii) its oxidation at high charging voltage.

Carbon material	Surface area (m ² g ⁻¹)	Pore diameter (nm)	Specific capacity (mA h g ⁻¹)
Super P	62	50	1736
Vulcan XC-72	250	2	762
Activated Carbon (AC)	2100	2	414
Carbon Nano Tube (CNT)	40	10	583
Graphite	6	—	560
Ball-milled graphite	480	—	1136
Mesocellular carbon foam-C	824	30	2500

Figure 22: Comparison of surface area, pore diameter, and specific capacity of various carbons ^{227, 228}.

Luntz and his coworkers reported the formation of a thin lithium carbonate (Li₂CO₃) layer at the Li₂O₂-C interface ²²⁹, denoting the instability of carbon in presence of Li₂O₂ at high voltages. Based on differential electrochemical mass spectroscopy (DEMS) and X-ray photoelectron spectroscopy (XPS) and the utilization of isotopically labeled ¹³C in the electrode, they were able to attribute the Li₂CO₃ formation to carbon decomposition via two possible mechanisms (*cf reactions 6 and 7*). Their study, using a LiTFSI/DME electrolyte, evidences that Li₂O₂ chemically reacts with the carbon electrode during discharge to form Li₂CO₃ at the carbon interface (*cf* Figure 23).

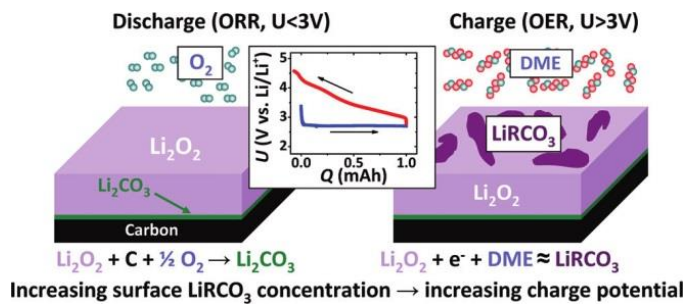
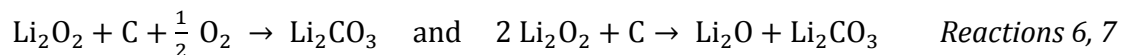


Figure 23: Schematic representation of side products formation in Li-O₂ batteries over charge and discharge ²²⁹.

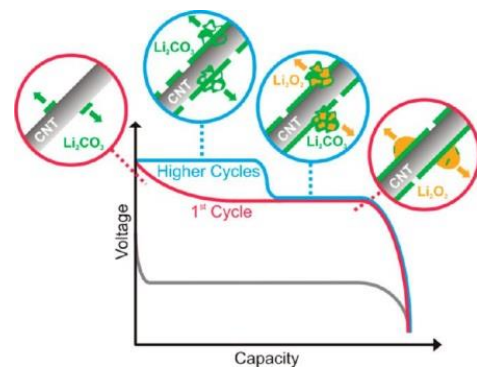


Figure 24: Schematic illustrating the morphological evolution of the discharge product during charge ²⁰⁵.

The formation of Li₂CO₃ was also reported by Gallant and her coworkers who used X-ray absorption near edge structure (XANES) spectroscopy to evidence the morphological changes undergone by Li₂O₂ and the formation of crystalline Li₂CO₃ during the first cycles ²⁰⁵. This was attributed to a side reaction between lithium peroxide and carbon nanotubes used as positive electrode in DME-based electrolyte. Li₂CO₃ re-oxidation is possible but incomplete after a few cycles, and occurs at a higher voltage plateau which expands with cycling (*cf* Figure 24).

Finally, the instability of carbon was also demonstrated in $\text{LiPF}_6/\text{TEGDME}$ and $\text{LiClO}_4/\text{DMSO}$ electrolytes by Bruce and his coworkers by labelling the air electrode with ^{13}C in order to determine the origin for the CO_2 formation observed by multiple other groups²³⁰. The presence of $^{13}\text{CO}_2$ in charge indicated the degradation of carbon at potentials higher than 3.5 V, while in discharge it was relatively stable and the main side reaction was coming from the electrolyte decomposition. Direct chemical reaction of carbon and Li_2O_2 also contributes to a small portion of Li_2CO_3 formation, which is in agreement with Luntz's work²²⁹. Together, these studies – among others – show clear evidence for carbon instability in Li- O_2 batteries, due to Li_2O_2 reactivity and oxidation at high potentials, hence calling for its replacement if the charge potential cannot be pushed further down (see catalyst effect later).

In that purpose, Bruce *et al.* used nano-porous gold (NPG) as an alternative to carbon at the air electrode, which shows > 100 cycles without accumulating Li_2CO_3 at the electrode surface, but with a limited capacity of 300 mAh/g_{Au} ¹⁹⁰. Yet, gold is not a practical solution due to its cost and high density (10x heavier than carbon) that drastically decreases the gravimetric capacity. To tackle this issue, the same group later used titanium carbide (TiC) as replacement of the NPG electrode, which exhibits a remarkable stability and also prevents the formation of Li_2CO_3 . Similarly, Zhou and coworkers²³¹ reported enhanced cyclability of a Li- O_2 cell using Ruthenium/Indium Tin Oxide (Ru/ITO) as air electrode. Figure 26 shows SEM images of the above-mentioned cathode in addition to other carbon-free air electrodes such as Co_3O_4 nano-rods²³²⁻²³⁶. A enhanced cycling stability was obtained when compared to carbon but at the price of a much lower gravimetric capacity (*cf* Figure 25).

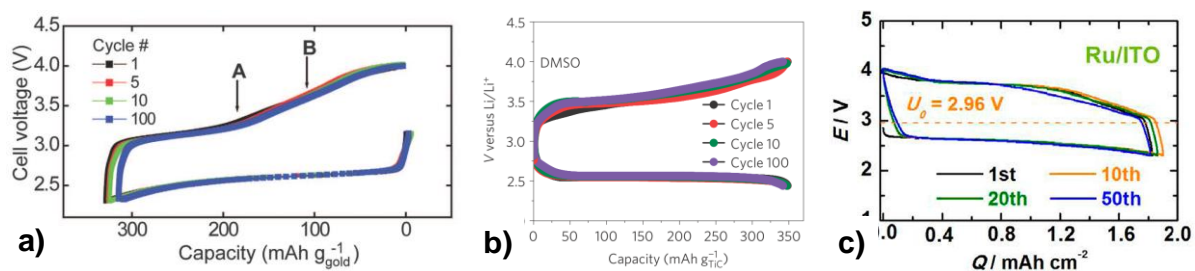


Figure 25: Voltage-Capacity profiles of Li- O_2 cells using NPG¹⁹⁰ (a), TiC¹⁹¹ (b), or Ru/ITO²³¹ (c) air electrode in DMSO- (a,b) or triglyme-based (c) electrolyte.

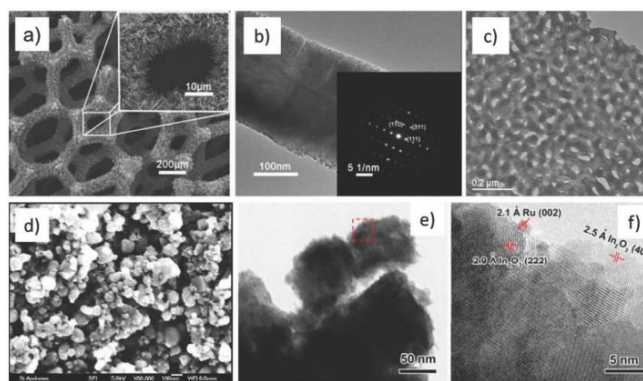


Figure 26: SEM and TEM images of various carbon-free Li-O₂ battery air electrodes²²⁷. Co₃O₄ nanorods on Ni mesh²³² (a,b); Nanoporous gold¹⁹⁰ (c); TiC¹⁹¹ (d); Ru/ITO²³¹ (e,f).

Another strategy to improve cathode stability consists in lowering the charge voltage so as to decrease the cathode degradation occurring under high oxidative conditions. It can be done using i) heterogeneous catalysts²³⁷ or ii) homogeneous ones such as redox mediators dissolved in the electrolyte²³⁸. Catalysts are used to promote the Li₂O₂ oxidation (and/or formation), so as to lower the charge potential and increase the kinetics of the reaction. Such approach has been successfully implemented to fuel cells, where the gas diffusion layer is studded with catalyst nanoparticles, mostly platinum and other noble metals²³⁹.

In Li-O₂ battery, lowering the charge voltage by adding small amounts of catalyst would significantly improve the carbon stability without jeopardizing the capacity associated to heavy material utilization. The mechanism of Li₂O₂ oxidation in presence of catalysts was studied by both Shao-Horn's²⁴⁰ and Wagemaker's²⁴¹ group, who evidenced the formation of a sub-stoichiometric intermediate which could be oxidized more easily than bulk Li₂O₂, hence reducing the overall charge voltage. However, finding a relevant catalyst is not an easy task, as pointed out by Luntz's group who showed that the most common ones (Au, MnO₂ and Pt nanoparticles) barely lowered the charge potential but rather increased CO₂ emissions²⁴² due to electrolyte degradation. Such lack of selectivity towards Li₂O₂ oxidation was later confirmed by Harding *et al.*²⁴³ who evidenced that most metallic catalysts actually lead to electrolyte decomposition. In addition, some of these catalysts react with lithium in the potential windows applied in Li-O₂ cells (*e.g.* MnO₂), making even more complex the comprehension of their catalytic activity.

Notwithstanding a few successful attempts²⁴⁴, such heterogeneous catalysis is by definition restricted by the limited contact point with Li₂O₂ arising from the punctual coverage of the cathode substrate by the active particles. These issues can be avoided with the utilization of homogeneous catalysts added to the solvent, also called redox mediator. Their use will be addressed in the next section focused more generally in electrolytes.

IV.1.c Electrolytes

Finding stable electrolytes towards reduced oxygen species generated at the cathode is one – if not the most – crucial challenge for Li-Air batteries^{183,188,206,245–247}. The instability of carbonate-based solvents that were initially used (for more than 10 years!) is now generally acknowledged by the community. It was first unraveled in 2011 by carefully monitoring the gases evolved upon charging PC- and EC-based Li-O₂ cells^{187–189}, with namely the evidence for the formation of side products such as Li₂CO₃, C₃H₆(OCO₂Li)₂ (Li propylene dicarbonate), MeCO₂Li (Li acetate), HCO₂Li (Li formate), CO₂ and H₂O during cycling, but no trace of Li₂O₂. This major discovery, which was evidenced by coupling galvanostatic, FTIR and DEMS analysis, send a warning to the community on the importance of gas analysis and the insufficiency of electrochemical characterization alone.

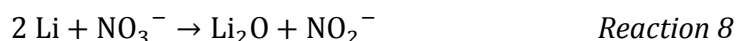
Glymes (i. e. DME, DEGDME, TEGDME), DMSO, and DMA are among today's most commonly used electrolytes in Metal-Air systems due to their decent stability towards oxygen reduced species. TEGDME is very attractive due to its extremely low volatility and has been the subject of many studies. Freunberger *et al.* reported that Li₂O₂ was the main discharge product formed in a Li-O₂ cell using 1M LiPF₆ in TEGDME as electrolyte and Csp/kynar as air electrode²⁴⁶. However, they also detected the formation and the accumulation of Li₂CO₃, CH₃CO₂Li, HCO₂Li, CO₂ and H₂O over cycling, at the expense of Li₂O₂ which disappeared after 5 cycles. The formation of parasitic species over cycling was independently confirmed by McCloskey *et al.* who used another lithium salt¹⁷⁵ (0.5 N Li triflate in TEGDME). DME-based electrolytes behave similarly, as reported by both Luntz's^{175,242,248} and Shao Horn's groups²⁰⁵. The reversible formation of Li₂O₂ was evidenced by various technics, however gas analysis revealed that CO₂ and H₂ are evolved in charge after a few cycles. It was later proposed that glymes were intrinsically stable in presence of chemically formed O₂⁻^{246,249} (*i.e.* formed by KO₂ dissolution), but not under electrochemical Li-O₂ battery cycling conditions^{197,250} (electro-oxidation, presence of O₂ and Li₂O₂, etc...). Additionally, the presence of impurities dissolved in the solvent and strongly reacting with O₂⁻ may bias the interpretation of these results^{245,251}, especially for long chains such as TEGDME which are hard to purify. In short, glymes are theoretically stables, but side reactions were spotted under real battery conditions which prevents their utilization for long-term cycling.

The use of dimethyl sulfoxide (DMSO) as an alternative to carbonates and glymes was early proposed by Laoire *et al.* who studied the ORR mechanism in various solvents²⁰⁶. Later on, Bruce and his coworkers reported 100 cycles with 95% capacity retention for a Li-O₂ cell using 0.1 M LiClO₄ in DMSO as electrolyte associated to a NGP cathode¹⁹⁰ and a

LiFePO₄ anode (metallic Li reacts with DMSO). Actually, the stability of DMSO-based electrolytes associated to carbon cathodes has been contested by Trahan *et al.* who failed to cycle such a cell for more than 10 cycles even with very limited capacity (300 mAh/gc ⇔ 10 % of the maximum discharge depth)²⁵². They invoke side reactions involving DMSO and O₂⁻, leading to LiOH formation at the cathode. Hence, DMSO instability was later confirmed by Aurbach's and Shao-Horn's groups^{250,253}.

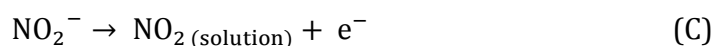
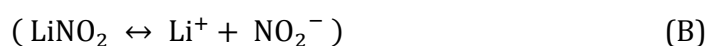
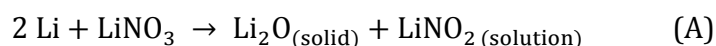
Aside from DMSO and glymes, amide-based electrolytes have been considered for Li-O₂ applications^{194,247,254,255}. A Dimethylformamide (DMF)-based cell was studied by XRD, FTIR and ¹H nuclear magnetic resonance (NMR) using either carbon or gold as air electrode²⁴⁷. In both cases, Li₂O₂ was detected during the first discharges but after the 10th cycle, only Li₂CO₃, MeCO₂Li and HCO₂Li were formed. Such poor results and its incompatibility with Li metal explain why DMF is barely used nowadays.

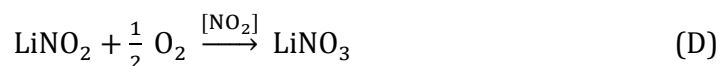
Based on theoretical studies^{250,256}, Liox group reported a N,N-dimethylacetamide (DMA)-based Li-O₂ battery with remarkable performances¹⁹³. This is especially explained by the use of 1 M LiNO₃ as lithium salt in presence of oxygen, which promotes the formation of a protective SEI on the Li surface according to *Reaction 8*.



In addition, the Li nitrate plays the role of redox mediator for the Li₂O₂ oxidation and decreases the charging voltage to a potential as low as 3.6 V. Hence, a cell using a carbon cathode was able to cycle 80 times at 0.1 mA/cm² when the discharge capacity was limited to ~ 220 mAh/g (1 mAh/cm²). In addition, a clever set-up enabling gas pressure monitoring confirmed that the quantity of gases released/uptaken over cycling was close to the theoretical expected value, therefore demonstrating limited side reactions for this system even after long-term cycling (> 2000 h)²⁵⁷.

Moreover, Liox researchers studied the formation mechanism of the SEI, which enables the use of lithium metal as anode with DMA (otherwise unstable) in Li-Li symmetric cells²⁵⁸. Interestingly, they noted a rapid failure of the system when the cell was cycled in argon instead of O₂ (all things being equal), suggesting an important role of dissolved oxygen. They proposed the following multistep mechanism:





It involves (A) the formation of the SEI (Li_2O) and soluble lithium nitrite (B). The latter is then oxidized in charge at ~ 3.6 V into nitrogen dioxide (C), which catalyzes LiNO_3 regeneration while consuming oxygen (D). It is then important to note that:

- The LiNO_3 regeneration occurs in presence of oxygen (*cf* D), which suggests a constant SEI regeneration explaining the long life-time of the anode. Such beneficial behavior is not observed in Li-S batteries where LiNO_3 is used as well ²⁵⁹, thus reinforcing the role played by oxygen in this mechanism.
- The dissolved $\text{NO}_2^-/\text{NO}_2$ redox couple is responsible for the low charging voltage: NO_2 is reduced in contact with Li_2O_2 and therefore promotes its oxidation at ~ 3.6 V.
- During these two processes, only a fraction of NO_2 reacts. Its concentration never reaches the solubility limit of the solvent, which explains why it was never identified as gaseous product

The redox properties of LiNO_3 (actually $\text{NO}_2^-/\text{NO}_2$) has also been reported in DEGDME ²⁶⁰, but the overall performances were not as good as in DMA, which was an impetus to develop redox mediators better adapted to other solvents.

IV.2 New trends

IV.2.a Redox mediators

As explained previously, the charging process is crucial for achieving better round trip efficiency as well as avoiding parasitic reactions. To reduce the large overpotential encountered during the oxidation of insulating Li_2O_2 , the use of redox mediators was first demonstrated by Liox Inc. and is nowadays foreseen as the solution of choice to tackle this limitation. A redox mediator is a soluble specie with a thermodynamically redox potential higher than that of the $\text{O}_2/\text{Li}_2\text{O}_2$ couple (2.96 V). Once oxidized during the charge process, the redox mediator is reduced during a reaction with Li_2O_2 (Li_2O_2 is oxidized), prior to be oxidized again and so on. By adjusting the potential of the redox mediator, one can expect to bring the charge potential of a Li- O_2 battery as low as $E^\circ(\text{O}_2/\text{Li}_2\text{O}_2)$. Moreover, in contrary to heterogeneous catalyst for which the surface in contact with Li_2O_2 is greatly limited – therefore limiting its effect – the use of dissolved species allows for accessing all the Li_2O_2 surface in contact with the electrolyte.

Various examples of redox mediator were reported in the recent literature, such as LiNO_3 in DMA and DEGDME^{193,257,260}. Later on, Bruce's group used the Tetrathiafulvalene redox couple (TTF/TTF⁺) in a Li-O₂ cell with a NPG electrode and DMSO-based electrolyte (1 M LiTFSI + 10 mM TFF)²⁶¹. The cell exhibits 0.8 V of polarization for 100 cycles with limited discharge of 300 mAh/g_{Au} and a current of 0.08 mA/cm². They were able to increase the current up to 1 mA/cm² and the polarization was 1.3 V, while the cell without TFF completely failed. In 2014, Bergner et al. reported that adding 10 mM TEMPO (2,2,6,6-tetramethylpiperidinyloxy) in a 1 M LiTFSI/DEGDME electrolyte reduced the charge potential by 0.5 V²⁶². Finally, the utilization of LiI (lithium iodine) in a TEGDME-based electrolyte associated to CNT fibrils led to overpotentials as low as 0.8 V for 900 cycles, as reported by Kisuk Kang's group²⁶³. However, this result has to be taken with caution since a recent work by Kwak *et al.* demonstrated the formation of additional side products associated to the I₂/I₃⁻ redox couple²⁶⁴. Similar side reactions could also explain the formation of LiOH which was recently reported by Grey *et al.* when using LiI as redox mediator in glymes²⁶⁵. Considering the large variety of potential redox mediator candidates, DFT calculation – which combines their ionization energy with the HOMO energy levels of the electrolyte and the Li₂O₂ – was proposed to narrow this list down and determine the most efficient redox mediators, such as DMPZ (Dimethylphenazine), whose beneficial effect in Li-O₂ batteries was experimentally confirmed²⁶⁶.

Other types of redox mediators are also used to promote the ORR in order to i) increase the discharge voltage and/or ii) increase the quantity of discharge product, both of which resulting in higher energy density. In a recent paper, Bruce and his coworkers studied the effect of DBBQ (2,5-di-tert-butyl-1,4-benzoquinone) on the discharge capacity of a glyme-based Li-O₂ cell using a GDL as cathode²⁶⁷. Adding 10 mM of DBBQ in the electrolyte increases the capacity (normalized in BET surface area) by 50 to 100 times and the discharge voltage by 0.1 to 0.15 V. SEM images show the growth of large Li₂O₂ particles fully covering the GDL surface. The surface growth mechanism, promoted by DBBQ and enabling such high capacity, will be explained in the next section

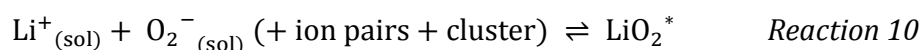
In summary, electrolyte stability is one of the most urgent challenges in non-aqueous Li-O₂ batteries to be solved. To date, only few solvents with acceptable stability were reported but they all suffer from the harsh cycling conditions. Redox mediators are currently attracting much attention as a way to solve this issue and might lead to increase the cycle number by one order of magnitude. Yet, an extra order of magnitude would still be necessary for commercial application, which requires a better understanding of the reaction

mechanism. The comprehension of the ORR mechanism in particular was significantly improved over the past 5 years, as detailed in the next section.

IV.2.b Unified ORR mechanism

In front of all the above-mentioned difficulties, it was understood that mastering the Li-O₂ technology would require a deep understanding of the chemistry at play, hence calling for fundamental studies on the reaction mechanism involved. In particular, much effort has been devoted to the study of the Oxygen Reduction Reaction (ORR) since: 1) it involves oxygen reduced species responsible for most stability issues previously reported and 2) it governs the morphology of the discharge product formed during reduction that then greatly influence the charging process. Until recently, two different models had been proposed. In one hand, the model supported by Luntz describes O₂ reduction into Li₂O₂ as a process taking place only on the surface of the electrode (2-D film, surface mechanism)^{248,268}. On the other hand, the model proposed by Abraham involves Li₂O₂ particles (3-D, solution mechanism)^{206,252,269} and is based on the Hard Soft Acid Base (HSAB) theory of Pearson²⁷⁰, i.e. the chemical reactivity of an acid and a base in solution. Both models were supported by experimental observations; however they are hardly compatible and have different implications regarding the rate, polarization and reversibility of Li₂O₂ formation/removal.

In 2014, L. Johnson and C. Li proposed a unified mechanism²⁰⁴ explaining both film and particle growth according to the solvents donor numbers (DN, defined as the solvation enthalpy of the Lewis acid SbCl₅ in a given solvent^{271,272}). Practically, a high DN solvent strongly solvates the Lewis acid Li⁺, which prevents its association with a base in solution such as O₂⁻. On the contrary, low DN solvents have low solvating power, leading to high Li⁺ availability. Overall, the donor number influences the equilibrium following the first reduction step:



Experimentally, rotation ring disc electrode (RRDE) and surface-enhanced Raman spectroscopy (SERS) technics revealed the existence of O₂⁻ in solution with high DN solvents, whereas LiO₂^{*} was detected at the surface of the electrode with low DN solvents (* indicates surface adsorbed species). This was the demonstration that low DN solvents shift equilibrium (9) to the right, which is consistent with the meaning of donor numbers.

Accordingly, the solubility of LiO₂ is increased with high DN solvents, which enables its disproportionation into Li₂O₂ away from the electrode so as to form large particles

(*Reaction 11*, solution mechanism). In contrast, in low DN solvents, LiO_2 stays near the surface of the electrode where it undergoes a second reduction leading to film formation (surface mechanism, *Reaction 12*).



In parallel, an analogous theory was established based on the Acceptor Number (AN) of the electrolyte, which determines the stability of O_2^- in solution. In agreement to the former explanation, Luntz's group reported the formation of large Li_2O_2 toroids when using high AN electrolytes, which strongly solvates O_2^- hence promoting a solution growth mechanism^{201,273}. Such theory rationalizes the influence of the Li salt and the solvent impurities^{201,202,225,274} on the discharge product morphology, since they can modify the AN of the overall electrolyte. This explains for instance the formation of large toroidal particles when significant amounts of water (AN = 55) or ethanol (AN = 37.9) were added to the electrolyte.

In addition, Shao-Horn's and Nazar's groups reported the absence of large particles formation at very high discharge rates due to the slow diffusion of O_2^- in solution limiting the particle growth. This stresses out the importance of the current density in controlling the discharge product's morphology^{195,200}, which does not contradict the DN and AN theories.

Finally, understanding the ORR mechanism has direct consequences on the choice of the solvent and the application. With low DN solvents (such as acetonitrile), the discharge capacity is limited by the surface of the Li_2O_2 film, acknowledging that its thickness cannot exceed 5 to 10 nm²⁰³. High surface area cathodes are then of prime importance when using these solvents. In contrast, this parameter has a limited influence in high DN solvents (such as DMSO) since Li_2O_2 can grow as long as the surface of the electrode remains electronically conducting to reduce O_2 into O_2^- .

IV.3 Challenges and perspectives in non-aqueous Li-O₂ batteries

For many years, rechargeable non-aqueous Li-O₂ batteries were promised a great future because of their high theoretical specific energy of ~ 3500 Wh/kg (with respect to the mass of active material at the anode and at the cathode)¹⁴⁴. However, the initial hopes were stained by the lack of comprehensive studies requiring time and dedication. The past five

years were marked by many fundamental discoveries enabling a better understanding of this unique and complex chemistry. Yet, many barriers remain before starting the development of practical Li-O₂ devices.

The air electrode is soon to be a solved issue: instability problems were identified and alternative materials were proposed. Reducing their weight and cost remains challenging, but the road has been paved. The perfect electrolyte has not been found and perhaps does not exist. Trying every existing solvent has not been a very successful strategy. Therefore, a stronger cooperation between organic chemists, battery experts and theoreticians so as to predict and synthesize this holy liquid is required. Meanwhile, the utilization of redox mediators showed promising results, and one can predict that coupling two mediators (one for the ORR, one for the OER) in the near future will enable the reversible formation of large Li₂O₂ without parasitic reactions and giving a large reversible capacity.

Finally, developing a suitable negative electrode is probably the most challenging issue that needs to be addressed. Both the utilization and replacement of lithium metal are problematic, mostly because of the strong oxidative operating conditions of Li-O₂ cells. Owing to their high theoretical capacity, metal alloys are considered as potential candidates but currently suffer from limited cycling performances.

Part of my thesis work is focused on developing an alternative anode based on lithiated silicon (Li_xSi). Previous studies tackling this approach were rare and elusive, hence calling for deeper investigation. Prior to consider the integration of silicon electrodes into full Li_xSi-O₂ cells, we studied the behavior of silicon with respect to lithium in Si half cells. In order to fully understand the factors currently limiting their utilization, the next section will focus on lithium-silicon alloys as well as on Si/SiO₂ composites in order to better put in context the impact of our work.

V Lithium-Silicon alloys

V.1 Electrochemical behavior and structural changes

First contributions on lithium-silicon alloys come from the metallurgical field ²⁷⁵⁻²⁷⁷. The first complete binary phase diagram ²⁷⁸ was described during the 80's and mentioned the existence of 4 defined compounds: Li_{1,7}Si (Li₁₂Si₇), Li_{2,3}Si (Li₇Si₃), Li_{3,25}Si (Li₁₃Si₄) and Li_{4,4}Si (Li₂₂Si₄) ²⁷⁹⁻²⁸¹. Meanwhile, it was reported that electrochemical lithiation of silicon at high temperature ^{103,104} (400-500 °C) occurred in agreement with this phase diagram ^{282,283},

ultimately leading to the $\text{Li}_{22}\text{Si}_4$ phase, which corresponds to a capacity of 4200 mAh per gram of silicon. However, $\text{Li}_{22}\text{Si}_4$ cannot be electrochemically formed at room temperature, for which the lithiation stops at $\text{Li}_{15}\text{Si}_4$ ²⁸⁴ (or $\text{Li}_{3.75}\text{Si}$, 3572 mAh/g_{Si}, 8300 mAh/cm³_{Si} or 3031 mAh/cm³_{Li₁₅Si₄}). These attractive theoretical values motivated many studies on mastering the lithium-silicon chemistry, which is particularly challenging given the massive volume changes in between the above-mentioned Li-Si phases (Figure 27). It is worth noting that owing to the linear $\Delta V = f(\Delta x)$ evolution, it is not possible to alleviate ΔV by shifting Δx .

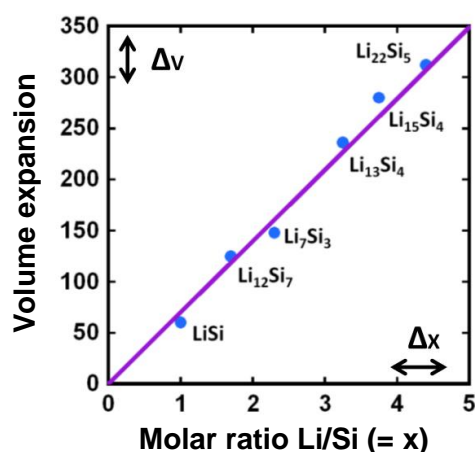


Figure 27: Volume expansion of Li_xSi particles as function of the Li/Si molar ratio⁸².

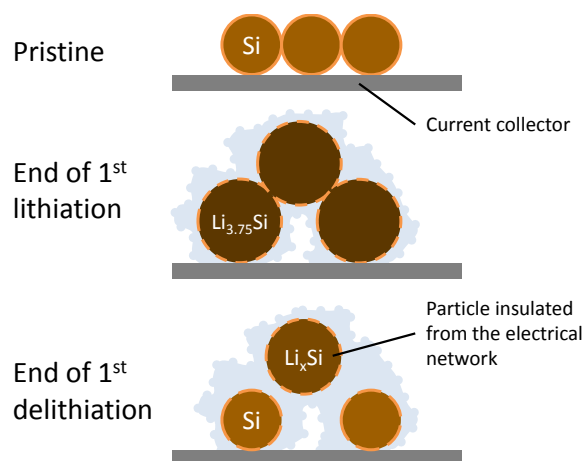


Figure 28: Schematic representation of a Si electrode during cycling (adapted from⁹).

Such important swelling/shrinking upon cycling implies i) the loss of the percolation network between the particles of active material, as represented in Figure 28; ii) a poor mechanical behavior of the electrode, for which the layer containing the active material is detached from the electrode²⁸⁵; iii) a huge mechanical stress leading to particle cracking; iv) deterioration of the SEI which cannot accommodate the volume change, and v) the perpetual SEI reformation on the newly exposed particle surface²⁸⁶⁻²⁸⁸. Facing so many challenges, much effort has been devoted to understand the structural changes occurring upon lithiation, which are responsible for the volume changes hindering the cycling performances.

In battery conditions, silicon does not usually crystallize during the lithiation process. Instead, it undergoes a phase transition from crystalline to amorphous, characterized by a voltage plateau at ~ 0.1 V. When nanoparticles are used ($< 1 \mu\text{m}$), they remain amorphous afterwards. Then, silicon is delithiated during a smooth and continuous charge process which indicates a single phase transition (solid solution)²⁸⁹.

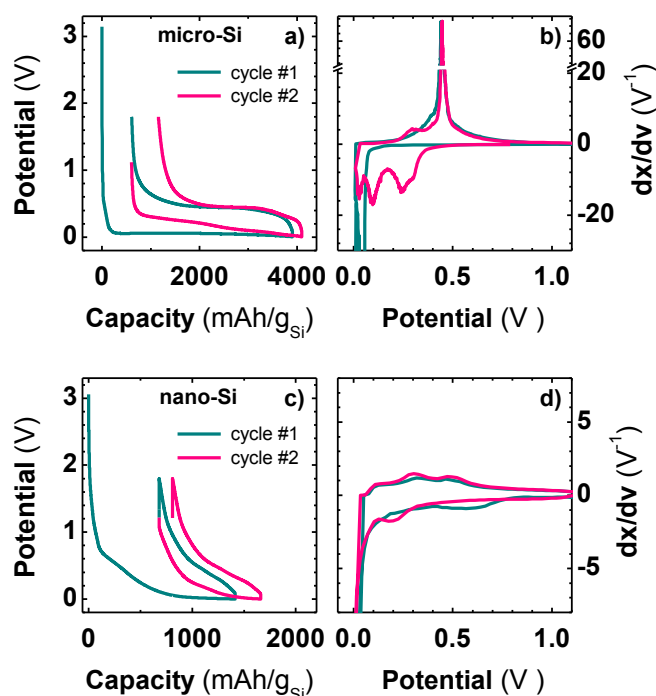


Figure 29: Voltage-capacity (a,c) and Derivative Capacity (b,d) profiles of a micro-Si/Csp/CMC // LP30 // Li (a,b) and a nano-Si/Csp/CMC // LP30 // Li (c,d) half-cell.

However, when large particles ($> 1\text{-}2\ \mu\text{m}$) are used, silicon may crystallize into the $\text{Li}_{15}\text{Si}_4$ phase at the end of the discharge at potentials $< 50\ \text{mV}$, which is observable by XRD. The formation of such crystalline phase modifies the electrochemical signature of the following charge, which shows a plateau at $\sim 0.4\ \text{V}$ associated to the two-phase transition from $\text{Li}_{15}\text{Si}_4$ to amorphous Li_xSi (cf Figure 29a,b). Having understood the lithiation/delithiation process, various strategies were considered to improve the cycle life of Si electrodes.

V.2 Limiting the impacts of volume expansions

V.2.a Morphology of the particles

The size of the particles and their assembly can reduce the impact of the volume expansion, hence leading to better cycling performances. For instance, using nanometric silicon particles reduces the total stress imposed to the electrode and improve its mechanical stability²⁹⁰⁻²⁹². Many studies confirm the beneficial effect of Si NP on cycling retention^{287,293,294}. However, for a given loading, the surface area is larger, which increases electrode/electrolyte side reaction and thus the irreversibility.

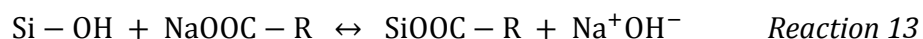
Some groups have synthesized vertically aligned Si nanowires with free space between each wire^{125,295}, hence enabling a radial volume expansion and reducing the stress

transferred to the electrode. High gravimetric capacity of 2700 mAh/g was reported, but the volumetric capacity was small owing to the low surface coverage. More complex architectures were also reported^{125,290} without significant gain in performances.

V.2.b Composite electrodes

One strategy employed to consolidate the percolation network consists in preparing electrodes with a large amount of polymeric binder in order to accommodate the volume changes. Their high resistivity is balanced by using conductive carbon particles, resulting in Si/C/binder composite electrodes after coating the corresponding ink on a copper foil substrate.

The first composite electrodes using PVDF showed poor performances owing to the low extensibility of PVDF, as reported by Dahn's group²⁹⁶. Styrene butadiene rubber (SBR) was then proposed due to its high flexibility, but gave similar results as PVDF²⁹⁷. It was only when sodium carboxymethyl cellulose (Na-CMC, or CMC) was used as a co-binder that cycling performances were improved¹¹⁸. The remarkable behavior of CMC is attributed to chemical factors (strong interaction between the hydroxyls groups at the Si surface and the carboxyl groups of the CMC^{116,117,296,298}, *cf Reaction 13*) rather than mechanical ones (only 5-8% elongation at rupture for CMC)²⁹⁸.

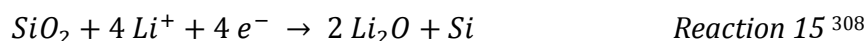
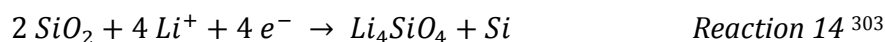


Various Si/C/CMC ratios were reported in the literature depending on the cycling conditions. Roué's group used only 12% CMC and reported ~1000 cycles when limiting the capacity at 1200 mAh/g_{Si}^{126,299}, whereas LRCS reported 110 cycles at > 3000 mAh/g_{Si}³⁰⁰ with 33 % of Si, C and CMC³⁰¹. Therefore, the electrode composition has to be subtly adjusted with respect to the cycling conditions, electrode loading and particle size as already mentioned. In the next section, we will show that the electrochemical performances might as well be affected by the electrolyte formulation.

V.2.c SEI and electrolyte additives

Silicon lithiation occurs at potentials below the stability windows of the commercial electrolytes. Practically, a small fraction of electrolyte is thus reduced at the electrode surface during the 1st discharge (shoulder at 0.8 V vs. Li⁺/Li⁰), thus forming an SEI^{133,135}. It is composed of reduced carbonate byproducts (ROLi, ROCO₂Li, Li₂CO₃, oxalates...) and salt degradation products (LiF, PF_x, Li_xPF_y...) ³⁰²⁻³⁰⁴ as deduced from various techniques such as NMR, XPS, STEM-EELS, TOF-SIMS³⁰⁵, AES, EIS^{306,307}, etc... Edström and coworkers also reported the existence of lithium silicates (Li₄SiO₄) and Li₂O in the inner layer of the SEI

based on XPS and PES measurements^{303,308}. These products might originate from the thin SiO₂ layer at the surface of Si particles participating to the SEI formation according to *Reactions 14* and *15* in discharge, although the exact origin is still under debate.



This protective SEI is necessary to the proper cell operation since it prevents further electrolyte degradation. However, silicon swelling and shrinking tend to damage this fragile layer which cannot accommodate such volume changes^{302,303}.

The mechanical properties of the SEI can be improved using electrolyte additives such as vinylene carbonate (VC)^{309,310} and fluoroethylene carbonate (FEC)^{129,130,311}. Beneficial effects regarding cycling retention (*cf* Figure 30) were reported using these additives, justifying their omnipresence in studies on Si electrodes. The reduction pathway is not clear yet but likely involves a radical anion leading to the polymerization of a thin film on the electrode surface^{130,312}.

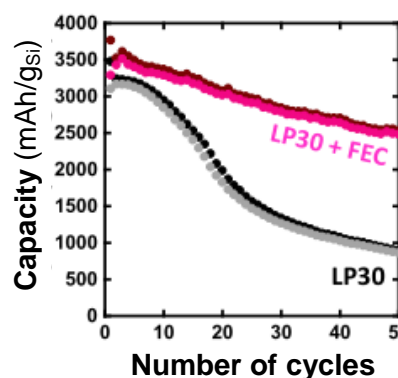


Figure 30: Influence of FEC (10 wt%) in LP30 electrolyte on capacity retention of Si/Csp/CMC [1:1:1] composite electrodes⁸² cycles vs. lithium.

Usually, both strategies mentioned in the former sections (composite electrode + electrolyte additives) are combined so as to limit the effect of volume changes. A last option consists in tackling the problem at source by using silicon derivative – such as alloys (Si-Sn, Si-Ag...) or oxides (SiO or SiO_x as described next) – undergoing smaller global volume changes upon lithiation as compared to pure Si.

V.2.d SiO_x compounds

Oxygen-deficient silicon oxides (SiO_x, 0 < x < 2) exhibit a smaller volume expansion along with a better cycling retention, but at the price of a lower capacity. Considering Si as

the only electroactive element, the theoretical capacities for $x = 0.5$, 1 and 1.5 would be 2780, 2276 and 1926 mAh/g_{SiO_x} respectively, which still outruns graphite by far.

In particular, silicon monoxide (SiO) was reported to be able to insert lithium reversibly^{124,313–317} but despite numerous studies, its chemical structure as well as its lithiation mechanism has been subject to debate for years. Two models were reported to describe the SiO structure: i) the Random Bonding (RB) model³¹⁸ describes SiO as a single-phase compound with Si–Si and Si–O bonds randomly distributed throughout (in agreement with G. Hass observations in 1950³¹⁹), and ii) the Random Mixture (RM) model (R. J. Temkin, 1975³²⁰) in which Si nanoclusters (< 10 nm) are randomly distributed within a SiO₂ matrix, which supports the initial observations by G. W. Brady defining SiO as “a stoichiometric mixture of SiO₂ + Si” in 1959³²¹. Recent studies seem to validate the random mixture (RM) model but stress out the importance of the interfacial region between n-Si and SiO₂ domains since it may involve 20 – 40% of the atoms^{322,323} (due to the very small size of the clusters).

Whatever the lithiation mechanism of SiO_x phases^{324–326}, a few trends seem to stand out, such as the irreversible formation of lithium silicates (mostly Li₄SiO₄) in oxygen-rich regions upon the 1st discharge, and the reversible formation of a Li-Si alloy in the Si clusters³²⁵ delivering the same charge-discharge characteristics as those observed for conventional amorphous Si electrodes^{127,324}. More specifically, a high O content causes a large initial irreversibility due to the silicate formation, which in return helps to buffer the volume expansion of the Si clusters and to improve the ionic conductivity as deduced from a combinatorial study of Si_{1-x}O_x compounds³²⁵. Realistic estimations of the SiO cycling performances give an energy density of 853 Wh/L, which is 18 % above graphite¹²⁷.

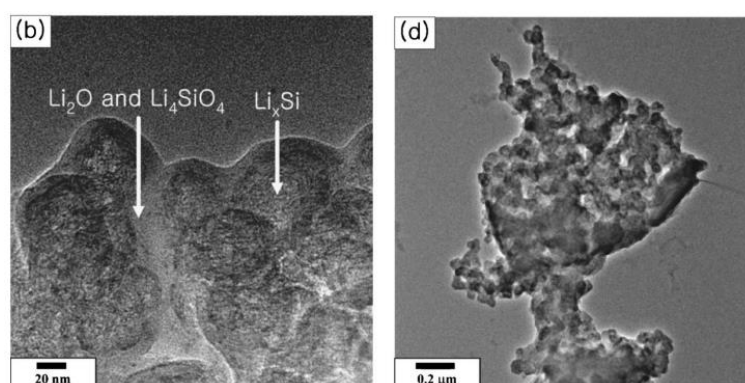


Figure 31: TEM images of SiO particles after 1 (b) and 20 (d) cycles³²⁴.

Lastly, a few studies discuss the potential utilization of SiO₂ as low-cost, environmentally-friendly anode material. However, its electro-activity towards lithium is highly controversial and probably size-dependent. While bulk silica is well known to be

highly insulating and electrochemically inert^{324,327,328}, nano-sized SiO₂ domains have the ability to form lithium silicates in reduction. This was reported by Kim *et al.* who performed ²⁹Si-NMR measurements on SiO particles, where Si nano-domains are surrounding by SiO₂ nano-clusters³²⁴. Independently, Philippe *et al.* observed a similar behavior for the native SiO₂ layer (< 10 nm) coating the surface of Si particles^{303,308}. In both cases, this reaction is irreversible and two possible pathways (*Reaction 14* and *15*, p.46) were proposed since both Li₂O and Li₄SiO₄ were observed.

On the contrary, two studies proposed the reversible lithiation of silica into the phyllosilicate Li₂Si₂O₅. Sun *et al.*³²⁹ used sputtered SiO₂ thin films (400 nm) while Chang *et al.*³³⁰ worked with composite electrodes with 70% of SiO₂ particles (44 μm). In their study, silica was showing an electrochemical activity only after ball-milling over a long period (12 to 36 h), which was attributed to the modification of the Si valence-state during the high energy mechanical milling. Both studies curiously report different charge-discharge profiles and derivate capacity curves.

In short, various strategies were adopted to counter the volume change inherent to silicon lithiation. Together, they led to significant improvements regarding capacity retention and cycling performances, which is one step forward practical/commercial utilization. Nevertheless, this later is hindered by the low coulombic efficiency observed during the first cycle due to i) the SEI formation and/or ii) irreversible structural changes within the electrode. In practice, some empirical technics based on prelithiation have been developed to overcome/compensate this irreversible capacity.

V.3 Prelithiation methods

In addition to minimize the initial irreversible capacity³³¹, the anode pre-lithiation would enable the use of lithium-free cathodes, which is particularly interesting for Lithium-Air batteries for instance, owing that the positive electrode – in contrast to Li-ion systems – does not act as a Li reservoir. The prelithiation can be achieved either by using prelithiated Si powder or by pretreating the Si electrode.

In the first case, Si powder is ball-milled with a lithiating agent (usually stabilized lithium metal powder (SLMP)) which produces Li_xSi (x > 3) then used as negative electrode³³¹⁻³³³. In the second case, the already prepared Si electrode is artificially pre-lithiated prior to the final cell assembly by bringing the electrode at a potential close to that of lithium. It can be performed in a conventional battery, which is not convenient and hardly

industrializable³³⁴. Another method consists in putting the electrode in capillary contact with a lithium foil soaked with electrolyte, as reported by Tarascon's, Cui's and Scrosati's groups in the case of Si^{145,146,335} and Li-Metal alloys³³⁶. The pressure then is maintained for several minutes/hours so as to fully lithiate the treated electrode and concomitantly form an SEI at the surface of the electrode. Cells are then assembled and started in charge (delithiation of the silicon electrode) and they usually show little or no irreversible capacity during the 2nd cycle³³¹, owing that the phenomenon usually responsible for the initial irreversible capacity (SEI formation, structural changes) have happened during the prelithiation. However, beside its efficacy, this method is hardly transferable to industry and does not allow for monitoring or controlling the lithiation/SEI formation process. In a recent study, Kim *et al.* address this issue by bridging both sides of a Si/Li half-cell with a resistor³³⁷. They report a fine control of the lithiation process when a 100 Ω resistor was used, and claim a possible transfer at industrial scale.

Such prelithiation technics enable coulombic efficiencies as high as 95 % for the subsequent cycles³³⁷, but the prospective industrialization will depend on the cost of the overall process.

V.4 Challenges and perspectives for lithium-silicon alloys

Silicon is a first-choice anode material owing to its high theoretical capacity and low potential for lithium insertion. However, it suffers from a large swelling/shrinking upon cycling, which jeopardizes its practical utilization. The development of composite electrodes containing a cohesive binder and a conductive additive highly improved the overall cycling performances. By combining a clever particle morphology and neat electrolytes additives, silicon electrodes may, in a close future, meet the standards of the industry, as it begin to be commercialized in C/Si composites.

In this work, we will use silicon as anode in Li-O₂ batteries. Prior to their integration in full cells, silicon electrodes were tested in half-cells so as to optimize their cycling retention and coulombic efficiency. Through this study, we will reveal the importance, together with its understanding, of the prelithiation process in enhancing the cycle-life of Si electrodes. We will also provide a full understanding of the lithiation process of SiO_x, hence opening a way to its possible utilization as additive in future Si-based composite electrodes.

VI Conclusions

We described in this chapter the wild journey taken from the battery technology to reach today's state of the art, which is clearly dominated by the Li-ion systems. This was achieved by significant research efforts to develop high-capacity anode and cathode materials in concert with suitable electrolytes, which led the Li-ion technology to power every portable electronic devices and most of the electrical vehicles nowadays. However, this technology is about to reach its theoretical limits while the costumers are always asking for more autonomy, which calls for the development of new systems with higher energy densities.

Among the technologies "beyond Li-ion", the Lithium-Air battery stands out as a promising candidate owing to its high gravimetric energy density of ~ 3500 Wh/kg. However, this technology has remained at the R&D stage for two decades due to the difficulty to master the chemistry at play and find the components which are stable in its oxidative environment. Overcoming these limitations requires a trustful investigation of the Li-O₂ system together with obtaining reproducible results. The latter – which is crucial due to the sensitivity of the Li-O₂ systems – will be the topic of the first chapter which focuses on the experimental procedure and more specifically to the test cell used for cycling our batteries.

CHAPTER 2: EXPERIMENTAL PROCEDURES AND NEW DESIGN OF THE LI-O₂ TEST CELL

In this chapter, we will first detail the experimental protocols which were used for preparing the different components and assembling the Li-O₂ cells. Facing cell-related issues during the first tests, we will then review the various cell design developed in the literature for testing Li-O₂ batteries in order to develop our own prototype. This opportunity was seized to integrate a pressure sensor which enables the collection of pneumatic data in addition to the usual electrochemical measurements. We will describe herein the multiple steps of the cell conception which led to its integration in the laboratory, while its utilization for testing Li-O₂ batteries will be discussed in the next chapter.

I Material preparation

I.1 Electrodes for Li-O₂ batteries

I.1.a Positive electrode

Porous composite carbon positive electrodes were prepared by drop-casting a slurry of Carbon Super P (Csp, Timcal Ltd) and 10 wt % PTFE (60 wt % dispersion in water, Sigma Aldrich) mixed in isopropanol (> 99.9 %, Sigma Aldrich) onto a 11 mm stainless steel mesh (AISI 316, 200 mesh, 0.05 mm diam wire, Alfa Aesar). After drying in ambient air, they were washed to remove the surfactants pertaining to the PTFE suspension, furtherly dried under vacuum in a Büchi oven at 180 °C overnight and transferred to an argon glove box without any air exposure.

In order to ensure a good reproducibility between each electrode – which is critical for obtaining reliable electrochemical results – the drop-casting step was done according to a standardized procedure (*cf* Figure 32): 18 µL of the slurry are sampled with a micropipette standing 7 cm above the targeted mesh, the distance being optimized with respect to the slurry viscosity so as to obtain a neat disc when the drop splashes on the grid (*cf* Figure 33).

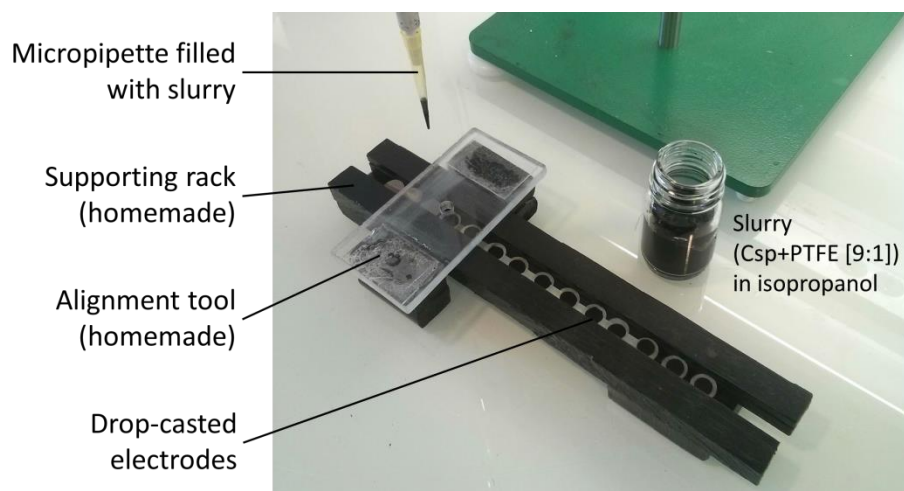


Figure 32: Photograph of the drop-casting procedure. The rack is used to hold and position the pristine stainless steel discs below the micropipette. It moves from the left to the right while the alignment tool is fixed and indicates with a hole where the drops fall. The pipet is refilled with the slurry for each new electrode.

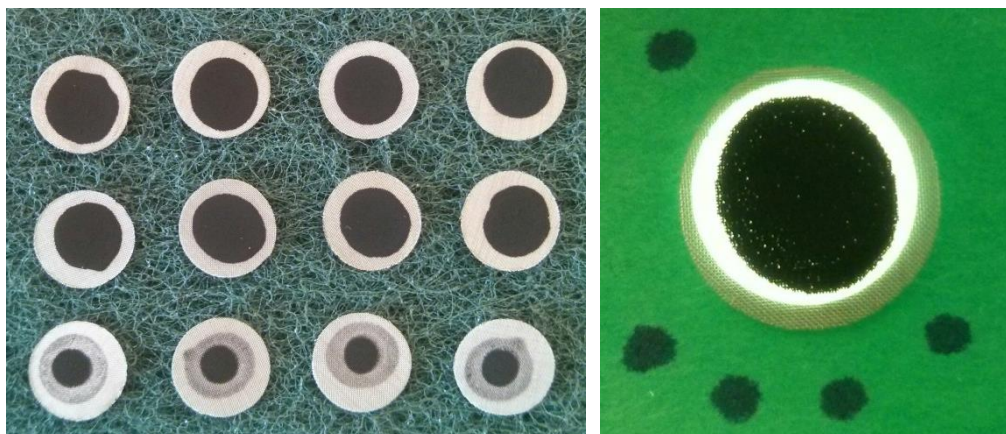


Figure 33: Photographs of dried air electrodes. The left picture shows front (top) and back (down) sides, while the right one shows the macro-porosity when the electrode is lightened from behind (the black dots were used for focusing the camera). The diameter of the stainless steel discs is 11 mm.

Using this protocol, a deposit of approximately $0.4 \text{ mg}_{\text{carbon}}$ on a surface of 0.4 cm^2 , corresponding to a carbon loading of 1.0 mg/cm^2 is achieved. Within this procedure, we experimented an error range of $\sim 10 \%$ between different batches (considering its average weight), and around 3% in a single batch. Therefore, we will in practice consider that within a batch, the weight of each electrode equals to the average one, thus acknowledging an acceptable error of 3% on all gravimetric quantities (current density, capacity, etc...). Such method seems more trustful than weighting each electrode individually owing to the small C loading and the mass variations between each mesh substrate.

I.1.b Negative electrode

Three types of negative electrodes were used as lithium source in Li-O₂ batteries: Lithium metal, pre-charged LiFePO₄ (LFP) composite electrodes and pre-lithiated silicon (Li_xSi) composite electrodes.

Li metal electrodes consist in 0.7 mm thick discs whose surface is scratched so as to remove any contamination prior to be pressed onto a metallic current collector. Their diameter was 9.0 and 11.5 mm for Swagelok-type cells and coin-cells, respectively.

The self-standing composite LiFePO₄ electrodes were made as follow: a few drops of isopropanol are gradually added to a mixture of LiFePO₄ powder, Csp and PTFE ([90:5:5] weight ratio) while this mixture is manually grinded until obtaining a plastic-like dough. This dough is then flattened down to 0.3 mm by rolling, and dried in ambient air before being punched into 11 mm diameter self-standing disks which were washed with a water/ethanol [1:2] solution and then dried at $150 \text{ }^\circ\text{C}$ under vacuum before being transferred into the glove box. Prior to be used as Li-source in Li-O₂ cells, LFP electrodes are

pre-charged in Li half-cells for 30 min (1/20th of the total capacity) so as to reach the flat charge plateau at ~ 3.45 V vs. Li⁺/Li⁰. The electrolyte used during the pre-charging is the same as in the subsequent Li-O₂ cell tests. The resulting negative electrodes are heavily loaded in LiFePO₄ (30 to 35 mg per cm²) with an equivalent of 4 to 5 times Li excess when compared to the fixed discharge capacity of the carbon air electrode.

Lastly, the preparation of silicon composite electrodes as well as the prelithiation methods leading to Li_xSi anodes for Li-O₂ batteries will be detailed in the 4th chapter focused on silicon electrodes.

I.2 Preparation of electrolytes

Numerous electrolytes were used during this work, the details of which are given below. For sake of clarity, they are all reported in Table 2 (*cf* p.58) annotated with their chemical formula and a few interesting properties. The electrolytes will herein be divided in two categories as function of their utilization in a) Li half-cells (which does not involve oxygen, such as Si/Li or LFP/Li cells), or b) Li-O₂-type cells (which involve O₂, *i.e.* Li/Csp/O₂, LFP/Csp/O₂ or Li_xSi/Csp/O₂ cells...).

I.2.a Electrolytes used in Li half-cells

Commercial LP30 (BASF, 1M LiPF₆ in ethylene carbonate / dimethyl carbonate [1:1] weight ratio) was used as electrolyte in LFP/Li half cells. The manufacturer specifications are < 10 ppm of water and < 30 ppm of hydrofluoric acid (HF). If not specified otherwise, 10 wt % of FEC (Fluoroethylene Carbonate, Sigma, 99 %) was added to the LP30 when cycling or pretreating Si/Li half-cells.

I.2.b Electrolytes in Li-O₂-type batteries

The electrolytes used in Li-, LFP- and Li_xSi-O₂ batteries were prepared in-house by mixing commercial salts and solvents. DMA (N,N-Dimethylacetamide, 99.8 % anhydrous, Alfa Aesar), DMSO (dimethylsulfoxide, 99.9 %, Carlo Erba), DME (1,2-dimethoxyethane, 99.9 %, Sigma Aldrich), DEGDME (diethylene glycol dimethyl ether, 99.5 % anhydrous, Sigma Aldrich) and TEGDME (tetraethylene glycol dimethyl ether, ≥ 99 %, Aldrich) were dried with activated molecular sieve (4 Å) for 3 days, so as to obtain a water content < 20 ppm as deduced by Karl Fischer titration. These last three solvents are often referred to as glyme polymers, also known as poly(ethylene oxide). In the literature, various names are used to refer to these solvents, such as monoglyme / 1G / dimethyl-PEO1 for DME, diglyme /

2G / DGME / dimethyl-PEO2 for DEGDME, and tetraglyme / 4G / TGME / dimethyl-PEO4 for TEGDME. Lithium salts LiNO₃ (lithium nitrate, 99 %, Alfa Aesar) and LiTFSI (lithium Bis(trifluoromethane)sulfonimide, 99.95 %, Sigma Aldrich) were dried under vacuum at 200 and 160 °C, respectively. In contrast, LiClO₄ (lithium perchlorate, battery grade, Aldrich) was used as received owing to its lower stability in temperature and sufficient purity. Appropriate solvents and salts were mixed together to prepare electrolytes of desired molarity.

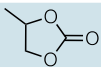
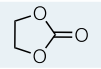
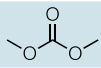
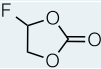
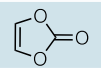
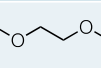
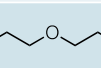
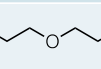
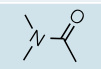
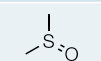
Short name	Long name	CAS	Boiling T° (°C)	O ₂ solubility [mmol/(L*bar)]	DN	AN	Formula
PC	Propylene carbonate	108-32-7	242 [a]		15.1 [d]		
EC	Ethylene carbonate	96-49-1	248 [a]		16.4 [d]		
DMC	Dimethyl carbonate	616-38-6	90.5 [a]		17.2 [d]		
FEC	Fluoroethylene carbonate	114435-02-8	212 [j]				
VC	Vinylene carbonate	872-36-6	162 [a]				
DME (monoglyme)	Dimethoxyethane	110-71-4	85 [b]	13.3 [b] or 10.1 [e]	22.0 [f]	10.2 [g]	
DEGDME (diglyme)	diethylene glycol dimethyl ether	111-96-6	162 [a]	6.4 [e]	19.2 [g]	9.9 [g]	
TEGDME (tetraglyme)	Tetraethylene glycol dimethyl ether	143-24-8	275.3 [a]	4.3 [e]	16.6 [h]	10.5 [i]	
DMA	N,N - Dimethylacetamide	127-19-5	165 [a]	5.4 [e]	27.8 [c]	13.6 [c]	
DMSO	Dimethylsulfoxide	67-68-5	189 [b]	2.2 [b]	29.8 [c]	19.3 [c]	

Table 2: Table of various solvents along with a few properties and their chemical structure. Refernces: [a]: 338; [b]: 339; [c]: 340; [d]: 341; [e]: 342; [f]: 343; [g]: 344; [h]: 345; [i]: 206; [j]: 346.

Once prepared, the battery components are assembled in the argon-filled glovebox. The positive and the negative electrodes are separated by 1 or 2 two vacuum-dried (overnight, 180 °C) glass fiber separators (Whatman GF/D, 675 μm) soaked with:

- 150 μL of electrolyte for Li-ion cells tested in Swagelok-type cells
- 100 μL of electrolyte for Li-ion cells tested in Coin Cells
- ~ 450 μL of electrolyte for Li-O₂ cells.

The different types of cell hardware used for Li-ion and Li-O₂ battery testing will be presented in the next section, as well as the reasons justifying their preferential utilization.

II Battery testing

II.1 Testing cells for Li-ion type batteries

II.1.a Two-electrode cells: Swagelok vs. Coin Cell

To perform the electrochemical characterizations, two types of cells were used, either Swagelok®-type (SW) or Coin cells (CC).

The SW cells were build based on the system described by Tarascon^{347,348} in 1984, which can be easily disassembled so as to recover the electrode/active material (Figure 34). The SW cells were used to perform *ex situ* prelithiation and post mortem analysis. However, the mechanical pressure applied to the electrodes is hardly reproducible due to the manual pressing of the cylinders, which may influence the electrochemical behavior of the SW cells and hamper the comparison of the electrochemical behaviors. This issue was tackled by using CC (Figure 35) sealed by an automatic crimping machine applying the same pressure to each cell. Therefore, CC were preferred over SW for studying the influence of sensitive parameters on the cell behavior as well as for long-term cycling owing to their better sealing.

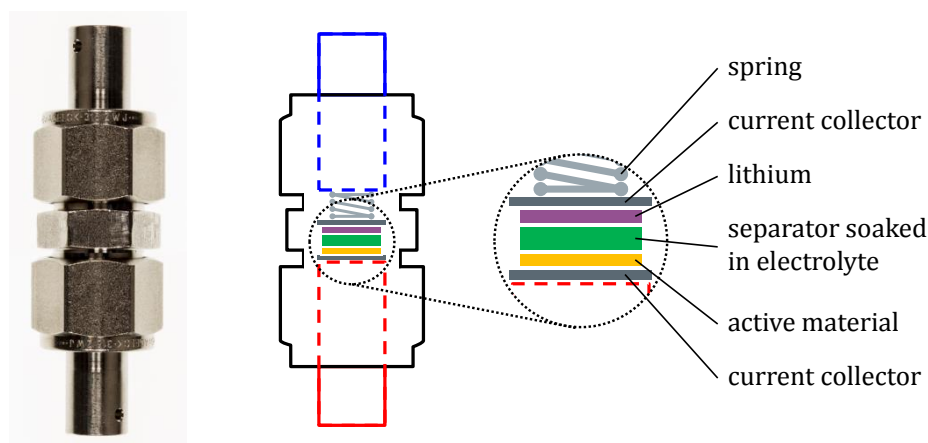


Figure 34: Photograph and schematic representation of a two-electrode Swagelok-type cell. The body, nuts and two cylindrical plungers are made of stainless steel AISI 316. The area of the cylinder in contact with the ferrules (not represented here) was polished so as to ensure proper sealing.

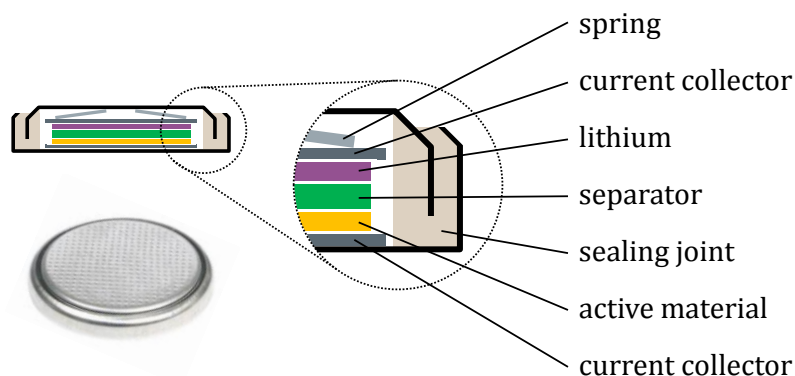


Figure 35: Photograph and schematic representation of a 2032 Coin Cell. A crimped CC has a thickness of 2.0 mm and a diameter of 32 mm.

II.1.b Three-electrode cell

For three-electrode measurements, we revisited the original design proposed by Tarascon *et al.*³⁴⁸ by using a 3-way T-connector instead of the usual 2-way straight-union connector (Figure 36). The side opening is used to connect the 3rd electrode which is usually a ring or a micro-electrode linked to the current collector *via* a Cu wire (Figure 37). The micro-electrode setup was used for Electrochemical Impedance Spectroscopy (EIS) so as to minimize the perturbations arising from the current lines between the positive and the negative electrode³⁴⁹.

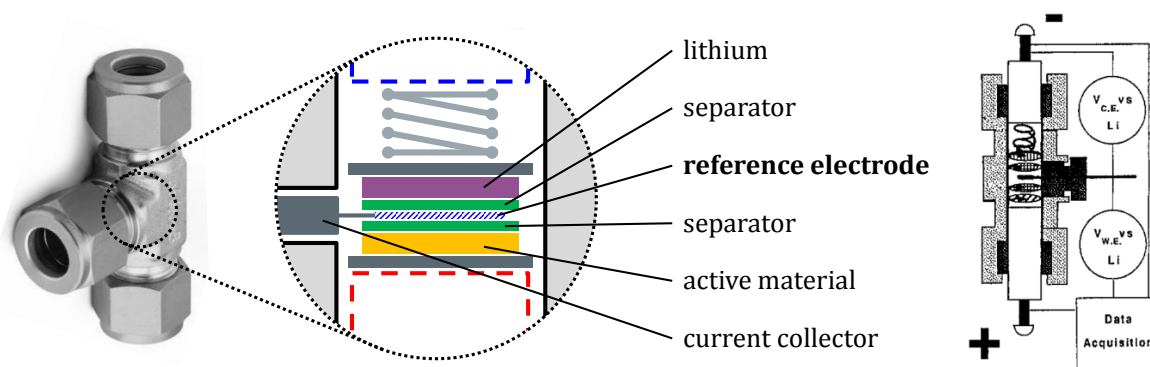


Figure 36: Photograph and schematic representation of a three-electrode cell based on a T-connector (left) as compared to the initial design by Tarascon *et al.*³⁴⁸ (right).



Figure 37: Photographs of the side current collector of a 3-electrode cell (a) and its utilization using a ring of self-standing LiFePO₄ (b) or a micro-electrode of Li touching a Cu wire (c) as reference electrode.

A large majority of research groups in the world are using either SW or CC for testing Li-ion batteries. At the opposite, there is no such uniformity of the testing devices in the field of Li-O₂ batteries, in which various designs of test cells exist, as presented next.

II.2 Testing cells for Li-O₂ batteries

When starting my PhD, the design of the Li-O₂ test cell used in our laboratory was similar to the one used by most research groups and inspired from a Li-ion cell. However, alternative designs – more elaborated – dedicated to Li-O₂ battery testing were proposed in the literature over the years. The main ones, which will be described in the following section, clearly reveal the limitation of our initial setup, hence calling for its replacement. Therefore, the design of the new testing cell capable of addressing the challenging question of the gas monitoring was the first goal of my PhD, which will be discussed in details in section III.

II.2.a Overview of common cells used in the literature

II.2.a.i Rudimentary cells

Most of the cells currently used for testing Li-O₂ batteries are Li-ion test cells which were modified so as to enable the use of a reactive gas inside the cell. It is usually done by drilling an aperture in the positive current collector and cycling the cell inside a sealed container filled with oxygen. Figure 38 and Figure 39 show how coin cells and Swagelok cells have been modified for testing Li-O₂ batteries.

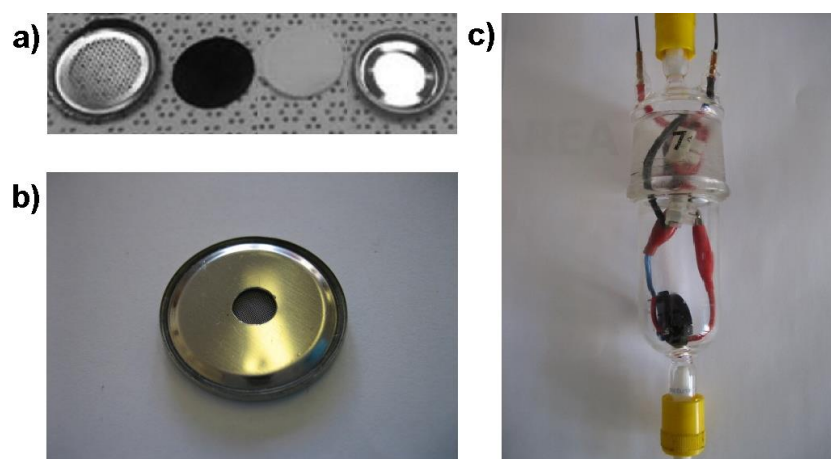


Figure 38: Photographs of two coin cell-type hardware for Li-O₂ batteries (a, b). The CC in (a) was cycled in a sealed container flowed by O₂²²⁵, while the CC in (b) was cycled in a closed glass jar filled with O₂³³⁴ (c).

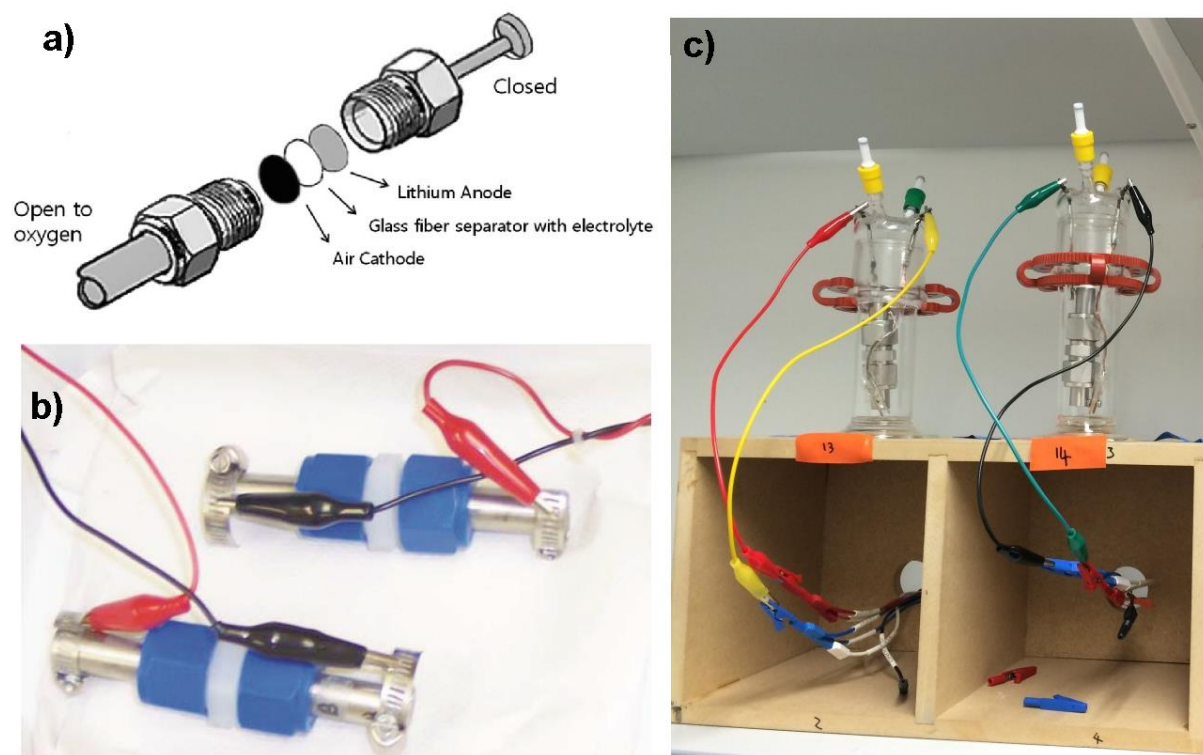


Figure 39: Schematic representation³⁵⁰ (a) of a Swagelok-type Li-O₂ battery using a tube as air current collector. Photographs of a plastic³⁵¹ (b) and two metallic²⁶⁵ (c) Li-O₂ SW cells cycled in O₂ atmosphere. (b) is an opened system (O₂ flowing in a plastic box), while (c) is a closed system (fixed amount of O₂).

The aforementioned cell designs fulfill the minimum requirement for the Li-O₂ system – *i.e.* enabling the oxygen to access the air electrode – but many drawbacks can be found, depending on the design:

- a) No information regarding gas evolution is collected,
- b) Some air may contaminate the cell during the O₂ filling process if a low-quality O₂ line is used (dead volumes containing air, bad connections...),

- c) The atmosphere may be slowly contaminated by a leak in the container even though it is slightly over pressurized ²²⁵,
- d) The horizontality of the cell is not always ensured (Figure 38c), which likely results in a partial/inhomogeneous wetting of the air cathode,
- e) Cells might be contaminating each other as they may be cycled in the same container (Figure 39b and ref ²²⁵)

Recognizing the limitations associated with early days' designs, numerous new setups dedicated to the study of Metal-Air batteries were developed. The most representative ones are presented in the next section.

II.2.a.ii Metal-air dedicated cells

Two examples of cells designed for testing Li-O₂ systems are shown in Figure 40. They include gas connections enabling a trustful filling/purging of the empty spaces inside the cell constituting a gas reservoir. Therefore, such systems drastically reduce the oxygen contamination as compared to rudimentary cells, and the electrodes are positioned horizontally.

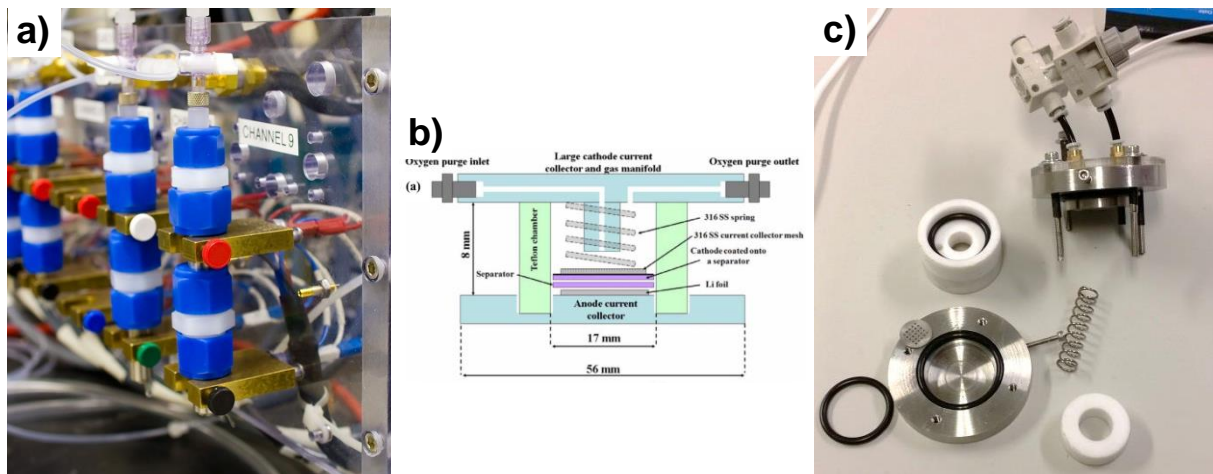


Figure 40: Li-O₂ cells with various designs. (a) Swagelok-type cells used by IBM ³⁵² – (b) Schematic of an alternative design developed at the MIT ^{274,353} – (c) Photograph of a disassembled cell inspired from (b) ³⁵⁴.

Regarding the gas supply, the cells in Figure 40a and b illustrate well the difference between a closed and an open system. The single opening on top of the SW cell (a) is used for filling the cell with a desired gas quantity which stays in the cell during cycling (*closed system*), while the two openings on both sides of cell (b) enable a constant flushing of the head space (*open system*). Two valves can be implemented to this setup to control the gas inlet/outlet, hence enabling to run the cell in a “closed” mode either after flushing it with O₂ (Figure 40c), or after assembling it in an O₂-filled glovebox (which was done at MIT and prevents a possible contamination due to the flushing process). It is worth noting that

discrepancies have been reported by Hartmann *et al.* for Na-O₂ cells when using a closed or a flowing system³⁴².

In summary, Li-O₂ test cells can be divided in two categories depending on their ability to well manage the gas-feeding process of the cell (static or dynamic). Having described the main setups used in the literature for testing metal-air systems, we will now focus on the test cells which were previously used in our laboratory, thus unveiling their limitations calling for their forthcoming replacement.

II.2.b Cells formerly used in our laboratory

Figure 41 represents the type of cell hardware previously used in the laboratory at the beginning of the thesis and developed in collaboration with P. G. Bruce and LRCS (Amiens, France). It is composed of a metallic Swagelok-type cell using an aluminum tube as top current collector and cycled inside a glass jar. Such cell is similar to what was described in section II.2.a.i (Figure 39), hence experiencing the same weaknesses, and leading to irreproducible results obtained when using this device. In addition, the components are costly, difficult to handle in the glovebox and very fragile. Combined together, those drawbacks led us to consider other alternatives for testing our Li-O₂ batteries.



Figure 41: Photograph of a typical Li-O₂ cell used in the lab (handmade glass container ≈ 1200 €).

A commercial test cell dedicated to the study of Li-O₂ batteries was purchased (~ 1000 \$) from MTI Corporation (Figure 42a). Its design is reminiscent of the schematic of Figure 40b excepted for the pressure gauge which was added on top of the device.

This cell was first used for cycling a DMSO-based Li-O₂ battery. Surprisingly, the potential recorded during the charge was not stable and oscillations between 3.7 and 4.2 V vs. Li⁺/Li⁰ were observed. In addition, post-mortem observations (Figure 42b) revealed a disastrous degradation of the hardware components. The most striking degradation was for instance the dark spots in the separator and the silverish coating found on the bottom part of the cell, both arising from the deterioration of the perforated current collector. Also, the O-ring rubber sold by MTI exhibited clear instability when using DMSO as solvent (Figure 42c).

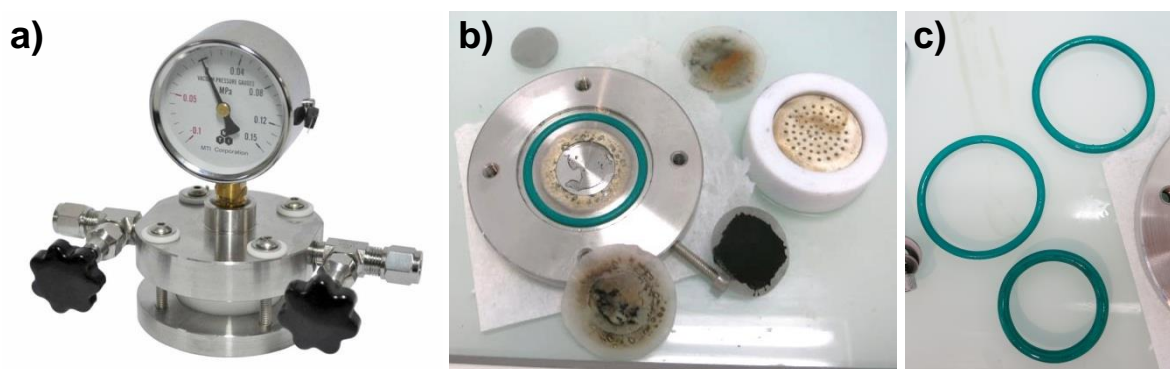


Figure 42: Photographs of an MTI Li-O₂ cell during cycling (a) and after cycling an LFP//DMSO//Csp//O₂ cell (b). Picture (c) shows the swelling (in thickness) and shrinking (in diameter) of the O-ring used during this test as compared to two pristine ones.

Moreover, the pressure gauge was not adapted to our experiments since the smallest marks scale (0.01 MPa = 0.1 bar) is above the theoretical variations expected from our experimental conditions.

Overall, it is clear that none of these setups would enable a trustful study of Li-O₂ batteries. This was an impetus for designing our own Metal-Air test cell, with the aim to improve the systems currently existing. In that purpose, we screened the new literature from the last couple of years and found that the most relevant studies were relying on gas measurements in addition to usual analysis technics. In particular, mass spectrometry (MS) stands out as the star technic for identifying the gas evolved upon cycling. In the next section, we will provide a brief overview of the different systems using MS, describe how it was implemented to Li-O₂ systems, and see if it can be considered as an alternative test cell for our experiments.

II.2.c Cells for gas analysis

Following the need for a better understanding of the chemistry at play in Li-O₂ systems, a lot of attention was recently paid to the gas generated during the cycling of Li-O₂ cells. Nowadays, the preferred method for studying the chemical composition of such gas

and thus gain additional information is called differential (or online) electrochemical mass spectrometry, also known as DEMS (or OEMS). These setups are composed of an electrochemical cell – such as those described in the “Metal-air dedicated cells” section (II.2.a.ii) – connected to a MS which analyzes, at regular time intervals, some gas sampled in the head space of the cell. The high sensitivity of this technic (a few tens of ppm) enables the identification and quantification of various gaseous species produced or consumed.

Three types of DEMS/OEMS set-ups can be distinguished as function of the sampling procedure (Figure 43):

- i) The *open* system (continuous flow) was first developed by Novák *et al.*³⁵⁵ and used to study Li-ion cells before being transferred to the Li-O₂ community^{187,246}. It employs a continuous flow of a gas carrier which collects the gases evolved inside the battery. Such gas mixture is then pushed into the MS to be analyzed. The carrier is usually argon, which requires flushing/purging the cell with O₂ at each half-cycle (before the discharge). The open system was then used by Bruce's^{190,230,261}, Nazar's³⁵⁶⁻³⁵⁸ and Winter's³⁵⁹ groups.
- ii) In contrast, the *closed* (integral) system, which was first developed by Gasteiger's group³⁶⁰, works with a fixed quantity of gas initially trapped in the cell headspace. This gas is slowly sampled through a capillary leak (1 μL/min) while its composition is modified owing to the gaseous species evolved during the charge. The purge/filling valves are only opened between each charge/discharge sequence so as to refill the cell with the appropriate gas (O₂ in discharge vs. Ar in charge).
- iii) Lastly, the *semi-closed* (dosing) system consists in sampling, at regular time intervals, a small fraction of the gas in the headspace while instantaneously replacing it by the exact same amount of neutral gas. This complex system was developed by Luntz's group at IBM^{188,248} and is currently used by Berg's team at PSI³⁶¹. Even though this system provides a better sensitivity over the other systems, it is far more complex to use and to control owing to the multiple valves operation which requires an automatized process.

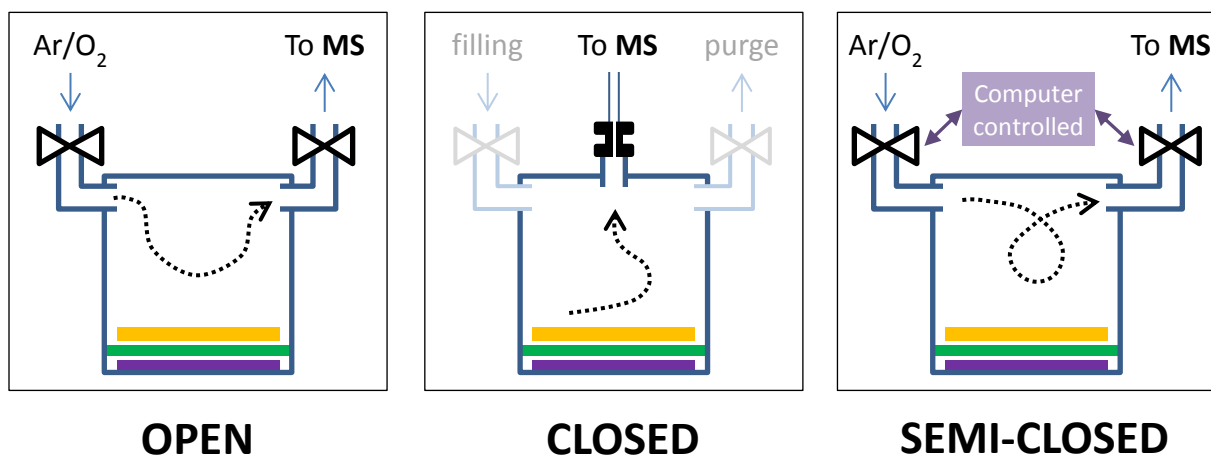


Figure 43: Schematic representation of the three types of DEMS/OEMS set-ups.

The use of DEMS and OEMS systems has enabled major breakthroughs in the field of Li-O₂ batteries, hence demonstrating the importance of gas analysis. Among them was the acknowledgement in 2011 of the carbonates-based electrolytes' instability towards the nucleophilic attack of the superoxide intermediate¹⁸⁷⁻¹⁸⁹, which were largely employed so far.

However, only a few laboratories across the world are equipped with one of these systems owing to their high cost and sensitive operation. Moreover, the extreme complexity of this technic does not allow for a fast and extensive study of Li-O₂ cells and chemistry. For this reason, the DEMS setup was not considered as a viable solution for the day-to-day study of Li-O₂ lab-scale batteries. Nonetheless, the idea of monitoring the gas evolved upon cycling was not put aside and resulted in the integration of a pressure sensor, which greatly improves the value of the test cell as compared to the classical ones mentioned above. The integration of this pressure sensor required a revisiting of the overall design of the cell, the latter being also governed by some practical specifications and a few factors which are discussed next. Together, they ensure the fabrication of a reliable device which does not reproduce the errors of the past.

III Design of the pressurized Li-O₂ test cell

III.1 Problematic

The overview of the different systems commonly used for testing/characterizing Li-O₂ systems unveiled their weaknesses, which led us to formulate the following problematic for the design of the new testing hardware: *How to build a test cell enabling i) to detect gas*

evolution upon long-term cycling and ii) to achieve reproducible results, while iii) being user-friendly so as to perform routine experiments?

Each of these requirements has practical implications which are discussed below point by point.

III.1.a Gas evolution monitoring

Properly addressing the issues related to the gas evolution/reduction upon cycling is essential for understanding Li-O₂ systems. Indeed, the overall reaction associated to lithium peroxide formation ($2 \text{Li}^+ + \text{O}_{2(\text{gas})} + 2 \text{e}^- \leftrightarrow \text{Li}_2\text{O}_2$) implies that two electrons are necessary to form/consume one molecule of dioxygen ($2 \text{e}^-/\text{O}_2$). The recent history of the Li-O₂ battery field and the misinterpretations in the absence of DEMS measurements regarding the cyclability in carbonate-based solvents (*cf* Chapter 2, section IV.1.c) shows that information related to gas analysis is as valuable as electrochemical data. Nonetheless, the development of such set-up is extremely complex and goes against the “routine and user-friendly” requirement, which is why we rather opted for the integration of a pressure sensor on the test cell. Such strategy, already mentioned in few papers^{178,257}, does not give access to the nature of the gaseous species but provides a constant monitoring of the pressure inside the cell, and hence the instantaneous e^-/gas ratio. This valuable information can be further exploited so as to deduce the efficiency of the system and the amount of parasitic reaction (*cf* Chapter 3).

III.1.b Reproducibility

In order to improve the reproducibility of our results, much effort has been devoted to minimize the factors of irreproducibility associated to the cell hardware. Firstly, the cells were built out of commercial spare parts (Figure 44), hence ensuring the similarity of each testing device. For information, to date, 15 strictly identical cells were built in our lab. Secondly, every part constituting the cell is made of stainless steel. This material was preferred over glass or plastic for various reasons:

- Handmade glass is expensive and brittle, while plastic is partially porous to water;
- Stainless steel enables an airtight connection between two pieces thanks to metal-to-metal joints, Swagelok-type double-ring tube fittings and PTFE-tapered threads. Such connections ensure the proper sealing of the gas reservoir and the gas filling system;
- Making a device out of spare parts enables an easy replacement of a defective one and an eventual modification of the global design.

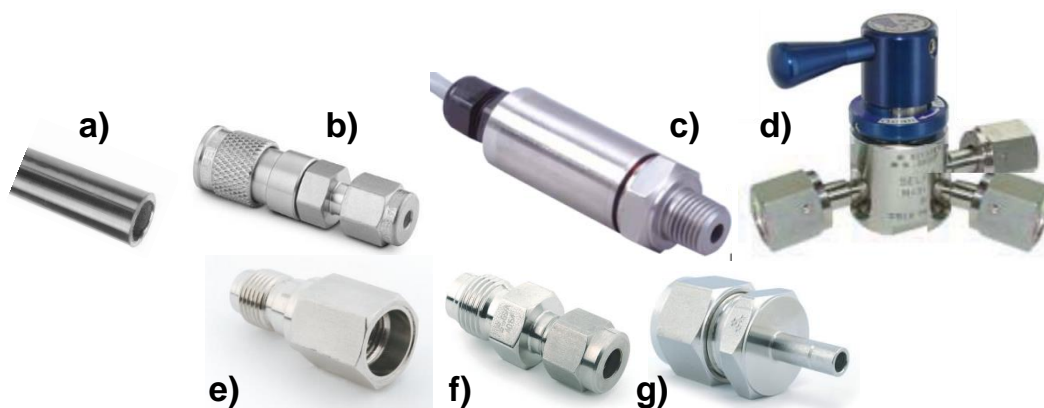


Figure 44: Spare parts of our pressurized cell. The 1st line (a-d) represents the vital components [tube fitting the SW cell (a), quick connector for gas inlet/outlet (b), pressure sensor (c), 3-way valve (d)] which are connected together using the connections shown in the 2nd line (e-g). All parts are commercially available except the ½ inch tube (a) which requires extra in-house cutting and polishing.

The specific set of parts shown in Figure 44 was chosen based on i) the price, which is why only series parts with standard connections were used (for instance, a valve on which both the pressure sensor and the ½ inch tube are directly connected can be tailor-made by the supplier, but at a very high price), and ii) the existence of matching connections to connect the spare parts together (threads, tube fittings, etc...).

Overall, the choice of an all-stainless-steel design drastically reduces the level of gas contamination while ensuring the high similarity of each test-cell.

III.1.c User-friendliness

Our new test cell is aimed at performing routine experiments on Li-O₂ batteries, so that testing Li-Air cells will become as easy as testing Li-ion batteries using SW or CC. The new design was therefore based on the Swagelok-type cell, which has two advantages: The first one is practical, since the battery community is familiar with the SW hardware which has been experienced for decades. The second one is scientific, owing that the use of the same cell design for Li-ion and Li-O₂ batteries (same dimensions, same electrode stacking, etc...) enables a straightforward comparison between both technologies.

In another extent, much effort has also been devoted toward developing a handy gas management system. A filling station, to which various gas bottles and a vacuum line are connected, was built to ease the oxygen filling procedure (see section III.3).

Lastly, our setup would not be user-friendly without a convenient way to record and process the pressure data. In practice, we are able to directly connect the sensor to the potentiostats and use the same software (EC-Lab, BioLogic) for both electrochemical and pressure data.

Having identified the main specifications related to the new test cell design, a first prototype which stood out as the best compromise was built. It was then slightly improved with time according to the feedbacks of the first users. Its most advanced version is presented in the next section.

III.2 Cell description

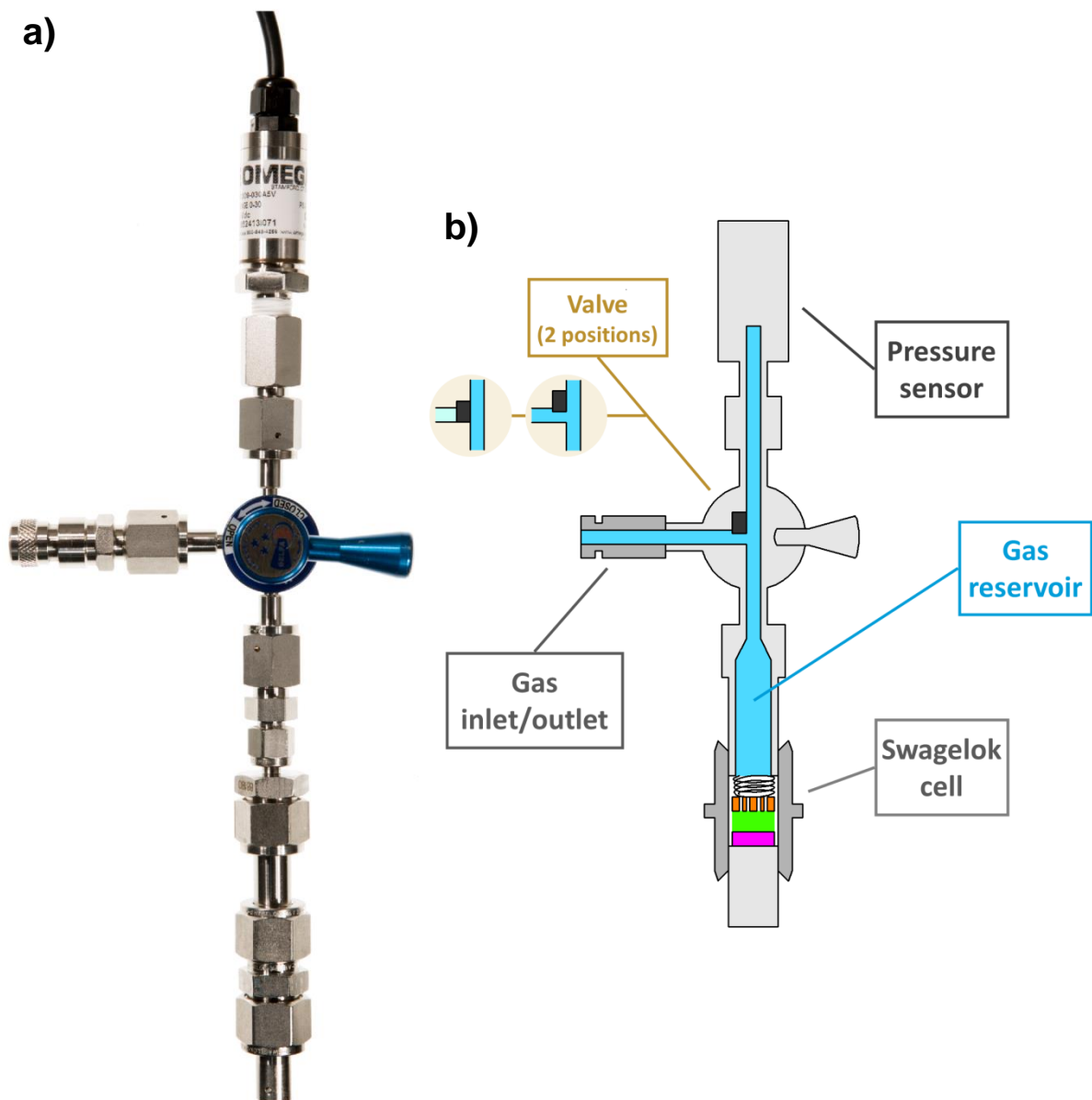


Figure 45: Picture (a) and schematic representation (b) of the newly designed Li-O₂ cell enabling *in operando* gas pressure monitoring within a range from 0 to 2.2 bar. The lower part is composed of a Swagelok cell, whom components (o-rings, nuts...) were not drawn in (b) for sake of clarity.

A picture of the newly designed Li-O₂ cell is presented in Figure 45a, together with its corresponding schematic representation in Figure 45b. It is composed of a gas reservoir (permanent assembly) positioned on top of a Swagelok-type electrochemical cell. The central part is a 2/3 valve (2 positions / 3 openings) used for insulating the gas reservoir from the left member (gas inlet/outlet), hence enabling the removal of the air trapped in the latter prior to purge the gas reservoir and to refill it with the desired gas. The overall volume of the abovementioned gas reservoir is close to 10 mL so as to obtain a good signal/noise ratio (S/N) while preventing large pressure changes during cycling which could influence the cell chemistry. In case of a typical Li-O₂ discharge ($\sim 1000 \text{ mAh/g} \equiv \sim 0.5 \text{ mAh}$), the expected ΔP for a 10 mL internal cell volume is $\sim 30 \text{ mbar}$, which corresponds to $S/N = 25$ and represent only 2 % variation of the overall pressure.

The gas reservoir does not include the gas inlet/outlet used for connecting the cell to a filling station (not displayed here, see section III.4.a) which acts as a hub connected to multiple gas bottles and a vacuum line. The pumping-filling procedure to replace argon – initially trapped in the cell during its assembly in the glovebox – by pure O₂ is repeated 7 times.

The pressure sensor is located on top of the valve and it is directly controlled by the potentiostat for *in operando* monitoring of the pressure during cycling. The highly specific features of the Biologic potentiostat drastically reduce the list of the compatible sensors available in the market. For this reason, a device working with a 10 V(dc) (or lower) power supply and returning an analogic voltage within a [0 - 10 V] potential range was chosen.

Turning to the lower part of the gas reservoir, it is composed of a polished stainless steel tube ($\frac{1}{2}$ inch in diameter) that fits into the top of a regular Swagelok cell. However, its design was slightly revisited as shown in Figure 46.

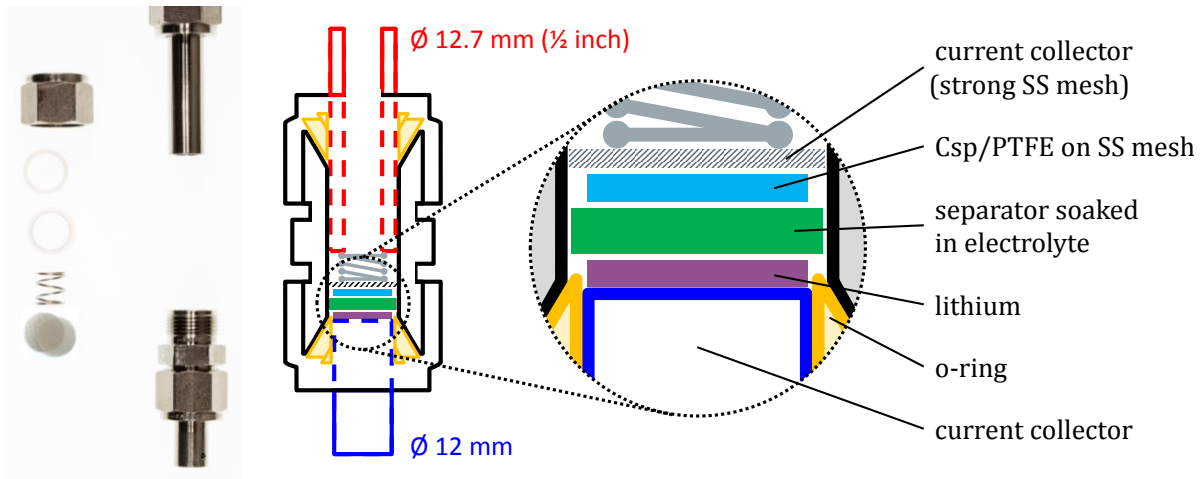


Figure 46: Photographic and schematic representation of a revisited SW cell design using a cylinder of 12 mm in diameter as negative current collector.

A 12 mm diameter cylinder was used as negative current collector (instead of 12.7 mm), which was lowered down to the ferrule level while the ferrule diameter was accordingly reduced to 12 mm. This enables:

- the utilization of a mylar-free SW, since the anode and its corresponding current collector are not in electrical contact with the SW core. It is worth noting that the contact between the positive current collector and the SW core has no effect on the electrochemical measurements.
- The easy washing of the SW cell without disassembling the bottom part (lower O-rings + nut + cylinder). Aside of the obvious time saving, it preserves the O-ring airtightness which would be jeopardized by multiple dis-/re-assembling processes (for information, 1 single O-ring = 2 €).

Lastly, two discs of rigid stainless steel mesh were used below the spring so as to spread its pressure onto the positive electrode without compromising oxygen diffusion.

The testing hardware being designed and assembled, our next step focuses on its use within the context of the Li-O₂ technology to provide reliable and trustful electrochemical and pneumatic data. However, obtaining trustworthy pneumatic data was rather challenging, as discussed in the next section.

III.3 Pressure measurement

III.3.a Sensor connection

The electrical connection of the commercial pressure sensors is composed of three bare wires that require a 3-track homemade electronic connector. Thus, stereo 3.5 mm Jack connectors were chosen for this reason, as well as for their universality and robustness. The male part was welded to the pressure sensor, while the female one was used in a homemade extension cable enabling the connection with the potentiostat (Figure 47). Note that only shielded cables and bulk metallic connectors were used so as to minimize the signal perturbation due to the ambient electrical noise.

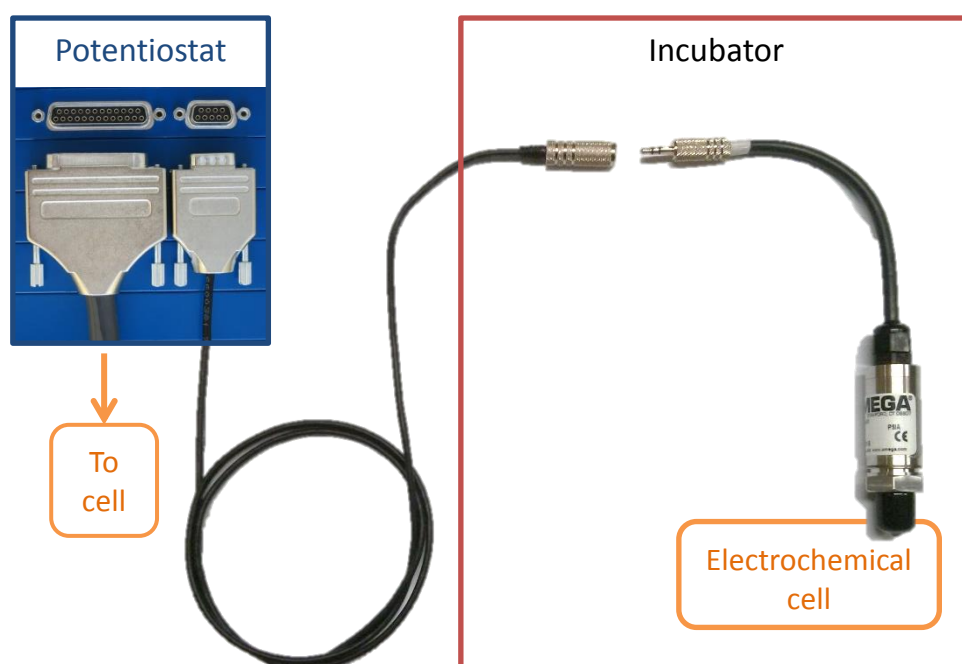


Figure 47: Schematic representation of a pressure sensor electrical network. The utility of the “Incubator” will be discussed in section III.4.b. The left image is a photograph of the back side of a Biologic potentiostat.

This setup enables the proper functioning of the sensor; however, it includes multiple connectors, welding and a long cable which may modify the overall setup resistance. Indeed, we found up to 10 mV discrepancy with the certificate of conformity, which corresponds to a non-negligible error of 4 mbar. The sensors were then re-calibrated according to the following procedure.

III.3.b Sensor calibration

The calibration of the sensors consists in determining the correlation coefficient linking the sensor signal (voltage) with the associated physical quantity (pressure). This procedure requires a known absolute pressure reference which is rather challenging to find.

After examining the possible options, the atmospheric pressure was chosen as the absolute reference. Its value – with a precision of 0.1 mbar – was obtained from the website of a meteorological station ³⁶² located 1 km away from the laboratory, at a height of 60 m above sea level. Coincidentally, the official NGF map of the Collège de France (Figure 48) revealed that our laboratory was at the same altitude, hence enabling the straightforward utilization of the weather station data. The comparison between the atmospheric pressure recorded by the station and by our sensors enables their accurate calibration (Figure 49).

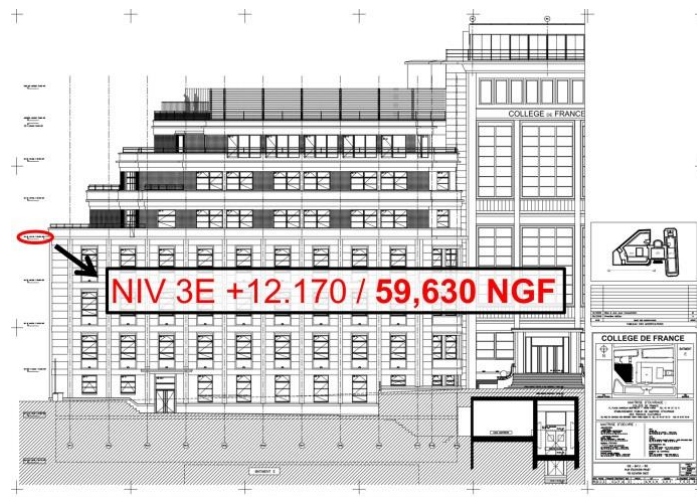


Figure 48: Official NPG (General France Level) map of Collège de France positioning our laboratory at 59.63 m above sea level (courtesy of the Patrimony Department of Collège de France).

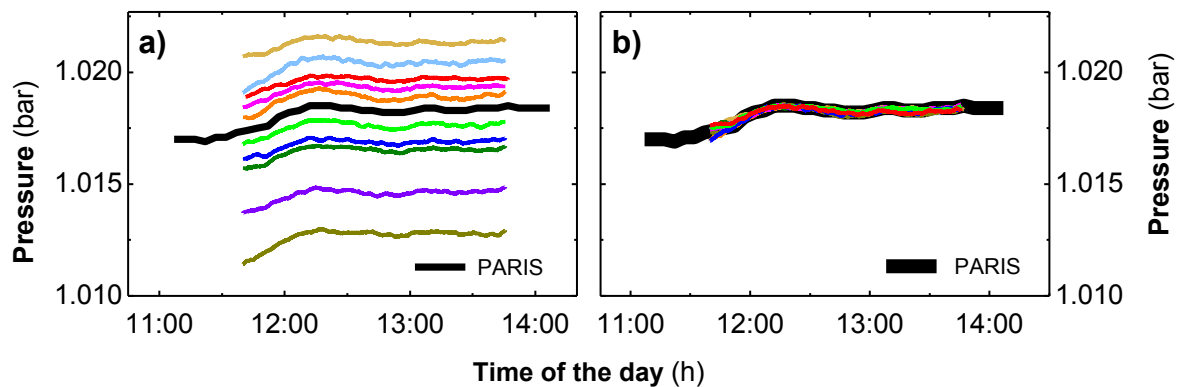


Figure 49: Time profile of the atmospheric pressure prior (a) and after (b) calibration. Colored lines correspond to our sensors while the thick black is the reference (weather station). The coefficients used prior calibration were found on the certificate of analysis of each sensor.

Lastly, two post-calibration tests were performed to confirm that the calibration was made successfully:

In one hand, we confirmed that the extension cable used for connecting the sensor to the potentiostat had no influence on the measurement, despite minor differences in the welding or cable length owing to the manual manufacture. Indeed, Figure 50a shows that a sensor connected to the potentiostat via seven different extension cables measures the same pressure.

On the other hand, we confirmed that the calibration was effective over a long period and over a larger pressure interval (Figure 50b).

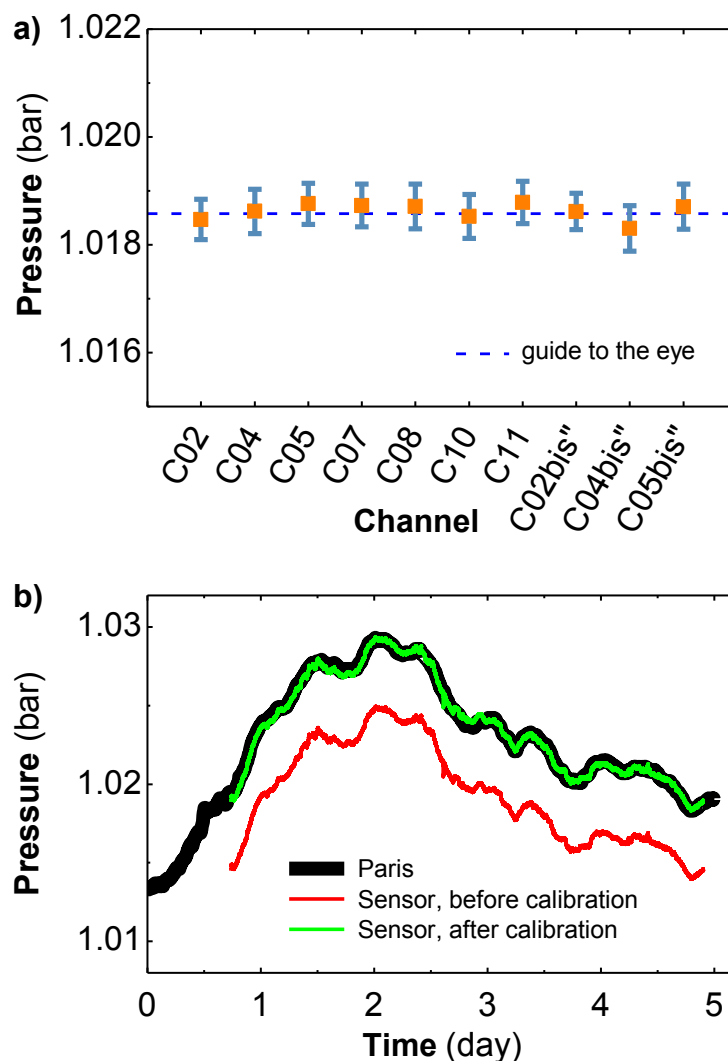


Figure 50: (a) Influence of the channel/cable on the measurement of a single P probe. The values reported herein are the average of a 2.30 minutes measurement. The three first channels were tested twice ("bis" label) to confirm the absence of atmospheric pressure changes within the overall experiment. (b) Atmospheric pressure measured in the laboratory by a pressure probe before and after calibration, as compared to the official atmospheric pressure (Paris).

In summary, we reported the development of practical electrical connections enabling an easy connection/disconnection of the pressure probe with the potentiostat. The influence of electrical network on the pneumatic data was minimized by the re-calibration of the sensors, which was performed in order to provide reliable and trustful test-cell hardware. However, such goal could not be reached without the development of satellite facilities which will be described below.

III.4 Related equipment

III.4.a Filling station

Considering the numerous issues arising from the presence of air contamination during the gas filling procedure (irreproducible results, trace of water, etc...), a special care was paid to establish a trustful way to fill the cells. For that purpose, a user-friendly and reliable filling station (Figure 51a) was built.

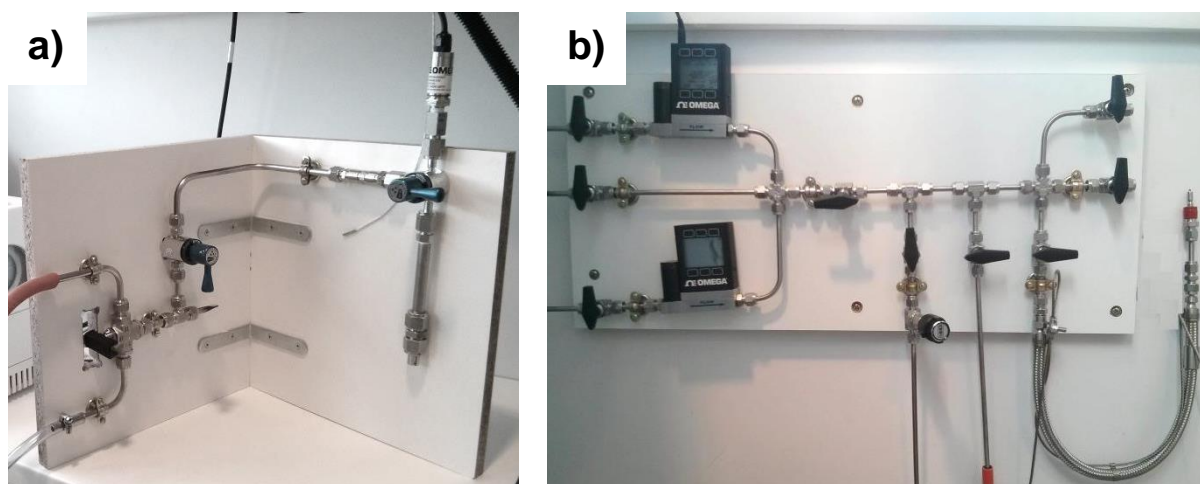


Figure 51: Photographs of two filling stations enabling a purging/refill of the cell with desire gas. The initial panel (a) was progressively replaced by a more advanced one (b).

The station is connected to the cell via a male quick connector that fits into the cell's female connector. Once coupled with the filling station, the cell is easily pumped/refilled by actuating a single 3-way valve several times. Note that the pressure is constantly monitored, which enables to fill each cell at the same absolute pressure (usually ~ 1.55 bar). Once loaded with the desired gas, the cells are unplugged from the filling station and put at rest (OCV) for 8 to 12 h prior to be cycled. This enables to equilibrate the temperature, to detect an accidental leak, and ensures a good O₂ dissolution in the electrolyte.

For broader use, it should be mentioned that during the writing of this manuscript, a more elaborated gas control panel (Figure 51b) was being build. It is connected to three gas

bottles (Ar, O₂ and CO₂) whose flow rates can be regulated by mass flow controllers, hence enabling the study of Li-Ar/O₂ and Li-O₂/CO₂ batteries with various gas compositions.

At this stage, having solved the filling issue, one had to address another important parameter to obtain reliable measures that is temperature.

III.4.b Temperature controlled chamber

A Li-O₂ cell – assembled in the new pressurized test cell configuration – was first cycled on a lab bench. The Pressure-Time profile measured is plotted in Figure 52c and compared with the pressure variations expected from an ideal Li-O₂ system (Figure 52b).

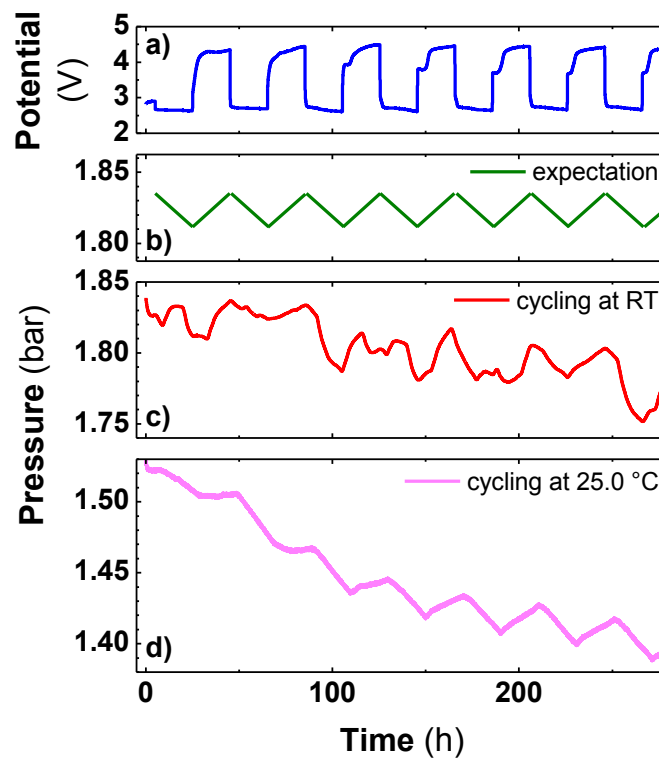


Figure 52: Voltage-Time (a) and Pressure-Time (b) profile of a Li//0.5 M LiTFSI in TEGDME//Csp//O₂ cell. (b) corresponds to the theoretical pressure evolution; (c) is the experimental pressure when the cell is cycled at room temperature (RT), and (d) is the experimental pressure when the cell is cycled inside an incubator at a fixed temperature of 25.0 °C.

Part of the discrepancies observed between the expected pressure variations and the measured ones were attributed to the temperature (T) variations inside the room due to day/night alternation and air conditioning. Indeed, given our experimental conditions (P = 1.5 bar; V = 10 mL), a 4 °C change results in a 20 mbar variation, value which is high as compared to the change in pressure (P) (\approx 30 mbar) expected for the (dis)charge of a Li-O₂ battery in our conditions (0.4 mg of C, 1000 mAh/g_C, 50 mA/g_C).

Our first trials to reduce the influence of T on the pressure measurement consisted in recording the room temperature upon cycling and correcting P from the temperature contribution based on the ideal gas law. However, this strategy was limited by the fast T changes in the room due to the air conditioning system, hence calling for a solution to run the cells under a controlled temperature.

To do this, an incubator (IPP 260, Memmert) was bought and equipped with a metallic structure and the connection cables, hence enabling the simultaneous testing of 14 pressurized cells in the absence of temperature variations (Figure 53). The pressure profile of a Li-O₂ cell cycled at a fixed temperature of 25.0 °C inside this chamber shows no fluctuation within one (dis)charge sequence (*cf* Figure 52d after 130 h), thus validating this strategy. It is worth noting that the peculiar behavior observed during the 130 first hours and the slow global pressure decay has a chemical origin which will be discussed in Chapter 3.

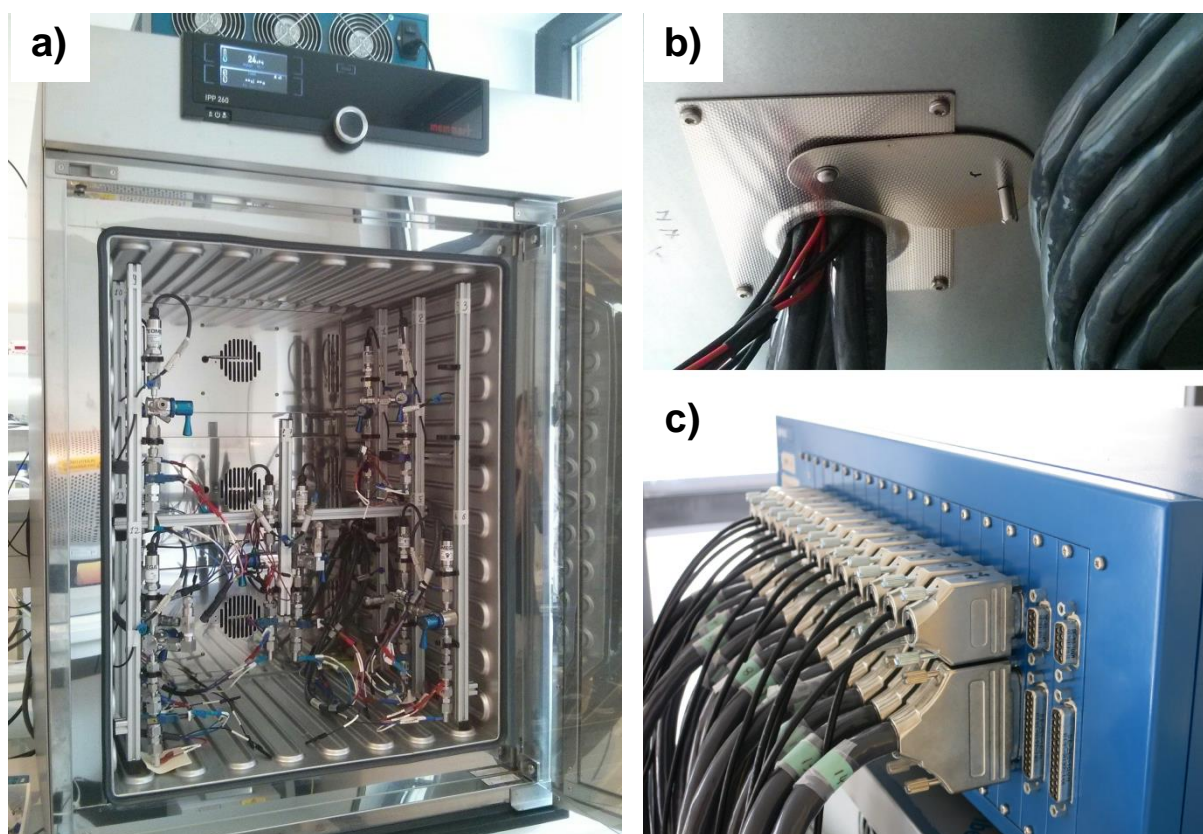


Figure 53: Photographs of the controlled temperature chamber. Front view showing the aluminum structure support the cycling cells (a); back aperture enabling cable connection (b); back panel of the Biologic potentiostat (c) connected to the pressure sensors (upper row) and the electrochemical cell (lower row).

The hardware being fully mastered (cell configuration, pressure measurements, stabilized temperature), preliminary tests were needed in order to establish the figures of merit of the pressurized cell.

IV Figures of merit of the pressurized cell

IV.1 Stability

The overriding figures of merit for such newly designed Li-O₂ cells are sensibility and stability. To be meaningful, the temperature has to be well managed all along the measurements. This was realized by performing all our experiments in the temperature incubator abovementioned, which provides a constant temperature set to 25.0 ± 0.1 °C. The temperature stability of the overall system is demonstrated in Figure 54a.

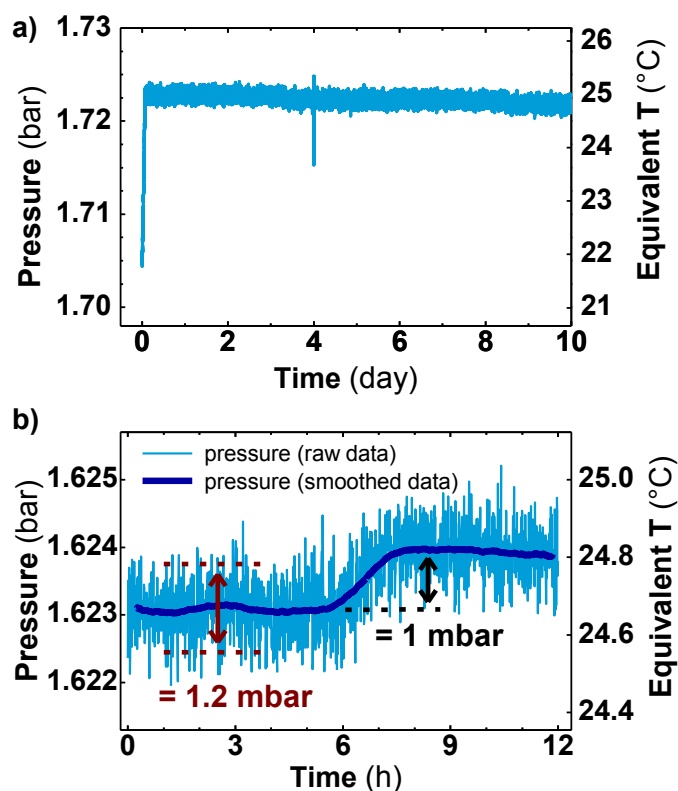


Figure 54: Pressure variations in a closed empty cell filled with O₂ a) during 10 days at 25.0 °C; the spike at 4 days is intentional (see main text); b) during 12 hours; the 1 mbar pressure increase (6 h) results from the addition of a small amount of gas into the cell. The equivalent temperature was calculated from the pressure value. The background noise shown by the red arrow was calculated as twice the standard deviation of a series of consecutive points.

Note that over a 10 days period at 1.72 bar, the pressure loss is only 1.1 mbar, equivalent to a leak rate of 64 ppm of gas per day ($4.1 \cdot 10^{-8}$ mol of gas/day). To quantify the extreme sensitivity of the pressure regarding temperature fluctuations, we also plotted on the y-axis the equivalent temperature calculated with the ideal gas equation ($PV = nRT$). Within such a scale, the sensitivity of the system is further exemplified by the large amplitude of the pressure spike (at day 4) which corresponds to a temperature change in the incubator from 25 °C to 23.6 °C, intentionally provoked by opening the incubator door

for 30 minutes. Let's recall that other temperature changes might also be generated by the dissolution of gaseous O₂ into the organic electrolyte. The standard enthalpy related to this reaction is reported in the range of few kJ/mol. With our setup, and assuming that the total heat associated to each charge/discharge (dissolution/release of gas O₂) sweep is instantaneously exchanged with the electrolyte, its T change would not exceed 0.3 °C degrees. In our cycling conditions, these 0.3 °C are spread over 20 h (one charge or discharge) and diffused through the metallic cell, hence the temperature change will be insignificant and the measurement won't be affected.

IV.2 Sensitivity

The sensitivity limit is deduced by observing the pressure variation driven by a small addition of gas in Figure 54b. The background noise in the raw data which is purely electrical and randomly distributed can be easily smoothed, hence enabling a better reading accuracy. Note that an increase of 1 mbar (equivalent to $3.7 \cdot 10^{-7}$ mol of gas, corresponding to 590 ppm of the total gas amount at 1.7 bar) is then easily observable. The smallest detectable variation is thus estimated to be around 0.5 mbar. This lower detection threshold corresponds to $1.8 \cdot 10^{-7}$ mol of gas (290 ppm at 1.7 bar), which is equivalent to a 9 μAh charge in the case of a Li-O₂ system, bearing in mind that the temperature fluctuations inside the incubator (≈ 0.05 °C, *i.e.* 0.25 mbar at 1.5 bar) are negligible in first approximation.

Thanks to those preliminary tests, the accuracy and sensitivity of our new setup were established. Their good values enable an accurate pneumatic study of Li-O₂ cells as presented in the following chapter.

V Conclusions

We presented herein the design of a new pressurized electrochemical test cell dedicated to Li-O₂ batteries whose development was motivated by the poor abilities of the cell initially used in our lab. After giving an overview of the Li-O₂ test cells developed worldwide and discussing the problematic arising from our will to develop a user-friendly device, we presented the design of the new pressurized cell and demonstrated its proper integration into the lab environment. The latter requires the utilization of a controlled temperature incubator, the design and the construction of a gas filling station preventing gas contamination, and the manufacturing of a relevant electrical network. Lastly, the figures of merit of the overall setup (test cell + related facilities) were established, hence demonstrating its relevance for accurately studying Li-O₂ systems.

The result of this study, which focuses on the stability of the most common Li-O₂ electrolytes, will be presented in the following chapter (Chapter 4). They emphasize the value added by a dual electrochemical/pneumatic characterization enabled by our pressurized cell, which allows for a rapid and reliable estimation of the amount of parasitic reactions, the chemistry of which could therefore be identified by a careful DEMS or OEMS study. The instability of their components explains the limits of current Li-O₂ batteries and motivates our future work, which will be presented in the next chapters of this thesis.

CHAPTER 3: STUDY OF LITHIUM-OXYGEN BATTERIES USING A PRESSURIZED ELECTROCHEMICAL TEST CELL

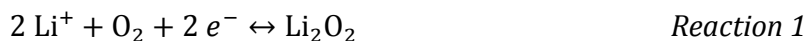
After having designed, build and calibrated our new test cells, a systemic study of the electrochemical behavior of different electrolytes previously reported for Li-O₂ systems was performed in order to definitively assess their stability and efficiency. Moreover, in addition to the electrolyte stability, side reactions such as cathode corrosion and lithium anode instability were assessed in order to develop a practical solution for the development of Li-O₂ cells showing long term stability.

I Prologue

I.1 Data interpretation

In the former chapter, we introduced our new home-designed Metal-Air test cell integrating a pressure sensor monitoring the gas evolution upon cycling. Prior to use this setup for testing Li-O₂ batteries, we will first discuss the possible options to plot/analyze the pressure data which will be used in the following part of this chapter.

In this work, the Li-O₂ cells were cycled in a galvanostatic mode (Figure 55a,b), which consists in applying a constant current, *i.e.* a constant quantity of electron per time unit. The consumption/evolution of O₂ being theoretically linearly correlated to the current density (*Reaction 1*), it should thus result in a linear pressure increase (or decrease) during a charge (or discharge) (Figure 55c).



The quantity of gas involved during this sequence can thus be measured and compared to the capacity so as to determine the “number of moles of electron required to consume/evolve one mole of O₂ (or gas)”, also written “e⁻/gas” ratio. Based on *Reaction 1*, it should equal 2 in the case of a perfect Li-O₂ system; however, this ideal scenario rarely happens in practice, where multiple electrochemical processes may influence the gas production rates, hence modifying this ratio as depicted in Figure 55. Three scenarii are considered: i) an ideal Li-O₂ cell (green, e⁻/gas = 2); ii) a Li-O₂ cell overconsuming and overproducing gas (red, e⁻/gas < 2); and iii) a Li-O₂ cell under-consuming and under-producing gas (blue, e⁻/gas > 2). The latter scenario was for instance observed by McCloskey *et al.* who reported 3.2 e⁻/gas during the first charge of a DME-based electrolyte. The e⁻/gas ratio was also used by Bruce and coworkers regarding CO₂ emissions, so as to corroborate the degradation mechanism of carbonate-based solvents.

The e⁻/gas ratio is thus a valuable asset when studying Li-O₂ batteries which, in the case of our pressure measurements, can be calculated by two methods. In one hand, one can consider the total pressure decrease (ΔP in Figure 55c) and compare it to the discharge capacity (*global method*). On the other hand, one can instead calculate the instantaneous gas emissions (Figure 55d), which is directly correlated to the e⁻/gas ratio knowing the current density (*derivative method*). Within such representation, it is worth noting that the *gas emission* ($\mu\text{mol/h}$) and the *e⁻/gas* scales are in reversed directions (a low gas emission corresponds to a high e⁻/gas ratio).

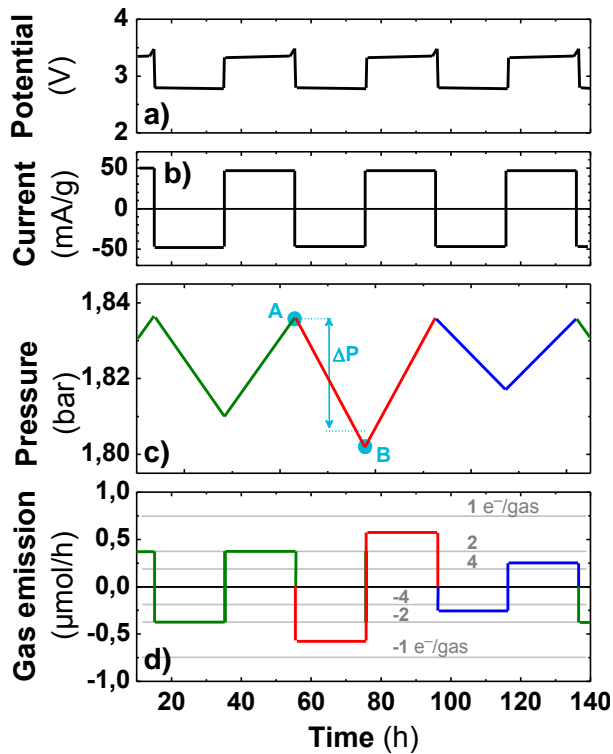


Figure 55: Simulated Potential-Time (a), Current-Time (b), Pressure-Time (c), and Gas Emission-Time (d) profiles of three Li-O₂ cells with different gas emission rates (not experimental data).

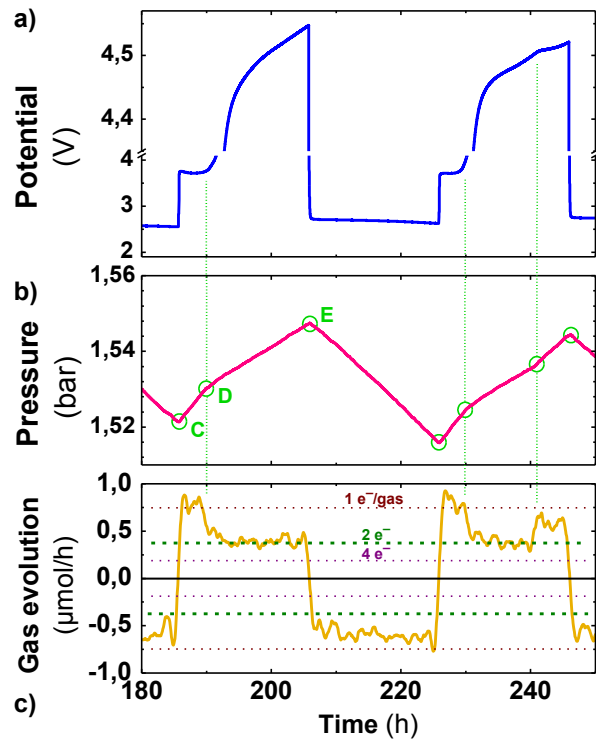


Figure 56: Experimental Potential-Time (a) and Pressure-Time (b) profiles of an actual Li/0.5 M LiTFSI in TEGDME/Csp/O₂ cell.

In practice, the *derivative method* will be favored over the *global* one owing to its ability to represent minor pressure changes as shown in Figure 56 and correlate them to a change in the cycling behavior. As a demonstrative example, we clearly see that some gas is evolved at a rate of $\sim 1 e^-/\text{gas}$ over the C-D segment, while it is close to 2 over D-E. Such variations, which are good indicators of the chemistry at play over cycling, would not be easily quantitatively observable by the *global method*.

Plotting the instantaneous gas emission is therefore a clever way to visualize the pressure data which provides a straightforward representation of the e^-/gas ratio. It gives an insight on the chemical reaction occurring in the system, which is very useful for quantifying parasitic reactions and comparing different Li-O₂ systems, as discussed later in this chapter.

1.2 Added value of Pressurized Cells for studying Li-O₂ batteries

Having developed a test cell capable of quantifying the gas evolved in a battery upon cycling, we will now focus our work on practical Li-O₂ systems using both electrochemical characterization and pressure monitoring. As explained previously, this new setup is

particularly relevant for detecting parasitical reactions since they modify the e^-/gas ratio. Bearing this in mind, we decided to investigate the stability of various electrolytes which, among all the battery components, are known to lack stability towards the radical superoxide ($\text{O}_2^{\cdot-}$) formed in reduction as well as high charging potentials.

In the past, gas analysis has been used to demonstrate the instability of carbonate-based electrolytes, and to suggest alternative solvents such as glymes, DMSO, DMA, etc... However, these studies were based on DEMS measurements limited to a single or a few cycles, owing to the practical difficulties to carry out such analysis over a long period. In our work, we will benefit from the convenience of our newly designed cell to extend the study to the long-term cycling (> 1000 hours) so as to detect the factors limiting the cycle life of current Li- O_2 batteries. Our setup will first be benchmarked with a DMA-based cell prior to be used for studying other electrolytes frequently employed in the literature such as glymes or DMSO. Noting their limited performances, we will then focus on parasitic reactions occurring in these systems and try to minimize their impact with the use of redox mediators. Finally, the overall results will be gathered and compared so as to determine the best choice among today's electrolytes.

II Lithium Nitrate in N,N-Dimethylacetamide (DMA)

Our pressurized set-up was first benchmarked with a Li- O_2 cell using a DMA-based electrolyte previously reported by Addison and coworkers at Liox¹⁹³. The typical cycling behavior (Figure 57a and b) with a discharge potential of about 2.7 V and a low charge potential ≈ 3.6 V vs. Li^+/Li^0 was obtained even though catalyst-free Carbon SP was used. This is typical of the dual role of LiNO_3 which acts as a redox mediator at the positive electrode on charge and which prevents at the negative electrode the reaction of metallic Li with DMA via the formation of a protective Li_2O layer (*cf* Chapter 1, section IV.1.c).

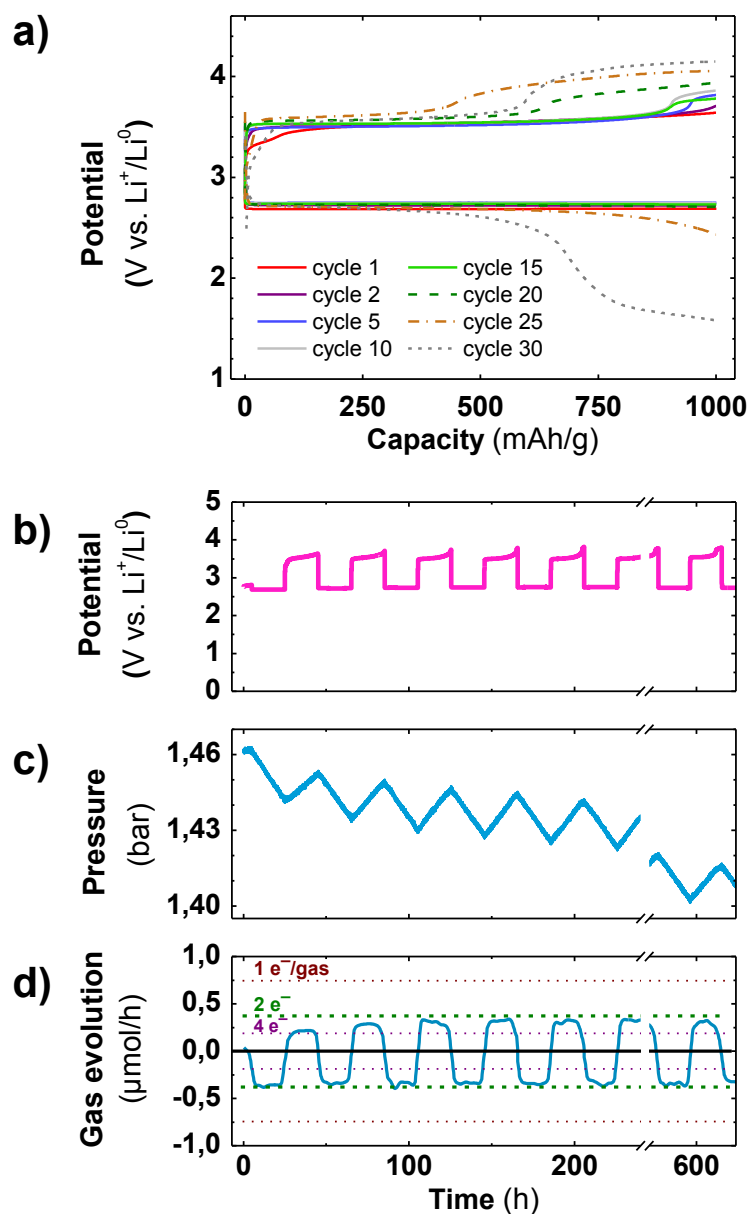


Figure 57: Electrochemical behavior of a $\text{O}_2//\text{Csp:PTFE [9:1]//2 M LiNO}_3$ in DMA//Li battery cycled at a current of $50 \text{ mA/g}_{\text{carbon}}$, with a capacity limited to $1000 \text{ mAh/g}_{\text{carbon}}$. a) Voltage-Capacity galvanostatic profile of some representative cycles; b) Voltage-Time profile (cycles #1-#6 and #15); c) pressure evolution inside the cell as function of time (cycles #1-#6 and #15); d) instantaneous gas release/uptake as function of time (cycles #1-#6 and #15). The horizontal green dashed lines represent the theoretical value of $\pm 2 e^-/\text{gas}$. The gravimetric capacities are reported with respect to the carbon mass.

Such an electrochemical cycling is associated both in charge and discharge to a linear response of the cell pressure with capacity (Figure 57c), similar to the results previously reported by Giordani *et al.*²⁵⁷. During the discharge, the pressure decreases as $\text{O}_{2(\text{g})}$ is consumed (reduced) while it increases during the charge owing to the $\text{O}_{2(\text{g})}$ evolution resulting from the decomposition of $\text{Li}_2\text{O}_{2(\text{s})}$. The Pressure-Time profile resembles to the ideal system previously depicted in Figure 55 (green line). Nevertheless a continuous decrease of the global pressure during cycling over hundreds of hours was measured, which

suggests that parasitic reactions, even though limited, irreversibly consume oxygen. Note that this slow loss in pressure (50 mbar within 25 days) is one order of magnitude larger than the leak rate previously measured in Chapter 2, section IV.1 (1.1 mbar in 10 days). To estimate the level of these parasitic reactions, the instantaneous gas evolution ($\mu\text{mol/h}$) was plotted (Figure 57d), enabling a direct comparison with the ideal Li-O₂ system (*Reaction 1*) for which the signal should be a square-wave, alternatively switching from + 0.37 $\mu\text{mol/h}$ to - 0.37 $\mu\text{mol/h}$.

Further exploiting Figure 57d, the gas emissions during the two first charges (3.46 and 2.59 e⁻/gas) are slightly lower than expected, which is consistent with the mechanism of SEI formation at the anode previously proposed²⁵⁸. This mechanism corresponds to the regeneration of the redox-mediator (NO₃⁻) that reacted at the anode during the SEI formation, and which consumes a fraction of the O₂ produced during the charge. In comparison, a blank-test cell without nitrates was mounted (using 0.5 M LiTFSI in DMA, and pre-charged LFP as anode), for which the gas was evolved at a rate of 2.55 and 2.22 e⁻/gas during the two first charges (*cf* Annex 1). Coming back to the LiNO₃/DMA system, the two first cycles differ from the subsequent ones and can be denoted as “formatting” cycles. In contrast, from the 3rd cycle, a “steady state domain” is reached, in which consecutive cycles show similar gas evolution profiles. After cycle #15 (~ 600 h), a second charge voltage plateau (4.1 V vs. Li⁺/Li) is spotted, and this feature continuously increases upon further cycling to finally account for almost half of the charge capacity at cycle #25 (Figure 57a). Thanks to the long-term reliability of our device, we could corroborate this second charge reaction with clear changes in the rate of pressure variations. This is nicely illustrated in Figure 58 that compares data of cycles #4 and #23. The two charge plateaus of cycle #23 at 3.55 V and 4.2 V (Figure 58a) clearly corresponds to two different slopes (Figure 58b) related to two different instantaneous gas emissions (Figure 58c). The low and high voltage reactions are proceeding at rates of 0.36 $\mu\text{mol/h}$ (2.07 e⁻/gas) and 0.24 $\mu\text{mol/h}$ (3.11 e⁻/gas), respectively. These variations of gas evolution reveal two distinct charge mechanisms, which precise origin would require additional chemical analysis. However, previous studies suggest that such high voltage charge phenomenon is associated to the release of gaseous CO₂¹⁹³, probably originating from side products oxidation (carbonates formed on the carbon electrode)²⁰⁵. Overall, these results show how pneumatic data are closely related to the electrochemical behavior and enable to accurately observe the aging of Li-O₂ cells over weeks/months of cycling.

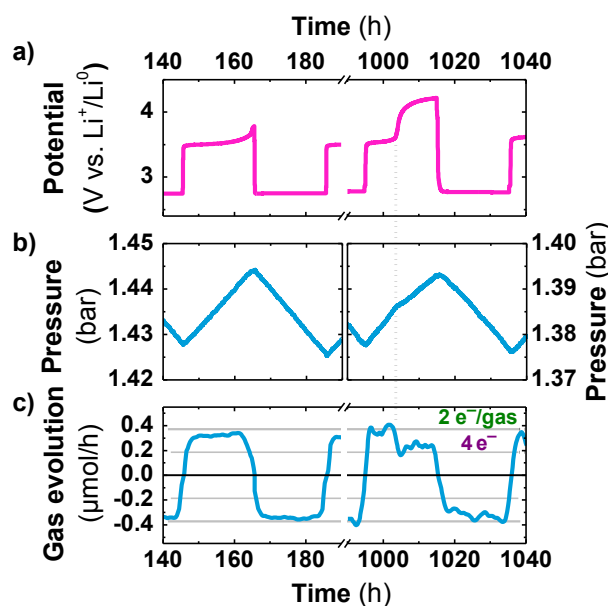


Figure 58: Electrochemical behavior of a O₂//Csp:PTFE [9:1]//2 M LiNO₃ in DMA//Li cycled at 50 mA/g_{carbon}, with a capacity limited to 1000 mAh/g_{carbon}. Only the 4th and 23rd cycles are shown. a) Voltage-Time profile; b) pressure evolution inside the cell as function of time; c) instantaneous gas release/uptake as function of time. The horizontal green dashed lines represent the theoretical value of $\pm 2 e^-/\text{gas}$.

III Tetraethyleneglycol dimethylether (TEGDME)

III.1 Electrochemical behavior

Being able to accurately detect minor irregularities in gas evolutions, we extended the use of our new set-up to study the long term performances of Li-O₂ batteries based on well-known solvents, with a specific attention to the Li-O₂ system using a TEGDME-based electrolyte shown in Figure 59a-d. This solvent has been widely studied by the Li-Air community due to its relatively good stability, high boiling point and very low volatility. The Voltage-Time profile of the Li/0.5 M LiTFSI in TEGDME/O₂ cell (Figure 59a and b) is comparable to those already reported for ether-based electrolytes using carbon cathodes²⁴⁵. The first cycle is characterized by a sharp potential drop prior to reach a 2.8 V discharge plateau, and a waving charge plateau at a potential above 4 V. On the subsequent cycles (#2 to #5), the discharge plateau is reached through a smoother potential decrease, whereas the charge is marked by the appearance of an additional initial voltage shoulder at 3.7 V. Such lowering of the potential on charge has already been reported elsewhere³⁶³ and was attributed to the surface of Li₂O₂ particles which decomposition is supposed to begin at 3.5 to 3.7 V¹⁹⁶, as opposed to bulk Li₂O₂ which is expected to react above 4 V. This singular electrochemical behavior is related to a gas evolution that strongly deviates from 2 e⁻/gas (Figure 59c and d), indicating at least one side reaction happening conjointly with Li₂O₂ oxidation. Pressure data also show that gas emissions observed during the first three

charges are much lower than the following ones, which indicates that a formatting process also occurs in TEGDME-based cells, whose chemical nature will be discussed in the next section.

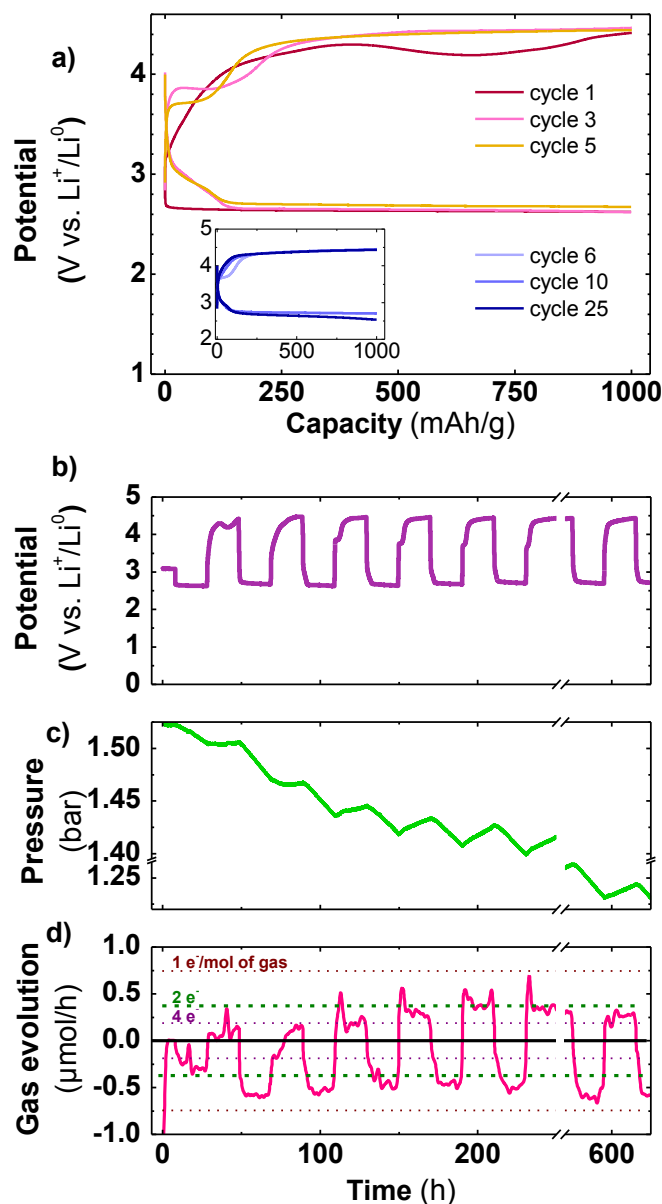


Figure 59: Electrochemical behavior of an $O_2//Csp:PTFE [9:1]//0.5 M LiTFSI$ in TEGDME//Li battery cycled at a current of $50 mA/g_{carbon}$, with a capacity limited to $1000 mAh/g_{carbon}$. a) Voltage-Capacity galvanostatic profile of some representative cycles; b) Voltage-Time profile (cycles #1-#6 and #15); c) pressure evolution inside the cell as function of time (cycles #1-#6 and #15); d) instantaneous gas release/uptake as function of time (cycles #1-#6 and #15). The horizontal green dashed lines represent the theoretical value of $\pm 2 e^-/gas$.

After the first three formatting cycles, a steady state domain is reached, for which the Voltage-Capacity curves look alike at each cycle (insert Figure 59a). Gases are then systematically consumed with a ratio $< 2 e^-/gas$ (discharge), while they are produced at a rate slightly higher than $2 e^-/gas$ (charge). This does not come as a surprise bearing in mind

that early works combining glymes-based electrolytes and carbon electrodes have revealed the existence of copious parasitic reactions^{248,229} associated to the formation of lithium carbonate in discharge and CO₂ evolution in charge^{205,207}, hence leading to a poor performance of the cells.

Overall, the TEGDME-based system does not perform as well as the DMA-based one discussed above (higher polarization, large deviations from the theoretical gas emissions...). In order to identify the parasitical reactions hindering its performances and to spot the cell components involved in these reactions, these two systems were compared using electrochemical impedance spectroscopy measurements, as detailed in the next section.

III.2 Identification of the parasitic reactions

III.2.a Comparing DMA- and TEGDME-based systems by impedance spectroscopy

The study of the LiNO₃/DMA and LiTFSI/TEGDME systems showed that they were both limited by the instability of (at least) one of their components, as spotted by the deviation from the theoretical gas evolution as discussed above. However, the simple monitoring of gas evolution does not provide information about the origin of the parasitic reactions and three-electrode electrochemical impedance spectroscopy (EIS) was used to independently assess the side reactions occurring at the positive and the negative electrode. The measurements were carried out using a microelectrode of Li as reference (Figure 37c, p.61) in the 3-electrode cell previously described (Figure 36, p.60) on top of which was mounted a pressurized cell.

EIS was first used to investigate the formatting cycles in TEGDME- and DMA-based systems which, at the first sight, may look similar as they both results in low gas emissions in charge. However, the LiNO₃, which is responsible for the limited oxygen evolution in the DMA-based cell, was not used in the TEGDME-based system, hence calling for a different explanation responsible for the sluggish gas emissions. For the TEGDME-based cell, EIS spectra recorded before and after the formatting cycles (cycle #1 and #4) show a large modification for both the positive (Figure 60d) and the negative (Figure 60e) electrodes. In contrary, only minor changes are observed upon cycling for the cell containing LiNO₃ in DMA (Figure 61). Nevertheless, the resistance of the negative electrode – given by the real part of the semi-circle observed in the Nyquist plot in Figure 61e – increases between cycles #1 and #4 and stabilizes afterwards. This increase corresponds to the formation of an SEI at the Li surface, hence confirming the explanation earlier proposed by Giordani *et al.*²⁵⁷ for the low gas emissions during the formatting cycles.

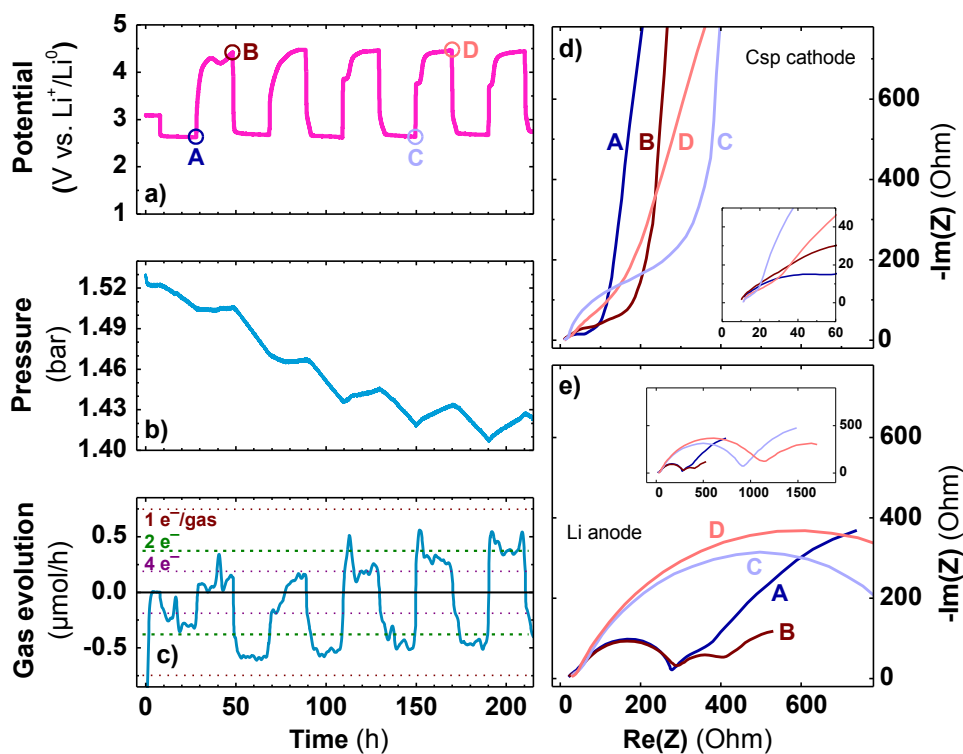


Figure 60: Potential-Time (a), Pressure-Time (b), and Gas Emission-Time (c) profiles of a Li/0.5 M LiTFSI in TEGDME/Csp/O₂ cell cycled at 50 mA/g_c with a limited capacity of 1000 mAh/g_c. Impedance spectra of the positive (d) and negative (e) electrodes at cycles #1 and #4 (end of discharge and charge).

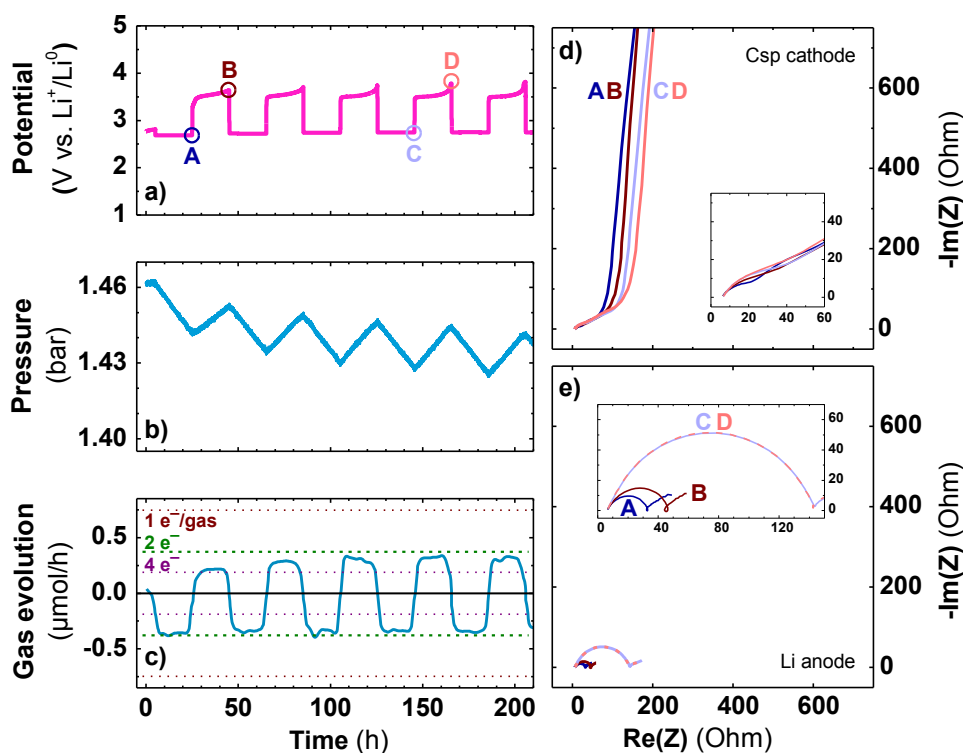


Figure 61: Potential-Time (a), Pressure-Time (b), and Gas Emission-Time (c) profiles of a Li/2 M LiNO₃ in DMA/Csp/O₂ cell cycled at 50 mA/g_c with a limited capacity of 1000 mAh/g_c. Impedance spectra of the positive (d) and negative (e) electrodes at cycles #1 and #4 (end of discharge and charge).

Focusing on the LiTFSI/TEGDME-based system, the EIS study reveals that both electrodes undergo drastic parasitic reactions during cycling, calling for an in depth study in order to develop a practical solution to tackle these limitations.

III.2.b Parasitic reactions at the positive and negative electrodes

In order to simplify this system, the Li anode was replaced by a pre-charged LFP electrode so as to prevent the side reactions associated to the presence of lithium metal and isolate the parasitic reactions occurring at the cathode. Such Li-free cell exhibits electrochemical and pneumatic behaviors (Figure 62) comparable to that of the cell containing lithium metal (Figure 59), hence suggesting that the positive electrode is the major source of parasitic reactions responsible for the formatting cycles, even though the degradation of the electrolyte cannot be ruled out by this experiment. This result is consistent with some studies previously mentioned reporting the instability of carbon at high potentials and its oxidation in presence of Li_2O_2 ^{229,248}.

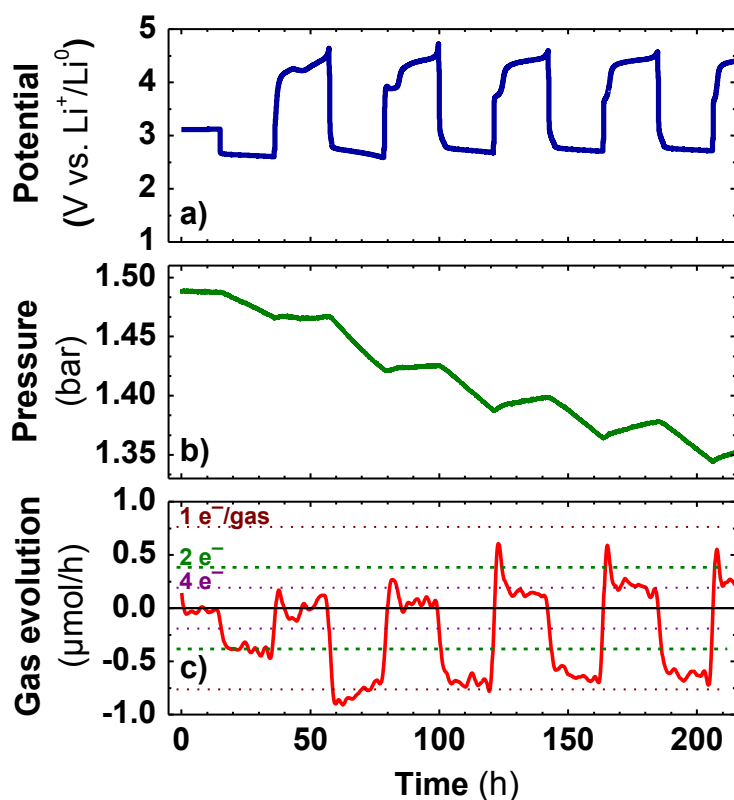


Figure 62: Potential-Time (a), Pressure-Time (b), and Gas Emission-Time (c) profiles of a pre-charged LFP/0.5 M LiTFSI in TEGDME/Csp/O₂ cell cycled at 50 mA/g_c with a limited capacity of 1000 mAh/g_c. The potential vs. Li^+/Li^0 was recalculated with respect to the LFP equilibrium potential (3.44 V). The small potential spikes at the end of the charge sequence are due to an inadequate pre-charging of the LFP electrode.

Lastly, in order to confirm that the process observed during charge at high potential was not simply due to electrolyte decomposition, a TEGDME-based Li-O₂ cell was cycled without limiting the capacity and without the use of high cut-off voltage (Figure 63). During the discharge, the e⁻/gas ratio is stable (2.1 e⁻/O₂) down to 2.3 V, suggesting that Li₂O₂ is formed all along the discharge. During the charge, the first wavy plateau at ~ 4.4 V, which accounts for about the same capacity as the initial discharge, is typical from the aforementioned “formatting process”. It is then followed by a second plateau at 4.78 V corresponding to the electrolyte decomposition (orange coloration of the separators was observed in post-mortem analysis) and for which a pressure drop is observed (not yet investigated).

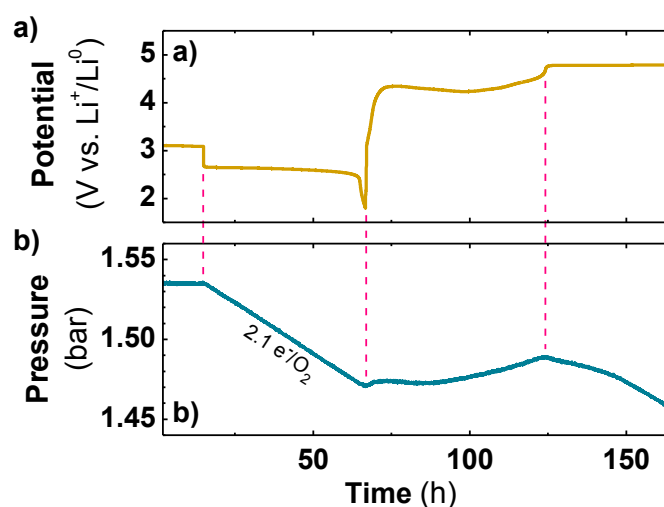


Figure 63: Potential-Time (a) and Pressure-Time (b) profiles of a Li/0.5 M LiTFSI in TEGDME/Csp/O₂ cell fully discharged down to 1.8 V and recharged in absence of high cutoff voltage.

Together, these two last experiments show that the formatting process responsible for the erratic gas emission upon charge is mostly involving the lack of stability of the carbon cathode. Nonetheless, the EIS spectra (Figure 61e) also spotted parasitic reactions which significantly increase the impedance of the negative electrode. In order to learn more about this process, a symmetric Li-Li cell was cycled in similar conditions (TEGDME electrolyte, pressurized cell in O₂ atmosphere...). The EIS measurements reveal a constant increase of the Li metal impedance throughout the experiment (> 12 days), hence indicating a relative instability of Li metal in presence of O₂ in TEGDME (Figure 64). However, this increase is notably slower than in a Li-O₂ cell, suggesting that compounds other than dissolved O₂ but related to the Li/O₂ chemistry (such as O₂⁻ or some side products coming from parasitic reactions at the cathode) also react with lithium metal.

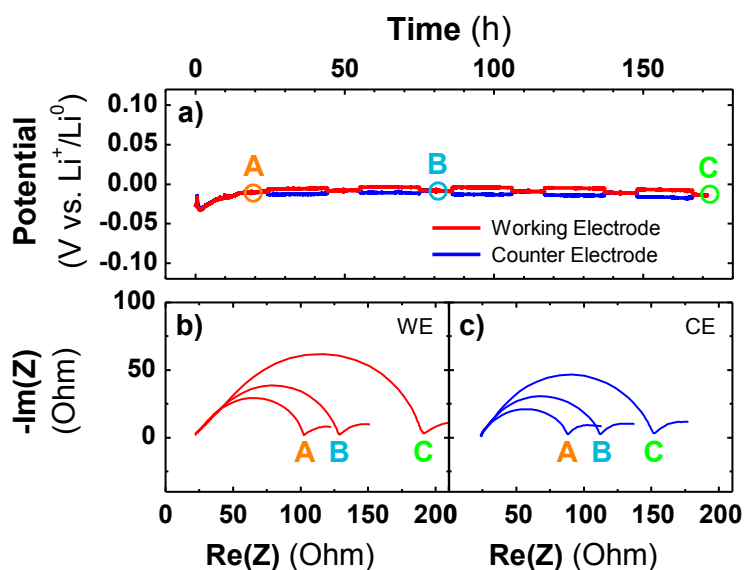


Figure 64: Impedance spectra of a Li/0.5 M LiTFSI in TEGDME/Li/O₂ cell doing successive plating/stripping sequences of 20 h with a current of 20 μA . The working electrode (WE, located at the bottom of the cell as usual in Li-O₂ cells) was always plated (b). The counter electrode (CE, located at the air side) was always stripped.

III.2.c Mitigating parasitic reactions using redox mediators

Having detected several parasitic reactions both at the positive and the negative electrode of LiTFSI/TEGDME-based cells, we tried to improve this system by using LiNO_3 , which shows beneficial effects at both electrodes in DMA-based cells (Li anode stabilization and decrease of the charging potential).

Curiously, the behavior of LiNO_3 drastically differs when used in TEGDME (Figure 65), in which three charge plateaus may be identified during the first cycles. The lower plateau (3.55 V), which corresponds to the nitrate redox activity usually observed in DMA, only accounts herein for $\sim 1/3$ of the first charge sequence. It disappears after the third cycle to the benefit of the 3.85 V plateau, which is consistent with a recent work from Aurbach's group who reported the same behavior using LiNO_3 in DEGDME²⁶⁰. However, these two low-voltage plateaus are progressively replaced by high-voltage one (4.33 V), which corresponds to the Li-O₂ chemistry usually observed in the LiTFSI/TEGDME system. This behavior denotes the inefficacy of LiNO_3 as a redox mediator in TEGDME, as confirmed by the large changes observed for the impedance at the positive electrode during cycling (Figure 65d) and the low pressure evolution recorded in charge (Figure 65c). On the other hand, the ability of LiNO_3 to form a protective SEI is preserved in TEGDME, as indicated by the stabilization of the impedance at the lithium metal electrode (Figure 65e).

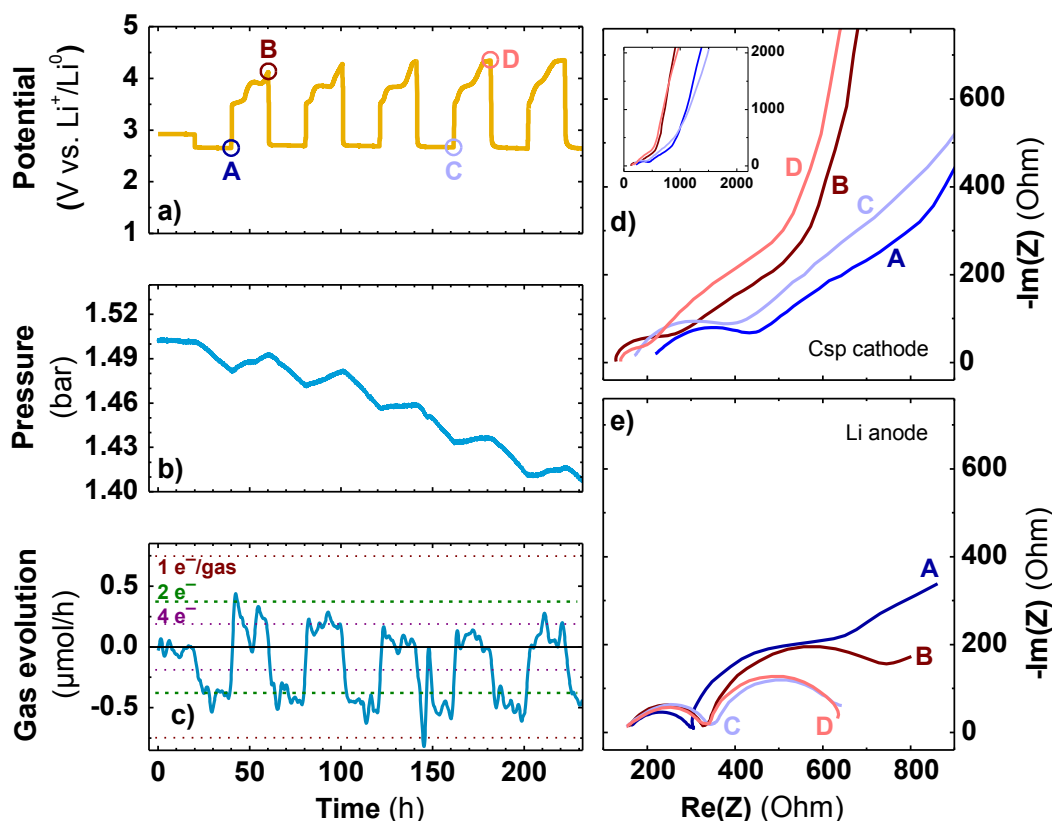


Figure 65: Potential-Time (a), Pressure-Time (b), and Gas Emission-Time (c) profiles of a Li/2 M LiNO₃ in TEGDME/Csp/O₂ cell cycled at 50 mA/gc with a limited capacity of 1000 mAh/gc. Impedance spectra of the positive (d) and negative (e) electrodes at cycles #1 and #4 (end of discharge and charge).

Overall, using LiNO₃ as Li salt in TEGDME-based electrolytes seems beneficial for short-term cycling (< 200 h) since it stabilizes the lithium metal anode. However, in order to confirm the sustainability of such strategy, the cycling behavior of LiNO₃/TEGDME (Figure 66) and LiTFSI/TEGDME (Figure 67) systems were compared over a long period. Comparatively, the utilization of LiNO₃ reduces/prevents the gas overconsumption in discharge and decreases the average charging potential. However, the latter effect is accompanied by a very low gas evolution (> 4 e⁻/gas) leading to a premature cell death, which occurs at cycle #15 for the LiNO₃-containing cell as compared to cycle #30 for the LiTFSI-containing one. This shows the cross-influence of the salt and the solvent, which should be seen as a binomial influencing together the cell performances. With this example, it is also worth noting that lower charge overpotentials do not necessarily imply a reduction of the amount of parasitical reactions, nor improve the cycle-life of the battery, as it is sometimes implied in studies lacking of gas monitoring/analysis.

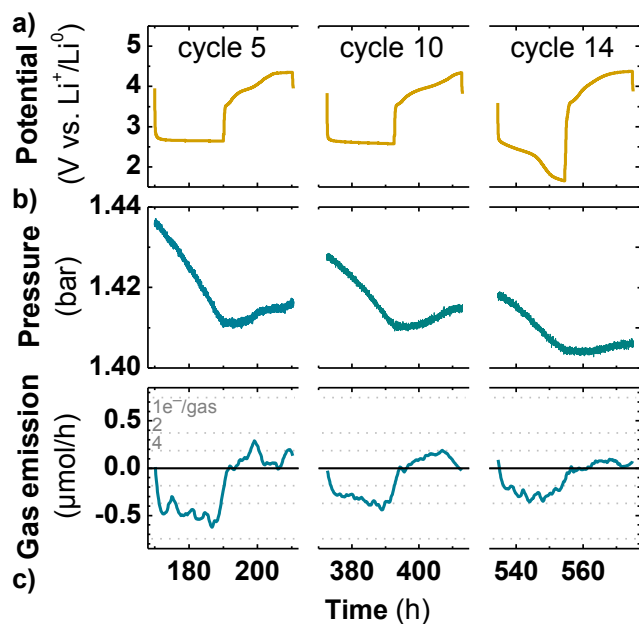


Figure 66: Potential- (a), Pressure- (b), and Gas Emission- (c) Time profiles of a Li/2 M LiNO₃ in TEGDME/Csp/O₂ cell cycled at 50 mA/g_c with a limited capacity of 1000 mAh/g_c. Only cycles #5, 10 and 14 are shown.

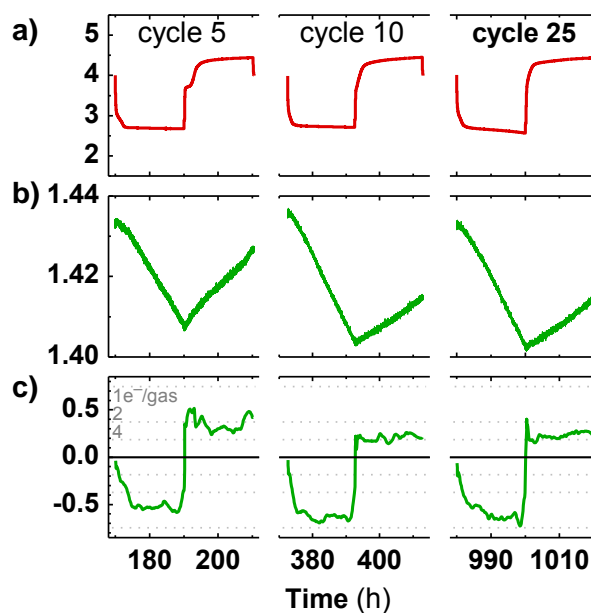


Figure 67: Potential- (a), Pressure- (b), and Gas Emission- (c) Time profiles of a Li/0.5 M LiTFSI in TEGDME/Csp/O₂ cell cycled at 50 mA/g_c with a limited capacity of 1000 mAh/g_c. Only cycles #5, 10 and 25 are shown.

Considering the poor performance of LiNO₃ as redox mediator in TEGDME, we investigated the utilization of lithium iodine as an alternative redox mediator. The cycling behavior of an Li-O₂ cell using 10 mM LiI + 0.5 M LiTFSI in TEGDME as electrolyte is reported in Figure 68 and shows no significant improvement of the overall TEGDME-based system. The charge plateau characteristic to the I₂/I₃⁻ redox couple at around 3.65 V vs. Li⁺/Li⁰ is only observed during the 3 first cycles and is accompanied by an erratic pressure evolution during charge. In discharge, the gas consumption rate is closer to the theoretical value than without LiI (*cf* the LiTFSI/TEGDME-based cell in Figure 59d), but this effect fades out after 150 h of cycling.

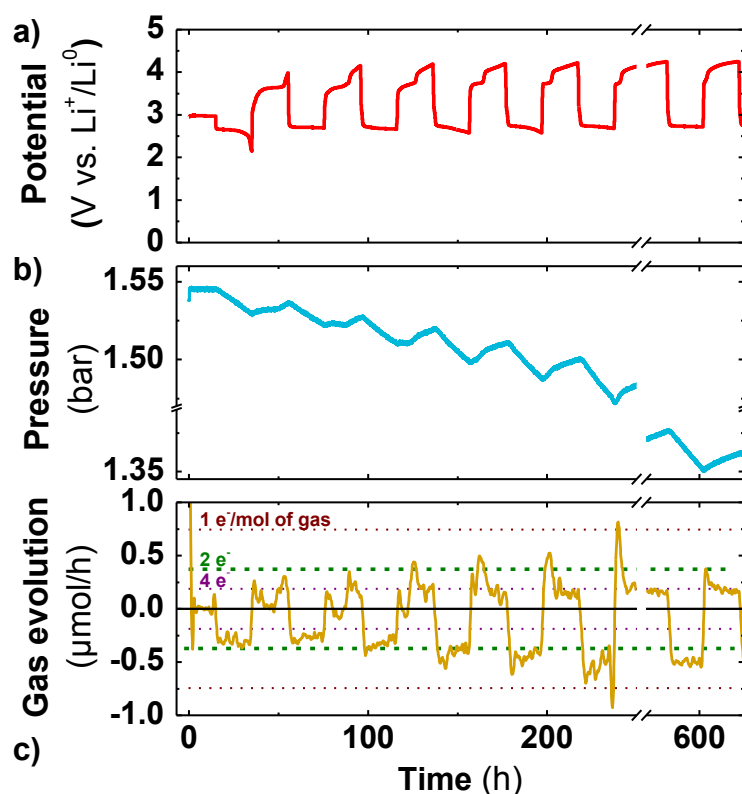


Figure 68: Potential-Time (a), Pressure-Time (b), and Gas Emission-Time (c) profiles of a Li/0.5 M LiTFSI + 10 mM LiI in TEGDME/Csp/O₂ cell cycled at 50 mA/gc with a limited capacity of 1000 mAh/gc.

None of the redox mediator tested herein were able to improve the long term cycling performances of the TEGDME-based system which, despite its common utilization in Li-O₂ batteries and over-optimists claims, suffers from important parasitic reactions at both the positive and the negative electrode. Being unable to minimize these undesired reactions, we focused on other electrolytes frequently used in the literature.

IV Influence of the glyme chain length

IV.1 DME vs. longer glymes

Our survey was extended to other glyme-based electrolytes to get further insights on the key role of their chain length on the performance of Li-O₂ cells. Aside DME – which was early reported in the Li-O₂ field as an alternative to carbonate-based solvents^{188,206} – we also focused on DEGDME which, despite being more volatile than TEGDME³⁶⁴, behave well for Li-O₂ batteries²⁴⁶ and even better for Na-O₂ batteries¹⁷⁸. The use of a medium chain length (*e.g.* DEGDME) led to identical Voltage-Time profiles (Figure 69a,b) to those obtained with TEGDME, which are associated with low gas evolution in charge (Figure 69c,d) and afterwards a poor round-trip efficiency on subsequent cycles. Not only the electrochemistry

but also the gas evolution and the aging of the cells upon cycling are strikingly similar for DEGDME and TEGDME, as observed when comparing Figure 69 and Figure 59 (p.91).

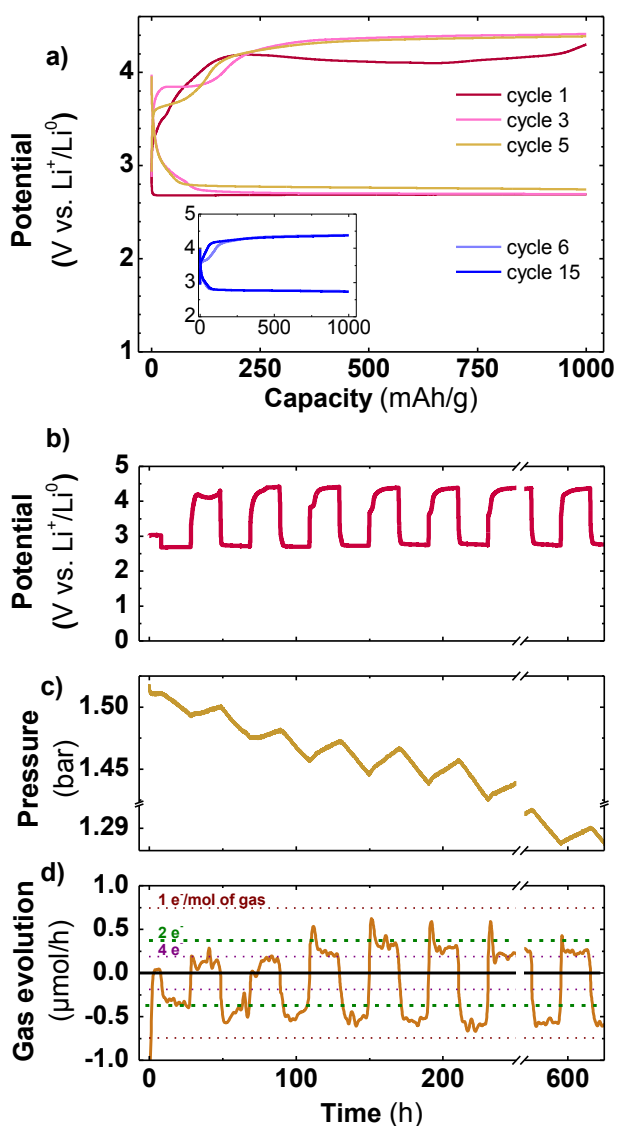


Figure 69: Voltage-Capacity (a), Voltage-Time (b), Pressure-Time (c) and Gas Emission-Time (d) profiles of a Li//0.5 M LiTFSI in DEGDME//Csp//O₂ battery cycled at a current of 50 mA/g_{carbon}, with a capacity limited to 1000 mAh/g_{carbon}.

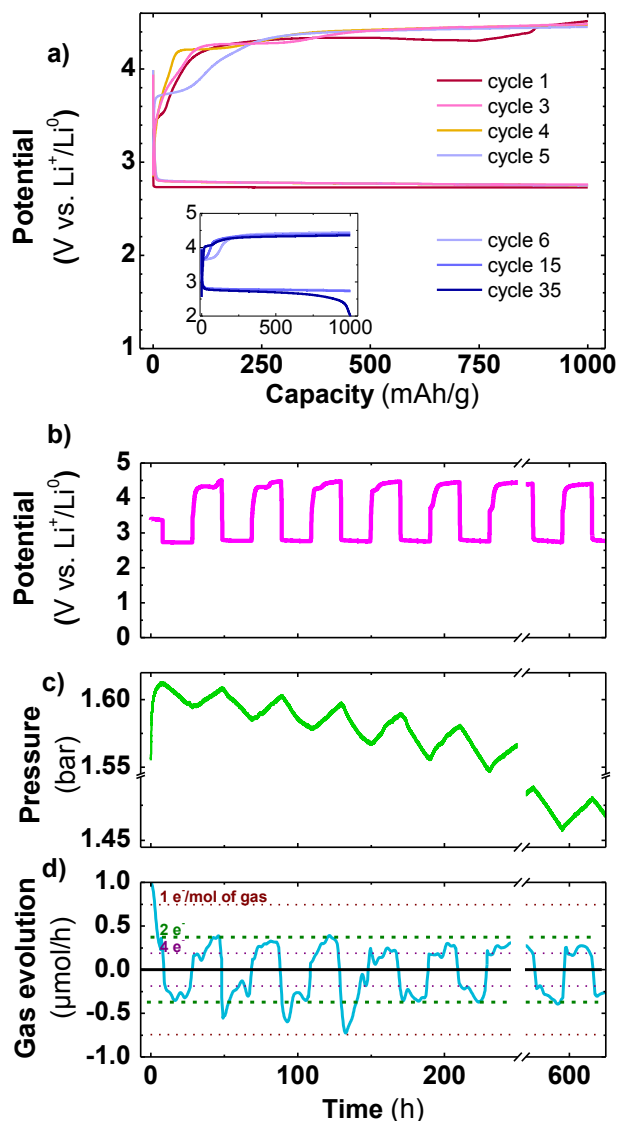


Figure 70: Voltage-Capacity (a), Voltage-Time (b), Pressure-Time (c) and Gas Emission-Time (d) profiles of a Li//0.5 M LiTFSI in DME//Csp//O₂ battery cycled at a current of 50 mA/g_{carbon}, with a capacity limited to 1000 mAh/g_{carbon}.

In contrast, glyme with shorter chain (*e.g.* DME) behaves differently (Figure 70). Although five formatting cycles are also necessary prior to reach the steady state, the gas evolution profile largely differs from the other glymes (DEGDME and TEGDME). Interestingly, the expected amount of gas is reached at the end of the three first charges for DME (Figure 70d), while a very low gas evolution was detected for DEGDME and TEGDME (Figure 69d and Figure 59d respectively). Moreover, gas emissions fluctuate a lot within one charge or discharge sequence, especially during the formatting cycles. This is consistent

with previous work of McCloskey and coworkers on the 1st cycle of a DME-based Li-O₂ cell which shows unsteady oxygen emission rates over the charging step which was requiring 3.2 e⁻/gas in average¹⁸⁸.

These results on glymes show clear evidence that DEGDME and TEGDME share a common mechanism towards ORR and OER, which is different from DME as deduced from the notable differences in their gas emission profiles. Acknowledging the similarities between TEGDME- and DEGDME-based systems, we focused on DME owing to its singular behavior and slightly better performances when compared to longer glymes (higher gas emissions in charge over the formatting cycles, less gas overconsumption in discharge...).

IV.2 Redox mediator in DME-based cells

Following our previous work using redox mediators, two cells using either 10 mM LiI + 0.5 M LiTFSI in DME or LiNO₃ saturated in DME as electrolyte were mounted to test if it could prevent the parasitic reactions encountered for DME-based cells. Note that a saturated (*sat.*) solution of LiNO₃ in DME was used because we could not dissolve 2 M. Based on the residual solid salt, the LiNO₃ concentration is < 1 M.

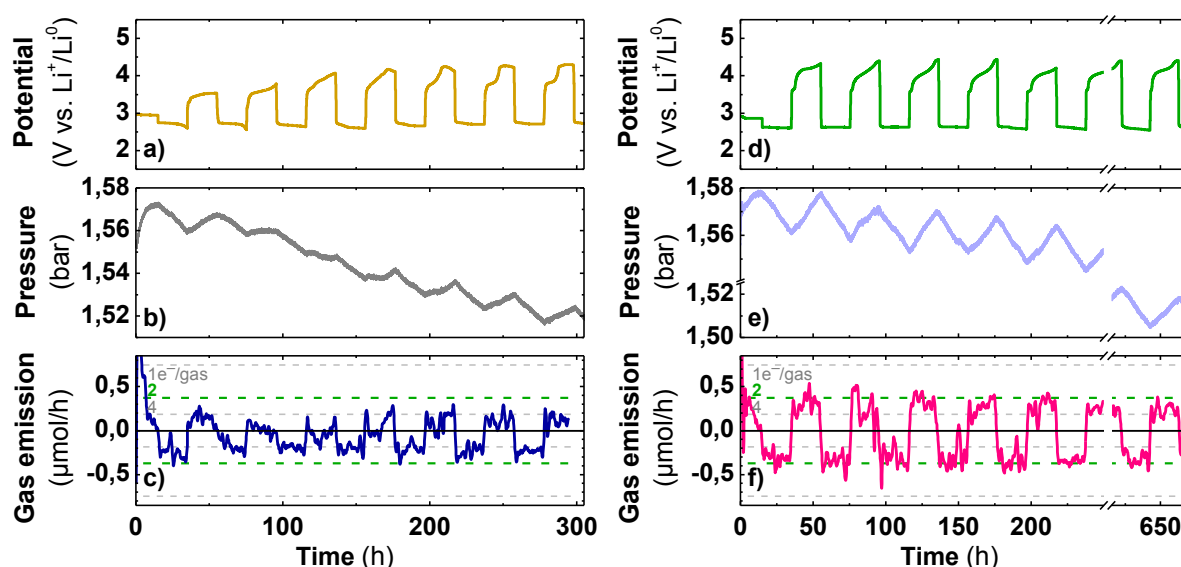


Figure 71: Potential-Time (a,d), Pressure-Time (b,e) and Gas Emission-Time (c,f) profiles of a Li//Csp//O₂ battery using 10 mM LiI + 0.5 M LiTFSI in DME (a-c) or LiNO₃ saturated in DME (d-f) as electrolyte. The current is 50 mA/g_{carbon}, and the capacity is limited to 1000 mAh/g_{carbon}.

Using LiI significantly reduces the cell polarization during the 3 first cycles, but it disturbs the pressure evolution which behaves abnormally in the meantime, hence indicating important parasitic reactions (Figure 71a,b). Their level remains high later on cycling (> 200 h) with gas emissions stabilizing around 3 and > 4 e⁻/gas in discharge and

charge respectively (Figure 71c), which leads to a cell death after 550 h of cycling. In contrast, the cell using LiNO_3 could sustain > 1000 h of cycling with an average gas emission of $2.1 \text{ e}^-/\text{gas}$ in discharge and $2.7 \text{ e}^-/\text{gas}$ in charge (Figure 71d-f). LiNO_3 thus reduces the amount of side reactions in charge when compared to the LiTFSI/DME system (Figure 70, $\sim 3.2 \text{ e}^-/\text{gaz}$), which is consistent with a lowering of the average charge plateau potential (4.07 V instead of 4.40 V), as shown in Figure 72. Curiously, the discharge plateau is also lower in presence of LiNO_3 (-0.17 V vs. the LiTFSI/DME system, and -0.14 V vs. the LiNO_3/DMA system) which might be due to a slower kinetics, or the lowest LiNO_3 concentration than in DMA. We did not investigate further this phenomenon.

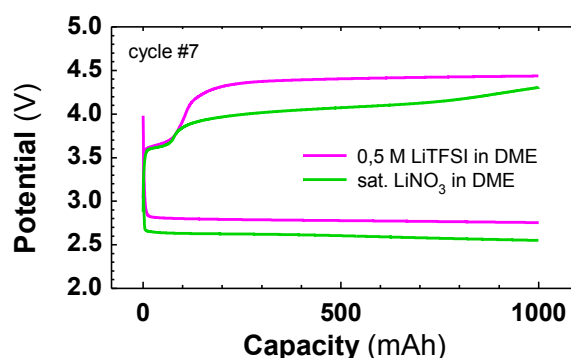


Figure 72: Potential-Time profile of the cycle #7 of a Li//Csp//O₂ battery using 10 mM LiI + 0.5 M LiTFSI in DME (cf Figure 70) or saturated (< 0.5 M) LiNO_3 in DME (cf Figure 71d-f) as electrolyte. The current is 50 mA/g_{carbon}, and the capacity is limited to 1000 mAh/g_{carbon}.

In short, we demonstrated the positive effect of using LiNO_3 in a DME-based system, which still exhibits slightly lower performances than the LiNO_3/DMA binomial. In contrast, no benefits were observed when using LiI as an alternative redox mediator neither in the TEGDME-based nor in the DME-based systems. This study shows that the use of a redox mediator is not sufficient for preventing the important side reactions occurring in glyme-based electrolytes. The latter are not suitable for long-term cycling when using carbon based electrodes, as previously reported, hence the need for more reliable electrodes and the study of other solvents such as DMSO as early proposed^{206,190}.

V Dimethyl Sulfoxide (DMSO)

We built some DMSO-based Li-O₂ cells and confirmed, via our experimental gas pressure setup, the consumption of $2.0 \text{ e}^-/\text{mol}$ of O₂ during the discharge process, implying that an oxygen reduction at a rate close to the one expected from *Reaction 1* (p.25) could be achieved and maintained over several dozens of hours of operation (Figure 73). However,

an average ratio of $2 e^-/\text{gas}$ over the whole charge could not be obtained owing to the reactivity of Li_2O_2 towards carbon, as reported by others¹⁹⁰. Presently, the charge was performed above 4.1 V, potential at which carbon is not stable. This implies a decrease of gas emissions leading to an equivalent value of 3 to $3.5 e^-/\text{gas}$ released and indicating extended side reactions. Hence, valuable information regarding the origin and role of these side reactions on cycling can be deduced from the pressure data as discussed in the next section.

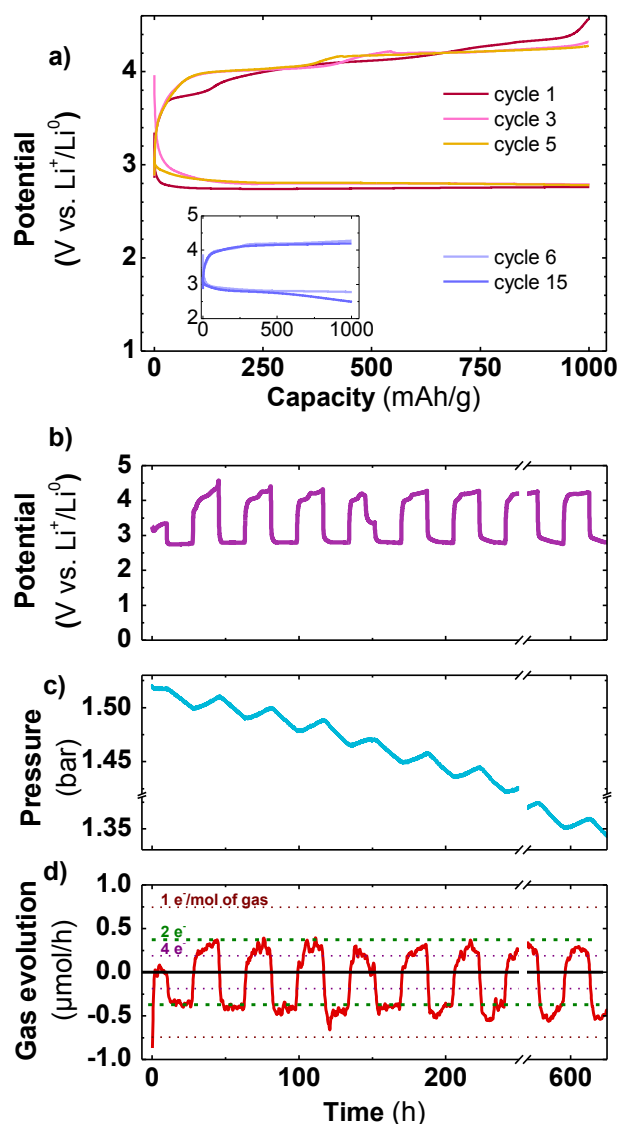


Figure 73: Voltage-Capacity (a), Voltage-Time (b), Pressure-Time (c) and Gas Emission-Time (d) profiles of a Li//0.5 M LiClO₄ in DMSO//Csp//O₂ battery cycled at a current of 50 mA/g_{carbon}, with a capacity limited to 1000 mAh/g_{carbon}.

V.1 Quantification of parasitic reactions

At this stage, for sake of clarity in quantifying the parasitic reactions associated to the electrolyte used in this study, all systems are compared in a single figure. The amount of

parasitic reactions is deduced from the ratio between the experimental and theoretical gas evolution rates, based on the assumption that a rate of $2 \text{ e}^-/\text{gas}$ would only involve oxygen (0 % of parasitic reaction). This ratio enables an estimation of the parasitic reactions, hence an assessment to the overall efficiency of the Li/O_2 reaction. These numbers, calculated from the pressure data, are summarized in Figure 74a for the first cycle and in Figure 74b once the steady state is reached (*i.e.* beyond the formatting cycles). Whatever the electrolyte considered, it is worth noticing the evolution in the level of parasitic reactions between the two figures, stressing the specificity of the formatting step previously mentioned. Please realize that the largest the percentage, the greater the amount of side reactions.

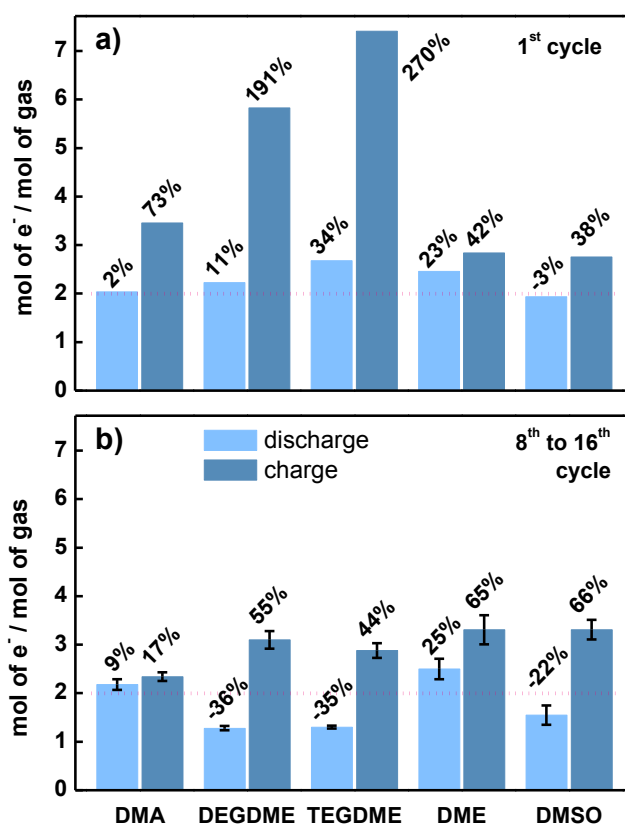


Figure 74: Estimation of the level of parasitic reactions as deduced from the gas evolution during the cycling of $\text{Li}-\text{O}_2$ cells, as a function of the electrolyte a) during the 1st cycle. For DME for instance, 2.46 and 2.84 e^-/gas were observed in discharge and charge respectively, corresponding to $(2.46-2)/2 = 23 \%$ and $(2.84-2)/2 = 42 \%$ of parasitic reaction. b) Average value from cycle #8 to cycle #16 (steady state). Error bars equal twice the standard deviation. Negative value indicates oxygen overconsumption. Horizontal dotted line is an eye-guide indicating the theoretical value.

Moreover, this figure conveys a few general trends of our electrolyte survey for $\text{Li}-\text{O}_2$ cells. We constantly observed that the first discharge is closer to the theoretical value than the subsequent ones, suggesting a progressive chemical deviation from the expected reaction with cycling. In contrast, the first charge always comes with gas emissions lower than expected, indicating irreversible transformations enlisting the formation of non-

volatile species which upon subsequent cycles enables, by a mechanism not deciphered yet, better efficiency.

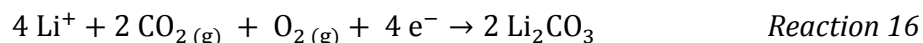
Overall, 2 M LiNO₃ in DMA appears as the most efficient electrolyte among those we investigated, although its efficacy and cycling performances are slightly lower than what was already published¹⁹³. This can be explained by the greater discharge capacity used in the present work (1000 mAh/g compared to 220 mAh/g). For sake of completion, the amount of parasitic reactions was also calculated in absence of LiNO₃ (LiTFSI/DMA electrolyte). It is lower during the 1st charge (no SEI formation) but higher in both charge and discharge over the steady-state domain (*cf* Annex 2).

For DMSO, we confirmed the presence of numerous parasitic reactions due to the use of a carbon electrode, an issue being presently solved by the development of efficient redox mediator (such as TFF) or carbon-free Au electrode^{261,190}. However, as it clearly appears in recent studies, high DN solvent such as DMSO tends to be unstable with the presence of O₂⁻ superoxide, and better solvent remain to be developed³⁶⁵.

Turning to glymes, we observed a large oxygen overconsumption during the steady state discharges for DEGDME and TEGDME but not for DME (Figure 74b), hence suggesting the importance of the glyme chain length. This overconsumption is likely due to parasitic reactions caused by the high reactivity of the superoxide radical formed during discharge, keeping in mind that the formation of O₂⁻ only requires 1 e⁻/O₂. Early reports suggest that glymes are intrinsically unstable in presence of O₂⁻ which will deprotonate a carbon of the ether chain, leading to polymerization or fragmentation into smaller molecules such as lithium acetate^{246,249}. On the contrary, other groups found that glymes, when intensively purified, were stable in presence of O₂⁻^{250,197}. This was confirmed by Schwenke *et al.* who demonstrated that only impurities, not clearly identified for commercial solvents, were directly reacting with O₂⁻²⁴⁵. Our results corroborate this explanation since the solvents used here were not furtherly purified besides drying with molecular sieve. Moreover, certificates of analysis indicate 1000/1200 ppm of impurities for TEGDME/DEGDME, much more than for DME (100 ppm). The DME is much easier to purify industrially because of its low boiling point (85 vs. 162 and 275 °C for DEGDME and TEGDME, respectively) which explains why high purity DME was commercially available as opposed to other glymes. Note that the overconsumption resulting from these impurities is never observed during the first cycle, which emphasizes the added value of using our pressurized Li-O₂ cells enabling gas monitoring over long-term cycling.

A more straightforward and likely explanation is nested in the aptitude of the electrolyte to absorb CO₂ as frequently reported in the literature^{366,179,367}. This gas, whose

origin will be explained in the next paragraph, might accumulate in the gas reservoir and lead to a Li-O₂/CO₂ battery. In presence of O₂ and CO₂, the system might follow the equation:



which corresponds to a ratio of 1.33 e⁻/gas, equivalent to a gas evolution of 0.56 μmol/h. The gas consumption rates observed in discharge using TEGDME (Figure 59d) and DEGDME (Figure 69d) are close to this value and even higher, suggesting that the presence of both solvent impurities and CO₂ might be responsible for the gas overconsumption. The formation of Li₂CO₃ could not be detected by XRD at the end of the second discharge; nevertheless this does not eliminate its presence as amorphous phase.

Parasitic reactions occurring during the charge of Li-O₂ cells are numerous, mainly due to the lack of stability of the cathode material. For instance, the release of CO₂ upon charge resulting from the decomposition of Li₂CO₃ coming from the corrosion of the carbon electrode by Li₂O₂ was independently demonstrated for DME and DMSO-based electrolytes by Luntz's and Bruce's groups respectively, via isotopic labelling of carbon and oxygen^{229,230}. This Li₂CO₃ decomposition could explain the spikes observed at the beginning of each charge for DEGDME and TEGDME in Figure 69d and Figure 59d respectively, during which gas is produced at a rate close to 0.56 μmol/h in accordance with *Reaction 16*. Beside CO₂, H₂ emissions were also reported by Addison's group for DMA-based Li-O₂ cells¹⁹³, and by Luntz's group in the case of glymes and DMSO^{183,188}.

VI Conclusions

In this chapter, we carried out an electrochemical survey of various electrolyte configurations used so far in this field, and from comparative studies, we could deduce that LiNO_3 in DMA was among the best of today's electrolytes, followed by LiNO_3 in DME and DMSO. We demonstrated the accuracy of our new setup and the possible use of impedance spectroscopy for carefully studying parasitic reactions in Li- O_2 cells

Overall, the omnipresence of these parasitic reactions, easily identified *via* the presently reported pneumatic data, tremendously affects the efficiency of C-based Li- O_2 systems. In this work, it was shown that all the components of the battery were affected by such unwanted reactions, namely i) the corrosion of the carbon at the positive electrode in glyme-based and DMSO-based cells when potentials were greater than 3.8 V upon charge, ii) the oxidation of the electrolyte and its impurities in DEGDME- and TEGDME- based cells, and iii) the instability of the metallic lithium anode.

If a few stable alternative positive electrodes have already been proposed (*e.g.* Au or TiC), the utilization of lithium metal remains a challenging issue, as indicated by its fast degradation in a TEGDME-based cell. Herein, we demonstrated that it could not be protected by LiNO_3 without jeopardizing the overall cell performances, hence calling for the development of new strategies such as the utilization of another anode material (for instance lithiated silicon Li_xSi) instead of Li. The next chapter will therefore be dedicated to develop a suitable silicon-based electrode capable of maintaining a high capacity for multiple cycles. In order to solve more efficiently the issues related to the lithium-silicon chemistry itself, Si composite electrodes will first be studied in half cell configuration. In a second stage, we will present the different prelithiation methods which can be used for obtaining an Li_xSi electrode, prior to consider their utilization in full $\text{Li}_x\text{Si-O}_2$ cells.

CHAPTER 4: DEVELOPMENT OF SI COMPOSITE ELECTRODES AS ANODE IN $\text{Li}_x\text{Si-O}_2$ BATTERIES

Owing to the strong parasitical reactions hindering the utilization of Li metal in practical Li-O₂ cells, we considered the use of lithiated silicon (Li_xSi) as alternative Li source for the system. Prior to integrate such electrodes in full $\text{Li}_x\text{Si-O}_2$ cells, we focused on mastering the Li-Si alloying process and investigate the effect of a few pre-lithiation techniques which, in addition to the lithiating the electrode, also tend to improve their overall performances.

I Si composite electrode with good cycling performance

In order to minimize the amount of parasitic reactions evidenced at the negative electrode in the former chapter, but also to improve the safety of practical Li-O_2 batteries, we decided to replace lithium metal by another anode material. Bearing in mind the research undertaken by the Li-ion community to deal with this issue and owing to the high capacity achieved at the positive electrode in Li-O_2 systems, our attention has focused on lithium-metal alloys and more especially the Li-Si binary which has a theoretical capacity of $3579 \text{ mAh/g}_{\text{Si}}$. However, Si particles are subject to huge volumetric changes upon lithiation (up to 275 % for the $\text{Si} \rightarrow \text{Li}_{15}\text{Si}_4$ reaction), which implies severe drawbacks including i) the cracking of the particles, ii) the loss of the percolation network between the particles of active material and iii) the promotion of side reactions (*i.e.* solvent reduction) owing to the creation of fresh surface newly exposed to the electrolyte at each cycle^{89,112,113,287,288,296,368}. These limitations are particularly challenging within the context of a $\text{Li}_x\text{Si-O}_2$ battery since they come in addition to parasitic reactions at the air cathode, which both decrease the amount of available Li in the system.

Several strategies have been developed in the literature to minimize this phenomenon and are discussed in this chapter. They enlist the size reduction of the silicon particles, the formulation of composite electrodes, and the use of electrolyte additives. Since Si has to be lithiated prior to be used in Li-O_2 cells, we will then investigate the different ways to pre-lithiate our electrodes. Depending on the technique used, we will demonstrate that these treatments may also improve the performances of Si electrodes through the reduction of the native SiO_2 layer coating the Si particles; a phenomenon which can be extended to pure SiO_2 particles. Finally, the feasibility of using Li_xSi electrodes as anode in Li-O_2 batteries will be discussed together with the limitations of such strategy and its possible ameliorations.

I.1 Composite electrode preparation

Owing to the significant swelling/shrinking of silicon upon its (de)lithiation, it cannot be used pure as anode material otherwise than in thin films, which do not provide a sufficient loading for our application. So far, the best results with higher Si loadings were obtained by developing composite electrodes comprising, in addition to Si particles, a binder suitable for enhancing the electrode mechanical integrity^{116–118,296,298,300,301} and carbon particles for improving the electronic conductivity.

In this thesis, silicon composite electrodes were made using a recipe developed by Bridel *et al.*³⁰⁰. A slurry was prepared by mixing the silicon powder, the Csp and the binder in deionized water with a Si/Csp/CMC ratio of either [2:1:1] or [1:1:1] depending on the batches. Further information concerning the nature and the origin of the silicon powders used to prepare the electrodes will be given in section I.2. Note that due to a natural air-exposure, Si particles may be recovered by a SiO_2 layer accounting for a non-negligible fraction of the Si content, and will therefore be referred to as Si/ SiO_2 particles. Na-Carboxy-Methyl-Cellulose (Na-CMC, Aldrich) with a molecular weight of 700 000 g/mol and a degree of substitution (DS) = 0.9 (\pm 0.1) was here used as polymeric binder. The three powders (Si/Csp/CMC) were first intimately mixed together by hand with a mortar and pestle prior to the addition of water, and the obtained slurry was then mechanically mixed for 2 minutes using a vertical rotor disperser (Ultra-Turrax®) spinning at \sim 15 000 rpm to ensure a good homogeneity. The syrup-like mixture was then casted on a 15 μm thick copper foil with a 450 μm slit and was left for drying in air overnight (Figure 75). 12.7 mm (1.27 cm^2) discs were punched out of this film and dried further at 105 $^\circ\text{C}$ under vacuum (\approx 20 mbar) before being transferred into the glove box without subsequent air exposure. The total powder loading per disc is \approx 2 mg (i.e. 10 % of the total powder + disk weight), which represents 1.6 mg/cm^2 . Hence, the typical loading of Si (or Si/ SiO_2) is comprised between 0.5 and 0.6 mg/cm^2 (0.6 to 0.7 $\text{mg}/\text{electrode}$). If not specified otherwise, the gravimetric capacities will refer to the mass of Si + SiO_2 regardless of the Si/ SiO_2 ratio.

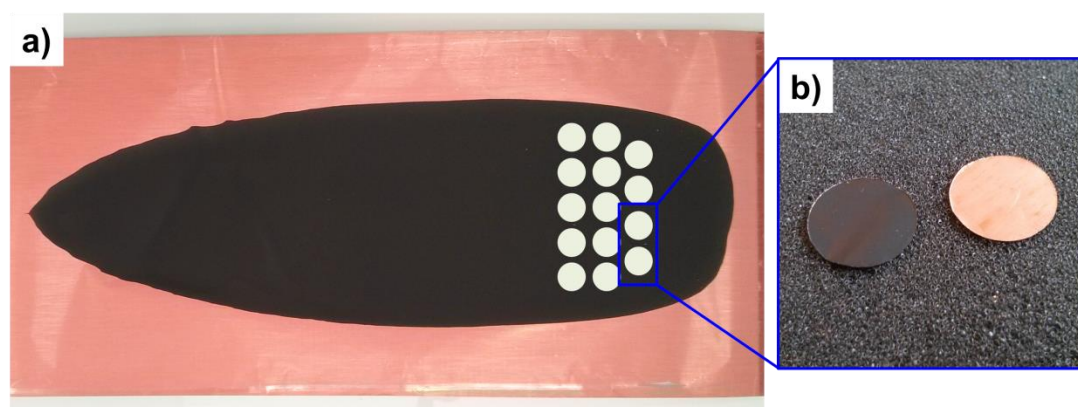


Figure 75: Photographs of a Si/ SiO_2 /Csp/CMC (1:1:1) film coated onto a Cu foil (a) and the corresponding 12.7 mm composite electrodes (b), recto and verso.

Due to the hydrophobicity of their pristine surface (Figure 76a) the Cu substrates had to be treated prior to coat the slurry. In that purpose, a thermal treatment consisting of heating the pristine substrate with an air gun set at 580 $^\circ\text{C}$ was used to form a thin layer of copper oxide reducing the hydrophobicity (Figure 76b).

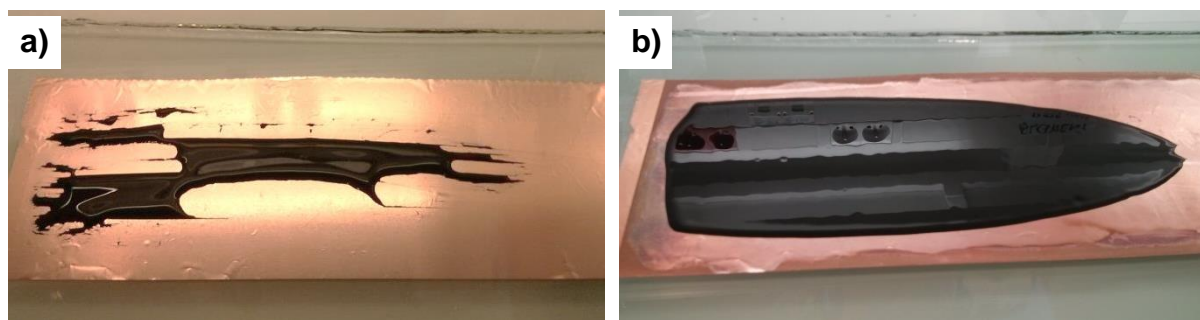


Figure 76: Photographs of two films freshly coated onto an untreated (a) and a treated (b) Cu substrate.

The homogeneity of the dried coating was determined by cutting and weighting 32 electrodes out of the same film, which evidences a Si loading distributed around a value of about 0.61 mg according to a Gaussian law (Figure 77). For this batch, 76 % of the electrodes deviates by less than 3.3 % from the average, and the Standard Deviation / Average (SD/A) ratio is 2.9 %.

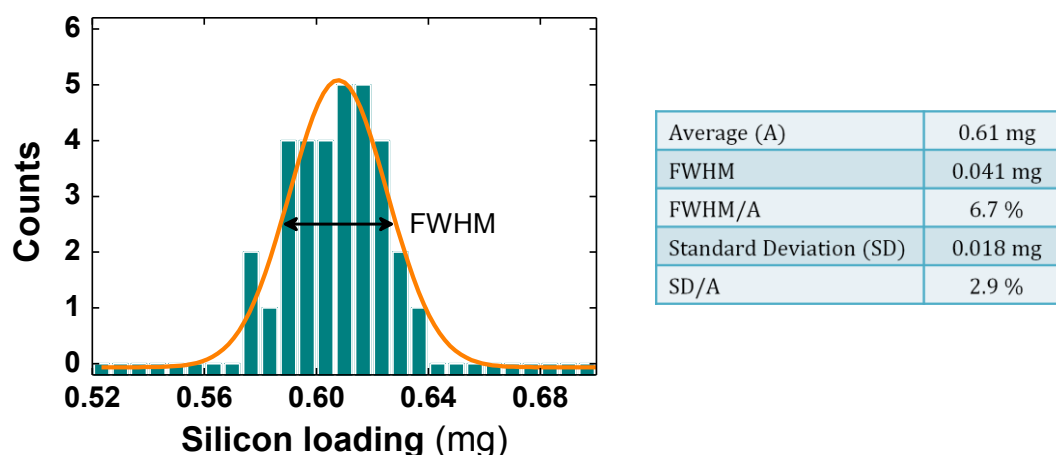


Figure 77: Mass distribution of 32 electrodes cut out of the same Si/Csp/CMC film.

Such good values testify of a good coating homogeneity enabling reproducible and trustworthy electrochemical tests.

I.2 Influence of the particle size on the cycling performances

As earlier mentioned, the utilization of Si as anode material in Li-O₂ batteries sets two main requirements which are i) a large capacity matching that of the cathode and ii) a good cycling retention which indicates no (or few) side reaction. Based on former studies, these characteristics are mostly governed by the size of the Si particles. Therefore, we first studied the effect of the particle size on Si composite electrodes prepared with three types of commercial Si particles: < 42 μm , 1-3 μm , and 100 nm (Alfa Aesar) denoted L-Si, M-Si and Si NP – for Large, Medium and Nano Particles – in the following (Figure 78).

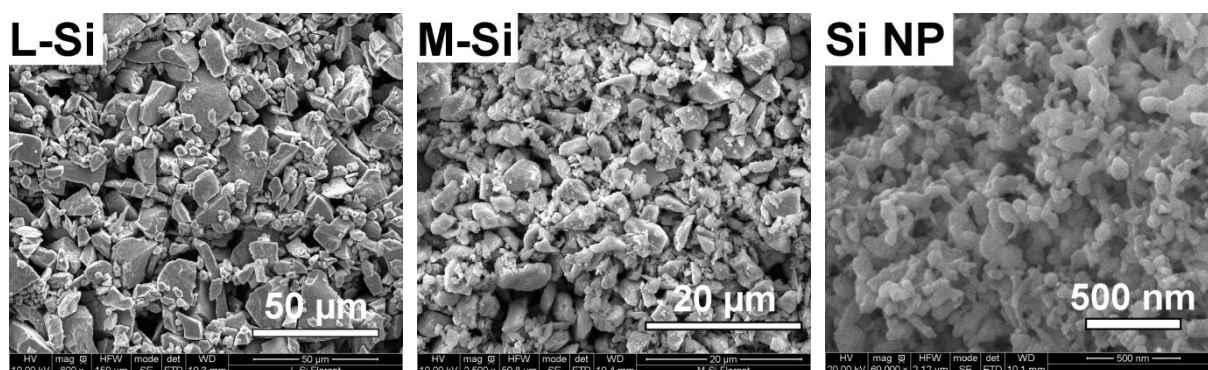


Figure 78: SEM images of L-Si (a), M-Si (b) and Si NP (c) particles as purchased.

Figure 79a shows major differences in the electrochemical behavior of Si/Csp/CMC//Li half-cells with respect to the particle size. The results obtained with the larger particles (L-Si & M-Si) are consistent with former reports using micrometric Si particles, with a 1st discharge/charge capacity close to the theoretical value (the slight overshoot in discharge is likely due to electrolytes degradation) and a charge plateau at ~ 0.4 V indicating the delithiation of the crystallized $\text{Li}_{15}\text{Si}_4$ phase. However, these electrodes suffer from a fast capacity decay upon cycling (Figure 79b) which decreases of 60 % during the 5 first cycles. This contrasts with the cell using Si NP which shows a sustained reversible capacity slightly increasing upon cycling and which corresponds to $\frac{1}{4}$ of the theoretical capacity of Si. Aside this low capacity – whose origin will be discussed in a following section – these results do not come as a surprise. They are further confirmed by previous literature reports showing that the best cycling performances are obtained for Si electrodes made of smaller particles.

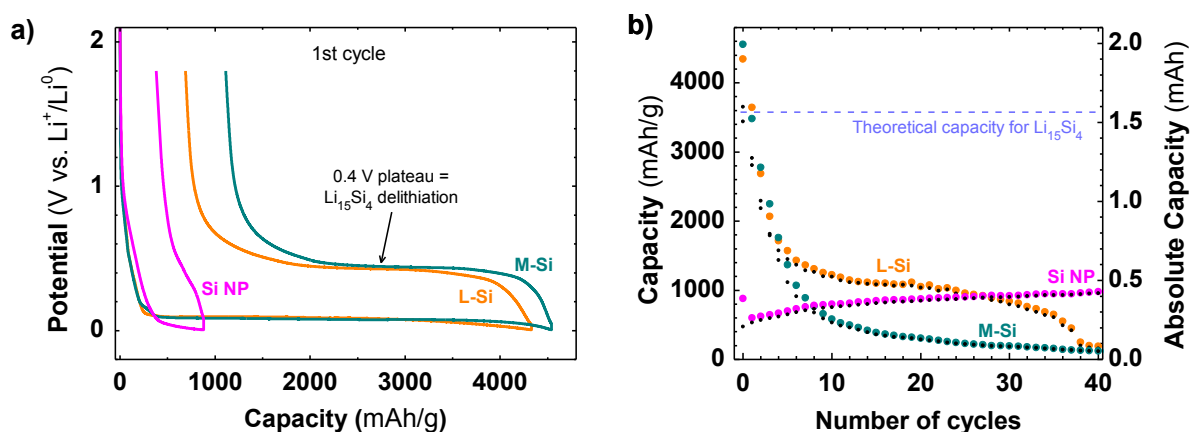


Figure 79: Voltage-Capacity (a) and Cycling Retention profile (b) of a Si/CMC/Csp[2:1:1]//LP30//Li half cell cycled at $C/2$ between 0 and 1.8 V as function of the Si particle size: $< 42 \mu\text{m}$ (Si-L); $1-3 \mu\text{m}$ (Si-M), and 100 nm (Si NP). In (b), colored dots = discharge, small black dots = charge.

Considering such results, the development of a long cycle-life Si electrode with high capacity thus requires either i) improving their cycle-life, or ii) increasing their overall

capacity. Both strategies will be explored in the next sections, starting with the utilization of an electrolyte additive aiming at improving the cycling retention of larger particles.

I.3 Improving the cycling retention of M-Si-based electrodes

Fluoroethylene carbonate (FEC) and vinylene carbonate (VC) are often used as electrolyte additives for Si-based cells in view of promoting the formation of a protective and flexible SEI able to accommodate the volume changes of Si particles upon cycling. With this in mind, various amounts of FEC were added to the electrolyte of a cell containing an M-Si based electrode with a M-Si/Csp/CMC ratio of [2:1:1] (Figure 80a). Within such configuration, the presence of FEC shows no effect on the cycling retention. This suggests that the fast capacity decay is rather due to the loss of electrical contact between the particles of active material, than to an SEI-related issue.

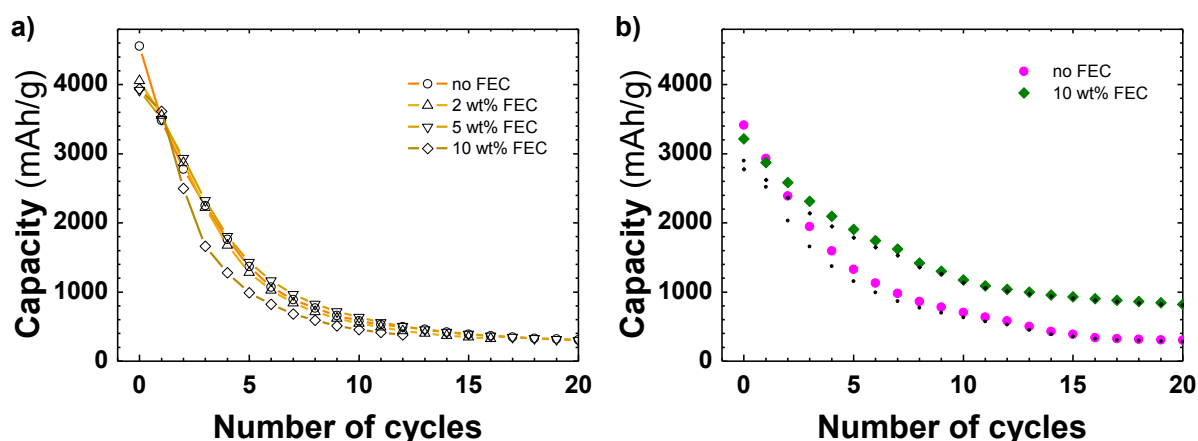


Figure 80: Cycling retention profiles of a M-Si/CMC/Csp[2:1:1]//Li (a) and a M-Si/CMC/Csp[1:1:1]//Li (b) half-cell cycled at $C/2$ between 0 and 1.8 V using LP30 as electrolyte with various amounts of FEC added. In (b), colored dots = discharge, small black dots = charge. For sake of clarity, (a) only shows the discharge capacity.

In order to maintain the electrical percolation between the Si particles upon cycling, the electrode formulation – Si/Csp/CMC ratio – was modified from [2:1:1] to [1:1:1]. The larger amount of binder provides better mechanical properties to the electrode, while the higher C ratio counterbalances the insulating nature of the binder. Figure 80b shows that decreasing the Si ratio does not significantly modify the electrochemical behavior of the electrode when cycled in LP30. However, this formulation exhibits better performance in presence of FEC, which enables a quasi-stabilization of the capacity at ~ 1000 mAh/g after the 10th cycle.

In summary, M-Si based electrodes are very attractive owing to their high initial capacity, but their practical utilization as anode in Li-O₂ batteries is hindered by their poor cycling retention, which could only be slightly improved by using FEC and decreasing the Si

ratio down to 33 %. Facing the numerous difficulties encountered with large Si particles, we focus our attention on the Si NP.

I.4 Improving the capacity of Si NP electrodes

As opposed to large Si particles, the Si NP electrodes show a low initial capacity ($\sim 750 \text{ mAh/g}$, $\approx 1/5$ of the theoretical capacity) which increases upon cycling (Figure 79b). However, even after 40 cycles, their capacity would hardly match those of a Li- O_2 cathode discharged at $1000 \text{ mAh/g}_{\text{carbon}}$ ($\equiv 0.4 \text{ mAh}$). The pristine Si NP were thus characterized with the hope to understand the origin of their low capacity and to provide solutions to enhance it.

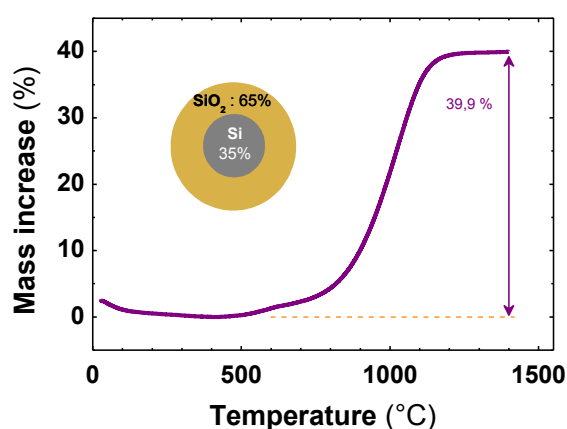


Figure 81: Thermogravimetric analysis (TGA) of the commercial Si NP (O_2/N_2 dry atmosphere, 10 K/min up to 1400°C).

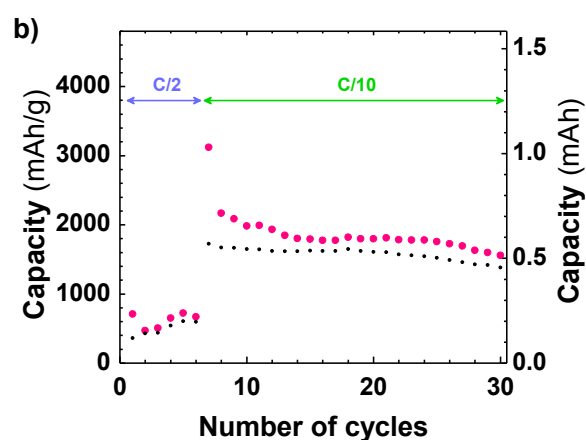


Figure 82: Cycling retention of a Si NP/CMC/Csp[2:1:1]/LP30//Li half-cell cycled between 0 and 1.8 V at C/2 (cycles #1 to #6) then at C/10 (from cycle #7). Colored dots = discharge, small black dots = charge.

From the mass increase (39.9 %) measured by TGA (Figure 81), the amount of Si in commercial Si NP was estimated to be 35.0 wt% (*i.e.* 65.0 wt% of SiO_2). The large fraction of SiO_2 is due to the high reactivity of the surface of the particles owing to their nanometric size and their shipment/handling under ambient atmosphere (air). By assuming a homogeneous coating of the Si particles, we could calculate the SiO_2 coating thickness to be between 11 and 14 nm (see Annex 3 for the thickness calculation and more SEM pictures). Based on a former report³⁶⁹, a coating of 7 to 15 nm would greatly affect the capacity of the Si NP owing to significant kinetic limitations. This hypothesis was confirmed by the capacity increase (from 800 to $\sim 2000 \text{ mAh/g}$) observed after changing the rate from C/2 to C/10 (Figure 82). Nevertheless, the cell exhibits a good cycling retention at C/10 since it was able to perform 25 cycles above 1500 mAh/g (0.5 mAh).

This is certainly sufficient for the preliminary testing of Li_xSi-O₂ cells, but the long-term application still requires a significant improvements regarding i) the capacity decay, ii) the coulombic efficiency – defined at the ratio between the capacity which can be obtained from the cell over the capacity which was formerly provided to that cell – and iii) the ability to maintain a high capacity at a high rate. These issues are addressed next by discussing the possible techniques used for pre-lithiating our Si electrodes.

II Influence of the pre-lithiation onto Si NP and their SiO₂ shell

Based on the best performances obtained for Si NP, such particles with an average size of 100 ± 50 nm will thus be used to carry out the prelithiation treatments. They will be referred as Si/SiO₂ NP owing to the large fraction of SiO₂ (65 wt%) at their surface.

II.1 Electrochemical pre-lithiation techniques

Lithiated silicon electrodes (Li_xSi) were obtained after an *in situ* electrochemical pre-lithiation *via* one of the four different techniques described next:

- The first one consists in cycling the Si electrode in a galvanostatic mode for one (or a few) cycle(s), and stopping the cell at the end of discharge (0 V vs. Li⁺/Li⁰). A low current density is used during this last discharge to maximize the electrode capacity.
- The second procedure (denoted "*shorted*" cells) consists of an externally controlled short circuit made by connecting, for a few to dozens of hours, both sides of the cell with a 100 Ohm resistor while monitoring the potential variation (Figure 83a). This step, equivalent to a "constant load discharge" (load = 100 Ω) is followed by a galvanostatic re-oxidation of the sample until 1.8 V vs. Li⁺/Li⁰.
- The third one (denoted "*plated*" cells, or PL) involves the application of a constant discharge current ($I_{PL} = -480 \text{ mA/g}$) without any cutoff voltage limitation so that the potential can reach negative values, thus enabling lithium plating to occur near -30 mV vs. Li⁺/Li⁰ (Figure 83b). Afterwards, Li plating proceeds as long as the negative current is applied. The charge involved during the plating sequence is $Q_{PL} = I_{PL} * t$, with t = duration of the discharge current (grey area in Figure 83b). A typical plating sequence (~ 20 h; $Q_{PL} \approx 6 \text{ mAh}$) provides nearly ~ 10 times the amount of Li necessary to fully lithiate the 0.6 mg Si/SiO₂ electrode ($0.78 \text{ mAh} \equiv 1300 \text{ mAh/g}$). On recharge, lithium stripping first

occurs at around + 25 mV vs. Li^+/Li^0 along a plateau and then, silicon starts to be delithiated as the voltage departs from this plateau.

- The fourth formatting method consists of a time-limited *potentiostatic discharge* by imposing a positive potential lying below the potential of formation of the Li-Si alloys instead of imposing a negative constant current (Figure 83c). We chose + 2 mV vs. Li^+/Li^0 so as to provide a strong driving force towards lithiation while keeping full control of the reaction and preventing lithium plating. The total charge (Q) of the potentiostatic discharge is easily measured with an accuracy of 0.4 % and can be split in two terms ($Q = Q_{\text{rev}} + Q_{\text{irrev}}$) as displayed in Figure 83c. The accuracy was determined bearing in mind the background noise and the current precision of the cyler (see Annex 6 for the detailed calculation).

Once pre-lithiated, the cells are further cycled in a galvanostatic mode (*post cycling*; 0-1.8 V; C/2) so as to verify the level of lithiation which was achieved, and observe any modifications of the electrochemical behavior of the treated cell.

In addition to the formation of Li_xSi , the use of different lithium pretreatments led to different electrochemical behavior for the treated cells. This was an impetus for studying the effects of the length and nature of the treatment on Si half-cell, as presented in the next paragraph.

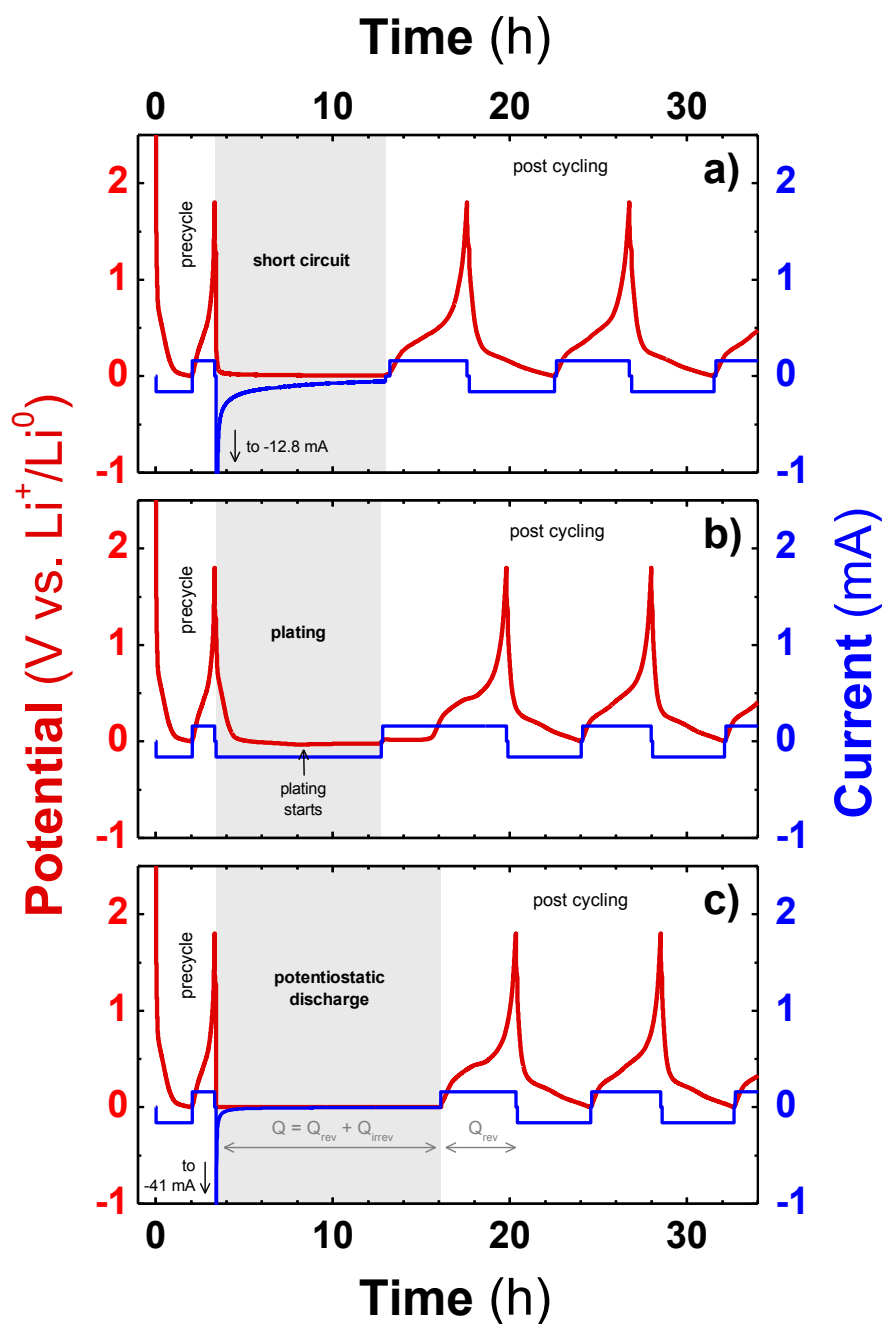


Figure 83: Voltage- & Current-Time profiles of Si/SiO₂/Csp/CMC // LP30 + 10% FEC // Li half-cells treated with (a) a controlled short-circuit, (b) a plating sequence, and (c) a potentiostatic discharge. Grey areas represent pretreatment sequences. Note that the length of the arrows in (c) representing the total Q and Q_{rev} capacities cannot be compared since the former is obtained under a floating current while the latter is at constant current.

II.2 Improved performances of prelithiated Si NP electrodes

II.2.a Effect of a short-circuit and a plating sequence

The galvanostatic profile of untreated electrodes shows sloping (dis)charge steps (Figure 84a,b) and derivative dx/dV traces evidencing two broad charge peaks (0.30 and 0.49 V) mirrored by two broad discharge signals (0.21 and 0.06 V) (Figure 84e). The

absence of a charge plateau at 0.4 V indicates the non-formation of the crystallized $\text{Li}_{15}\text{Si}_4$ phase, in agreement with previous reports on Si nanoparticles^{370,371} or indicating kinetic limitations. The first discharge (660 mAh/g) and charge (250 mAh/g) capacities are much lower than expected based on the Si^0 content of the powder (1250 mAh/g) but they slowly increase while cycling to finally reach a maximum (865 mAh/g) after ~ 100 "activation" cycles (Figure 84f). The increase in capacity can be attributed to a progressive cracking of the SiO_2 layer that improves the accessibility to Si and therefore its lithiation. It is confirmed by i) the increase in intensity of the broad peaks associated to the Li-Si alloying in the derivative plots (Figure 84e), and ii) the apparition of a small sharp peak at 0.45 V indicating the formation of the fully lithiated $\text{Li}_{15}\text{Si}_4$ crystalline phase.

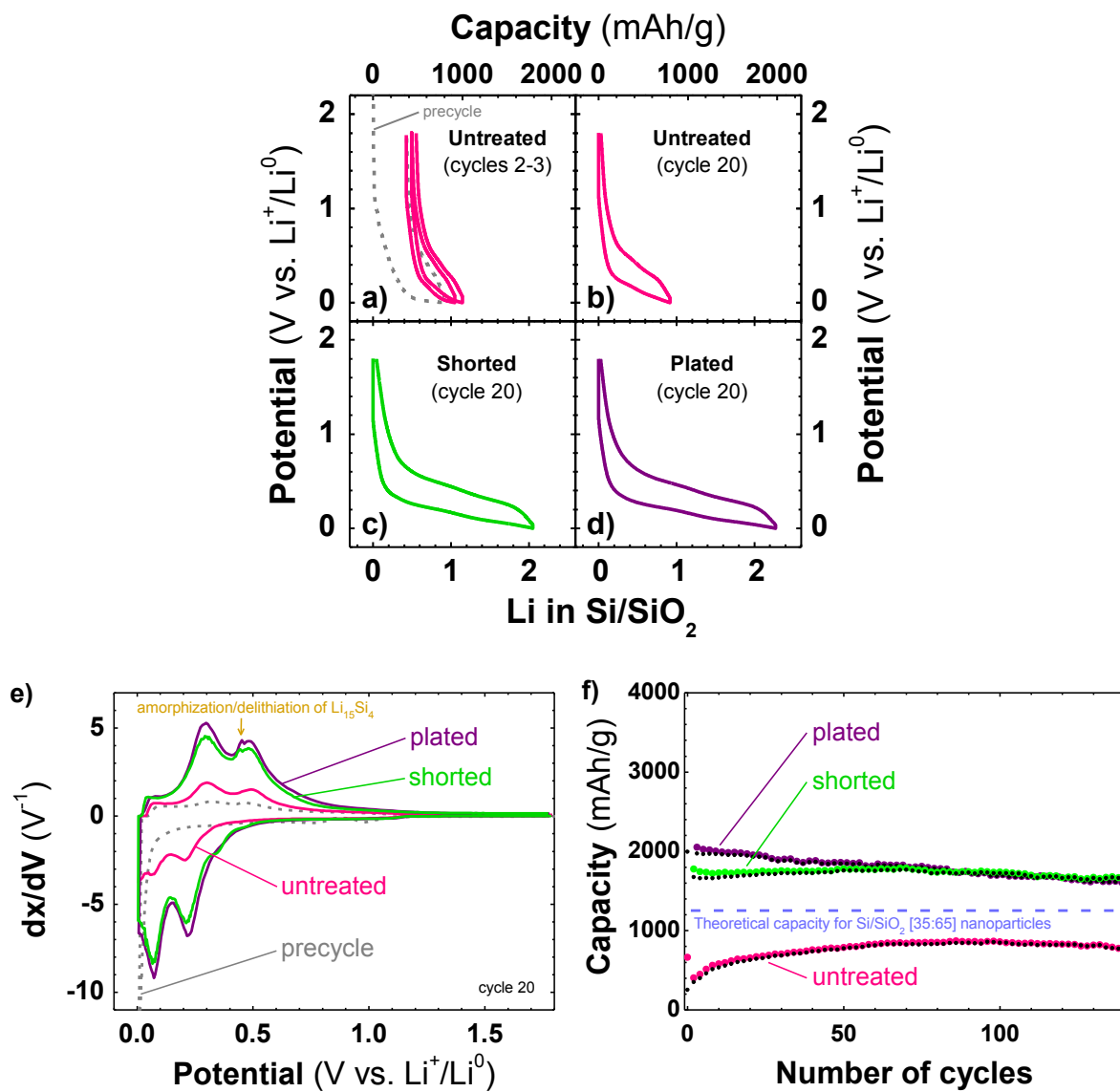


Figure 84: Voltage-Composition profiles (a-d), Derivative Capacity profiles at cycle #20 (e), and Capacity Retention plot (f) of untreated, plated or shorted $\text{Si/SiO}_2/\text{Csp}/\text{CMC} // \text{LP30} + 10\% \text{FEC} // \text{Li}$ half-cells. The current is $480 \text{ mAh/g}_{\text{Si/SiO}_2}$ ($\sim \text{C}/2$). In (f), colored dots = discharge capacity, small black dots = charge capacity.

In order to more rapidly reach this maximum in capacity, electrodes were prelithiated by either plating or short-circuiting the cell as described in section II.1 and in Figure 83a,b. Both prelithiated electrodes show sustained capacities with values that are more than twice those of untreated electrodes (~ 1800 mAh/g vs. ~ 800 mAh/g) (Figure 84c,d,f). This confirms the efficacy of the formatting steps to lithiate the Si core. Surprisingly, these high capacity values exceed by far the expected maximum theoretical capacity solely based on the initial Si^0 metal content (1250 mAh/g). However, this excess of capacity is clearly associated to the reversible Li-Si alloying process, based on the evolution of the derivative plots (Figure 84e) which show more intense (dis)charge Li-Si characteristic features, implying that both pre-treatments increase the quantity of electrochemically active silicon. This result is of practical importance since such electrodes having enhanced capacities show also good cycle life with capacity decays ranging from 2 % (*shorted* cell) to 15 % (*plated* cells) over 100 cycles. It is worth noting that the capacity decay is higher in absence of FEC in the electrolyte (15 % in 40 cycles for the plated cell, *cf* Annex 7).

Regarding the plating process, a question is to know if the increase in capacity is due to an electrochemical process (*i.e.* requires a reducing current) or to a chemical one resulting from the contact between the plated Li and the Si electrode (*i.e.* occurring even at the OCV). To answer this question, we compared the capacity of some cells left at the OCV after a short plating sequence to other cells plated for a long time (Figure 85). The Capacity-Retention plot (Figure 85b) shows the necessity of applying a reducing current for reaching a high capacity relatively quickly (20 h of plating gives a better capacity than 50 h of OCV). A slight increase of the capacity with the resting time is nonetheless observed, which confirms the existence of a very slow chemical process creating active Si domains from SiO_2 while consuming the plated Li. The latter is indicated by the absence of charge plateau at ~ 0.2 V (typical to Li stripping) beyond 20 h of OCV. When no plated Li remains, the electrode starts to be self-delithiated as evidenced by the slope break of the open circuit potential at around 30 h (Cell 3). This self-discharge phenomenon will be more carefully examined in section III.2.a which focuses on recovering the Si electrodes after the prelithiation.

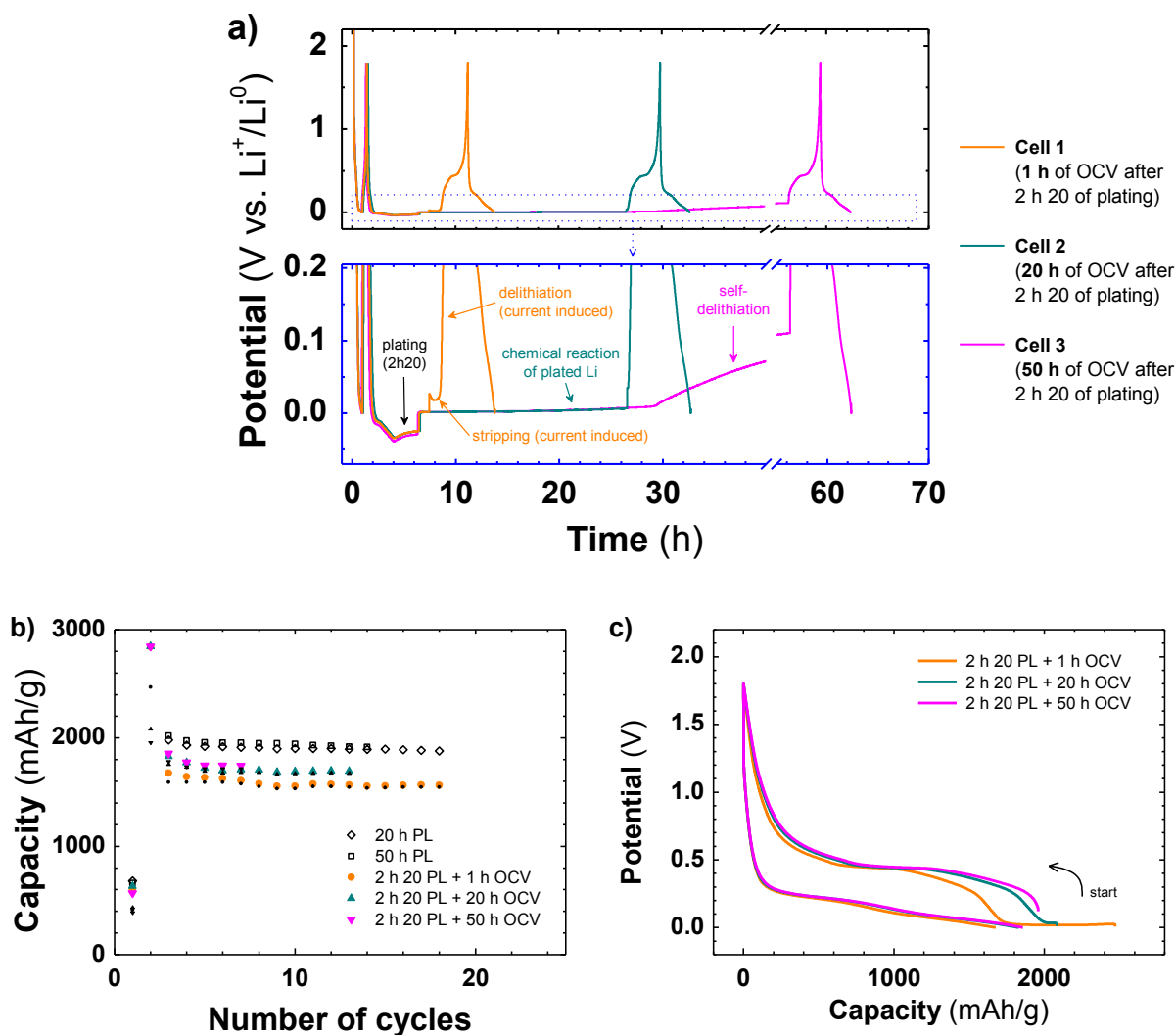


Figure 85: Potential-Time (a), Capacity Retention (b) and Potential-Capacity (c) profiles of three $\text{Si}|\text{SiO}_2/\text{Csp}/\text{CMC}$ [2:1:1] // LP30 + 10% FEC // Li half-cells as function of the resting time following a 2h20 plating sequence. For sake of clarity, only the first cycles are plotted in (a). In (b), colored dots = discharge, small black dots = charge, and the discharge capacity of two cells plated for 20 and 50 h was added for comparison.

II.2.b Investigating the SiO_2 reduction process using a potentiostatic discharge

To further exploit the capacity increase phenomenon – which cannot be adequately controlled by either lithium plating or a short circuit – we explore a potentiostatic discharge protocol as an alternative mean to prelithiate the Si electrode, with the hope of preserving the cycling stability and capacity improvements observed with the other formatting treatments. The procedure involves the application of a constant + 2 mV voltage during 3 to 44 h prior to galvanostatic cycling (Figure 83c). Such treatment enables reliable recording of the voltage and current evolution, as opposed to the short circuit protocol, which inflicts a

severe potential drop on the cell when connecting the resistor that is not easy to monitor. After the potentiostatic discharge, the capacities were found to monotonically increase with increasing lengths of pretreatment (Figure 86a). Regarding the electrochemical behavior of each cell, we note that the capacity does not increase upon cycling when pretreatments longer than 15 hours are applied. We hypothesize that this is the amount of time required to complete the cracking process of the SiO₂ shell.

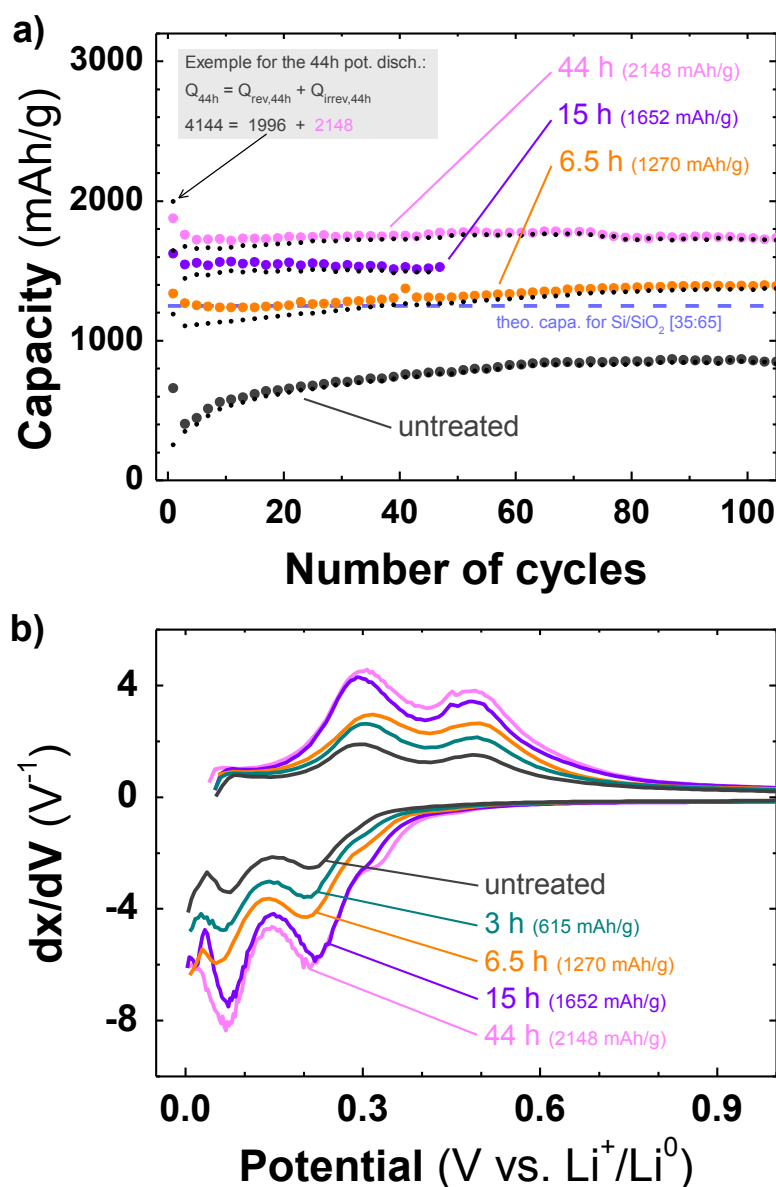


Figure 86: Capacity Retention (a) and Derivative Capacity (b) profiles for Si/SiO₂ (35:65)/Csp/CMC // LP30 + 10% FEC // Li half-cells as function of the pretreatment (potentiostatic discharge) time. For each cell, the value of the irreversible capacity (Q_{irrev} , see Figure 83c for details) corresponding to the treatment time is indicated in parenthesis. In (a), colored dots = discharge, small black dots = charge.

Similar to the plated and shorted electrodes, the capacity increase is clearly attributed to an increasing amount of active Si, based on the peak growth in the dx/dV

traces (Figure 86b). For pretreatments longer than 6.5 h, the capacity clearly exceeds the theoretical maximum value (1250 mAh/g), thus demonstrating the feasibility to electrochemically reduce SiO₂ into active Si using potentiostatic discharge.

The yield of this reaction (SiO₂ → Si) can be estimated by comparing Q_{rev} that is directly related to the total active Si content including the portion derived from SiO₂, with Q_{irrev} obtained by subtracting Q_{rev} from the total capacity of the potentiostatic sequence Q (Figure 83c). Such a calculation is done by assuming the absence of other possible irreversible processes. In particular, the electrolyte reduction is neglected since the SEI formed during the pre-formatting cycle in the presence of FEC passivates the electrode surface, hence preventing further solvent reduction¹¹⁴.

Figure 87 shows a linear correlation between Q_{irrev} and the capacity of the electrodes after the potentiostatic discharge, which suggests that the length of the pretreatment governs the extent of the silica reduction process. The dashed lines correspond to 3 different scenarios: (1) the full conversion of silica into active Si, (2) the chemically assisted electrochemical formation of nesosilicate (Li₄SiO₄) in addition of active Si, and (3) the absence of silica reduction. The first scenario corresponds to the conversion reaction: $SiO_2 + 4 Li \rightarrow Si + 2 Li_2O$ ($\Delta E^\circ \approx 0.7 V$ vs Li⁺/Li⁰)³⁷² which, despite its kinetic limitations (> 1 V overpotentials)³²⁸, was reported in a few papers^{308,373}. The theoretical capacity associated with the reaction for our Si/SiO₂ (35:65) NPs is 2340 mAh/g (= 0.35*3579 + 0.65*1673). Scenario #2 corresponds to the reaction: $2 SiO_2 + 4 Li \rightarrow Si + Li_4SiO_4$, resulting in a theoretical capacity of 1796 mAh/g (= 0.35*3579 + 0.65*836) for our particles. This mechanism has been proposed to explain the formation of Li₄SiO₄ in SiO compounds^{316,324,374,375} and at the surface of Si/SiO₂ particles^{303,308}, in which nesosilicate was observed by TEM³²⁴ and XPS^{303,308,316,375} measurements. The high ionic conductivity of Li₄SiO₄³⁷⁶ may be responsible for the remarkable Li ion transfer properties of SiO compounds³¹⁷. Lastly, scenario #3 describes SiO₂ as inactive, a case in which the treatment would have no effect on the capacity.

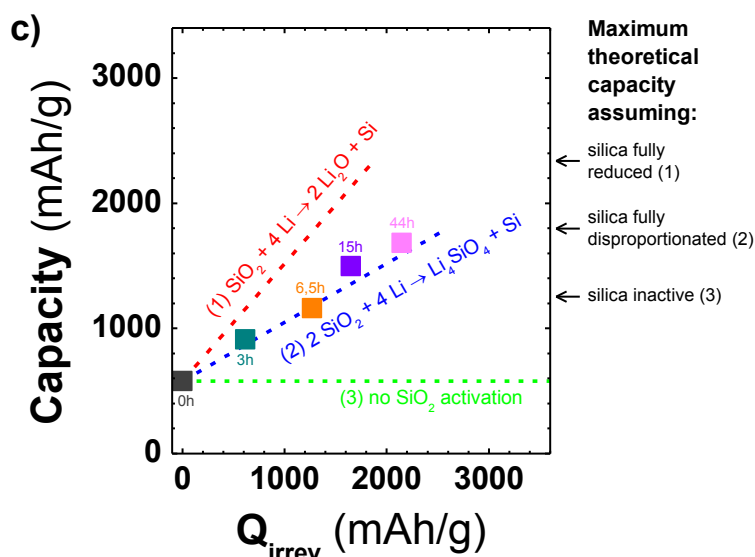


Figure 87: Reversible post-treatment capacity (average of cycles #10 to #20) of the four Si/SiO₂(35:65)/Csp/CMC // LP30 + 10% FEC // Li half-cells reported in Figure 86, as function of the irreversible capacity (Q_{irrev} , value in parenthesis in Figure 86). Dashed lines indicate the capacity gains according to scenarios 1, 2 or 3 (cf main text).

Whether purely coincidental or not, our experimental results nicely fit scenario #2, hence confirming previous studies^{303,308,316,324,325,373}. Further exploiting this reaction scheme means that 79 % of the initial SiO₂ content must have been reduced to account for the capacity of the cell treated for 44 h (1683 mAh/g). Although in agreement with previous studies, caution has to be exercised prior to fully eliminate scenario #1, since our reported capacity values were obtained by assuming i) the full lithiation of Si particles, which was not proved, and ii) the cessation of SEI growth beyond the first cycle. It is worth mentioning at this stage that we could not detect, *via* post mortem XRD measurement, the presence of Li₄SiO₄ in treated cells, suggesting most likely its amorphous nature under our operating conditions.

We demonstrated herein, *via* the use of the *potentiostatic discharge* method, the possibility to reduce SiO₂ supported on Si particles into active Si in a well-controlled fashion. Till now, all of the presented results were obtained using Si/SiO₂ nanoparticles; thus the burning question of whether electro-active Si can be produced from pure silica remains.

II.3 Reduction of pure silica

To answer this question, electrodes containing SiO₂ nanospheres (150-200 nm) – instead of Si/SiO₂ NP – made *via* the Stöber method³⁷⁷ were galvanostatically cycled with and without potentiostatic discharge. When not pretreated, almost no capacity could be accessed (Figure 88a), as confirmed by the dx/dV plot similar to the blank Csp/CMC test electrode (Figure 88b). In contrast, the characteristic features associated with Li-Si

reactions are observed on the Potential-Composition profiles (Figure 88c) and dx/dV plots after 60 and 250 hours of *potentiostatic discharge*; the intensity of the signals increasing with pretreatment times (Figure 88a,b). Note that the SiO_2 reduction can be initially initiated when drastically reducing the discharge rate ($> C/50$) which is highly time-consuming (*cf* Annex 8).

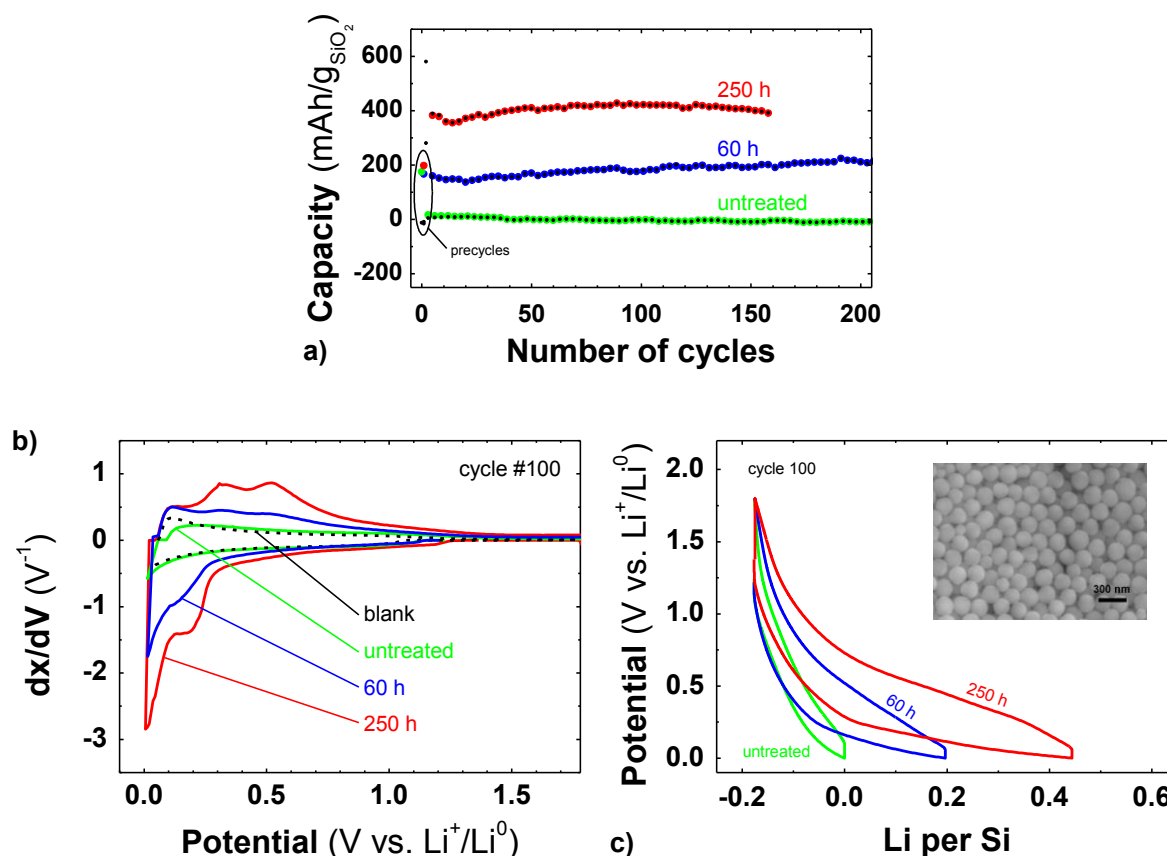


Figure 88: Capacity Retention (a), Derivative Capacity (b) and Voltage-Composition profiles (c) for $\text{SiO}_2/\text{Csp}/\text{CMC}$ // LP30 + 10% FEC // Li half-cells as function of the pretreatment (potentiostatic discharge) time. Insert in (c) is a SEM image of pristine SiO_2 particles prior to electrode fabrication. Blank test in (b) was performed with a Csp/CMC (1:1) electrode and the related capacity was subtracted from other cell capacities. Accordingly, the composition profiles in (c) were purposely shifted towards the left to account for the Csp capacity. In (a), color dots = discharge, small black dots = charge.

This indicates the feasibility to trigger the electrochemical activity of Si – and cycling it for > 150 cycles – from pure silica after a long treatment. Yet, the reduction is limited to 51 % of the initial SiO_2 content even after 250 h of treatment (calculation based on scenario #2), which corresponds to a 44 nm-thick layer of lithiated silica ($\text{Li}_{15}\text{Si}_4 + \text{Li}_4\text{SiO}_4$) for a 200 nm particle homogeneously lithiated at its surface. The limitation of the silica reduction process is attributed to the insulating character of SiO_2 which prevents the reduction from proceeding beyond a threshold penetration depth of $\sim 45/50$ nm. This hypothesis was confirmed by solely achieving a 15 % SiO_2 conversion yield for 500 nm SiO_2 particles (Figure 89), which corresponds to a homogeneous lithiated silica layer of 48 nm, in agreement with

the former statement. Finally, for the sake of completeness, we checked i) the influence of the pretreatment length time on a silicon-free (*i.e.* Csp/CMC) electrode and did not find any visible change in the electrochemical behavior, and ii) that the glass fiber separator (mainly composed of a $\text{Na}_2\text{O} - \text{SiO}_2$ mixture) was not reduced during the treatment. For the latter, a Cu//glass fiber//Li cell was assembled, for which no activity with respect to lithium was observed after a potentiostatic discharge.

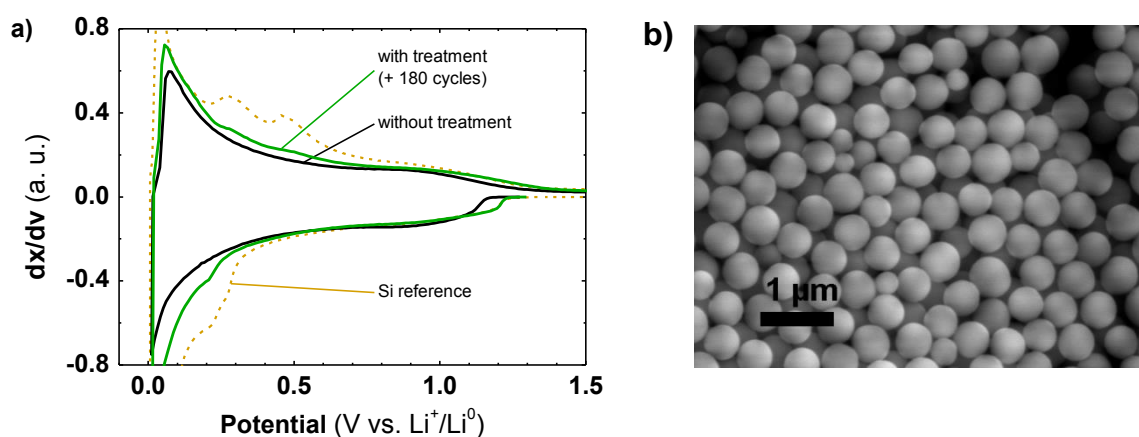


Figure 89: Derivative capacity profile (a) and SEM image (b) of a $\text{SiO}_2/\text{Csp}/\text{CMC} // \text{LP30} + 10\% \text{FEC} // \text{Li}$ half-cell pretreated for 130 h (potentiostatic discharge) prior to be and cycled 180 times.

In conclusion, we demonstrated that the silica reduction process accompanying the prelithiation of Si/ SiO_2 particles could similarly happen with pure silica particles. In the case of Si/ SiO_2 particles, the three treatments (*controlled short circuit*, *plating*, and *potentiostatic discharge*) were shown to significantly increase the reversible capacity of the electrodes while enabling stable cycling at constant capacity for hundreds of cycles (see Annex 4 and Annex 5 for the long term cycling). We believe that both the cracking of the silica shell and the reduction of SiO_2 into electroactive Si are crucial to achieve the extra capacity.

This dual effect is of prime interest within the context of replacing Li metal in Li- O_2 batteries by Li_xSi electrodes since it provides the extra-capacity required for balancing the high-capacity air electrode. The integration of Si electrodes prelithiated *via* such methods into full $\text{Li}_x\text{Si-O}_2$ batteries is described next.

III Lithium-Air batteries using lithiated silicon as anode

The assembly of a full $\text{Li}_x\text{Si-O}_2$ battery is a multistep process which begins with prelithiating a silicon electrode in a Li half-cell, as detailed in the former section. It is then disassembled in the glovebox so as to recover the Li_xSi electrode, which is washed and dried

before being used as the anode (*i.e.* Li source) in a $\text{Li}_x\text{Si//Csp//O}_2$ cell. However, the utilization of a Li_xSi electrode in an O_2 cell instead of a half cell requires the adjustment of a few parameters, especially to deal with the limited quantity of Li in the system, which is discussed next.

III.1 The Li_xSi electrodes within the context of Li-Air batteries

III.1.a Electrode loading

In the former section, Si electrodes were optimized to achieve a good cycling retention while little attention was paid to the electrode loading. However, this parameter becomes decisive when lithiated silicon is used as the lithium source in a $\text{Li}_x\text{Si-O}_2$ system owing to i) the parasitic reactions occurring during the washing process – for instance with its impurities, *cf* section III.2.c – and during the cycling, which consume Li and ii) the necessity to extract lithium at a relatively low potential (< 0.6 V) so as to maintain a high energy density at the full cell level (Figure 90). In order to improve the absolute capacity of the Si anode, we tried to increase the tap density by preparing thicker electrodes (use of 650 μm bar coater instead of 500 μm). However, they tend to crack while drying, and some pieces of active material were detached from the Cu substrate during the washing step.

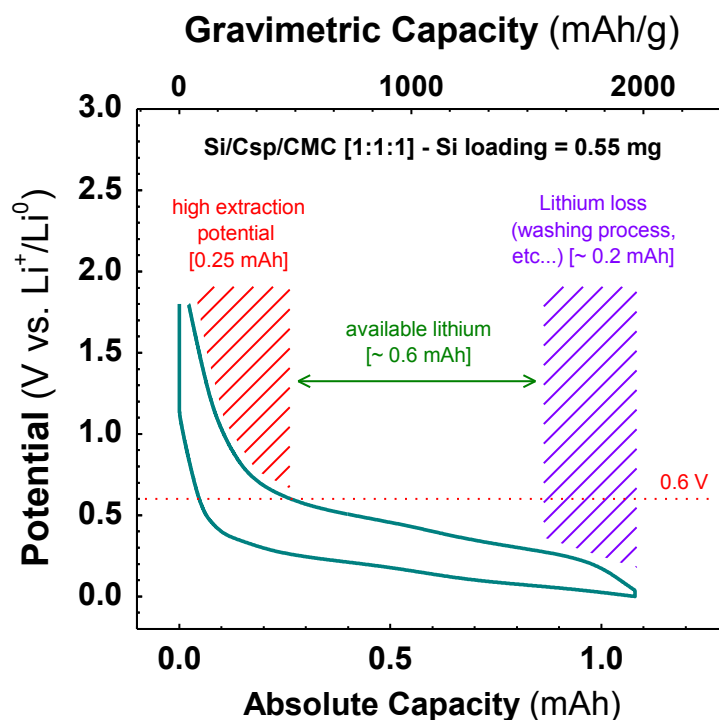


Figure 90: Potential-Capacity profile of a $\text{Si/SiO}_2/\text{Csp/CMC}[1:1:1] // \text{LP30} + 10\% \text{ FEC} // \text{Li}$ half-cell after a 44 h potentiostatic discharge. Once integrated in a full $\text{Li}_x\text{Si-O}_2$ cell, only 0.6 out of 1.08 mAh can be used owing to various lithium losses and if the Li extraction potential is limited to 0.6 V.

A more successful strategy consisted in using a Si/Csp/CMC ratio of [2:1:1] (instead of [1:1:1]) enabling absolute capacities as high as ~ 1.5 mAh/electrode ($750 \text{ mAh/g}_{\text{electrode}} \equiv 1.2 \text{ mAh/cm}^2$) with a good efficiency ($\sim 98\%$) and a limited impact on the cycling retention (cf Annex 9). Unless specified otherwise, the [2:1:1] electrode composition will be used in our following work. However, we will see that in some cases, increasing the tap density is not sufficient to compensate for the Li losses (purple area in Figure 90), which calls for an alternative strategy.

III.1.b Balancing Li losses

To overcome the loss of lithium, we will sometimes use a strategy consisting in stopping a cell at the end of a short plating sequence so as to form a thin layer of metallic Li on top of the electrode, which preserves the Li_xSi phase during the transfer into the $\text{Li}_x\text{Si-O}_2$ cell. This strategy is illustrated in Figure 91a in which the electrode may either be recovered after 2 h of plating (orange circles), or at the end of a standard galvanostatic discharge to 0 V (green circles). The electrodes prelithiated by such means will be referred to as $p\text{-Li}_x\text{Si}$ electrodes (p for plated).

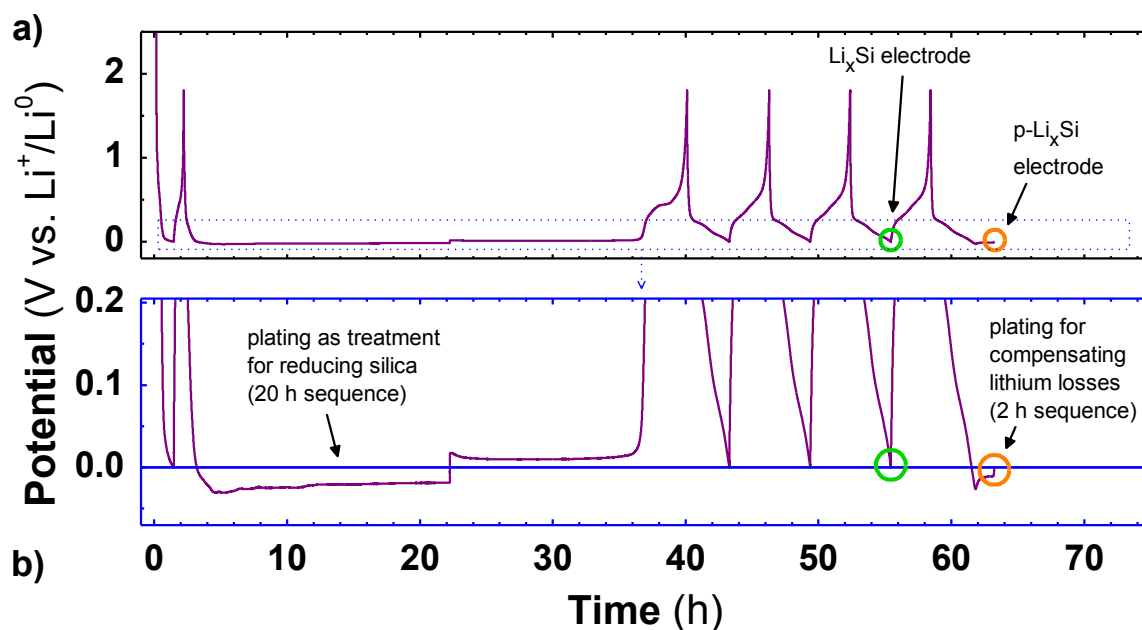


Figure 91: Large (a) and zoomed (b) Potential-Time profiles of a Si|SiO₂/Csp/CMC[2:1:1]/LP30 + 10 % FEC//Li half-cell treated with a 20 h plating sequence, which can be stopped and recovered in a “regular” lithiated state (green circle) or in a plated state (orange circle). The captions in (b) highlight the distinct functions of the two plating sequences.

The purpose of this short plating sequence – which may be used for compensating eventual Li losses – shall not be confused with the long initial plating sequence used for reducing silica (Figure 91b). Since this electrochemical treatment governs the capacity of Si

electrodes, we will now focus on this crucial step to find the fastest way to obtain the highest capacities.

III.1.c Prelithiation sequence

Based on our mastering of the prelithiation processes, we tried to identify the most relevant method in order to achieve the best performances using the new [2:1:1] electrode composition (Figure 92).

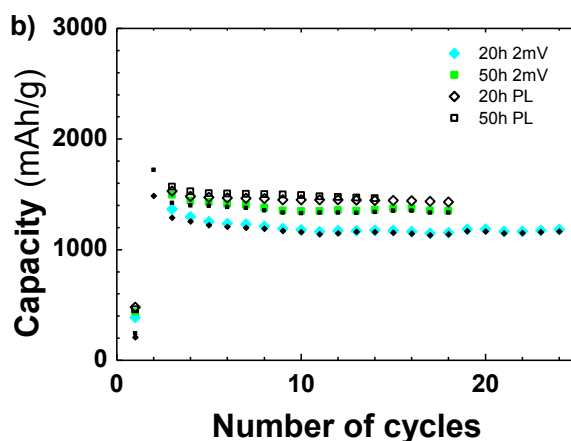


Figure 92: Capacity Retention profile for Si/SiO₂/Csp/CMC [2:1:1] // LP30 + 10% FEC // Li half-cells as function of the pretreatment's nature and duration. The large dots represent to the discharge capacity while the small black dots correspond to the charge (only plotted for the potentiostatic discharge for sake of clarity). The *short-circuit* method was not studied here owing to its redundancy with the *potentiostatic discharge*.

The best results are obtained with the plating technique, which shows after 20 h of treatment a higher reversible capacity than the 50 h potentiostatic discharge. Moreover, we do not observe any significant gain in capacity between the cell plated for 20 and 50 h. For these reasons, a **20 h plating sequence** was chosen as the preferred method for enhancing the capacity of Si/SiO₂ electrodes during the prelithiation.

III.2 Recovering the Li_xSi electrode

III.2.a Resting time after lithiation

Earlier in this chapter (section II.2.a), we were able to detect the self-oxidation of a Li_xSi electrode resting at the OCV; phenomenon which will always happen prior recovering the electrode (time to transfer the cell into the glovebox, cell stopped during the night, etc...). In order to quantify the capacity which could be lost during this self-discharge, a cell was discharged to 0 V and rested for 50 h prior to be charged again (Figure 93).

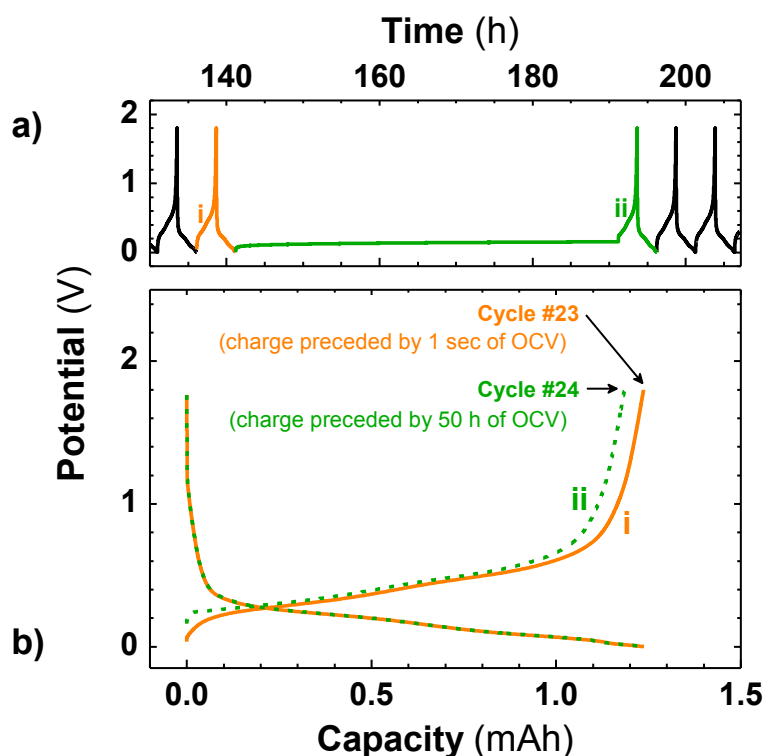


Figure 93: Potential-Time (a) and Potential-Capacity (b) profiles of a $\text{Si/SiO}_2/\text{Csp}/\text{CMC}$ [2:1:1] // LP30 + 10% FEC // Li half-cell stopped in discharge and rested for 50 h between cycles #23 and #24. The cell was treated by a plating treatment of 2h20 at cycle #2 (not shown here, cf Figure 85).

The comparison between the capacity of the charge following the 50 h OCV and the capacity of a regular charge (which starts 1 second after the end of the previous discharge) reveals a capacity loss of only 4 % (1.185 mAh for charge #23 vs. 1.235 mAh for charge #24). It corresponds to an average self-discharge current of 1.0 μA indicating the relatively high stability of the fully lithiated Li_xSi phase, hence suggesting that prelithiated electrode can be recovered without significant Li losses even after one day.

III.2.b Glass Fiber vs. Celgard-type separator

Once prelithiated, the Si/Li half-cell is entered into the glovebox and disassembled so as to recover the Li_xSi electrode. When a glass fiber separator was used, we were not able to clean the electrode without damaging it, owing to some fibers attached at its surface (Figure 94a,d). To prevent this phenomenon, a celgard separator (Celgard® 2325, 25 μm microporous tri-layer membrane (PP/PE/PP)) was added on top of the anode so as to protect its electrode surface while the glass-fiber separators ensured a proper electrolyte impregnation. The celgard does not attach to the electrode surface and enables a homogeneous prelithiation (Figure 94b) and plating (Figure 94c).

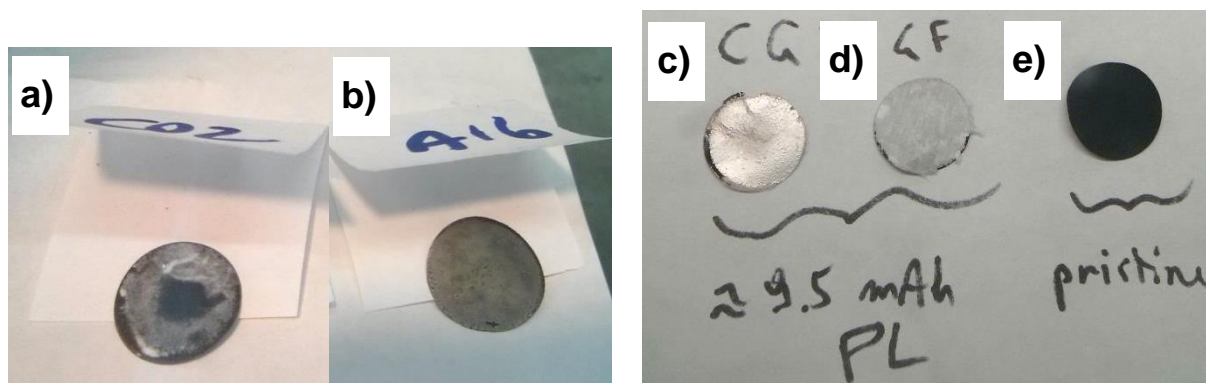


Figure 94: Photographs of some Li_xSi electrodes recovered at the end of discharge (a,b) and after 17 h of plating (c,d) as compared to a pristine Si electrode (e). (a) and (d) were in contact with a glass fiber separator in the Si/Li prelithiation half-cell, while (b) and (c) used a celgard separator.

Adding this extra layer has no impact on the electrochemical behavior of Li/Si cells, as confirmed by the perfect reproducibility obtained in presence or absence of celgard after both 20 h and 50 h of plating (Figure 95), but modifies the surface aspect of the electrode. Hence, considering such results, a celgard separator will always be used for prelithiating the Si electrodes. Moreover, this experiment further confirms the uselessness of treating an electrode with a plating sequence longer than 20 h.

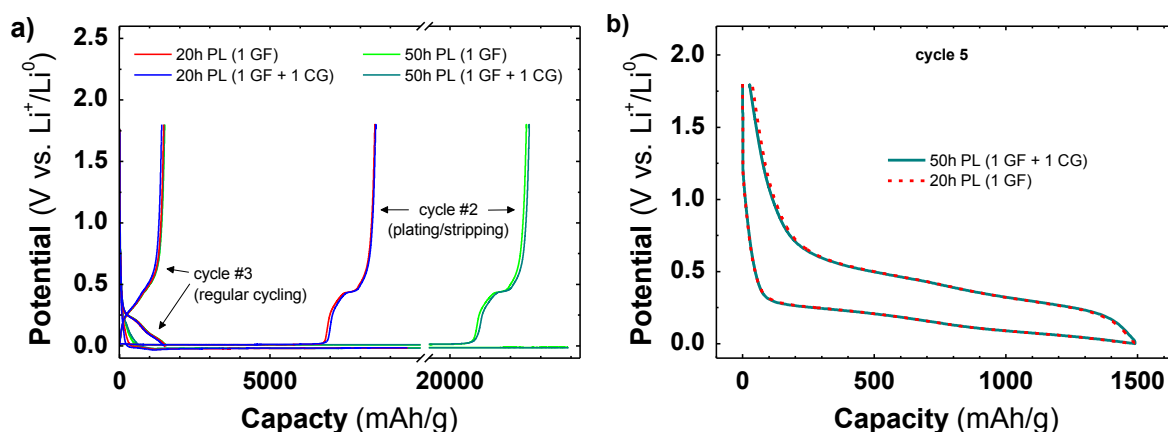


Figure 95: Potential-Capacity profiles of cycles #2 and #3 (a), and cycle #5 (b) of some $\text{Si|SiO}_2/\text{Csp}/\text{CMC}$ [2:1:1] // LP30 + 10% FEC // Li half-cells treated with a plating sequence of 20 h or 50 h, in presence or absence of celgard separator. In the figure caption, GF = glass fiber, while CG = celgard.

III.2.c Washing process and cycling in a Li-O_2 electrolyte

Various solvents were considered for the treatment/prelithiation step, including the usual Li-O_2 electrolytes in addition to LP30+FEC. Surprisingly, we were not able to plate any Li when a glyme-based electrolyte was used, which suggests the instability of these solvents below 0 V vs. Li^+/Li^0 (see Annex 10 for the plating sequence in DME and TEGDME). DMA was not tested lest the presence of two Li surfaces, including one in a highly divided form, would disturb the subsequent LiNO_3 chemistry. It was also reported that DMA can only be used for

cycling Li in presence of both LiNO_3 and O_2 ²⁵⁷, which is not practical for a pretreatment step. Therefore, a mixture of LP30 + 10 % FEC was used for prelithiating the Si electrodes, which shows the advantage of forming a neat SEI accommodating the volume changes of the Si NP. However, this mixture composed of carbonate species which must be avoided in Li-O_2 batteries due to their high instability, justifying a washing step prior integrating the prelithiated silicon electrode into full $\text{Li}_x\text{Si-O}_2$ cells. Dimethoxyethane (DME) was used as washing solvent owing to its better compatibility with the Li-O_2 chemistry, its high volatility and the high purity of the commercial product. Such precautions are needed to minimize the Li losses over the washing step, but the latter cannot be completely avoided due to the self-discharge process discussed earlier.

In order to estimate the amount of lithium lost during the overall process in real conditions, a Li_xSi electrode was washed and cycled again in a Li half-cell presenting the same experimental conditions as a Li-O_2 battery (O_2 atmosphere, 0.5 M LiTFSI in TEGDME as electrolyte and 8 h of initial OCV) (Figure 96a).

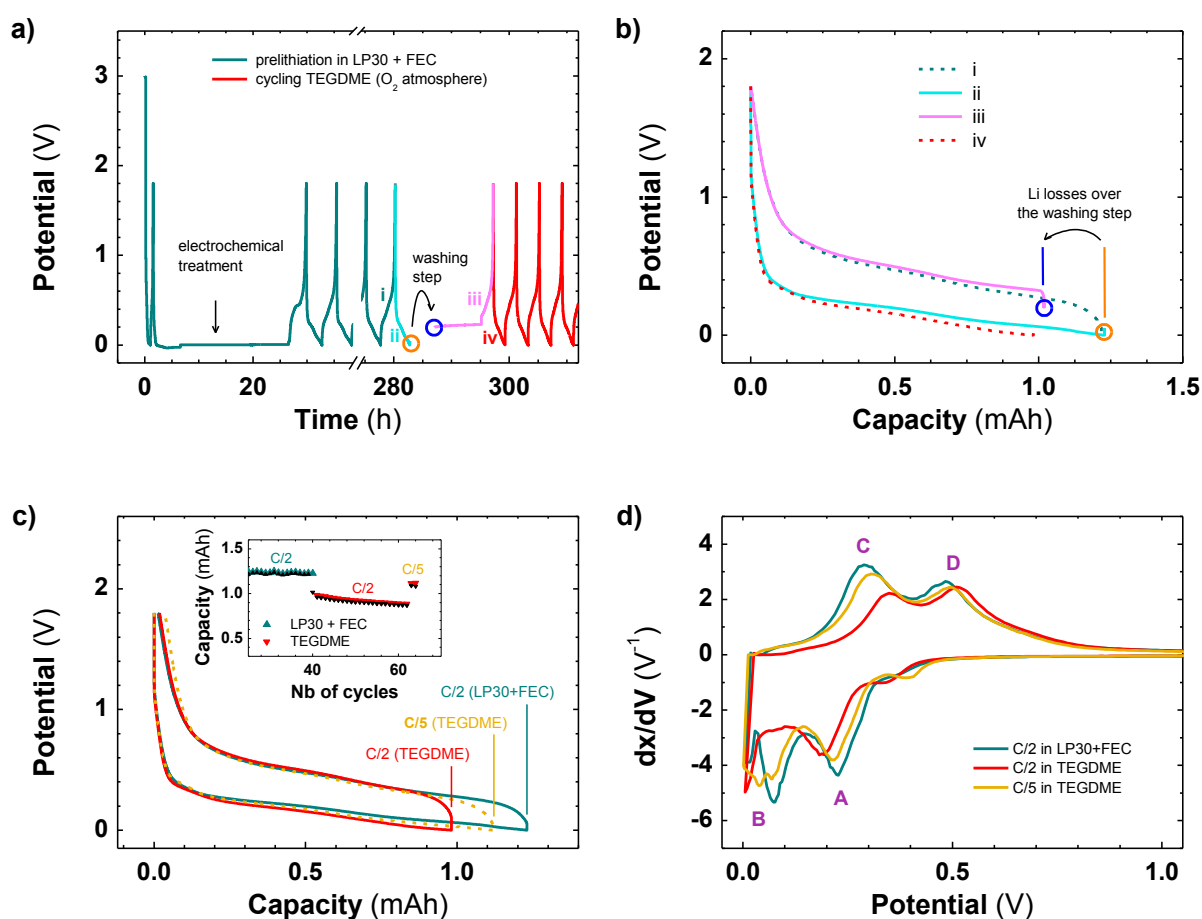


Figure 96: Potential-Time (a), Potential-Capacity (b,c) and Derivative capacity (d) profiles of a $\text{Si/SiO}_2/\text{Csp}/\text{CMC}$ [2:1:1] electrodes cycled first in a $\text{Si} // \text{LP30} + 10\% \text{FEC} // \text{Li}$ half-cell (prelithiation step) at C/2, then recovered/washed at cycle #40, and then cycled in a $\text{Si} // 0.5 \text{ M LiTFSI in TEGDME} // \text{Li} // \text{O}_2$ half-cell at C/2 then C/5.

The lithium loss – difference in capacity before and after the washing step (*cf* orange and blue circles in Figure 96b) – corresponds to 17 % (~ 0.2 mAh) of the capacity before washing^{ix}. It is attributed to i) the self-discharge phenomenon and ii) side reactions with impurities, which both happen in the washing and the Li-O_2 solvent, and are inevitable. Moreover, the reversible capacity of the Si electrode cycled in TEGDME is lower than in LP30+FEC (~ 0.95 mAh vs. 1.23 mAh, *cf* insert in Figure 96c) which is attributed to kinetic limitations due to the higher viscosity of TEGDME and its lower conductivity. It was confirmed by the shift of the reduction peaks (A and B) towards lower potentials in the dx/dV plot (Figure 96d) when replacing LP30+FEC by TEGDME. The reversible capacity in TEGDME could be increased by reducing the current density to C/5 (corresponding to $195 \mu\text{A} \equiv 95 \text{ mA/g}_{\text{electrode}}$), suggesting that this issue should not be a limiting factor in a full $\text{Li}_x\text{Si-O}_2$ cells owing to the low current usually applied ($20 \mu\text{A}$). Lastly, the slow capacity decay observed in the TEGDME-based electrolyte is probably due to a weakening of the SEI during the washing step, which cannot be properly reformed in absence of FEC.

Having detailed and optimized the different steps leading to high performance Li_xSi electrodes, we now focus on their practical utilization into full $\text{Li}_x\text{Si-O}_2$ cells.

III.3 Study of full $\text{Li}_x\text{Si-O}_2$ batteries

III.3.a Experimental setup

A pressurized three-electrode cell (Figure 97) consisting of a Csp cathode (10 % PTFE onto SS mesh, ~ 0.4 mg of Csp) in an oxygen atmosphere, a lithium ring as reference electrode, and a prelithiated silicon electrode (~ 1.5 mAh/electrode) as counter electrode was used for the electrochemical study of full $\text{Li}_x\text{Si-O}_2$ cells. If not specified otherwise, the Si electrodes are always treated by a 20 h plating sequence (for obtaining high capacities) and cycled a few times prior to be stopped in a lithiated state (the capacity and stopping conditions of each electrode will be specified individually). For sake of simplicity, the rigorous $\text{Li}_x\text{Si}|\text{SiO}_2/\text{Csp}/\text{CMC}$ [2:1:1] notation will be shortened to “ Li_xSi ”.

Using such setup, it is possible to independently measure the potential of each electrode over cycling (Figure 97a) and the corresponding pressure variations (Figure 97b).

^{ix} Note that the Si electrode used for this experiment corresponds to Cell 2 in Figure 85 (also used for Figure 93). Note that its capacity (~ 1.25 mAh) is relatively low as compared to the electrodes usually used in the full $\text{Li}_x\text{Si-O}_2$ cells (~ 1.5 mAh).

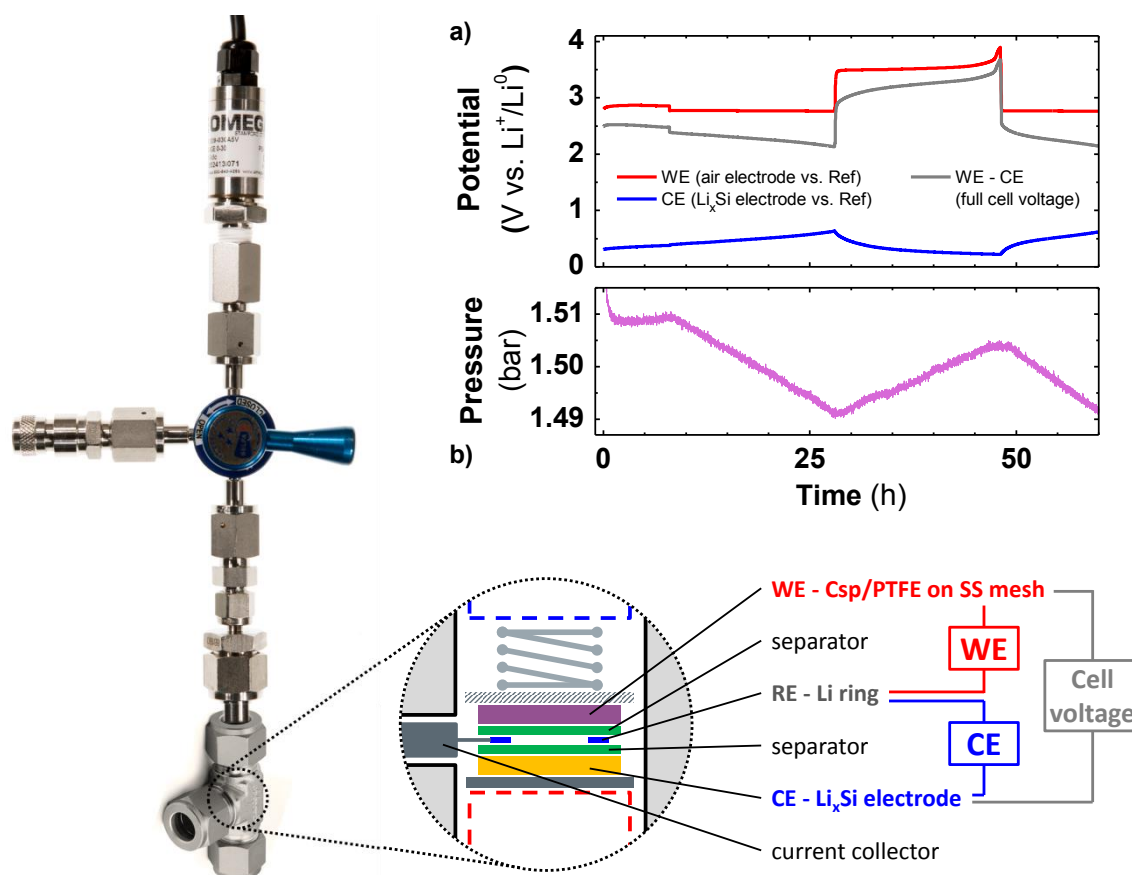


Figure 97: Photograph and schematic representation of a three-electrode pressurized electrochemical cell enabling to record independently the potential of the cathode and anode (a) as well as the pressure evolution (b).

Considering the results obtained in the former chapter, we decided to focus our study on two systems using DMA and TEGDME as solvents.

III.3.b $\text{Li}_x\text{Si-O}_2$ full cells using high capacity Si electrodes

Figure 98 shows the electrochemical behavior of two $\text{Li}_x\text{Si-O}_2$ cells containing Li_xSi electrodes prelithiated with a capacity of ~ 1.55 mAh (discharge to 0 V, cf green circles in Figure 91, p.129), using either 2 M LiNO_3 in DMA (Figure 98a,b) or 0.5 M LiTFSI in TEGDME (Figure 98c,d) as electrolyte. While the electrochemical behavior of the air electrode and the pressure evolution are similar to what was obtained using a Li anode, the Si electrode is quickly delithiated which leads to a total cell voltage of 0 V within less than five cycles.

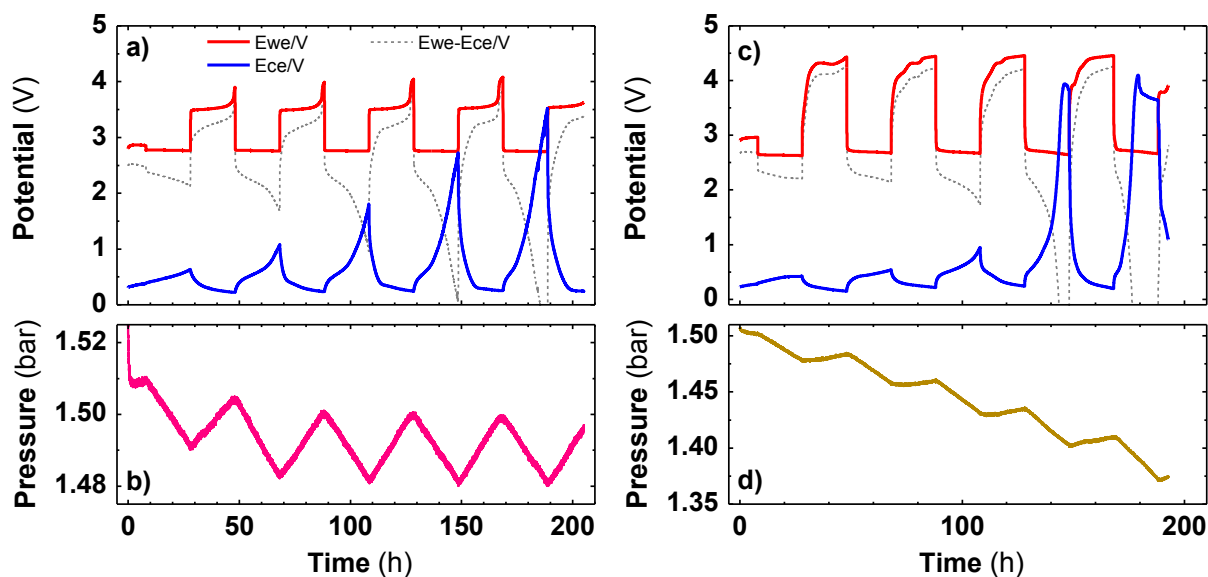


Figure 98: Potential-Time (a,c) and Pressure-Time (b,d) profiles of two $\text{Li}_x\text{Si} // \text{Csp} // \text{O}_2$ cells using 2 M LiNO_3 in DMA (a,b) and 0.5 M LiTFSI in TEGDME (c,d) as electrolyte, and cycled at a current of $50 \mu\text{A/g}_{\text{carbon}}$ with a capacity limited to $1000 \text{mAh/g}_{\text{carbon}}$ (0.4mAh). The Li_xSi electrode was prepared by galvanostatic discharge stopped at 0 V, enabling a capacity of $\sim 1.55 \text{mAh}$.

Based on our former results on Li-O_2 systems, this fast delithiation is likely due the parasitic reactions occurring during the formatting cycles: in the DMA-based cell, the presence of LiNO_3 promotes the formation of an SEI made of Li_2O at the surface of the Li_xSi anode, while the cycle-life of the TEGDME-based system is hindered by side reactions occurring at the air electrode (C corrosion, etc...). Both reactions decrease the amount of Li available for the Li-O_2 reaction, which only equals to 5 % and 28 % of its initial content at the end of the 2nd discharge for the DMA- and TEGDME-based systems, respectively (Figure 99).

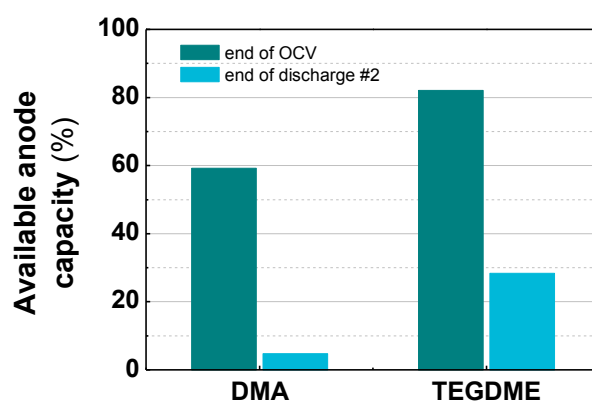


Figure 99: Relative Capacity of the Li_xSi anode at different stages of the cycling as function of the electrolyte used. It is equivalent to the amount of Li available for the Li-O_2 reaction. The % values are estimated from the anode potential and with respect to its prelithiation capacity.

III.3.c $\text{Li}_x\text{Si-O}_2$ full cells using $p\text{-Li}_x\text{Si}$ electrodes

In order to compensate for the Li lost over the formatting cycles, the $\text{Li}_x\text{Si-O}_2$ cells were mounted using a $p\text{-Li}_x\text{Si}$ electrode, *i.e.* with a small amount of Li plated on its surface (*cf* orange circles in Figure 91, p.129). A short plating sequence (~ 1.5 h of Li plating $\equiv \sim 0.6$ mAh) enables to double the cycle-life of the cells (*cf* synoptic cycling retention plots in Figure 102a), which indicates that the extra Li quantity improved the performances but was not sufficient for mitigating a significant fraction of the side reactions.

More interestingly, the use of $p\text{-Li}_x\text{Si}$ electrodes gives a better insight in the SEI formation when LiNO_3 is used. In presence of nitrates, a rapid delithiation of the anode occurs *via* the formation of the SEI, which starts as soon as the cell is assembled (Figure 100a). Note that due to the fast kinetics of this reaction and the time needed to fill the cell with O_2 prior to start the data acquisition, we were not able to record the departure of the potential from the Li stripping plateau. In contrast, the plated Li is stable in the absence of LiNO_3 (initial OCV $\approx +3$ mV vs. Li^+/Li^0), as confirmed by electrochemical stripping observed prior to the anode delithiation during the first discharge (Figure 100b).

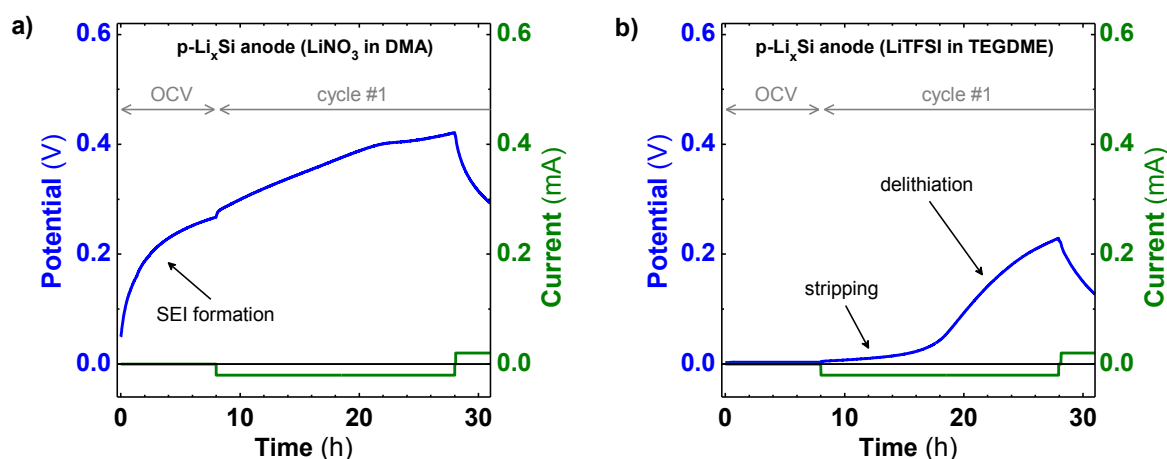


Figure 100: Potential-Time and Current-Time profiles of a $p\text{-Li}_x\text{Si} // \text{Csp} // \text{O}_2$ cell using 2 M LiNO_3 in DMA (a) or 0.5 M LiTFSI in TEGDME (b) as electrolyte, and cycled at a current of $50 \mu\text{A}/g_{\text{carbon}}$ with a capacity limited to $1000 \text{mAh}/g_{\text{carbon}}$ (0.4 mAh). The $p\text{-Li}_x\text{Si}$ electrode was prepared by discharging it without any cutoff voltage for 4h30 enabling its full lithiation (~ 1.5 mAh) and a Li plating equivalent to ~ 0.6 mAh.

In order to further improve the cycle-life of our full cells, we tried to minimize the side reactions occurring in the system by limiting the depth of discharge.

III.3.d $\text{Li}_x\text{Si-O}_2$ full cells with limited depth of discharge

Figure 101 shows the electrochemical behavior of a $p\text{-Li}_x\text{Si-O}_2$ cell cycled with a charge/discharge limited to $500 \text{mAh}/g_{\text{carbon}}$. For this experiment, a slightly loaded Csp electrode was chosen (0.3 mg instead of 0.4 mg of Csp) to limit the extent of one cycle to

$1/10^{\text{th}}$ of the Si electrode capacity. Such strategy – combined with the “plating trick” discussed previously – drastically improves the cycle-life of the full cell leading to more than 35 cycles.

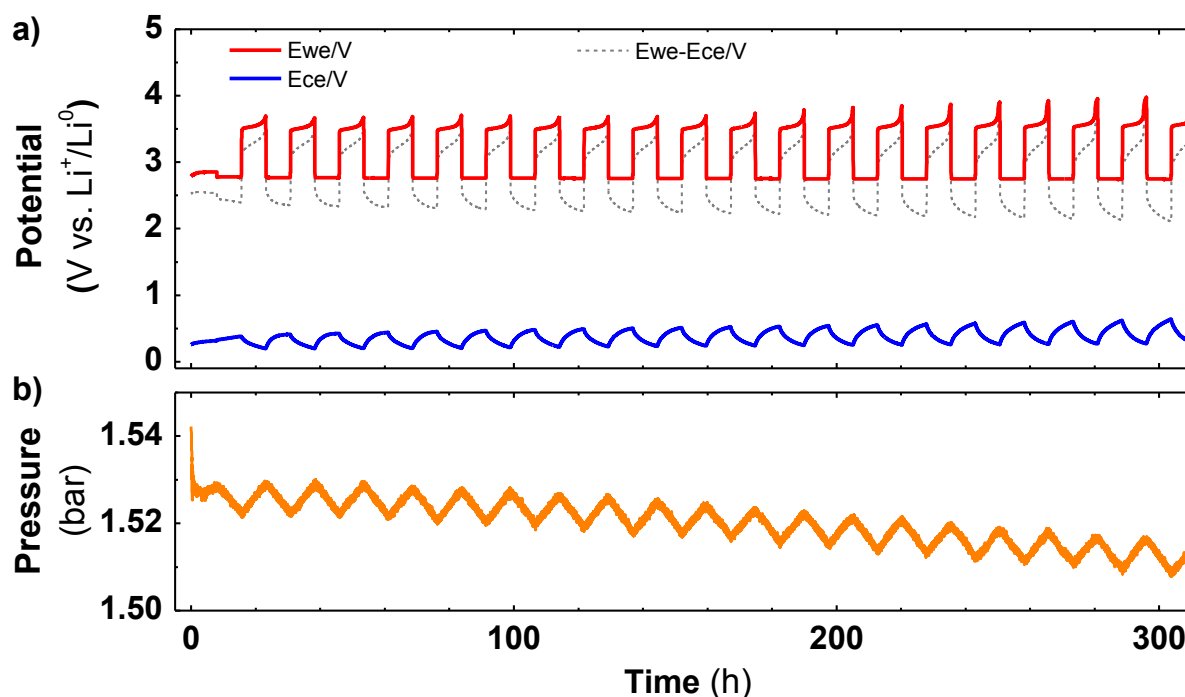


Figure 101: Potential-Time (a) and Pressure-Time (b) profiles of a $p\text{-Li}_x\text{Si} // 2 \text{ M LiNO}_3$ in DMA // Csp // O_2 cell cycled at a current of $50 \mu\text{A}/\text{g}_{\text{carbon}}$ with a capacity limited to $500 \text{ mAh}/\text{g}_{\text{carbon}}$ (0.15 mAh). The $p\text{-Li}_x\text{Si}$ electrode was prepared by discharging it without any cutoff voltage for 4h40 enabling its full lithiation (~ 1.5 mAh) and a Li plating equivalent to ~ 0.6 mAh. Only the 20 first cycles are shown here.

One of the main reasons for such improvement is most likely rooted in the discharge capacity (500 vs. $1000 \text{ mAh}/\text{g}_{\text{carbon}}$) which prevents the formation of large Li_2O_2 particles that are difficult to re-oxidized in charge. Additionally, it minimizes the volume changes of the Si particles which preserves the SEI from cracking and prevents the side reactions caused by a direct contact between the Li_xSi particles and the electrolyte (and its impurities). The same strategy was used to increase the cycle-life of a $\text{Li}_x\text{Si} // 0.5 \text{ M LiTFSI}$ in TEGDME // Csp // O_2 cell, which could hold 21 cycles when the capacity was limited to $300 \text{ mAh}/\text{g}$ ^x (see Annex 11 for the Potential- and Pressure-Time profiles).

All the results obtained so far with full $\text{Li}_x\text{Si-O}_2$ batteries are summarized in Figure 102, in which the full cell voltage at the end of the discharge sequence is reported as function of the number of cycles ^{xi} (Figure 102a). It shows the benefits of limiting the depth

^x We chose $300 \text{ mAh}/\text{g}$ for the TEGDME-based system (vs. $500 \text{ mAh}/\text{g}$ in DMA) because of i) more important cathodic side reactions, and ii) the use of a regular Li_xSi electrode (vs. a $p\text{-Li}_x\text{Si}$ in DMA).

^{xi} The “full-cell potential vs. number of cycles” plot is the equivalent to the capacity retention plot in a system limited by the depth of discharge instead of the cutoff voltage. It is mostly governed by the anode potential owing to the flat potential (~ 2.7 V) of the air electrode during the discharge.

of discharge for achieving more cycles, a strategy which is frequently encountered in the literature^{190,191,193,378} although not realistic for practical applications.

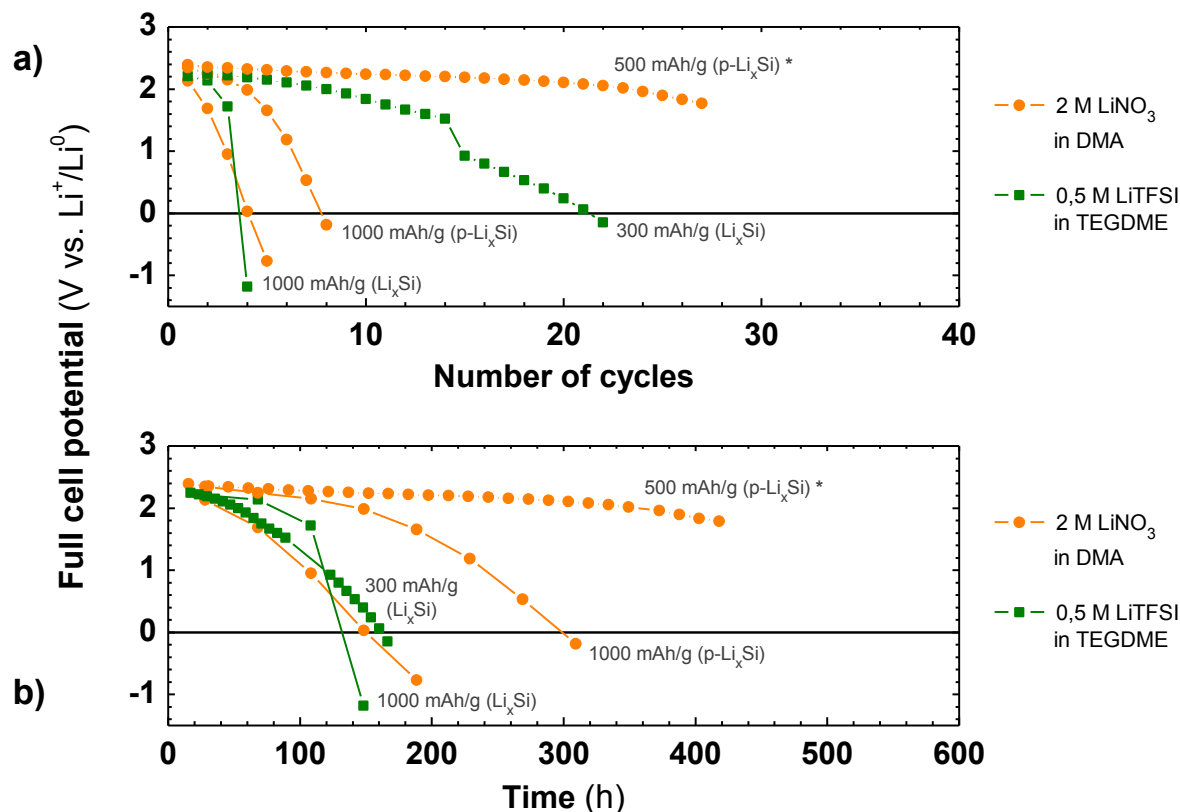


Figure 102: Full-cell potential (end of the discharge sequence) as function of the number of cycles (a) and time of cycling (b) for all $\text{Li}_x\text{Si-O}_2$ cells according to the electrolyte, anode prelithiation, and capacity. The labels indicate the depth of discharge and the prelithiation type. *: the cell was involuntarily stopped due to multiple power cuts in the building.

The second plot (Figure 102b) indicates the length of the cycling, which reveals a significant difference between the two electrolytes. For the DMA-based cell, limiting the depth of discharge from 1000 to 500 mAh/g doubles the battery life (the cell was stopped after 430 h due to a power cut but may have lasted $\sim 550/600$ h otherwise, as compared to ~ 300 h using 1000 mAh/g and a $p\text{-Li}_x\text{Si}$ anode), while the TEGDME-based cell cycled at 300 mAh/g only lives $\sim 20\%$ longer than when it is cycled at 1000 mAh/g. This suggests that for the latter systems, the battery-life is only marginally affected by the cycling conditions and its consequences earlier mentioned (volume changes of the Si NP, size of the Li_2O_2 particles, etc...).

The origin of the Li losses may therefore be nested in the crossover of reactive species like oxygen, as previously reported^{146,378}. In order to verify this hypothesis, a two-compartment cell including a physical barrier protecting the negative electrode was

conceived. This strategy will be discussed next and its outcome will be the last subject of this thesis.

III.3.e Improving the cycle-life of the Li_xSi anode with a physical protection

In order to protect the anode from the O_2 cross-over, an interlayer composed of a solid electrolyte (Lithium-ion Conductive Glass-ceramics (LICGS), LATP-type^{xii}, 200 μm thick, Ohara Inc.) was integrated into our electrochemical cell. Located between the anode and the cathode, it acts as a selective cationic membrane permeable to Li^+ ions only. It is therefore possible to use two distinct electrolytes on each side of the battery, such as LP30 + FEC on the silicon side while TEGDME is used at the air electrode.

Based on the *in situ* XRD cell design³⁷⁹, we developed a testing hardware (referred as “Ohara cell”) enabling the use of a 1*1 inch LATP membrane, and can be adapted to our pressured setup (Figure 103).

^{xii} $\text{Li}_{1+x+y}\text{Al}_x\text{Ti}_{2-x}\text{Si}_y\text{P}_{3-y}\text{O}_{12}$ (NASICON type), $\sigma = 3 \cdot 10^{-3}$ S/cm at 25 °C.

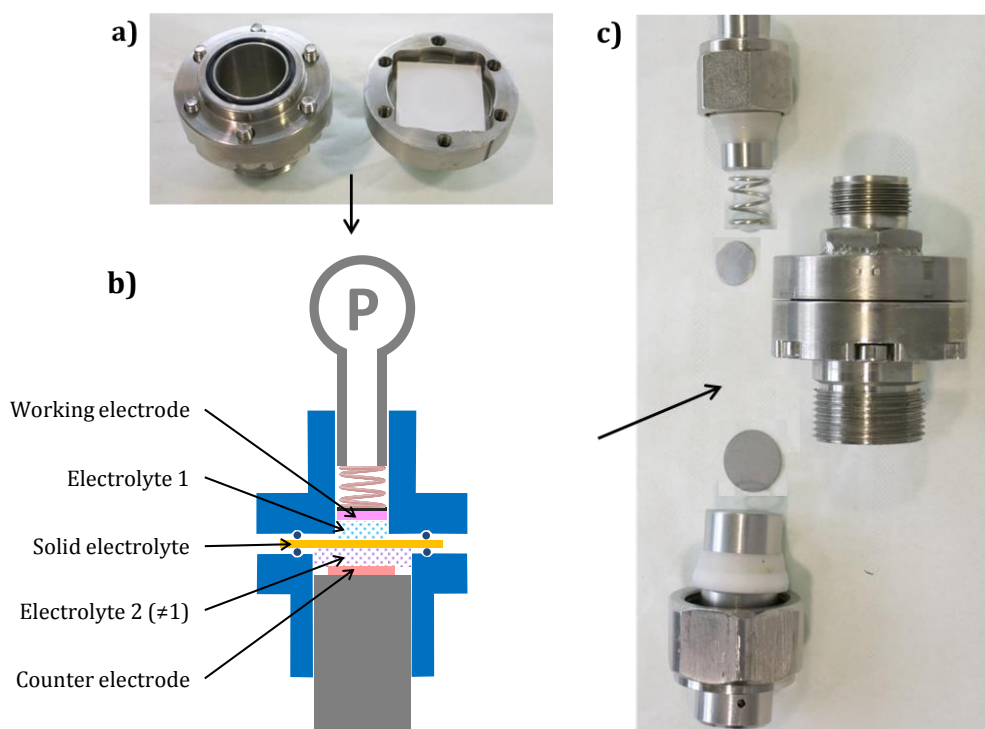


Figure 103: Photographs (a,c) and schematic representation (b) of a two-compartment "Ohara" cell.

The device was first benchmarked with a well-known system using LiFePO_4 – cycled in LP30 – as working electrode, and lithium metal – cycled in 0.5 M LiTFSI in TEGDME – as counter electrode (Figure 104). The polarization of the system is similar to what was obtained in a regular coin cell with a two-fold higher current density, which is not a surprise owing to the higher resistivity induced by the ceramic membrane. This experiment confirms the proper functioning of the two-compartment cell, which may now be used for studying the $\text{Li}_x\text{Si-O}_2$ battery.

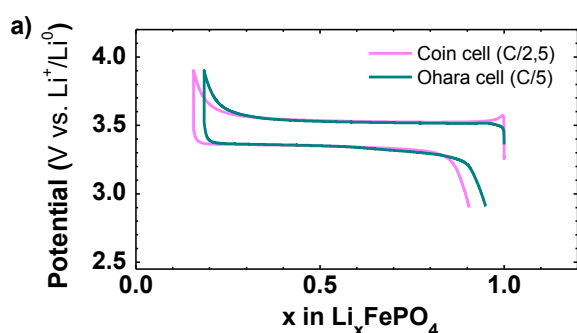


Figure 104: Potential-Composition profile a composite $\text{LiFePO}_4/\text{Csp}/\text{PVDF}$ electrode cycled vs. Li in the Ohara cell composed of LFP // LP30 // LATP // 0.5 M LiTFSI in TEGDME // Li (green line), and in a regular LFP // LP30 // Li coin cell (pink line). The current density is 29 mA/g in the Ohara cell, and 57 mA/g in the coin cell.

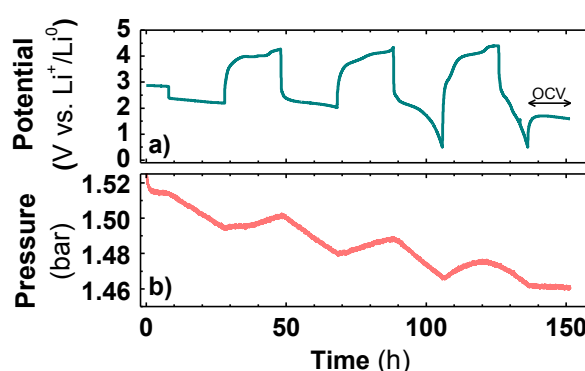


Figure 105: Potential-Time (a) and Pressure-Time (b) profiles of an Ohara cell Li_xSi // LP30 + 10 % FEC // LATP // 0.5 M LiTFSI in TEGDME // Csp // O_2 , cycled at a current of $50 \mu\text{A}/\text{g}_{\text{carbon}}$ with a capacity limited to $1000 \text{mAh}/\text{g}_{\text{Carbon}}$ (0.4 mAh) and a lower cutoff voltage of 0.5 V. The Li_xSi electrode was prepared by galvanostatic discharge to 0 V, enabling a capacity of $\sim 1.5 \text{mAh}$.

The lower compartment of the Ohara cell consisted of a Li_xSi electrode and a separator soaked with LP30 + 10 % FEC, while the upper one contained the Csp air electrode and a separator soaked with 0.5 M LiTFSI in TEGDME. The O_2 was contained in a pressurized gas reservoir (similar to those formerly use) which was mounted on top of the Ohara cell. Using this configuration, only three cycles at 1000 mAh/g could be performed prior to reach a full-cell potential of 0 V. Even in absence of third electrode, we could identify the origin of the failure based on the shape of the potential during cycle #3. It indicates that the voltage drop of the full cell is due to an increase of the anode voltage owing to side reactions consuming Li, which could not be compensated by the high loading of the Li_xSi electrode.

Despite the originality of such set-up, we did not succeed in improving the cycle-life of the $\text{Li}_x\text{Si-O}_2$ system using in the Ohara cell due to the high amount of Li lost during the formatting cycles. This would require many trials so as to optimize the cycling parameters, which we have not done owing to the practical difficulties for carrying out this kind of experiment without breaking the very brittle and expensive LICGS membrane.

IV Conclusions

In this chapter, the use of Silicon as anode material in Lithium-Air batteries was discussed. First, we focused on the Li-Si alloying process in order to develop an electrode capable of sustaining a high capacity for numerous cycles. This was achieved by using silicon nanoparticles embedded in a composite electrode in concert with developing electrochemical pretreatments – namely a *short circuit*, a *plating sequence*, and a *potentiostatic discharge* – boosting their capacity. This effect was assigned to the reduction of the SiO_2 layer coating the Si NP into electroactive Si; phenomenon which was also demonstrated when using pure SiO_2 particles. This result is not anodyne knowing that previous works reporting the electro-reduction of silica were only dealing with extremely small (< 30 nm) SiO_2 domains^{374,380,381}.

Having developed high capacity, long cycle-life Si electrodes, we then focused on their integration into full $\text{Li}_x\text{Si-O}_2$ cells. The preparation of the lithiated silicon anodes enlists a few intermediary steps, such as the prelithiation sequence or the washing process, which were all optimized. The behavior of the Li_xSi electrodes in full Li-Air cells was reported in two systems, respectively using a DMA-based and a TEGDME-based electrolyte. Owing to inevitable side reactions neutralizing the available Li, the performances of the full cells were limited when compared to the similar systems using Li as anode. Nonetheless, we could identify the reasons of the cell failure in both systems, and were able to improve the cycle-life of a DMA-based $\text{Li}_x\text{Si-O}_2$ cell to more than 430 h (> 30 cycles) by reducing the capacity of the air electrode. We could reproduce what was reported in other papers also using this strategy and/or another one consisting in cycling the cell at a very high rate (less than a few hours per cycle), which is therefore totally impractical.

It remains from this study that replacing the Li electrode in Li- O_2 cells by an alloy still remains as a hurdle for the development of Li-Air batteries, but we are convinced that further investigating the possible ways to overcome the Li losses during the initial cycles is the key to a significant progress.

GENERAL CONCLUSIONS

Among all the battery technologies “beyond Li-ion”, the Lithium-Air technology is one of the most promising in term of capacity, but its complex chemistry has prevented any practical applications so far. The work accomplished during this thesis was an opportunity to contribute to the development of this technology, and follows the recent trend observed in the literature which focuses on understanding the fundamental chemical mechanism at play, rather than focusing on performances with the risk to over-sell and/or propose irreproducible results.

Three main topics were covered during this manuscript:

- In line with the former statement and acknowledging the lack of reliable Li-O₂ test-cell in our lab at the beginning of the thesis, a new electrochemical cell dedicated to the study of the Metal-Air systems was designed and built. It enlists a pressure sensor monitoring the gas consumption/evolution in the cell during cycling, hence giving access to the e⁻/gas ratio which reveals valuable information on the chemistry of the systems studied. More importantly, our setup can sustain thousands of hours of operation enabling long-term cycling characterization, which cannot be undertaken by usual gas analysis technics such as DEMS or OEMS.

Our pressurized cells can be mounted onto the Swagelok[®] system used worldwide for testing Li-ion batteries, which testifies the universality of our device. Its user-friendliness is therefore reinforced by the simplicity of the purging/filling procedure and the possibility to control the pressure sensor directly from the potentiostat. For these reasons, it is used everyday in the lab for routine analysis of Li-O₂ systems, but also for testing other metal-air technologies and more generally any material whose electrochemical behavior enlists gas uptake and/or gas release upon cycling (*e.g.* Li-rich layered compounds, organic electrode materials...). Moreover, this setup can be used for the fundamental determination of the gas solubility (O₂, CO₂, etc...) in various solvent/salt combinations.

Lastly, an obvious optimization of the present system lies in its coupling to a mass spectrometer so as to determine not only the amount but also the nature of the gas released without jeopardizing the sensibility of the measurements; a task being presently undertaken.

- Using our newly-designed device, we carried out an electrochemical survey of various electrolyte configurations used so far in this field, namely LiTFSI in DME, DEGDME and TEGDME, LiNO₃ in DMA, and LiClO₄ in DMSO. Each system was characterized with respect to the e⁻/gas ratio, which evidences the presence of a few formatting cycles during the first hours of cycling, during which the electrochemical

(and gas evolution) behavior largely differs from what is observed further on cycling. Based on former reports, these formatting cycles were attributed to the formation of an SEI at the anode surface in the LiNO_3/DMA system, while they resulted from side reactions involving the carbon cathode in the glyme- and DMSO-based systems.

From this comparative study, we could deduce that the LiNO_3/DMA formulation was among the best of today's electrolytes, owing to the low level of parasitic reactions which enables a long-term cycling over more than 1300 h (> 35 cycles at 1000 mAh/g). The cycle-life of other electrolytes was hindered by parasitic reactions including for instance the instability of the metallic lithium anode, whose replacement by another high-capacity anode material was discussed in the third axis of this thesis.

- Owing to its very high capacity, lithiated silicon was studied in order to serve as Li source in full Li-O_2 cells. Prior to reach that end, we focused on mastering the Li-Si alloying process in order to develop a high-capacity and long-term cycling electrode. This was achieved by using silicon nanoparticles embedded in a composite electrode in concert with developing electrochemical pretreatments – namely a *short circuit*, a *plating sequence*, and a *potentiostatic discharge* – for boosting their capacity. A systematic survey of these pretreatments indicated that the extra capacity arose from the electro-reduction of the native SiO_2 layer coating the Si NP into active Si and most likely Li_4SiO_4 , as reported for SiO_x compounds. The treated electrodes could sustain > 200 cycles at around 2000 mAh/g. In the meantime, this effect was extended to pure, homemade SiO_2 particles which could be reduced up to 50 % *via* a long potentiostatic discharge.

Having developed high capacity, long cycle-life Si electrodes, we focused on their integration into full $\text{Li}_x\text{Si-O}_2$ cells. The preparation of the Li_xSi electrodes requires a few intermediary steps, which were all optimized prior to study the behavior of the lithiated electrodes in full cells using two electrolytes formerly studied that are the LiNO_3/DMA and the $\text{LiTFSI}/\text{TEGDME}$ couples. Without surprise, their cycle-life was hindered by the amount of lithium trapped in the parasitic reactions – earlier evidenced in our Li-O_2 study – which we could partially compensate in the LiNO_3/DMA system by plating a small amount of Li onto the Li_xSi electrode. When this strategy was used and the capacity limited to 500 mAh/g, we managed to cycle the cell for more than 400 h, which is among the best cycle-life reported so far for a full $\text{Li}_x\text{Si-O}_2$ cell (Figure 106). Nonetheless, nor such capacity restrictions neither the very fast cycling used by H. Zhou *et al.*³⁷⁸ that allow them to obtain 100 cycles (Figure 106b) are viable for practical applications.

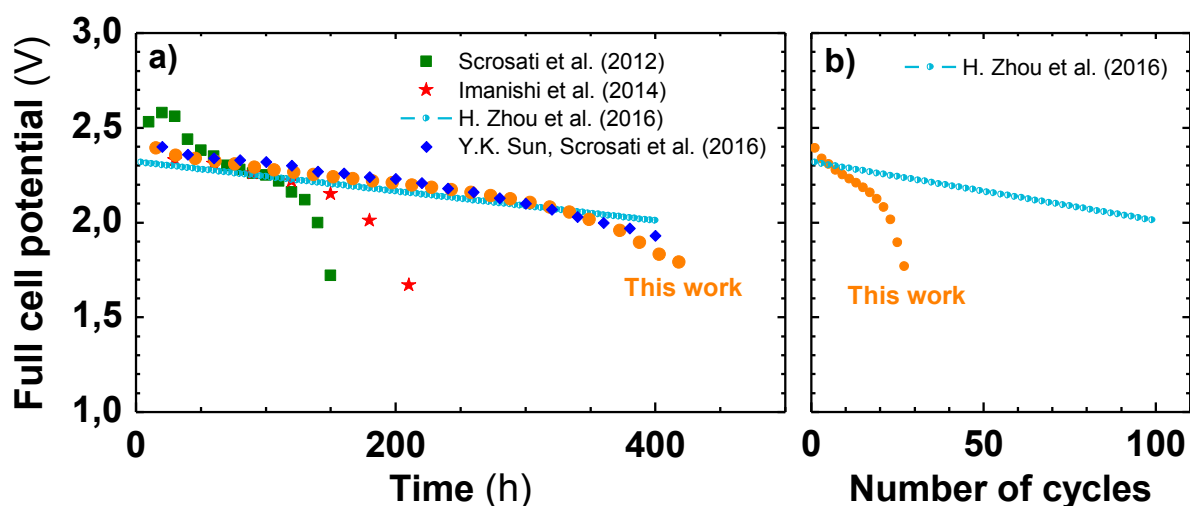


Figure 106: Comparison of the potential at the end of discharge between various full $\text{Li}_x\text{Si-O}_2$ full cells reported in the literature ^{146,147,378,382} and our work as function of the time of cycling (a) or the number of cycles (b). One dot represents one cycle. The values of other group's work were extracted and/or interpolated from their publications. * : hybrid aqueous(+)/organic(-) full Li-O_2 cell ¹⁴⁷.

The development of the Lithium-Air technology requires the understanding of chemical mechanisms involving a triple point between a gas (so far O_2), a liquid (the electrolyte) and a solid (the cathode); a complex scheme with which the battery community is not familiar. Based on the relatively slow evolution of the fuel cell area – which also involves a triple point but has the significant advantage of starting with pure gases! –, the development of a functional Lithium-Air battery prototype will take some time.

Within this context, the analytical device that was developed during this thesis and which enables a fine monitoring of the gas inside an Li-O_2 battery is of prime interest. Therefore, more analytical tools must be cleverly adapted (and not simply translated) from the Li-ion to the Li-O_2 community in order to get more insight into the fundamental mechanisms.

The main issue now is to find a way to minimize (and ideally delete) the parasitic reactions which slowly leads to a premature cell death. Many efforts have been devoted to that end, and some are currently focused on developing redox mediators that would enable the complete oxidation of Li_2O_2 particles at lower potentials, hence reducing the risk to damage the cathode material.

Finally, the stability of the electrolyte must be improved, either directly by identifying/developing a new electrolyte, or indirectly by lowering the charge potential and/or controlling the reactivity of the superoxide, which is mainly at the origin of parasitic reactions. In this context, we are convinced that further investigating full Li-Air batteries *via*

General conclusions

simple fundamental experiences (*e.g.* the $\text{Li}_x\text{Si-O}_2$ cell herein) – which can directly quantify the Li losses hence the parasitical reactions – are the key towards significant progresses.

Bibliography

1. United Nations. *Adoption Of The Paris Agreement, Conference of the Parties, Twenty-first session.* (2015).
2. Bernstein, L., Bosch, P., Canziani, O., Chen, Z., Christ, R., Davidson, O., Hare, W., Huq, S., Karoly, D., Kattsov, V. & others. *Climate change 2007: Synthesis report: An assessment of the intergovernmental panel on climate change.* (IPCC, 2008).
3. *Climate change 2014: synthesis report.* (Intergovernmental Panel on Climate Change, 2015).
4. Miller, R. L., Schmidt, G. A., Nazarenko, L. S., Tausnev, N., Bauer, S. E., DelGenio, A. D., Kelley, M., Lo, K. K., Ruedy, R., Shindell, D. T., *et al.* CMIP5 historical simulations (1850–2012) with GISS ModelE2. *J. Adv. Model. Earth Syst.* **6**, 441–478 (2014). doi:10.1002/2013MS000266
5. Hansen, J., Nazarenko, L., Ruedy, R., Sato, M., Willis, J., Del Genio, A., Koch, D., Lacis, A., Lo, K., Menon, S. & others. Earth's energy imbalance: Confirmation and implications. *science* **308**, 1431–1435 (2005).
6. *Climate change 2014: mitigation of climate change: Working Group III contribution to the Fifth Assessment Report of the Intergovernmental Panel on Climate Change.* (Cambridge University Press, 2014).
7. *Global Greenhouse Gas Emissions Data.*
8. Global Carbon Project (GCP). URL: <http://www.globalcarbonproject.org/carbonbudget/>
9. Bridel, J.-S. 'Optimisation de composites silicium-polymère-carbone pour électrodes négatives d'accumulateurs lithium-ion'. *PhD Def. - LRCS Amiens Fr.* (2011).
10. Manicore -. URL: <http://www.manicore.com/documentation/energie.html>
11. Venezuela. *Le Moci* URL: <http://www.lemoci.com/fiche-pays/venezuela/>
12. Energies et Economie: Revue Mondiale Septembre 2015. URL: <http://www.2000watts.org/index.php/energytrend/petrole/peak-oil/1152-energies-et-economie-revue-mondiale-septembre-2015.html>
13. Death in the Air: Air Pollution Costs Money and Lives. *World Bank* URL: <http://www.worldbank.org/en/news/infographic/2016/09/08/death-in-the-air-air-pollution-costs-money-and-lives>
14. International Energy Agency. IEA - Report: World Balances for 2014. (2014). URL: <http://www.iea.org/statistics/statisticssearch/report/?country=WORLD&product=balances&year=2014>
15. Tarascon, J.-M. & Armand, M. Issues and challenges facing rechargeable lithium batteries. *Nature* **414**, 359–367 (2001). doi:10.1038/35104644
16. Cheng, F., Liang, J., Tao, Z. & Chen, J. Functional materials for rechargeable batteries. *Adv. Mater.* **23**, 1695–1715 (2011). doi:10.1002/adma.201003587
17. Pillot, C. *Battery Market Development for Consumer Electronics, Automotive, and Industrial: Materials Requirements and Trends.* (Avicenne Energy, 2015).
18. *Commissariat Général au Développement Durable, Etudes & Documents: Les véhicules Electriques en perspective. Analyse coûts-avantages et demande potentielle. n°41 mai 2011.*
19. Association nationale pour le développement de la mobilité électrique. Quelle est la place de la France sur le marché européen du véhicule électrique ? *Avere-France* URL: http://www.aver-france.org/Site/Article/?article_id=6515

20. Association nationale pour le développement de la mobilité électrique. Le vélo à assistance électrique dope les ventes de cycles en 2015! *Avere-France* URL: http://www.avery-france.org/Site/Article/?article_id=6531
21. und Auskünfte, U. & Swiss Federal Energy Office. Statistique globale suisse de l'énergie 2014. (2014).
22. Ministère du Développement Durable. *La production d'électricité et l'effacement de consommation en France*. (2015).
23. China Energy News. *National Power Planning Research Center. Forecast of Power Generation Capacity and Power Demand Development of China in the Future*. (2013).
24. US Energy Information Administration. *Electric Power Monthly*. (2015).
25. Scotiabank. *Global Auto Report*. (2016).
26. International Energy Agency. *Global EV Outlook 2015*. (2016).
27. Ipsos. *Les Français, la mobilité et les véhicules électriques - Enquête pour Avere-France et Mobivia Groupe*. (2014).
28. ADEME. Chiffres clés et observations - Chiffres clés. *ADEME* (2016). URL: <http://www.ademe.fr/expertises/mobilite-transport/chiffres-cles-observations/chiffres-cles>
29. Bruce, P. G., Freunberger, S. A., Hardwick, L. J. & Tarascon, J.-M. Li-O₂ and Li-S batteries with high energy storage. *Nat. Mater.* **11**, 19–29 (2012). doi:10.1038/nmat3191
30. F.R.S, M. A. V. & P.R.S, R. H. S. J. B. B. K. B. I. On the electricity excited by the mere contact of conducting substances of different kinds. *Philos. Mag. Ser. 1* **7**, 289–311 (1800). doi:10.1080/14786440008562590
31. Planté, G. (1834-1889). Recherches sur l'électricité : de 1859 à 1879. *Lilliad - Univ. Lille - Sci. Technol.* (2013).
32. Jungner, J. *Swedish Patent, 15, 567; German Patent 163, 170*. (1901).
33. Percheron-Guégan, A. & Welter, J.-M. in *Hydrogen in Intermetallic Compounds I* (ed. Schlapbach, D. L.) 11–48 (Springer Berlin Heidelberg, 1988).
34. Feng, F., Geng, M. & Northwood, D. O. Electrochemical behaviour of intermetallic-based metal hydrides used in Ni/metal hydride (MH) batteries: a review. *Int. J. Hydrog. Energy* **26**, 725–734 (2001). doi:10.1016/S0360-3199(00)00127-0
35. CORPORATION, T. M. Toyota Global Site | The Hybrid that Started it All. *Toyota Motor Corporation Global Website* URL: http://www.toyota-global.com/company/toyota_traditions/innovation/nov2008_feb2009_1.html
36. Tarascon, J.-M. & Simon, P. *Electrochemical Energy Storage*. (John Wiley & Sons, 2015).
37. Larcher, D. & Tarascon, J.-M. *Science of Lithium - The Science and Practice of Lithium Therapy*. (2014).
38. Moore, G. E. Cramming more components onto integrated circuits. *Read. Comput. Archit. - Electron.* **38**, (1965).
39. Moore, G. E. & others. Progress in digital integrated electronics. *SPIE Milest. Ser. MS* **178**, 179–181 (2004).
40. Tarascon, J.-M. *L'énergie : stockage électrochimique et développement durable*. (Collège de France, 2013).
41. Tarascon, J.-M. *Chimie du solide et énergie. Exemples et avenir d'une science millénaire: Leçon inaugurale prononcée le jeudi 23 janvier 2014*. (Collège de France, 2015).
42. Steel, B. C. H. *Fast ion transport in solids: Solid state batteries and devices*. (North Holland Pub. Co., 1973).
43. Armand, M. B. *Fast ion transport in solids: Solid state batteries and devices*. (North Holland Pub. Co., 1973).
44. Rouxel, J., Danot, M. & Bichon, M. Les composites intercalaires NaxTiS₂. Etude générale des phases NaxTiS₂ et KxTiS₂. *Bull Soc Chim* **11**, 3930–3936 (1971).

45. Whittingham, M. S. Intercalation chemistry and energy storage. *J. Solid State Chem.* **29**, 303–310 (1979). doi:10.1016/0022-4596(79)90187-7
46. Orsini, F., du Pasquier, A., Beaudouin, B., Tarascon, J. M., Trentin, M., Langenhuizen, N., de Beer, E. & Notten, P. In situ SEM study of the interfaces in plastic lithium cells. *J. Power Sources* **81–82**, 918–921 (1999). doi:10.1016/S0378-7753(98)00241-9
47. Vashishta, P., Mundy, J. N. & Shenoy, G. K. *Fast ion transport in solids: electrodes, and electrolytes*. (North Holland, 1979).
48. LES BATTERIES LMP (LITHIUM MÉTAL POLYMÈRE). *www.bluecar.fr* (2014). URL: <http://www.bluecar.fr/les-batteries-lmp-lithium-metal-polymere>
49. Murphy, D. W., Di Salvo, F. J., Carides, J. N. & Waszczak, J. V. Topochemical reactions of rutile related structures with lithium. *Mater. Res. Bull.* **13**, 1395–1402 (1978). doi:10.1016/0025-5408(78)90131-9
50. Lazzari, M. & Scrosati, B. A Cyclable Lithium Organic Electrolyte Cell Based on Two Intercalation Electrodes. *J. Electrochem. Soc.* **127**, 773–774 (1980). doi:10.1149/1.2129753
51. Nagaura, T. & Tozawa, K. Lithium ion rechargeable battery. *Prog Batter. Sol. Cells* **9**, 209 (1990).
52. Murphy, D. W. & Christian, P. A. Solid State Electrodes for High Energy Batteries. *Science* **205**, 651–656 (1979). doi:10.1126/science.205.4407.651
53. Mizushima, K., Jones, P. C., Wiseman, P. J. & Goodenough, J. B. Li_xCoO_2 ($0 < x < 1$): A new cathode material for batteries of high energy density. *Mater. Res. Bull.* **15**, 783–789 (1980).
54. Thackeray, M. M., David, W. I. F., Bruce, P. G. & Goodenough, J. B. Lithium insertion into manganese spinels. *Mater. Res. Bull.* **18**, 461–472 (1983). doi:10.1016/0025-5408(83)90138-1
55. Madhavi, S., Subba Rao, G. V., Chowdari, B. V. R. & Li, S. F. Y. Effect of aluminium doping on cathodic behaviour of $\text{LiNi}_0.7\text{Co}_0.3\text{O}_2$. *J. Power Sources* **93**, 156–162 (2001). doi:10.1016/S0378-7753(00)00559-0
56. Kosova, N. V., Devyatkina, E. T. & Kaichev, V. V. Optimization of $\text{Ni}^{2+}/\text{Ni}^{3+}$ ratio in layered $\text{Li}(\text{Ni},\text{Mn},\text{Co})\text{O}_2$ cathodes for better electrochemistry. *J. Power Sources* **174**, 965–969 (2007). doi:10.1016/j.jpowsour.2007.06.051
57. Cao, H., Zhang, Y., Zhang, J. & Xia, B. Synthesis and electrochemical characteristics of layered $\text{LiNi}_0.6\text{Co}_0.2\text{Mn}_0.2\text{O}_2$ cathode material for lithium ion batteries. *Solid State Ion.* **176**, 1207–1211 (2005). doi:10.1016/j.ssi.2005.02.023
58. Ma, L., Self, J., Nie, M., Glazier, S., Wang, D. Y., Lin, Y.-S. & Dahn, J. R. A systematic study of some promising electrolyte additives in $\text{Li}[\text{Ni}_{1/3}\text{Mn}_{1/3}\text{Co}_{1/3}]\text{O}_2/\text{graphite}$, $\text{Li}[\text{Ni}_{0.5}\text{Mn}_{0.3}\text{Co}_{0.2}]/\text{graphite}$ and $\text{Li}[\text{Ni}_{0.6}\text{Mn}_{0.2}\text{Co}_{0.2}]/\text{graphite}$ pouch cells. *J. Power Sources* **299**, 130–138 (2015). doi:10.1016/j.jpowsour.2015.08.084
59. Kim, J.-S., Johnson, C. S. & Thackeray, M. M. Layered $x\text{LiMO}_2 \cdot (1-x)\text{Li}_2\text{M}'\text{O}_3$ electrodes for lithium batteries: a study of $0.95\text{LiMn}_0.5\text{Ni}_0.5\text{O}_2 \cdot 0.05\text{Li}_2\text{TiO}_3$. *Electrochem. Commun.* **4**, 205–209 (2002). doi:10.1016/S1388-2481(02)00251-5
60. Kim, J.-S., Johnson, C. S., Vaughey, J. T., Thackeray, M. M., Hackney, S. A., Yoon, W. & Grey, C. P. Electrochemical and Structural Properties of $x\text{Li}_2\text{M}'\text{O}_3 \cdot (1-x)\text{LiMn}_0.5\text{Ni}_0.5\text{O}_2$ Electrodes for Lithium Batteries ($\text{M}' = \text{Ti}, \text{Mn}, \text{Zr}; 0 \leq x \leq 0.3$). *Chem. Mater.* **16**, 1996–2006 (2004). doi:10.1021/cm0306461
61. Thackeray, M. M., Johnson, C. S., Vaughey, J. T., Li, N. & Hackney, S. A. Advances in manganese-oxide ‘composite’ electrodes for lithium-ion batteries. *J. Mater. Chem.* **15**, 2257–2267 (2005). doi:10.1039/B417616M
62. Johnson, C. S., Li, N., Lefief, C., Vaughey, J. T. & Thackeray, M. M. Synthesis, Characterization and Electrochemistry of Lithium Battery Electrodes: $x\text{Li}_2\text{MnO}_3 \cdot (1 -$

- x)LiMn_{0.333}Ni_{0.333}Co_{0.333}O₂ ($0 \leq x \leq 0.7$). *Chem. Mater.* **20**, 6095–6106 (2008). doi:10.1021/cm801245r
63. Sathiya, M., Rouse, G., Ramesha, K., Laisa, C. P., Vezin, H., Sougrati, M. T., Doublet, M.-L., Foix, D., Gonbeau, D., Walker, W., Prakash, A. S., Ben Hassine, M., Dupont, L. & Tarascon, J.-M. Reversible anionic redox chemistry in high-capacity layered-oxide electrodes. *Nat. Mater.* **12**, 827–835 (2013). doi:10.1038/nmat3699
64. Saubanère, M., McCalla, E., Tarascon, J.-M. & Doublet, M.-L. The intriguing question of anionic redox in high-energy density cathodes for Li-ion batteries. *Energy Env. Sci* **9**, 984–991 (2016). doi:10.1039/C5EE03048J
65. Koga, H., Croguennec, L., Ménétrier, M., Mannessiez, P., Weill, F., Delmas, C. & Belin, S. Operando X-ray Absorption Study of the Redox Processes Involved upon Cycling of the Li-Rich Layered Oxide Li_{1.20} Mn_{0.54} Co_{0.13} Ni_{0.13} O₂ in Li Ion Batteries. *J. Phys. Chem. C* **118**, 5700–5709 (2014). doi:10.1021/jp412197z
66. Grimaud, A., Hong, W. T., Shao-Horn, Y. & Tarascon, J.-M. Anionic redox processes for electrochemical devices. *Nat. Mater.* **15**, 121–126 (2016).
67. Armstrong, A. R., Holzapfel, M., Novák, P., Johnson, C. S., Kang, S.-H., Thackeray, M. M. & Bruce, P. G. Demonstrating oxygen loss and associated structural reorganization in the lithium battery cathode Li [Ni_{0.2}Li_{0.2}Mn_{0.6}] O₂. *J. Am. Chem. Soc.* **128**, 8694–8698 (2006).
68. Sathiya, M., Ramesha, K., Rouse, G., Foix, D., Gonbeau, D., Prakash, A. S., Doublet, M. L., Hemalatha, K. & Tarascon, J.-M. High Performance Li₂Ru_{1-y}MnyO₃ ($0.2 \leq y \leq 0.8$) Cathode Materials for Rechargeable Lithium-Ion Batteries: Their Understanding. *Chem. Mater.* **25**, 1121–1131 (2013). doi:10.1021/cm400193m
69. McCalla, E., Prakash, A. S., Berg, E., Saubanère, M., Abakumov, A. M., Foix, D., Klobes, B., Sougrati, M.-T., Rouse, G., Lepoivre, F., Mariyappan, S., Doublet, M.-L., Gonbeau, D., Novak, P., Tendeloo, G. V., Hermann, R. P. & Tarascon, J.-M. Reversible Li-Intercalation through Oxygen Reactivity in Li-Rich Li-Fe-Te Oxide Materials. *J. Electrochem. Soc.* **162**, A1341–A1351 (2015). doi:10.1149/2.0991507jes
70. Watanabe, N. & Fukuda, M. *Primary Cell for Electric Batteries. Patent US 3536532. Available at <http://www.google.com/patents?id=pCRqAAAAEBAJ>*. (1970).
71. Braeuer, K. & Moyes, K. R. *High Energy Density Battery. Patent US 3514337. Available at <http://www.google.com/patents/US3514337>*.
72. Dunning, J. S., Tiedemann, W. H., Hsueh, L. & Bennion, D. N. A Secondary, Nonaqueous Solvent Battery. *J. Electrochem. Soc.* **118**, 1886–1890 (1971). doi:10.1149/1.2407861
73. Hunger, H. F. & Heymach, G. J. Cathodic Discharge of Graphite Intercalation Compounds in Organic Electrolytes. *J. Electrochem. Soc.* **120**, 1161–1168 (1973). doi:10.1149/1.2403654
74. Armand, M. & Touzain, P. Proceedings of the Franco American Conference on Intercalation Compounds of Graphite Graphite intercalation compounds as cathode materials. *Mater. Sci. Eng.* **31**, 319–329 (1977). doi:10.1016/0025-5416(77)90052-0
75. Yazami, R. & Touzain, P. A reversible graphite-lithium negative electrode for electrochemical generators. *J. Power Sources* **9**, 365–371 (1983). doi:10.1016/0378-7753(83)87040-2
76. Mohri, M., Yanagisawa, N., Tajima, Y., Tanaka, H., Mitate, T., Nakajima, S., Yoshida, M., Yoshimoto, Y., Suzuki, T. & Wada, H. 4th International Meetings on Lithium Batteries Rechargeable lithium battery based on pyrolytic carbon as a negative electrode. *J. Power Sources* **26**, 545–551 (1989). doi:10.1016/0378-7753(89)80176-4
77. Yoshino, A., Sanachika, K. & Nakajima, T. *Secondary battery*. (Google Patents, 1987).
78. Nishi, Y., Azuma, H. & Omaru, A. *Non aqueous electrolyte cell. Patent US 4959281. Issued September 25, 1990.*

79. Interview with Dr. Akira Yoshino | R&D | Asahi Kasei. *Asahi Kasei Corporation* URL: http://www.asahi-kasei.co.jp/asahi/en/r_and_d/interview/yoshino.html
80. Larcher, D., Beattie, S., Morcrette, M., Edström, K., Jumas, J.-C. & Tarascon, J.-M. Recent findings and prospects in the field of pure metals as negative electrodes for Li-ion batteries. *J. Mater. Chem.* **17**, 3759–3772 (2007). doi:10.1039/B705421C
81. Palacín, M. R. Recent advances in rechargeable battery materials: a chemist's perspective. *Chem. Soc. Rev.* **38**, 2565 (2009). doi:10.1039/b820555h
82. Toudjine, A. 'Optimisation de l'électrode négative à base de silicium pour les batteries lithium-ion'. *PhD Def. - LRCS Amiens Fr.* (2016).
83. Ohzuku, T., Ueda, A. & Yamamoto, N. Zero-Strain Insertion Material of Li [Li₁ / 3Ti₅ / 3] O₄ for Rechargeable Lithium Cells. *J. Electrochem. Soc.* **142**, 1431–1435 (1995). doi:10.1149/1.2048592
84. Panero, S., Reale, P., Ronci, F., Albertini, V. R. & Scrosati, B. Structural and electrochemical study on Li (Li₁/3Ti₅/3) O₄ anode material for lithium ion batteries. *Ionics* **6**, 461–465 (2000).
85. Zaghib, K., Armand, M. & Gauthier, M. Electrochemistry of Anodes in Solid-State Li-Ion Polymer Batteries. *J. Electrochem. Soc.* **145**, 3135–3140 (1998). doi:10.1149/1.1838776
86. Wagemaker, M., Borghols, W. J. H. & Mulder, F. M. Large Impact of Particle Size on Insertion Reactions. A Case for Anatase Li_xTiO₂. *J. Am. Chem. Soc.* **129**, 4323–4327 (2007). doi:10.1021/ja067733p
87. Deng, D., Kim, M. G., Lee, J. Y. & Cho, J. Green energy storage materials: Nanostructured TiO₂ and Sn-based anodes for lithium-ion batteries. *Energy Environ. Sci.* **2**, 818 (2009). doi:10.1039/b823474d
88. Thackeray, M. M., David, W. I. F. & Goodenough, J. B. High-temperature lithiation of α-Fe₂O₃: A mechanistic study. *J. Solid State Chem.* **55**, 280–286 (1984). doi:10.1016/0022-4596(84)90278-0
89. Winter, M. & Besenhard, J. O. Electrochemical lithiation of tin and tin-based intermetallics and composites. *Electrochimica Acta* **45**, 31–50 (1999). doi:10.1016/S0013-4686(99)00191-7
90. Poizot, P., Laruelle, S., Grugeon, S., Dupont, L. & Tarascon, J.-M. Nano-sized transition-metal oxides as negative-electrode materials for lithium-ion batteries. *Nature* **407**, 496–499 (2000). doi:10.1038/35035045
91. Kang, Y.-M., Kim, K.-T., Kim, J.-H., Kim, H.-S., Lee, P. S., Lee, J.-Y., Liu, H. K. & Dou, S. X. Electrochemical properties of Co₃O₄, Ni-Co₃O₄ mixture and Ni-Co₃O₄ composite as anode materials for Li ion secondary batteries. *J. Power Sources* **133**, 252–259 (2004). doi:10.1016/j.jpowsour.2004.02.012
92. Hosono, E., Fujihara, S., Honma, I. & Zhou, H. The high power and high energy densities Li ion storage device by nanocrystalline and mesoporous Ni/NiO covered structure. *Electrochem. Commun.* **8**, 284–288 (2006). doi:10.1016/j.elecom.2005.11.023
93. Gillot, F., Ménétrier, M., Bekaert, E., Dupont, L., Morcrette, M., Monconduit, L. & Tarascon, J. M. Vanadium diphosphides as negative electrodes for secondary Li-ion batteries. *J. Power Sources* **172**, 877–885 (2007). doi:10.1016/j.jpowsour.2007.05.043
94. Xiang, J. Y., Tu, J. P., Wang, X. L., Huang, X. H., Yuan, Y. F., Xia, X. H. & Zeng, Z. Y. Electrochemical performances of nanostructured Ni₃P–Ni films electrodeposited on nickel foam substrate. *J. Power Sources* **185**, 519–525 (2008). doi:10.1016/j.jpowsour.2008.06.084
95. Sun, Q. & Fu, Z.-W. An Anode Material of CrN for Lithium-Ion Batteries. *Electrochem. Solid-State Lett.* **10**, A189–A193 (2007). doi:10.1149/1.2745087

96. Pereira, N., Balasubramanian, M., Dupont, L., McBreen, J., Klein, L. C. & Amatucci, G. G. The Electrochemistry of Germanium Nitride with Lithium. *J. Electrochem. Soc.* **150**, A1118–A1128 (2003). doi:10.1149/1.1587724
97. Fu, Z.-W., Li, C.-L., Liu, W.-Y., Ma, J., Wang, Y. & Qin, Q.-Z. Electrochemical Reaction of Lithium with Cobalt Fluoride Thin Film Electrode. *J. Electrochem. Soc.* **152**, E50–E55 (2005). doi:10.1149/1.1839512
98. Takada, K., Iwamoto, K. & Kondo, S. Lithium iron sulfide as an electrode material in a solid state lithium battery. *Solid State Ion.* **117**, 273–276 (1999). doi:10.1016/S0167-2738(98)00413-5
99. Oumellal, Y., Rougier, A., Nazri, G. A., Tarascon, J.-M. & Aymard, L. Metal hydrides for lithium-ion batteries. *Nat. Mater.* **7**, 916–921 (2008). doi:10.1038/nmat2288
100. Yao, N. P., Herédy, L. A. & Saunders, R. C. Emf Measurements of Electrochemically Prepared Lithium-Aluminum Alloy. *J. Electrochem. Soc.* **118**, 1039–1042 (1971). doi:10.1149/1.2408242
101. Gay, E. C., Vissers, D. R., Martino, F. J. & Anderson, K. E. Performance Characteristics of Solid Lithium-Aluminum Alloy Electrodes. *J. Electrochem. Soc.* **123**, 1591–1596 (1976). doi:10.1149/1.2132652
102. Lai, S.-C. Solid lithium-silicon electrode. *J. Electrochem. Soc.* **123**, 1196 (1976).
103. Sharma, R. A. & Seefurth, R. N. Thermodynamic Properties of the Lithium-Silicon System. *J. Electrochem. Soc.* **123**, 1763–1768 (1976). doi:10.1149/1.2132692
104. Seefurth, R. N. & Sharma, R. A. Investigation of Lithium Utilization from A Lithium-Silicon Electrode. *J. Electrochem. Soc.* **124**, 1207–1214 (1977). doi:10.1149/1.2133529
105. Seefurth, R. N. & Sharma, R. A. Dependence of Lithium-Silicon Electrode Potential and Lithium Utilization on Reference Electrode Location. *J. Electrochem. Soc.* **127**, 1101–1104 (1980). doi:10.1149/1.2129824
106. Wen, C. J. & Huggins, R. A. Chemical diffusion in intermediate phases in the lithium-tin system. *J. Solid State Chem.* **35**, 376–384 (1980). doi:10.1016/0022-4596(80)90535-6
107. Weppner, W. & Huggins, R. A. Thermodynamic Properties of the Intermetallic Systems Lithium-Antimony and Lithium-Bismuth. *J. Electrochem. Soc.* **125**, 7–14 (1978). doi:10.1149/1.2131401
108. Weppner, W. & Huggins, R. A. Determination of the Kinetic Parameters of Mixed-Conducting Electrodes and Application to the System Li₃Sb. *J. Electrochem. Soc.* **124**, 1569–1578 (1977). doi:10.1149/1.2133112
109. Wen, C. J. & Huggins, R. A. Electrochemical Investigation of the Lithium-Gallium System. *J. Electrochem. Soc.* **128**, 1636–1641 (1981). doi:10.1149/1.2127701
110. Tedmon, C. S. & Hagel, W. C. Electrochemical Formation of Lithium Alloys from Molten Lithium Fluoride. *J. Electrochem. Soc.* **115**, 151–157 (1968). doi:10.1149/1.2411053
111. James, S. D. & DeVries, L. E. Structure and Anodic Discharge Behavior of Lithium-Boron Alloys in the LiCl - KCl Eutectic Melt. *J. Electrochem. Soc.* **123**, 321–327 (1976). doi:10.1149/1.2132818
112. Dey, A. N. Electrochemical Alloying of Lithium in Organic Electrolytes. *J. Electrochem. Soc.* **118**, 1547 (1971). doi:10.1149/1.2407783
113. Obrovac, M. N. & Krause, L. J. Reversible Cycling of Crystalline Silicon Powder. *J. Electrochem. Soc.* **154**, A103–A108 (2007). doi:10.1149/1.2402112
114. Mazouzi, D., Delpuech, N., Oumellal, Y., Gauthier, M., Cerbelaud, M., Gaubicher, J., Dupré, N., Moreau, P., Guyomard, D., Roué, L. & Lestriez, B. New insights into the silicon-based electrode's irreversibility along cycle life through simple gravimetric method. *J. Power Sources* **220**, 180–184 (2012). doi:10.1016/j.jpowsour.2012.08.007
115. Yoon, T., Nguyen, C. C., Seo, D. M. & Lucht, B. L. Capacity Fading Mechanisms of Silicon Nanoparticle Negative Electrodes for Lithium Ion Batteries. *J. Electrochem. Soc.* **162**, A2325–A2330 (2015). doi:10.1149/2.0731512jes

116. Li, J., Lewis, R. B. & Dahn, J. R. Sodium Carboxymethyl Cellulose A Potential Binder for Si Negative Electrodes for Li-Ion Batteries. *Electrochem. Solid-State Lett.* **10**, A17–A20 (2007). doi:10.1149/1.2398725
117. Hochgatterer, N. S., Schweiger, M. R., Koller, S., Raimann, P. R., Wöhrle, T., Wurm, C. & Winter, M. Silicon/Graphite Composite Electrodes for High-Capacity Anodes: Influence of Binder Chemistry on Cycling Stability. *Electrochem. Solid-State Lett.* **11**, A76–A80 (2008). doi:10.1149/1.2888173
118. Liu, W.-R., Yang, M.-H., Wu, H.-C., Chiao, S. M. & Wu, N.-L. Enhanced Cycle Life of Si Anode for Li-Ion Batteries by Using Modified Elastomeric Binder. *Electrochem. Solid-State Lett.* **8**, A100–A103 (2005). doi:10.1149/1.1847685
119. Wang, G. X., Sun, L., Bradhurst, D. H., Zhong, S., Dou, S. X. & Liu, H. K. Innovative nanosize lithium storage alloys with silica as active centre. *J. Power Sources* **88**, 278–281 (2000). doi:10.1016/S0378-7753(00)00385-2
120. Hatchard, T. D., Obrovac, M. N. & Dahn, J. R. A Comparison of the Reactions of the SiSn, SiAg, and SiZn Binary Systems with L3i. *J. Electrochem. Soc.* **153**, A282–A287 (2006). doi:10.1149/1.2140607
121. Nguyen, B. P. N., Gaubicher, J. & Lestriez, B. Analogy between electrochemical behaviour of thick silicon granular electrodes for lithium batteries and fine soils micromechanics. *Electrochimica Acta* **120**, 319–326 (2014). doi:10.1016/j.electacta.2013.12.126
122. Larcher, D., Beaulieu, L. Y., MacNeil, D. D. & Dahn, J. R. In Situ X-Ray Study of the Electrochemical Reaction of Li with η' - Cu₆Sn₅. *J. Electrochem. Soc.* **147**, 1658–1662 (2000). doi:10.1149/1.1393413
123. Mukaibo, H., Momma, T. & Osaka, T. Changes of electro-deposited Sn–Ni alloy thin film for lithium ion battery anodes during charge discharge cycling. *J. Power Sources* **146**, 457–463 (2005). doi:10.1016/j.jpowsour.2005.03.043
124. Yang, J., Takeda, Y., Imanishi, N., Capiglia, C., Xie, J. Y. & Yamamoto, O. SiO_x-based anodes for secondary lithium batteries. *Solid State Ion.* **152–153**, 125–129 (2002). doi:10.1016/S0167-2738(02)00362-4
125. Szczech, J. R. & Jin, S. Nanostructured silicon for high capacity lithium battery anodes. *Energy Environ. Sci.* **4**, 56–72 (2010). doi:10.1039/C0EE00281J
126. Gauthier, M., Mazouzi, D., Reyter, D., Lestriez, B., Moreau, P., Guyomard, D. & Roué, L. A low-cost and high performance ball-milled Si-based negative electrode for high-energy Li-ion batteries. *Energy Environ. Sci.* **6**, 2145–2155 (2013). doi:10.1039/C3EE41318G
127. Obrovac, M. N. & Chevrier, V. L. Alloy Negative Electrodes for Li-Ion Batteries. *Chem. Rev.* **114**, 11444–11502 (2014). doi:10.1021/cr500207g
128. Aurbach, D., Gamolsky, K., Markovsky, B., Gofer, Y., Schmidt, M. & Heider, U. On the use of vinylene carbonate (VC) as an additive to electrolyte solutions for Li-ion batteries. *Electrochimica Acta* **47**, 1423–1439 (2002). doi:10.1016/S0013-4686(01)00858-1
129. Choi, N.-S., Yew, K. H., Lee, K. Y., Sung, M., Kim, H. & Kim, S.-S. Effect of fluoroethylene carbonate additive on interfacial properties of silicon thin-film electrode. *J. Power Sources* **161**, 1254–1259 (2006). doi:10.1016/j.jpowsour.2006.05.049
130. Etacheri, V., Haik, O., Goffer, Y., Roberts, G. A., Stefan, I. C., Fasching, R. & Aurbach, D. Effect of Fluoroethylene Carbonate (FEC) on the Performance and Surface Chemistry of Si-Nanowire Li-Ion Battery Anodes. *Langmuir* **28**, 965–976 (2011). doi:10.1021/la203712s
131. Aurbach, D., Talyosef, Y., Markovsky, B., Markevich, E., Zinigrad, E., Asraf, L., Gnanaraj, J. S. & Kim, H.-J. Design of electrolyte solutions for Li and Li-ion batteries: a review. *Electrochimica Acta* **50**, 247–254 (2004). doi:10.1016/j.electacta.2004.01.090

132. Tarascon, J. M. & Guyomard, D. New electrolyte compositions stable over the 0 to 5 V voltage range and compatible with the $\text{Li}_{1+x}\text{Mn}_2\text{O}_4$ /carbon Li-ion cells. *Solid State Ion.* **69**, 293–305 (1994). doi:10.1016/0167-2738(94)90418-9
133. Xu, K. Nonaqueous Liquid Electrolytes for Lithium-Based Rechargeable Batteries. *Chem. Rev.* **104**, 4303–4418 (2004). doi:10.1021/cr030203g
134. Suo, L., Borodin, O., Wang, C. & Xu, K. (Invited) Aqueous Interphase Enables Safe, Green and Low Cost Li-Ion Chemistry. *Meet. Abstr.* **MA2016-01**, 465–465 (2016).
135. Peled, E. The Electrochemical Behavior of Alkali and Alkaline Earth Metals in Nonaqueous Battery Systems—The Solid Electrolyte Interphase Model. *J. Electrochem. Soc.* **126**, 2047–2051 (1979). doi:10.1149/1.2128859
136. Balbuena, P. B. & Wang, Y. *Lithium-Ion Batteries: Solid-Electrolyte Interphase*. (World Scientific, 2004).
137. Huggins, R. A. Lithium alloy negative electrodes. *J. Power Sources* **81–82**, 13–19 (1999). doi:10.1016/S0378-7753(99)00124-X
138. Aurbach, D., Markovsky, B., Salitra, G., Markevich, E., Talyossef, Y., Koltypin, M., Nazar, L., Ellis, B. & Kovacheva, D. Review on electrode–electrolyte solution interactions, related to cathode materials for Li-ion batteries. *J. Power Sources* **165**, 491–499 (2007). doi:10.1016/j.jpowsour.2006.10.025
139. Fenton, D. E., Parker, J. M. & Wright, P. V. Complexes of alkali metal ions with poly (ethylene oxide). *polymer* **14**, 589 (1973).
140. Armand, M. Polymer solid electrolytes - an overview. *Solid State Ion.* **9**, 745–754 (1983). doi:10.1016/0167-2738(83)90083-8
141. Tarascon, J.-M., Gozdz, A. S., Schmutz, C., Shokoohi, F. & Warren, P. C. Proceedings of the 10th International Conference on Solid State Ionics Performance of Bellcore’s plastic rechargeable Li-ion batteries. *Solid State Ion.* **86**, 49–54 (1996). doi:10.1016/0167-2738(96)00330-X
142. Quartarone, E. & Mustarelli, P. Electrolytes for solid-state lithium rechargeable batteries: recent advances and perspectives. *Chem. Soc. Rev.* **40**, 2525–2540 (2011). doi:10.1039/C0CS00081G
143. Thangadurai, V., Narayanan, S. & Pinzaru, D. Garnet-type solid-state fast Li ion conductors for Li batteries: critical review. *Chem. Soc. Rev.* **43**, 4714–4727 (2014). doi:10.1039/C4CS00020J
144. Manthiram, A. & Li, L. Hybrid and Aqueous Lithium-Air Batteries. *Adv. Energy Mater.* **5**, n/a-n/a (2015). doi:10.1002/aenm.201401302
145. Hassoun, J., Kim, J., Lee, D.-J., Jung, H.-G., Lee, S.-M., Sun, Y.-K. & Scrosati, B. A contribution to the progress of high energy batteries: A metal-free, lithium-ion, silicon–sulfur battery. *J. Power Sources* **202**, 308–313 (2012). doi:10.1016/j.jpowsour.2011.11.060
146. Hassoun, J., Jung, H.-G., Lee, D.-J., Park, J.-B., Amine, K., Sun, Y.-K. & Scrosati, B. A Metal-Free, Lithium-Ion Oxygen Battery: A Step Forward to Safety in Lithium-Air Batteries. *Nano Lett.* **12**, 5775–5779 (2012). doi:10.1021/nl303087j
147. Teranishi, R., Si, Q., Mizukoshi, F., Kawakubo, M., Matsui, M., Takeda, Y., Yamamoto, O. & Imanishi, N. Silicon anode for rechargeable aqueous lithium–air batteries. *J. Power Sources* **273**, 538–543 (2015). doi:10.1016/j.jpowsour.2014.09.024
148. Un nouveau prototype de batterie plein de promesses - Communiqués et dossiers de presse - CNRS. URL: <http://www2.cnrs.fr/presse/communiqué/4325.htm?debut=68>
149. Murgia, M. Bosch invents new electric car battery to double mileage. (2015).
150. Dyson acquires Sakti3 for \$90M to help commercialize ‘breakthrough’ solid-state battery tech. *VentureBeat* URL: <http://venturebeat.com/2015/10/19/dyson-acquires-sakti3-for-90m-to-help-commercialize-breakthrough-solid-state-battery-tech/>

151. Carrington, D. Dyson could become next Tesla with its electric car, says expert. *The Guardian* (2016).
152. Luntz, A. C., Voss, J. & Reuter, K. Interfacial Challenges in Solid-State Li Ion Batteries. *J. Phys. Chem. Lett.* **6**, 4599–4604 (2015). doi:10.1021/acs.jpcllett.5b02352
153. Feng, J. K., Yan, B. G., Liu, J. C., Lai, M. O. & Li, L. All solid state lithium ion rechargeable batteries using NASICON structured electrolyte. *Mater. Technol.* **28**, 276–279 (2013). doi:10.1179/1753555713Y.0000000085
154. Adelhelm, P., Hartmann, P., Bender, C. L., Busche, M., Eufinger, C. & Janek, J. From lithium to sodium: cell chemistry of room temperature sodium–air and sodium–sulfur batteries. *Beilstein J. Nanotechnol.* **6**, 1016–1055 (2015). doi:10.3762/bjnano.6.105
155. Grande, L., Paillard, E., Hassoun, J., Park, J.-B., Lee, Y.-J., Sun, Y.-K., Passerini, S. & Scrosati, B. The Lithium/Air Battery: Still an Emerging System or a Practical Reality? *Adv. Mater.* **27**, 784–800 (2015). doi:10.1002/adma.201403064
156. Gröger, O., Gasteiger, H. A. & Suchsland, J.-P. Review—Electromobility: Batteries or Fuel Cells? *J. Electrochem. Soc.* **162**, A2605–A2622 (2015).
157. Zhang, S. S. Liquid electrolyte lithium/sulfur battery: Fundamental chemistry, problems, and solutions. *J. Power Sources* **231**, 153–162 (2013). doi:10.1016/j.jpowsour.2012.12.102
158. Ma, L., Hendrickson, K. E., Wei, S. & Archer, L. A. Nanomaterials: Science and applications in the lithium–sulfur battery. *Nano Today* **10**, 315–338 (2015). doi:10.1016/j.nantod.2015.04.011
159. Mikhaylik, Y. V., Kovalev, I., Schock, R., Kumaresan, K., Xu, J. & Affinito, J. High Energy Rechargeable Li-S Cells for EV Application: Status, Remaining Problems and Solutions. *ECS Trans.* **25**, 23–34 (2010). doi:10.1149/1.3414001
160. Jayaprakash, N., Shen, J., Moganty, S. S., Corona, A. & Archer, L. A. Porous Hollow Carbon@Sulfur Composites for High-Power Lithium–Sulfur Batteries. *Angew. Chem. Int. Ed.* **50**, 5904–5908 (2011). doi:10.1002/anie.201100637
161. Zheng, G., Zhang, Q., Cha, J. J., Yang, Y., Li, W., Seh, Z. W. & Cui, Y. Amphiphilic Surface Modification of Hollow Carbon Nanofibers for Improved Cycle Life of Lithium Sulfur Batteries. *Nano Lett.* **13**, 1265–1270 (2013). doi:10.1021/nl304795g
162. Zheng, G., Yang, Y., Cha, J. J., Hong, S. S. & Cui, Y. Hollow Carbon Nanofiber-Encapsulated Sulfur Cathodes for High Specific Capacity Rechargeable Lithium Batteries. *Nano Lett.* **11**, 4462–4467 (2011). doi:10.1021/nl2027684
163. Rauh, R. D., Abraham, K. M., Pearson, G. F., Surprenant, J. K. & Brummer, S. B. A Lithium/Dissolved Sulfur Battery with an Organic Electrolyte. *J. Electrochem. Soc.* **126**, 523–527 (1979). doi:10.1149/1.2129079
164. Yang, Y., McDowell, M. T., Jackson, A., Cha, J. J., Hong, S. S. & Cui, Y. New Nanostructured Li₂S/Silicon Rechargeable Battery with High Specific Energy. *Nano Lett.* **10**, 1486–1491 (2010). doi:10.1021/nl100504q
165. Elazari, R., Salitra, G., Gershinsky, G., Garsuch, A., Panchenko, A. & Aurbach, D. Rechargeable lithiated silicon–sulfur (SLS) battery prototypes. *Electrochem. Commun.* **14**, 21–24 (2012). doi:10.1016/j.elecom.2011.10.020
166. Pang, Q., Kundu, D., Cuisinier, M. & Nazar, L. F. Surface-enhanced redox chemistry of polysulphides on a metallic and polar host for lithium-sulphur batteries. *Nat. Commun.* **5**, 4759 (2014). doi:10.1038/ncomms5759
167. Tao, X., Wang, J., Ying, Z., Cai, Q., Zheng, G., Gan, Y., Huang, H., Xia, Y., Liang, C., Zhang, W. & Cui, Y. Strong Sulfur Binding with Conducting Magnéli-Phase Ti_nO_{2n-1} Nanomaterials for Improving Lithium–Sulfur Batteries. *Nano Lett.* **14**, 5288–5294 (2014). doi:10.1021/nl502331f
168. Qiu, L., Zhang, S., Zhang, L., Sun, M. & Wang, W. Preparation and enhanced electrochemical properties of nano-sulfur/poly(pyrrole-co-aniline) cathode material

- for lithium/sulfur batteries. *Electrochimica Acta* **55**, 4632–4636 (2010). doi:10.1016/j.electacta.2010.03.030
169. Su, Y.-S. & Manthiram, A. Lithium–sulphur batteries with a microporous carbon paper as a bifunctional interlayer. *Nat. Commun.* **3**, 1166 (2012). doi:10.1038/ncomms2163
170. Su, Y.-S. & Manthiram, A. A new approach to improve cycle performance of rechargeable lithium–sulfur batteries by inserting a free-standing MWCNT interlayer. *Chem. Commun.* **48**, 8817 (2012). doi:10.1039/c2cc33945e
171. Hwang, J.-Y., Kim, H. M., Lee, S.-K., Lee, J.-H., Abouimrane, A., Khaleel, M. A., Belharouak, I., Manthiram, A. & Sun, Y.-K. High-Energy, High-Rate, Lithium–Sulfur Batteries: Synergetic Effect of Hollow TiO₂-Webbed Carbon Nanotubes and a Dual Functional Carbon-Paper Interlayer. *Adv. Energy Mater.* **6**, n/a-n/a (2016). doi:10.1002/aenm.201501480
172. Skotheim, T. A., Sheehan, C. J., Mikhaylik, Y. V. & Affinito, J. *Lithium anodes for electrochemical cells*. (Google Patents, 2004).
173. Aurbach, D., Pollak, E., Elazari, R., Salitra, G., Kelley, C. S. & Affinito, J. On the Surface Chemical Aspects of Very High Energy Density, Rechargeable Li–Sulfur Batteries. *J. Electrochem. Soc.* **156**, A694 (2009). doi:10.1149/1.3148721
174. Yang, Y., Zheng, G. & Cui, Y. A membrane-free lithium/polysulfide semi-liquid battery for large-scale energy storage. *Energy Environ. Sci.* **6**, 1552 (2013). doi:10.1039/c3ee00072a
175. McCloskey, B. D., Valery, A., Luntz, A. C., Gowda, S. R., Wallraff, G. M., Garcia, J. M., Mori, T. & Krupp, L. E. Combining Accurate O₂ and Li₂O₂ Assays to Separate Discharge and Charge Stability Limitations in Nonaqueous Li–O₂ Batteries. *J. Phys. Chem. Lett.* **4**, 2989–2993 (2013). doi:10.1021/jz401659f
176. McCloskey, B. D., Garcia, J. M. & Luntz, A. C. Chemical and Electrochemical Differences in Non-aqueous Li–O₂ and Na–O₂ Batteries. *J. Phys. Chem. Lett.* (2014). doi:10.1021/jz500494s
177. Abraham, K. M. & Jiang, Z. A Polymer Electrolyte-Based Rechargeable Lithium/Oxygen Battery. *J. Electrochem. Soc.* **143**, 1–5 (1996).
178. Hartmann, P., Bender, C. L., Vračar, M., Dürr, A. K., Garsuch, A., Janek, J. & Adelhelm, P. A rechargeable room-temperature sodium superoxide (NaO₂) battery. *Nat. Mater.* **12**, 228–232 (2013). doi:10.1038/nmat3486
179. Lim, H.-K., Lim, H.-D., Park, K.-Y., Seo, D.-H., Gwon, H., Hong, J., Goddard, W. A., Kim, H. & Kang, K. Toward a Lithium–‘Air’ Battery: The Effect of CO₂ on the Chemistry of a Lithium–Oxygen Cell. *J. Am. Chem. Soc.* **135**, 9733–9742 (2013). doi:10.1021/ja4016765
180. Sun, Q., Yadegari, H., Banis, M. N., Liu, J., Xiao, B., Li, X., Langford, C., Li, R. & Sun, X. Towards Sodium–‘Air’ Battery: Revealing the Critical Role of Humidity. *J. Phys. Chem. C* (2015). doi:10.1021/acs.jpcc.5b02673
181. Gallagher, K. G., Goebel, S., Greszler, T., Mathias, M., Oelerich, W., Eroglu, D. & Srinivasan, V. Quantifying the promise of lithium–air batteries for electric vehicles. *Energy Environ. Sci.* **7**, 1555–1563 (2014). doi:10.1039/C3EE43870H
182. Read, J. Characterization of the Lithium/Oxygen Organic Electrolyte Battery. *J. Electrochem. Soc.* **149**, A1190 (2002). doi:10.1149/1.1498256
183. McCloskey, B. D., Bethune, D. S., Shelby, R. M., Mori, T., Scheffler, R., Speidel, A., Sherwood, M. & Luntz, A. C. Limitations in Rechargeability of Li–O₂ Batteries and Possible Origins. *J. Phys. Chem. Lett.* **3**, 3043–3047 (2012). doi:10.1021/jz301359t
184. Battino, R., Rettich, T. R. & Tominaga, T. The Solubility of Oxygen and Ozone in Liquids. *J. Phys. Chem. Ref. Data* **12**, 163–178 (1983). doi:10.1063/1.555680

185. Kretschmer, C. B., Nowakowska, J. & Wiebe, R. Solubility of Oxygen and Nitrogen in Organic Solvents from -25° to 50° C. *Ind. Eng. Chem.* **38**, 506–509 (1946). doi:10.1021/ie50437a018
186. Hartmann, P., Bender, C. L., Sann, J., Dürr, A. K., Jansen, M., Janek, J. & Adelhelm, P. A comprehensive study on the cell chemistry of the sodium superoxide (NaO₂) battery. *Phys. Chem. Chem. Phys.* **15**, 11661 (2013). doi:10.1039/c3cp50930c
187. Freunberger, S. A., Chen, Y., Peng, Z., Griffin, J. M., Hardwick, L. J., Bardé, F., Novák, P. & Bruce, P. G. Reactions in the Rechargeable Lithium–O₂ Battery with Alkyl Carbonate Electrolytes. *J. Am. Chem. Soc.* **133**, 8040–8047 (2011). doi:10.1021/ja2021747
188. McCloskey, B. D., Bethune, D. S., Shelby, R. M., Girishkumar, G. & Luntz, A. C. Solvents' Critical Role in Nonaqueous Lithium–Oxygen Battery Electrochemistry. *J. Phys. Chem. Lett.* **2**, 1161–1166 (2011). doi:10.1021/jz200352v
189. Xu, W., Xu, K., Viswanathan, V. V., Towne, S. A., Hardy, J. S., Xiao, J., Nie, Z., Hu, D., Wang, D. & Zhang, J.-G. Reaction mechanisms for the limited reversibility of Li–O₂ chemistry in organic carbonate electrolytes. *J. Power Sources* **196**, 9631–9639 (2011). doi:10.1016/j.jpowsour.2011.06.099
190. Peng, Z., Freunberger, S. A., Chen, Y. & Bruce, P. G. A Reversible and Higher-Rate Li–O₂ Battery. *Science* **337**, 563–566 (2012). doi:10.1126/science.1223985
191. Ottakam Thotiyl, M. M., Freunberger, S. A., Peng, Z., Chen, Y., Liu, Z. & Bruce, P. G. A stable cathode for the aprotic Li–O₂ battery. *Nat. Mater.* **12**, 1050–1056 (2013). doi:10.1038/nmat3737
192. Semino, R., Zaldívar, G., Calvo, E. J. & Laria, D. Lithium solvation in dimethyl sulfoxide-acetonitrile mixtures. *J. Chem. Phys.* **141**, 214509 (2014). doi:10.1063/1.4902837
193. Walker, W., Giordani, V., Uddin, J., Bryantsev, V. S., Chase, G. V. & Addison, D. A Rechargeable Li–O₂ Battery Using a Lithium Nitrate/ N,N -Dimethylacetamide Electrolyte. *J. Am. Chem. Soc.* **135**, 2076–2079 (2013). doi:10.1021/ja311518s
194. Sharon, D., Hirsberg, D., Afri, M., Garsuch, A., Frimer, A. A. & Aurbach, D. Reactivity of Amide Based Solutions in Lithium–Oxygen Cells. *J. Phys. Chem. C* **118**, 15207–15213 (2014). doi:10.1021/jp506230v
195. Lu, Y.-C., Kwabi, D. G., Yao, K. P. C., Harding, J. R., Zhou, J., Zuin, L. & Shao-Horn, Y. The discharge rate capability of rechargeable Li–O₂ batteries. *Energy Environ. Sci.* **4**, 2999–3007 (2011). doi:10.1039/C1EE01500A
196. Gallant, B. M., Kwabi, D. G., Mitchell, R. R., Zhou, J., Thompson, C. V. & Shao-Horn, Y. Influence of Li₂O₂ morphology on oxygen reduction and evolution kinetics in Li–O₂ batteries. *Energy Environ. Sci.* **6**, 2518–2528 (2013). doi:10.1039/c3ee40998h
197. Black, R., Oh, S. H., Lee, J.-H., Yim, T., Adams, B. & Nazar, L. F. Screening for Superoxide Reactivity in Li–O₂ Batteries: Effect on Li₂O₂/LiOH Crystallization. *J. Am. Chem. Soc.* **134**, 2902–2905 (2012). doi:10.1021/ja2111543
198. Meini, S., Piana, M., Beyer, H., Schwammlein, J. & Gasteiger, H. A. Effect of Carbon Surface Area on First Discharge Capacity of Li–O₂ Cathodes and Cycle-Life Behavior in Ether-Based Electrolytes. *J. Electrochem. Soc.* **159**, A2135–A2142 (2012). doi:10.1149/2.011301jes
199. Mitchell, R. R., Gallant, B. M., Shao-Horn, Y. & Thompson, C. V. Mechanisms of Morphological Evolution of Li₂O₂ Particles during Electrochemical Growth. *J. Phys. Chem. Lett.* **4**, 1060–1064 (2013). doi:10.1021/jz4003586
200. Adams, B. D., Radtke, C., Black, R., Trudeau, M. L., Zaghbi, K. & Nazar, L. F. Current density dependence of peroxide formation in the Li–O₂ battery and its effect on charge. *Energy Environ. Sci.* **6**, 1772–1778 (2013). doi:10.1039/C3EE40697K
201. Aetukuri, N. B., McCloskey, B. D., García, J. M., Krupp, L. E., Viswanathan, V. & Luntz, A. C. Solvating additives drive solution-mediated electrochemistry and enhance toroid

- growth in non-aqueous Li-O₂ batteries. *Nat. Chem.* **7**, 50–56 (2015). doi:10.1038/nchem.2132
202. Schwenke, K. U., Metzger, M., Restle, T., Piana, M. & Gasteiger, H. A. The Influence of Water and Protons on Li₂O₂ Crystal Growth in Aprotic Li-O₂ Cells. *J. Electrochem. Soc.* **162**, A573–A584 (2015). doi:10.1149/2.0201504jes
203. Viswanathan, V., Thygesen, K. S., Hummelshøj, J. S., Nørskov, J. K., Girishkumar, G., McCloskey, B. D. & Luntz, A. C. Electrical conductivity in Li₂O₂ and its role in determining capacity limitations in non-aqueous Li-O₂ batteries. *J. Chem. Phys.* **135**, 214704 (2011). doi:10.1063/1.3663385
204. Johnson, L., Li, C., Liu, Z., Chen, Y., Freunberger, S. A., Ashok, P. C., Praveen, B. B., Dholakia, K., Tarascon, J.-M. & Bruce, P. G. The role of Li₂O solubility in O₂ reduction in aprotic solvents and its consequences for Li-O₂ batteries. *Nat. Chem.* **6**, 1091–1099 (2014). doi:10.1038/nchem.2101
205. Gallant, B. M., Mitchell, R. R., Kwabi, D. G., Zhou, J., Zuin, L., Thompson, C. V. & Shao-Horn, Y. Chemical and Morphological Changes of Li-O₂ Battery Electrodes upon Cycling. *J. Phys. Chem. C* **116**, 20800–20805 (2012). doi:10.1021/jp308093b
206. Laoire, C. O., Mukerjee, S., Abraham, K. M., Plichta, E. J. & Hendrickson, M. A. Influence of Nonaqueous Solvents on the Electrochemistry of Oxygen in the Rechargeable Lithium–Air Battery. *J. Phys. Chem. C* **114**, 9178–9186 (2010). doi:10.1021/jp102019y
207. Lu, Y.-C. & Shao-Horn, Y. Probing the Reaction Kinetics of the Charge Reactions of Nonaqueous Li-O₂ Batteries. *J. Phys. Chem. Lett.* **4**, 93–99 (2013). doi:10.1021/jz3018368
208. Noked, M., Schroeder, M. A., Pearse, A. J., Rubloff, G. W. & Lee, S. B. Protocols for Evaluating and Reporting Li-O₂ Cell Performance. *J. Phys. Chem. Lett.* **7**, 211–215 (2016). doi:10.1021/acs.jpcllett.5b02613
209. Aurbach, D. *Oral presentation*. (2015).
210. Aurbach, D. *Oral presentation*. (2016).
211. Visco, S. J., Nimon, E., Katz, B., De Jonghe, L. C. & Chu, M.-Y. Lithium metal aqueous batteries. in *12th International Meeting on Lithium Batteries, Nara, Japan* (2004).
212. Visco, S. J., Nimon, Y. S., Katz, B. D. & De Jonghe, L. C. *Active metal fuel cells*. (Google Patents, 2009).
213. Visco, S. J., Nimon, V. Y., Petrov, A., Pridatko, K., Goncharenko, N., Nimon, E., Jonghe, L. D., Volfkovich, Y. M. & Bograchev, D. A. Aqueous and nonaqueous lithium-air batteries enabled by water-stable lithium metal electrodes. *J. Solid State Electrochem.* **18**, 1443–1456 (2014). doi:10.1007/s10008-014-2427-x
214. Stevens, P., Toussaint, G., Caillon, G., Viaud, P., Vinatier, P., Cantau, C., Fichet, O., Sarrazin, C. & Mallouki, M. Development of a Lithium Air Rechargeable Battery. *ECS Trans.* **28**, 1–12 (2010). doi:10.1149/1.3507922
215. Stevens, P., Toussaint, G., Puech, L. & Vinatier, P. Very High Specific Area Lithium-Air Battery. *ECS Trans.* **50**, 1–11 (2013). doi:10.1149/05025.0001ecst
216. Lancel, G. Thèse Gilles Lancel. *PhD Manuscr.* (2016).
217. Bertolotti, B., Messaoudi, H., Chikh, L., Vancaeyzeele, C., Alfonsi, S. & Fichet, O. Stability in alkaline aqueous electrolyte of air electrode protected with fluorinated interpenetrating polymer network membrane. *J. Power Sources* **274**, 488–495 (2015). doi:10.1016/j.jpowsour.2014.10.059
218. Bertolotti, B., Chikh, L., Vancaeyzeele, C., Alfonsi, S. & Fichet, O. Assemblies of protective anion exchange membrane on air electrode for its efficient operation in aqueous alkaline electrolyte. *J. Power Sources* **274**, 636–644 (2015). doi:10.1016/j.jpowsour.2014.10.079

219. Hashimoto, T. & Hayashi, K. Aqueous and Nonaqueous Sodium-Air Cells with Nanoporous Gold Cathode. *Electrochimica Acta* **182**, 809–814 (2015). doi:10.1016/j.electacta.2015.09.153
220. Senthilkumar, B., Khan, Z., Park, S., Seo, I., Ko, H. & Kim, Y. Exploration of cobalt phosphate as a potential catalyst for rechargeable aqueous sodium-air battery. *J. Power Sources* **311**, 29–34 (2016). doi:10.1016/j.jpowsour.2016.02.022
221. Haering, R. R., Stiles, J. A. & Brandt, K. *Lithium molybdenum disulphide battery cathode*. (Google Patents, 1980).
222. Assary, R. S., Lu, J., Du, P., Luo, X., Zhang, X., Ren, Y., Curtiss, L. A. & Amine, K. The Effect of Oxygen Crossover on the Anode of a Li–O₂ Battery using an Ether-Based Solvent: Insights from Experimental and Computational Studies. *ChemSusChem* **6**, 51–55 (2013). doi:10.1002/cssc.201200810
223. Shui, J.-L., Okasinski, J. S., Kenesei, P., Dobbs, H. A., Zhao, D., Almer, J. D. & Liu, D.-J. Reversibility of anodic lithium in rechargeable lithium–oxygen batteries. *Nat. Commun.* **4**, 2255 (2013). doi:10.1038/ncomms3255
224. Laoire, C. O., Mukerjee, S., Plichta, E. J., Hendrickson, M. A. & Abraham, K. M. Rechargeable Lithium/TEGDME-LiPF₆O Battery. *J. Electrochem. Soc.* **158**, A302 (2011). doi:10.1149/1.3531981
225. Cho, M. H., Trottier, J., Gagnon, C., Hovington, P., Clément, D., Vijh, A., Kim, C.-S., Guerfi, A., Black, R., Nazar, L. & Zaghbi, K. The effects of moisture contamination in the Li–O₂ battery. *J. Power Sources* **268**, 565–574 (2014). doi:10.1016/j.jpowsour.2014.05.148
226. Girishkumar, G., McCloskey, B., Luntz, A. C., Swanson, S. & Wilcke, W. Lithium–Air Battery: Promise and Challenges. *J. Phys. Chem. Lett.* **1**, 2193–2203 (2010). doi:10.1021/jz1005384
227. Bhatt, M. D., Geaney, H., Nolan, M. & O'Dwyer, C. Key scientific challenges in current rechargeable non-aqueous Li–O₂ batteries: experiment and theory. *Phys. Chem. Chem. Phys.* **16**, 12093–12130 (2014). doi:10.1039/C4CP01309C
228. Franco, A. A. & Xue, K.-H. Carbon-Based Electrodes for Lithium Air Batteries: Scientific and Technological Challenges from a Modeling Perspective. *ECS J. Solid State Sci. Technol.* **2**, M3084–M3100 (2013). doi:10.1149/2.012310jss
229. McCloskey, B. D., Speidel, A., Scheffler, R., Miller, D. C., Viswanathan, V., Hummelshøj, J. S., Nørskov, J. K. & Luntz, A. C. Twin Problems of Interfacial Carbonate Formation in Nonaqueous Li–O₂ Batteries. *J. Phys. Chem. Lett.* **3**, 997–1001 (2012). doi:10.1021/jz300243r
230. Ottakam Thotiyl, M. M., Freunberger, S. A., Peng, Z. & Bruce, P. G. The Carbon Electrode in Nonaqueous Li–O₂ Cells. *J. Am. Chem. Soc.* **135**, 494–500 (2013). doi:10.1021/ja310258x
231. Li, F., Tang, D.-M., Chen, Y., Golberg, D., Kitaura, H., Zhang, T., Yamada, A. & Zhou, H. Ru/ITO: A Carbon-Free Cathode for Nonaqueous Li–O₂ Battery. *Nano Lett.* **13**, 4702–4707 (2013). doi:10.1021/nl402213h
232. Cui, Y., Wen, Z. & Liu, Y. A free-standing-type design for cathodes of rechargeable Li–O₂ batteries. *Energy Environ. Sci.* **4**, 4727 (2011). doi:10.1039/c1ee02365a
233. Cao, J., Liu, S., Xie, J., Zhang, S., Cao, G. & Zhao, X. Tips-Bundled Pt/Co₃O₄ Nanowires with Directed Peripheral Growth of Li₂O₂ as Efficient Binder/Carbon-Free Catalytic Cathode for Lithium–Oxygen Battery. *ACS Catal.* 241–245 (2014). doi:10.1021/cs501392p
234. Gao, R., Zhu, J., Xiao, X., Hu, Z., Liu, J. & Liu, X. Facet-Dependent Electrocatalytic Performance of Co₃O₄ for Rechargeable Li–O₂ Battery. *J. Phys. Chem. C* **119**, 4516–4523 (2015). doi:10.1021/jp511363p

235. Kim, D. S. & Kim, S. B. Electrochemical performance of surface modified CNF/Co₃O₄ composite for Li-air batteries. *J. Electroceramics* **33**, 246–251 (2014). doi:10.1007/s10832-014-9957-6
236. Song, M. J., Kim, I. T., Kim, Y. B. & Shin, M. W. Self-standing, binder-free electrospun Co₃O₄/carbon nanofiber composites for non-aqueous Li-air batteries. *Electrochimica Acta* **182**, 289–296 (2015). doi:10.1016/j.electacta.2015.09.100
237. Black, R., Lee, J.-H., Adams, B., Mims, C. A. & Nazar, L. F. The Role of Catalysts and Peroxide Oxidation in Lithium–Oxygen Batteries. *Angew. Chem.* **125**, 410–414 (2013). doi:10.1002/ange.201205354
238. Li, C., Fontaine, O., Freunberger, S. A., Johnson, L., Grugeon, S., Laruelle, S., Bruce, P. G. & Armand, M. Aprotic Li–O₂ Battery: Influence of Complexing Agents on Oxygen Reduction in an Aprotic Solvent. *J. Phys. Chem. C* **118**, 3393–3401 (2014). doi:10.1021/jp4093805
239. Zhang, S., Yuan, X.-Z., Hin, J. N. C., Wang, H., Friedrich, K. A. & Schulze, M. A review of platinum-based catalyst layer degradation in proton exchange membrane fuel cells. *J. Power Sources* **194**, 588–600 (2009). doi:10.1016/j.jpowsour.2009.06.073
240. Yao, K. P. C., Risch, M., Sayed, S. Y., Lee, Y.-L., Harding, J. R., Grimaud, A., Pour, N., Xu, Z., Zhou, J., Mansour, A., Bardé, F. & Shao-Horn, Y. Solid-state activation of Li₂O₂ oxidation kinetics and implications for Li–O₂ batteries. *Energy Env. Sci* **8**, 2417–2426 (2015). doi:10.1039/C5EE00967G
241. Ganapathy, S., Adams, B. D., Stenou, G., Anastasaki, M. S., Goubitz, K., Miao, X.-F., Nazar, L. F. & Wagemaker, M. The nature of Li₂O₂ oxidation in a Li–O₂ battery revealed by operando X-ray diffraction. *J. Am. Chem. Soc.* 15807–15808 (2014). doi:10.1021/ja508794r
242. McCloskey, B. D., Scheffler, R., Speidel, A., Bethune, D. S., Shelby, R. M. & Luntz, A. C. On the Efficacy of Electrocatalysis in Nonaqueous Li–O₂ Batteries. *J. Am. Chem. Soc.* **133**, 18038–18041 (2011). doi:10.1021/ja207229n
243. Harding, J. R., Lu, Y.-C., Tsukada, Y. & Shao-Horn, Y. Evidence of catalyzed oxidation of Li₂O₂ for rechargeable Li–air battery applications. *Phys. Chem. Chem. Phys.* **14**, 10540–10546 (2012). doi:10.1039/C2CP41761H
244. Lu, J., Lei, Y., Lau, K. C., Luo, X., Du, P., Wen, J., Assary, R. S., Das, U., Miller, D. J., Elam, J. W., Albishri, H. M., El-Hady, D. A., Sun, Y.-K., Curtiss, L. A. & Amine, K. A nanostructured cathode architecture for low charge overpotential in lithium–oxygen batteries. *Nat. Commun.* **4**, 2383 (2013). doi:10.1038/ncomms3383
245. Schwenke, K. U., Meini, S., Wu, X., Gasteiger, H. A. & Piana, M. Stability of superoxide radicals in glyme solvents for non-aqueous Li–O₂ battery electrolytes. *Phys. Chem. Chem. Phys.* **15**, 11830 (2013). doi:10.1039/c3cp51531a
246. Freunberger, S. A., Chen, Y., Drewett, N. E., Hardwick, L. J., Bardé, F. & Bruce, P. G. The Lithium–Oxygen Battery with Ether-Based Electrolytes. *Angew. Chem. Int. Ed.* **50**, 8609–8613 (2011). doi:10.1002/anie.201102357
247. Chen, Y., Freunberger, S. A., Peng, Z., Bardé, F. & Bruce, P. G. Li–O₂ Battery with a Dimethylformamide Electrolyte. *J. Am. Chem. Soc.* **134**, 7952–7957 (2012). doi:10.1021/ja302178w
248. McCloskey, B. D., Scheffler, R., Speidel, A., Girishkumar, G. & Luntz, A. C. On the Mechanism of Nonaqueous Li–O₂ Electrochemistry on C and Its Kinetic Overpotentials: Some Implications for Li–Air Batteries. *J. Phys. Chem. C* **116**, 23897–23905 (2012). doi:10.1021/jp306680f
249. Takechi, K., Higashi, S., Mizuno, F., Nishikoori, H., Iba, H. & Shiga, T. Stability of solvents against superoxide radical species for the electrolyte of lithium–air battery. *ECS Electrochem. Lett.* **1**, A27–A29 (2012). doi:10.1149/2.010201eel

250. Bryantsev, V. S., Giordani, V., Walker, W., Blanco, M., Zecevic, S., Sasaki, K., Uddin, J., Addison, D. & Chase, G. V. Predicting Solvent Stability in Aprotic Electrolyte Li–Air Batteries: Nucleophilic Substitution by the Superoxide Anion Radical ($O_2^{\cdot -}$). *J. Phys. Chem. A* **115**, 12399–12409 (2011). doi:10.1021/jp2073914
251. Lepoivre, F., Grimaud, A., Larcher, D. & Tarascon, J.-M. Long-Time and Reliable Gas Monitoring in Li-O₂ Batteries via a Swagelok Derived Electrochemical Cell. *J. Electrochem. Soc.* **163**, A923–A929 (2016). doi:10.1149/2.0421606jes
252. Trahan, M. J., Mukerjee, S., Plichta, E. J., Hendrickson, M. A. & Abraham, K. M. Studies of Li-Air Cells Utilizing Dimethyl Sulfoxide-Based Electrolyte. *J. Electrochem. Soc.* **160**, A259–A267 (2012). doi:10.1149/2.048302jes
253. Sharon, D., Afri, M., Noked, M., Garsuch, A., Frimer, A. A. & Aurbach, D. Oxidation of Dimethyl Sulfoxide Solutions by Electrochemical Reduction of Oxygen. *J. Phys. Chem. Lett.* **4**, 3115–3119 (2013). doi:10.1021/jz4017188
254. Bryantsev, V. S. & Faglioni, F. Predicting Autoxidation Stability of Ether- and Amide-Based Electrolyte Solvents for Li–Air Batteries. *J. Phys. Chem. A* **116**, 7128–7138 (2012). doi:10.1021/jp301537w
255. Bryantsev, V. S., Giordani, V., Walker, W., Uddin, J., Lee, I., van Duin, A. C. T., Chase, G. V. & Addison, D. Investigation of Fluorinated Amides for Solid–Electrolyte Interphase Stabilization in Li–O₂ Batteries Using Amide-Based Electrolytes. *J. Phys. Chem. C* **117**, 11977–11988 (2013). doi:10.1021/jp402844r
256. Bryantsev, V. S., Uddin, J., Giordani, V., Walker, W., Addison, D. & Chase, G. V. The identification of stable solvents for nonaqueous rechargeable Li-air batteries. *J. Electrochem. Soc.* **160**, A160–A171 (2013). doi:10.1149/2.027302jes
257. Giordani, V., Walker, W., Bryantsev, V. S., Uddin, J., Chase, G. V. & Addison, D. Synergistic Effect of Oxygen and LiNO₃ on the Interfacial Stability of Lithium Metal in a Li/O₂ Battery. *J. Electrochem. Soc.* **160**, A1544–A1550 (2013). doi:10.1149/2.097309jes
258. Uddin, J., Bryantsev, V. S., Giordani, V., Walker, W., Chase, G. V. & Addison, D. Lithium Nitrate As Regenerable SEI Stabilizing Agent for Rechargeable Li/O₂ Batteries. *J. Phys. Chem. Lett.* **4**, 3760–3765 (2013). doi:10.1021/jz402025n
259. Elazari, R., Salitra, G., Talyosef, Y., Grinblat, J., Scordilis-Kelley, C., Xiao, A., Affinito, J. & Aurbach, D. Morphological and Structural Studies of Composite Sulfur Electrodes upon Cycling by HRTEM, AFM and Raman Spectroscopy. *J. Electrochem. Soc.* **157**, A1131–A1138 (2010). doi:10.1149/1.3479828
260. Sharon, D., Hirsberg, D., Afri, M., Chesneau, F., Lavi, R., Frimer, A. A., Sun, Y.-K. & Aurbach, D. Catalytic Behavior of Lithium Nitrate in Li-O₂ Cells. *ACS Appl. Mater. Interfaces* **7**, 16590–16600 (2015). doi:10.1021/acsami.5b04145
261. Chen, Y., Freunberger, S. A., Peng, Z., Fontaine, O. & Bruce, P. G. Charging a Li–O₂ battery using a redox mediator. *Nat. Chem.* **5**, 489–494 (2013). doi:10.1038/nchem.1646
262. Bergner, B. J., Schuermann, A., Peppler, K., Garsuch, A. & Janek, J. TEMPO: A Mobile Catalyst for Rechargeable Li-O₂ Batteries. *J. Am. Chem. Soc.* (2014). doi:10.1021/ja508400m
263. Lim, H.-D., Song, H., Kim, J., Gwon, H., Bae, Y., Park, K.-Y., Hong, J., Kim, H., Kim, T., Kim, Y. H., Lepró, X., Ovalle-Robles, R., Baughman, R. H. & Kang, K. Superior Rechargeability and Efficiency of Lithium–Oxygen Batteries: Hierarchical Air Electrode Architecture Combined with a Soluble Catalyst. *Angew. Chem. Int. Ed.* **53**, 3926–3931 (2014). doi:10.1002/anie.201400711
264. Kwak, W.-J., Hirshberg, D., Sharon, D., Shin, H.-J., Afri, M., Park, J.-B., Garsuch, A., Chesneau, F. F., Frimer, A. A., Aurbach, D. & Sun, Y.-K. Understanding the behavior of Li–oxygen cells containing LiI. *J. Mater. Chem. A* **3**, 8855–8864 (2015). doi:10.1039/C5TA01399B

265. Liu, T., Leskes, M., Yu, W., Moore, A. J., Zhou, L., Bayley, P. M., Kim, G. & Grey, C. P. Cycling Li-O₂ batteries via LiOH formation and decomposition. *Science* **350**, 530–533 (2015). doi:10.1126/science.aac7730
266. Lim, H.-D., Lee, B., Zheng, Y., Hong, J., Kim, J., Gwon, H., Ko, Y., Lee, M., Cho, K. & Kang, K. Rational design of redox mediators for advanced Li–O₂ batteries. *Nat. Energy* **1**, 16066 (2016). doi:10.1038/nenergy.2016.66
267. Gao, X., Chen, Y., Johnson, L. & Bruce, P. G. Promoting solution phase discharge in Li–O₂ batteries containing weakly solvating electrolyte solutions. *Nat. Mater.* (2016). doi:10.1038/nmat4629
268. Viswanathan, V., Nørskov, J. K., Speidel, A., Scheffler, R., Gowda, S. & Luntz, A. C. Li–O₂ Kinetic Overpotentials: Tafel Plots from Experiment and First-Principles Theory. *J. Phys. Chem. Lett.* **4**, 556–560 (2013). doi:10.1021/jz400019y
269. Allen, C. J., Hwang, J., Kautz, R., Mukerjee, S., Plichta, E. J., Hendrickson, M. A. & Abraham, K. M. Oxygen Reduction Reactions in Ionic Liquids and the Formulation of a General ORR Mechanism for Li–Air Batteries. *J. Phys. Chem. C* **116**, 20755–20764 (2012). doi:10.1021/jp306718v
270. Pearson, R. G. Hard and Soft Acids and Bases. *J. Am. Chem. Soc.* **85**, 3533–3539 (1963). doi:10.1021/ja00905a001
271. Gutmann, V. Solvent effects on the reactivities of organometallic compounds. *Coord. Chem. Rev.* **18**, 225–255 (1976). doi:10.1016/S0010-8545(00)82045-7
272. Kwabi, D. G., Bryantsev, V. S., Batcho, T. P., Itkis, D. M., Thompson, C. V. & Shao-Horn, Y. Experimental and Computational Analysis of the Solvent-Dependent O₂/Li⁺–O₂[–] Redox Couple: Standard Potentials, Coupling Strength, and Implications for Lithium–Oxygen Batteries. *Angew. Chem. Int. Ed.* **55**, 3129–3134 (2016). doi:10.1002/anie.201509143
273. Khetan, A., Luntz, A. & Viswanathan, V. Trade-Offs in Capacity and Rechargeability in Nonaqueous Li–O₂ Batteries: Solution-Driven Growth versus Nucleophilic Stability. *J. Phys. Chem. Lett.* **6**, 1254–1259 (2015). doi:10.1021/acs.jpcllett.5b00324
274. Meini, S., Piana, M., Tsiouvaras, N., Garsuch, A. & Gasteiger, H. A. The Effect of Water on the Discharge Capacity of a Non-Catalyzed Carbon Cathode for Li–O₂ Batteries. *Electrochem. Solid-State Lett.* **15**, A45 (2012). doi:10.1149/2.005204esl
275. Böhm, H. The lithium–silicon system. *Z. Met.* **50**, 44–46 (1959).
276. Axel, H., Schäfer, H. & Weiss, A. Die Kristallstruktur von Lithiumsilicid Li₂Si. *Angew. Chem.* **77**, 379–380 (1965). doi:10.1002/ange.19650770809
277. Böhm, H. DAS SYSTEM LITHIUM–SILIZIUM. *Z. Met.* **50**, 44–46 (1959).
278. van der Marel, C., Vinke, G. J. B. & van der Lugt, W. The phase diagram of the system lithium–silicon. *Solid State Commun.* **54**, 917–919 (1985). doi:10.1016/0038-1098(85)90155-3
279. von Schnering, H. G., Nesper, R., Curda, J. & Tebbe, K.-F. Li₁₂Si₇, a Compound Having a Trigonal Planar Si₄ Cluster and Planar Si₅ Rings. *Angew. Chem. Int. Ed. Engl.* **19**, 1033–1034 (1980). doi:10.1002/anie.198010331
280. von Schnering, N. G., Nesper, R., Tebbe, K. & Kurda, J. Structure and properties of Li₁₄Si₆ (Li₂. 33Si), the violet phase in the lithium–silicon system. *Z. Met.* **71**, 357–363 (1980).
281. Nesper, R. & von Schnering, H. G. Li₂₁Si₅, a Zintl phase as well as a Hume-Rothery phase. *J. Solid State Chem.* **70**, 48–57 (1987). doi:10.1016/0022-4596(87)90176-9
282. Boukamp, B. A., Lesh, G. C. & Huggins, R. A. All-Solid Lithium Electrodes with Mixed-Conductor Matrix. *J. Electrochem. Soc.* **128**, 725 (1981). doi:10.1149/1.2127495
283. Wen, C. J. & Huggins, R. A. Chemical diffusion in intermediate phases in the lithium–silicon system. *J. Solid State Chem.* **37**, 271–278 (1981). doi:10.1016/0022-4596(81)90487-4

284. Obrovac, M. N. & Christensen, L. Structural Changes in Silicon Anodes during Lithium Insertion/Extraction. *Electrochem. Solid-State Lett.* **7**, A93 (2004). doi:10.1149/1.1652421
285. Limthongkul, P., Jang, Y.-I., Dudney, N. J. & Chiang, Y.-M. Electrochemically-driven solid-state amorphization in lithium-silicon alloys and implications for lithium storage. *Acta Mater.* **51**, 1103–1113 (2003). doi:10.1016/S1359-6454(02)00514-1
286. Li, H., Huang, X., Chen, L., Zhou, G., Zhang, Z., Yu, D., Jun Mo, Y. & Pei, N. The crystal structural evolution of nano-Si anode caused by lithium insertion and extraction at room temperature. *Solid State Ion.* **135**, 181–191 (2000). doi:10.1016/S0167-2738(00)00362-3
287. Besenhard, J. O., Yang, J. & Winter, M. Will advanced lithium-alloy anodes have a chance in lithium-ion batteries? *J. Power Sources* **68**, 87–90 (1997). doi:10.1016/S0378-7753(96)02547-5
288. Beaulieu, L. Y., Eberman, K. W., Turner, R. L., Krause, L. J. & Dahn, J. R. Colossal Reversible Volume Changes in Lithium Alloys. *Electrochem. Solid-State Lett.* **4**, A137 (2001). doi:10.1149/1.1388178
289. Beaulieu, L. Y., Hewitt, K. C., Turner, R. L., Bonakdarpour, A., Abdo, A. A., Christensen, L., Eberman, K. W., Krause, L. J. & Dahn, J. R. The Electrochemical Reaction of Li with Amorphous Si-Sn Alloys. *J. Electrochem. Soc.* **150**, A149 (2003). doi:10.1149/1.1530151
290. Graetz, J., Ahn, C. C., Yazami, R. & Fultz, B. Highly Reversible Lithium Storage in Nanostructured Silicon. *Electrochem. Solid-State Lett.* **6**, A194–A197 (2003). doi:10.1149/1.1596917
291. Liu, X. H., Wang, J. W., Huang, S., Fan, F., Huang, X., Liu, Y., Krylyuk, S., Yoo, J., Dayeh, S. A., Davydov, A. V., Mao, S. X., Picraux, S. T., Zhang, S., Li, J., Zhu, T. & Huang, J. Y. In situ atomic-scale imaging of electrochemical lithiation in silicon. *Nat. Nanotechnol.* **7**, 749–756 (2012). doi:10.1038/nnano.2012.170
292. Wolfenstine, J. Critical grain size for microcracking during lithium insertion. *J. Power Sources* **79**, 111–113 (1999). doi:10.1016/S0378-7753(99)00052-X
293. Li, H., Huang, X., Chen, L., Wu, Z. & Liang, Y. A High Capacity Nano - Si Composite Anode Material for Lithium Rechargeable Batteries. *Electrochem. Solid-State Lett.* **2**, 547–549 (1999). doi:10.1149/1.1390899
294. Kasavajjula, U., Wang, C. & Appleby, A. J. Nano- and bulk-silicon-based insertion anodes for lithium-ion secondary cells. *J. Power Sources* **163**, 1003–1039 (2007). doi:10.1016/j.jpowsour.2006.09.084
295. Chan, C. K., Peng, H., Liu, G., McIlwrath, K., Zhang, X. F., Huggins, R. A. & Cui, Y. High-performance lithium battery anodes using silicon nanowires. *Nat. Nanotechnol.* **3**, 31–35 (2008). doi:10.1038/nnano.2007.411
296. Timmons, A. & Dahn, J. R. In Situ Optical Observations of Particle Motion in Alloy Negative Electrodes for Li-Ion Batteries. *J. Electrochem. Soc.* **153**, A1206 (2006). doi:10.1149/1.2194611
297. Yen, J.-P., Chang, C.-C., Lin, Y.-R., Shen, S.-T. & Hong, J.-L. Effects of Styrene-Butadiene Rubber/Carboxymethylcellulose (SBR/CMC) and Polyvinylidene Difluoride (PVDF) Binders on Low Temperature Lithium Ion Batteries. *J. Electrochem. Soc.* **160**, A1811–A1818 (2013).
298. Lestriez, B., Bahri, S., Sandu, I., Roué, L. & Guyomard, D. On the binding mechanism of CMC in Si negative electrodes for Li-ion batteries. *Electrochem. Commun.* **9**, 2801–2806 (2007). doi:10.1016/j.elecom.2007.10.001
299. Reyter, D., Rousselot, S., Mazouzi, D., Gauthier, M., Moreau, P., Lestriez, B., Guyomard, D. & Roué, L. An electrochemically roughened Cu current collector for Si-based electrode

- in Li-ion batteries. *J. Power Sources* **239**, 308–314 (2013). doi:10.1016/j.jpowsour.2013.03.108
300. Bridel, J.-S., Azais, T., Morcrette, M., Tarascon, J.-M. & Larcher, D. Key Parameters Governing the Reversibility of Si/Carbon/CMC Electrodes for Li-Ion Batteries†. *Chem. Mater.* **22**, 1229–1241 (2010). doi:10.1021/cm902688w
301. Beattie, S. D., Larcher, D., Morcrette, M., Simon, B. & Tarascon, J.-M. Si Electrodes for Li-Ion Batteries—A New Way to Look at an Old Problem. *J. Electrochem. Soc.* **155**, A158 (2008). doi:10.1149/1.2817828
302. Pereira-Nabais, C., Światowska, J., Chagnes, A., Gohier, A., Zanna, S., Seyeux, A., Tran-Van, P., Cojocar, C.-S., Cassir, M. & Marcus, P. Insight into the Solid Electrolyte Interphase on Si Nanowires in Lithium-Ion Battery: Chemical and Morphological Modifications upon Cycling. *J. Phys. Chem. C* **118**, 2919–2928 (2014). doi:10.1021/jp409762m
303. Philippe, B., Dedryvère, R., Allouche, J., Lindgren, F., Gorgoi, M., Rensmo, H., Gonbeau, D. & Edström, K. Nanosilicon Electrodes for Lithium-Ion Batteries: Interfacial Mechanisms Studied by Hard and Soft X-ray Photoelectron Spectroscopy. *Chem. Mater.* **24**, 1107–1115 (2012). doi:10.1021/cm2034195
304. Arreaga-Salas, D. E., Sra, A. K., Roodenko, K., Chabal, Y. J. & Hinkle, C. L. Progression of Solid Electrolyte Interphase Formation on Hydrogenated Amorphous Silicon Anodes for Lithium-Ion Batteries. *J. Phys. Chem. C* **116**, 9072–9077 (2012). doi:10.1021/jp300787p
305. Dupré, N., Moreau, P., De Vito, E., Quazuguel, L., Boniface, M., Bordes, A., Rudisch, C., Bayle-Guillemaud, P. & Guyomard, D. Multiprobe Study of the Solid Electrolyte Interphase on Silicon-Based Electrodes in Full-Cell Configuration. *Chem. Mater.* **28**, 2557–2572 (2016). doi:10.1021/acs.chemmater.5b04461
306. Radvanyi, E., Vito, E. D., Porcher, W. & Larbi, S. J. S. An XPS/AES comparative study of the surface behaviour of nano-silicon anodes for Li-ion batteries. *J. Anal. At. Spectrom.* **29**, 1120–1131 (2014). doi:10.1039/C3JA50362C
307. Lee, Y. M., Lee, J. Y., Shim, H.-T., Lee, J. K. & Park, J.-K. SEI Layer Formation on Amorphous Si Thin Electrode during Precycling. *J. Electrochem. Soc.* **154**, A515–A519 (2007). doi:10.1149/1.2719644
308. Philippe, B., Dedryvère, R., Gorgoi, M., Rensmo, H., Gonbeau, D. & Edström, K. Improved Performances of Nanosilicon Electrodes Using the Salt LiFSI: A Photoelectron Spectroscopy Study. *J. Am. Chem. Soc.* **135**, 9829–9842 (2013). doi:10.1021/ja403082s
309. Chen, L., Wang, K., Xie, X. & Xie, J. Enhancing Electrochemical Performance of Silicon Film Anode by Vinylene Carbonate Electrolyte Additive. *Electrochem. Solid-State Lett.* **9**, A512–A515 (2006). doi:10.1149/1.2338771
310. Chen, L., Wang, K., Xie, X. & Xie, J. Effect of vinylene carbonate (VC) as electrolyte additive on electrochemical performance of Si film anode for lithium ion batteries. *J. Power Sources* **174**, 538–543 (2007). doi:10.1016/j.jpowsour.2007.06.149
311. Xu, C., Lindgren, F., Philippe, B., Gorgoi, M., Björefors, F., Edström, K. & Gustafsson, T. Improved Performance of the Silicon Anode for Li-Ion Batteries: Understanding the Surface Modification Mechanism of Fluoroethylene Carbonate as an Effective Electrolyte Additive. *Chem. Mater.* **27**, 2591–2599 (2015). doi:10.1021/acs.chemmater.5b00339
312. Martin, L., Martinez, H., Ulldemolins, M., Pecquenard, B. & Le Cras, F. Evolution of the Si electrode/electrolyte interface in lithium batteries characterized by XPS and AFM techniques: The influence of vinylene carbonate additive. *Solid State Ion.* **215**, 36–44 (2012). doi:10.1016/j.ssi.2012.03.042

313. Netz, A., Huggins, R. A. & Weppner, W. The formation and properties of amorphous silicon as negative electrode reactant in lithium systems. *J. Power Sources* **119–121**, 95–100 (2003). doi:10.1016/S0378-7753(03)00132-0
314. Nagao, Y., Sakaguchi, H., Honda, H., Fukunaga, T. & Esaka, T. Structural Analysis of Pure and Electrochemically Lithiated SiO Using Neutron Elastic Scattering. *J. Electrochem. Soc.* **151**, A1572–A1575 (2004). doi:10.1149/1.1787173
315. Tabuchi, T., Yasuda, H. & Yamachi, M. Li-doping process for Li_xSiO -negative active material synthesized by chemical method for lithium-ion cells. *J. Power Sources* **146**, 507–509 (2005). doi:10.1016/j.jpowsour.2005.03.100
316. Miyachi, M., Yamamoto, H., Kawai, H., Ohta, T. & Shirakata, M. Analysis of SiO Anodes for Lithium-Ion Batteries. *J. Electrochem. Soc.* **152**, A2089 (2005). doi:10.1149/1.2013210
317. Yamada, Y., Iriyama, Y., Abe, T. & Ogumi, Z. Kinetics of Electrochemical Insertion and Extraction of Lithium Ion at SiO. *J. Electrochem. Soc.* **157**, A26 (2010). doi:10.1149/1.3247598
318. Philipp, H. R. Amorphous and Liquid Semiconductors Optical and bonding model for non-crystalline SiO_x and SiO_xN_y materials. *J. Non-Cryst. Solids* **8**, 627–632 (1972). doi:10.1016/0022-3093(72)90202-5
319. Hass, G. Preparation, Structure, and Applications of Thin Films of Silicon Monoxide and Titanium Dioxide. *J. Am. Ceram. Soc.* **33**, 353–360 (1950). doi:10.1111/j.1151-2916.1950.tb14151.x
320. Temkin, R. J. An analysis of the radial distribution function of SiO_x . *J. Non-Cryst. Solids* **17**, 215–230 (1975). doi:10.1016/0022-3093(75)90052-6
321. Brady, G. W. A Study of Amorphous SiO. *J. Phys. Chem.* **63**, 1119–1120 (1959). doi:10.1021/j150577a020
322. Schulmeister, K. & Mader, W. TEM investigation on the structure of amorphous silicon monoxide. *J. Non-Cryst. Solids* **320**, 143–150 (2003). doi:10.1016/S0022-3093(03)00029-2
323. Hohl, A., Wieder, T., van Aken, P. A., Weirich, T. E., Denninger, G., Vidal, M., Oswald, S., Deneke, C., Mayer, J. & Fuess, H. An interface clusters mixture model for the structure of amorphous silicon monoxide (SiO). *J. Non-Cryst. Solids* **320**, 255–280 (2003). doi:10.1016/S0022-3093(03)00031-0
324. Kim, T., Park, S. & Oh, S. M. Solid-State NMR and Electrochemical Dilatometry Study on Li^{+} Uptake/Extraction Mechanism in SiO Electrode. *J. Electrochem. Soc.* **154**, A1112 (2007). doi:10.1149/1.2790282
325. Al-Maghrabi, M. A., Suzuki, J., Sanderson, R. J., Chevri er, V. L., Dunlap, R. A. & Dahn, J. R. Combinatorial Studies of $\text{Si}_{1-x}\text{O}_x$ as a Potential Negative Electrode Material for Li-Ion Battery Applications. *J. Electrochem. Soc.* **160**, A1587–A1593 (2013). doi:10.1149/2.115309jes
326. Hwa, Y., Park, C.-M. & Sohn, H.-J. Modified SiO as a high performance anode for Li-ion batteries. *J. Power Sources* **222**, 129–134 (2013). doi:10.1016/j.jpowsour.2012.08.060
327. Lee, J.-I., Lee, K. T., Cho, J., Kim, J., Choi, N.-S. & Park, S. Chemical-Assisted Thermal Disproportionation of Porous Silicon Monoxide into Silicon-Based Multicomponent Systems. *Angew. Chem. Int. Ed.* **51**, 2767–2771 (2012). doi:10.1002/anie.201108915
328. Saint, J., Morcrette, M., Larcher, D., Laffont, L., Beattie, S., P er es, J.-P., Talaga, D., Couzi, M. & Tarascon, J.-M. Towards a Fundamental Understanding of the Improved Electrochemical Performance of Silicon–Carbon Composites. *Adv. Funct. Mater.* **17**, 1765–1774 (2007). doi:10.1002/adfm.200600937
329. Sun, Q., Zhang, B. & Fu, Z.-W. Lithium electrochemistry of SiO_2 thin film electrode for lithium-ion batteries. *Appl. Surf. Sci.* **254**, 3774–3779 (2008). doi:10.1016/j.apsusc.2007.11.058

330. Chang, W.-S., Park, C.-M., Kim, J.-H., Kim, Y.-U., Jeong, G. & Sohn, H.-J. Quartz (SiO₂): a new energy storage anode material for Li-ion batteries. *Energy Environ. Sci.* **5**, 6895 (2012). doi:10.1039/c2ee00003b
331. Zhao, J., Lu, Z., Liu, N., Lee, H.-W., McDowell, M. T. & Cui, Y. Dry-air-stable lithium silicide–lithium oxide core–shell nanoparticles as high-capacity prelithiation reagents. *Nat. Commun.* **5**, 5088 (2014). doi:10.1038/ncomms6088
332. Zhou, H., Wang, X. & Chen, D. Li-Metal-Free Prelithiation of Si-Based Negative Electrodes for Full Li-Ion Batteries. *ChemSusChem* **8**, 2737–2744 (2015). doi:10.1002/cssc.201500287
333. Forney, M. W., Ganter, M. J., Staub, J. W., Ridgley, R. D. & Landi, B. J. Prelithiation of Silicon–Carbon Nanotube Anodes for Lithium Ion Batteries by Stabilized Lithium Metal Powder (SLMP). *Nano Lett.* **13**, 4158–4163 (2013). doi:10.1021/nl401776d
334. Li, C. ‘Study of Rechargeable Aprotic Li-O₂ Batteries’. *PhD Def. - LRCS Amiens Fr.* (2013).
335. Liu, N., Hu, L., McDowell, M. T., Jackson, A. & Cui, Y. Prelithiated Silicon Nanowires as an Anode for Lithium Ion Batteries. *ACS Nano* **5**, 6487–6493 (2011). doi:10.1021/nn2017167
336. Bridel, J.-S., Grugeon, S., Laruelle, S., Hassoun, J., Reale, P., Scrosati, B. & Tarascon, J.-M. Decomposition of ethylene carbonate on electrodeposited metal thin film anode. *J. Power Sources* **195**, 2036–2043 (2010). doi:10.1016/j.jpowsour.2009.10.038
337. Kim, H. J., Choi, S., Lee, S. J., Seo, M. W., Lee, J. G., Deniz, E., Lee, Y. J., Kim, E. K. & Choi, J. W. Controlled Prelithiation of Silicon Monoxide for High Performance Lithium-Ion Rechargeable Full Cells. *Nano Lett.* **16**, 282–288 (2016). doi:10.1021/acs.nanolett.5b03776
338. Lide, D. R. *CRC Handbook of Chemistry and Physics, 85th Edition.* (CRC Press, 2004).
339. Montalti, M., Credi, A., Prodi, L. & Gandolfi, M. T. *Handbook of Photochemistry, Third Edition.* (Taylor & Francis, 2006).
340. Donor and acceptor numbers for various solvents. *Pure Appl. Chem.* **51**, 1697–1712 (1979).
341. Marcus, Y. The effectivity of solvents as electron pair donors. *J. Solut. Chem.* **13**, 599–624 (1984).
342. Hartmann, P., Grübl, D., Sommer, H., Janek, J., Bessler, W. G. & Adelhelm, P. Pressure Dynamics in Metal–Oxygen (Metal–Air) Batteries: A Case Study on Sodium Superoxide Cells. *J. Phys. Chem. C* **118**, 1461–1471 (2014). doi:10.1021/jp4099478
343. Plewa, A., Kalita, M. & Siekierski, M. Estimation of ion pair formation constants of lithium salts in mixtures of glymes and 1,4-dioxane. *Electrochimica Acta* **53**, 1527–1534 (2007). doi:10.1016/j.electacta.2007.04.017
344. Das, B. & Hazra, D. K. Conductance of Selected Alkali Metal Salts in Aqueous Binary Mixtures of 2-Methoxyethanol at 25°C. *J. Solut. Chem.* **27**, 1021–1031 doi:10.1023/A:1022652305008
345. Mamantov, G. & Popov, A. I. *Chemistry of nonaqueous solutions: current progress.* (VCH, 1994).
346. Fluoroethylene carbonate - FEC - H61502 - Alfa Aesar. URL: <https://www.alfa.com/fr/catalog/H61502/>
347. Tarascon, J.-M. *Mo₆Se₆ solid state electrode for secondary lithium batteries.* (Google Patents, 1986).
348. Guyomard, D. & Tarascon, J. M. Li Metal-Free Rechargeable LiMn₂O₄ / Carbon Cells: Their Understanding and Optimization. *J. Electrochem. Soc.* **139**, 937–948 (1992). doi:10.1149/1.2069372

349. Delacourt, C., Ridgway, P. L., Srinivasan, V. & Battaglia, V. Measurements and Simulations of Electrochemical Impedance Spectroscopy of a Three-Electrode Coin Cell Design for Li-Ion Cell Testing. *J. Electrochem. Soc.* **161**, A1253–A1260 (2014).
350. Han, S.-M., Kim, J.-H. & Kim, D.-W. Evaluation of the Electrochemical Performance of a Lithium-Air Cell Utilizing Diethylene Glycol Diethyl Ether-Based Electrolyte. *J. Electrochem. Soc.* **161**, A856–A862 (2014).
351. Beattie, S. D., Manolescu, D. M. & Blair, S. L. High-Capacity Lithium–Air Cathodes. *J. Electrochem. Soc.* **156**, A44 (2009). doi:10.1149/1.3005989
352. IBM's Battery 500 gets new material partners, inhales for real in 2020. *www.zemotoring.com* URL: <http://www.zemotoring.com/news/2012/04/ibms-battery-500-gets-new-material-partners-inhales-for-real-in-2020>
353. Lu, Y.-C., Gasteiger, H. A., Parent, M. C., Chiloyan, V. & Shao-Horn, Y. The Influence of Catalysts on Discharge and Charge Voltages of Rechargeable Li–Oxygen Batteries. *Electrochem. Solid-State Lett.* **13**, A69 (2010). doi:10.1149/1.3363047
354. Tan, P., Shyy, W., Wu, M. C., Huang, Y. Y. & Zhao, T. S. Carbon electrode with NiO and RuO₂ nanoparticles improves the cycling life of non-aqueous lithium-oxygen batteries. *J. Power Sources* **326**, 303–312 (2016). doi:10.1016/j.jpowsour.2016.07.012
355. Novák, P., Goers, D., Hardwick, L., Holzapfel, M., Scheifele, W., Ufheil, J. & Würsig, A. Advanced in situ characterization methods applied to carbonaceous materials. *J. Power Sources* **146**, 15–20 (2005). doi:10.1016/j.jpowsour.2005.03.129
356. Adams, B. D., Black, R., Radtke, C., Williams, Z., Mehdi, B. L., Browning, N. D. & Nazar, L. F. The Importance of Nanometric Passivating Films on Cathodes for Li–Air Batteries. *ACS Nano* **8**, 12483–12493 (2014). doi:10.1021/nn505337p
357. Kundu, D., Black, R., Adams, B., Harrison, K., Zavadil, K. & Nazar, L. F. Nanostructured Metal Carbides for Aprotic Li–O₂ Batteries: New Insights into Interfacial Reactions and Cathode Stability. *J. Phys. Chem. Lett.* **6**, 2252–2258 (2015). doi:10.1021/acs.jpcllett.5b00721
358. Kundu, D., Black, R., Berg, E. J. & Nazar, L. F. A highly active nanostructured metallic oxide cathode for aprotic Li–O₂ batteries. *Energy Env. Sci* **8**, 1292–1298 (2015). doi:10.1039/c4ee02587c
359. Hahn, H., Wagner, R., Schappacher, F., Winter, M. & Nowak, S. In operando X-shaped cell online electrochemical mass spectrometry (OEMS): New online analysis enables insight into lab scale lithium ion batteries during operation. *J. Electroanal. Chem.* **772**, 52–57 (2016). doi:10.1016/j.jelechem.2016.04.023
360. Tsiouvaras, N., Meini, S., Buchberger, I. & Gasteiger, H. A. A Novel On-Line Mass Spectrometer Design for the Study of Multiple Charging Cycles of a Li–O₂ Battery. *J. Electrochem. Soc.* **160**, A471–A477 (2013). doi:10.1149/2.042303jes
361. He, M., Castel, E., Laumann, A., Nuspl, G., Novák, P. & Berg, E. J. In Situ Gas Analysis of Li₄Ti₅O₁₂ Based Electrodes at Elevated Temperatures. *J. Electrochem. Soc.* **162**, A870–A876 (2015). doi:10.1149/2.0311506jes
362. Station météo de Paris - Meteo Paris - Le premier site météo pour Paris et l'île-de-France. URL: <http://www.meteo-paris.com/ile-de-france/station-meteo-paris.html>
363. Nemanick, E. J. Electrochemistry of lithium–oxygen batteries using microelectrode voltammetry. *J. Power Sources* **247**, 26–31 (2014). doi:10.1016/j.jpowsour.2013.08.043
364. Xu, W., Xiao, J., Zhang, J., Wang, D. & Zhang, J.-G. Optimization of Nonaqueous Electrolytes for Primary Lithium/Air Batteries Operated in Ambient Environment. *J. Electrochem. Soc.* **156**, A773 (2009). doi:10.1149/1.3168564
365. Kwabi, D. G., Batcho, T. P., Amanchukwu, C. V., Ortiz-Vitoriano, N., Hammond, P., Thompson, C. V. & Shao-Horn, Y. Chemical Instability of Dimethyl Sulfoxide in Lithium–Air Batteries. *J. Phys. Chem. Lett.* **5**, 2850–2856 (2014). doi:10.1021/jz5013824

366. Gowda, S. R., Brunet, A., Wallraff, G. M. & McCloskey, B. D. Implications of CO₂ Contamination in Rechargeable Nonaqueous Li-O₂ Batteries. *J. Phys. Chem. Lett.* **4**, 276–279 (2013). doi:10.1021/jz301902h
367. Liu, Y., Wang, R., Lyu, Y., Li, H. & Chen, L. Rechargeable Li/CO₂-O₂ (2 : 1) battery and Li/CO₂ battery. *Energy Environ. Sci.* **7**, 677 (2014). doi:10.1039/c3ee43318h
368. Ryu, J. H., Kim, J. W., Sung, Y.-E. & Oh, S. M. Failure Modes of Silicon Powder Negative Electrode in Lithium Secondary Batteries. *Electrochem. Solid-State Lett.* **7**, A306 (2004). doi:10.1149/1.1792242
369. Sim, S., Oh, P., Park, S. & Cho, J. Critical Thickness of SiO₂ Coating Layer on Core@Shell Bulk@Nanowire Si Anode Materials for Li-Ion Batteries. *Adv. Mater.* **25**, 4498–4503 (2013). doi:10.1002/adma.201301454
370. Hatchard, T. D. & Dahn, J. R. In Situ XRD and Electrochemical Study of the Reaction of Lithium with Amorphous Silicon. *J. Electrochem. Soc.* **151**, A838 (2004). doi:10.1149/1.1739217
371. Wang, F., Wu, L., Key, B., Yang, X.-Q., Grey, C. P., Zhu, Y. & Graetz, J. Electrochemical Reaction of Lithium with Nanostructured Silicon Anodes: A Study by In-Situ Synchrotron X-Ray Diffraction and Electron Energy-Loss Spectroscopy. *Adv. Energy Mater.* **3**, 1324–1331 (2013). doi:10.1002/aenm.201300394
372. Xun, S., Song, X., Wang, L., Grass, M. E., Liu, Z., Battaglia, V. S. & Liu, G. The Effects of Native Oxide Surface Layer on the Electrochemical Performance of Si Nanoparticle-Based Electrodes. *J. Electrochem. Soc.* **158**, A1260–A1266 (2011). doi:10.1149/2.007112jes
373. Guo, B., Shu, J., Wang, Z., Yang, H., Shi, L., Liu, Y. & Chen, L. Electrochemical reduction of nano-SiO₂ in hard carbon as anode material for lithium ion batteries. *Electrochem. Commun.* **10**, 1876–1878 (2008). doi:10.1016/j.elecom.2008.09.032
374. Yan, N., Wang, F., Zhong, H., Li, Y., Wang, Y., Hu, L. & Chen, Q. Hollow Porous SiO₂ Nanocubes Towards High-performance Anodes for Lithium-ion Batteries. *Sci. Rep.* **3**, (2013). doi:10.1038/srep01568
375. Miyachi, M., Yamamoto, H. & Kawai, H. Electrochemical Properties and Chemical Structures of Metal-Doped SiO Anodes for Li-Ion Rechargeable Batteries. *J. Electrochem. Soc.* **154**, A376–A380 (2007). doi:10.1149/1.2455963
376. West, A. R. Ionic conductivity of oxides based on Li₄SiO₄. *J. Appl. Electrochem.* **3**, 327–335 doi:10.1007/BF00613041
377. Stöber, W., Fink, A. & Bohn, E. Controlled growth of monodisperse silica spheres in the micron size range. *J. Colloid Interface Sci.* **26**, 62–69 (1968).
378. Wu, S., Zhu, K., Tang, J., Liao, K., Bai, S., Yi, J., Yamauchi, Y., Ishida, M. & Zhou, H. A Long-Life Lithium Ion Oxygen Battery Based on Commercial Silicon Particles as the Anode. *Energy Env. Sci* (2016). doi:10.1039/C6EE01512C
379. Morcrette, M., Chabre, Y., Vaughan, G., Amatucci, G., Leriche, J.-B., Patoux, S., Masquelier, C. & Tarascon, J.-M. In situ X-ray diffraction techniques as a powerful tool to study battery electrode materials. *Electrochimica Acta* **47**, 3137–3149 (2002). doi:10.1016/S0013-4686(02)00233-5
380. Favors, Z., Wang, W., Bay, H. H., George, A., Ozkan, M. & Ozkan, C. S. Stable Cycling of SiO₂ Nanotubes as High-Performance Anodes for Lithium-Ion Batteries. *Sci. Rep.* **4**, (2014). doi:10.1038/srep04605
381. Gao, B., Sinha, S., Fleming, L. & Zhou, O. Alloy Formation in Nanostructured Silicon. *Adv. Mater.* **13**, 816–819 (2001). doi:10.1002/1521-4095(200106)13:11<816::AID-ADMA816>3.0.CO;2-P
382. Kwak, W.-J., Shin, H.-J., Reiter, J., Tsiouvaras, N., Hassoun, J., Passerini, S., Scrosati, B. & Sun, Y.-K. Understanding problems of lithiated anodes in lithium oxygen full-cells. *J Mater Chem A* **4**, 10467–10471 (2016). doi:10.1039/C6TA03013K

Annexes

Annex 1 (Chapter 3 - II): Electrochemical performances of a DMA-based system without nitrates (1/2).

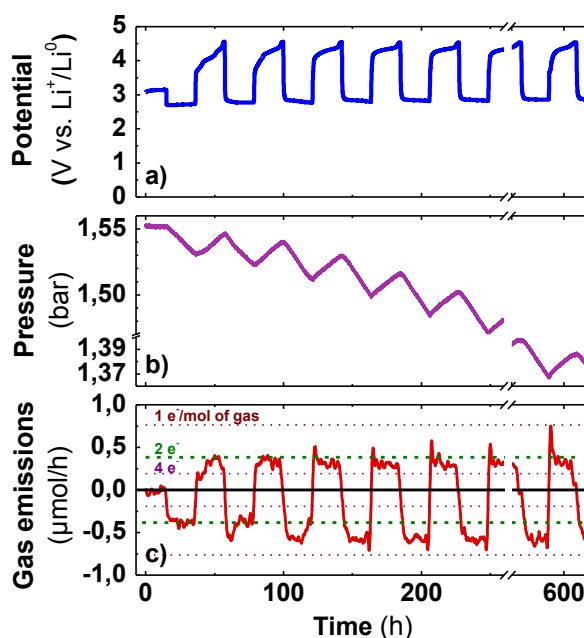


Figure 107: Potential-Time (a), Pressure-Time (b) and Gas emissions (c) of an $O_2//Csp:PTFE [9:1]//0.5 M LiTFSI$ in DMA// $LiFePO_4$ battery cycled at a current of $50 mA/g_{carbon}$, with a capacity limited to $1000 mAh/g_{carbon}$. Only cycles #1-#6 and #15 are shown. In (c), the horizontal green dashed lines represent the theoretical value of $\pm 2 e^-/gas$. The gravimetric capacities are reported with respect to the carbon mass.

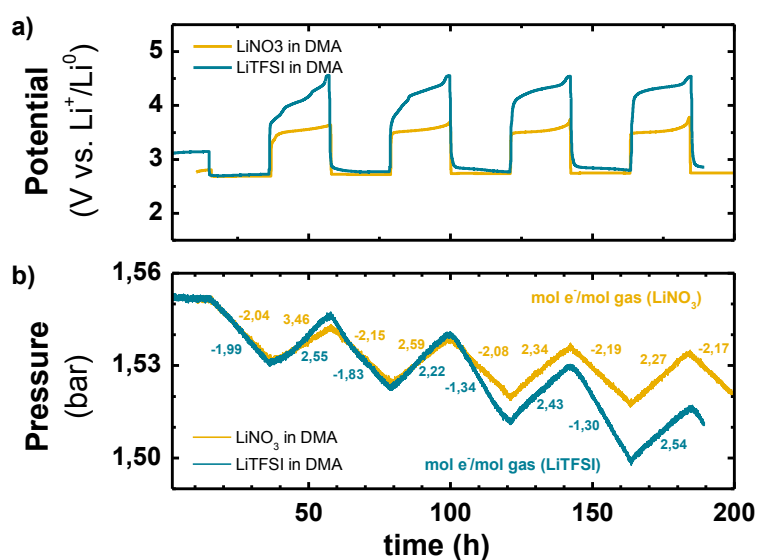


Figure 108: Effect of the salt on the Potential-Time (a) and Pressure-Time (b) profiles of the DMA-based system. Both cells are cycled in the same conditions. The $2 M LiNO_3/DMA$ -based cell uses Li as counter electrode while the $0.5 M LiTFSI/DMA$ -based one uses a pre-charged $LiFePO_4$ composite electrode. In (a), the potential vs. Li^+/Li^0 was recalculated with respect to the equilibrium potential of $LiFePO_4$ ($3.44 V$). The numbers in (b) represent the average " e^-/gas " value for one (dis)charge sequence.

Annex 2 (Chapter 3 - V.1): Electrochemical performances of a DMA-based system without nitrates (2/2).

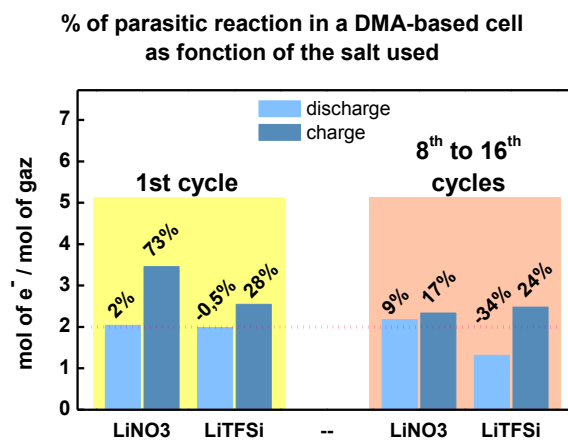
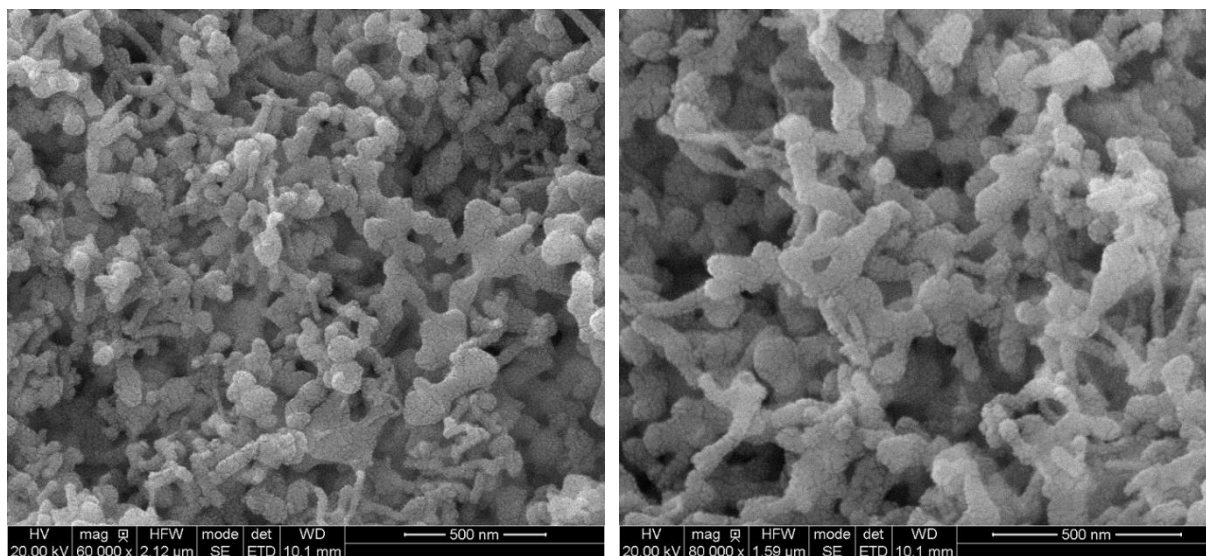


Figure 109: Estimation of the level of parasitic reactions for two DMA-based cells as function of the electrolyte used. Negative value indicates oxygen overconsumption. Horizontal dotted line is an eye-guide indicating the theoretical value.

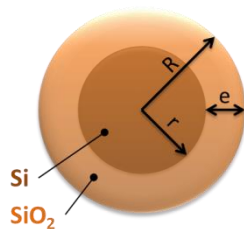
Annex 3 (Chapter 4 - I.4): Calculation of the thickness of a SiO₂ coating layer.

The morphology of the Si NP is not clearly defined, as evidenced by the SEM pictures below:



The thickness of the SiO₂ layer was estimated using three model particle shape, namely a sphere, a cube, and a square-based pellet, as detailed below.

Sphere model:

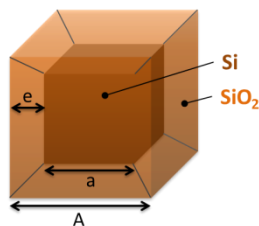


$$r = R * \sqrt[3]{\frac{1}{1 + \frac{d_{Si}}{d_{SiO_2}} * \alpha}}$$

with $\alpha = \left(\frac{1}{\tau_{Si}} - 1\right)$

Using $R = 50 \text{ nm}$, and $\tau_{Si} = 35 \%$ (determined by TGA), then $r = 35 \text{ nm}$ and $e = 15 \text{ nm}$.

Cube model:

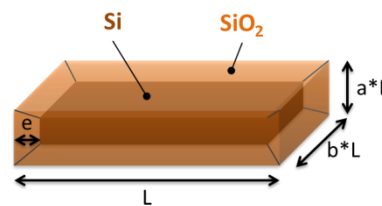


$$r = A * \sqrt[3]{\frac{1}{1 + \frac{d_{Si}}{d_{SiO_2}} * \alpha}}$$

with $\alpha = \left(\frac{1}{\tau_{Si}} - 1\right)$

Using $A = 100 \text{ nm}$, and $\tau_{Si} = 35 \%$, then $a = 70 \text{ nm}$ and $e = 15 \text{ nm}$. Using $A = 81 \text{ nm}$ (same volume as the sphere model), then $a = 56 \text{ nm}$ and $e = 12.5 \text{ nm}$.

Pellet model:



The general formula is given by :

$$(L - 2e) * (aL - 2e) * (bL - 2e) * \left(1 + \frac{d_{Si}}{d_{SiO_2}} * \alpha\right) = abL^3$$

We chose $L = 100 \text{ nm}$, $b = 1$, and $a = 0.524$ (sphere volume), then $e = 11.4 \text{ nm}$.

[Values: silicon density = 2.33; SiO₂ density (amorphous) = 2.2]

Annex 4 (Chapter 4 - II.3): Long term cycling of treated electrodes.

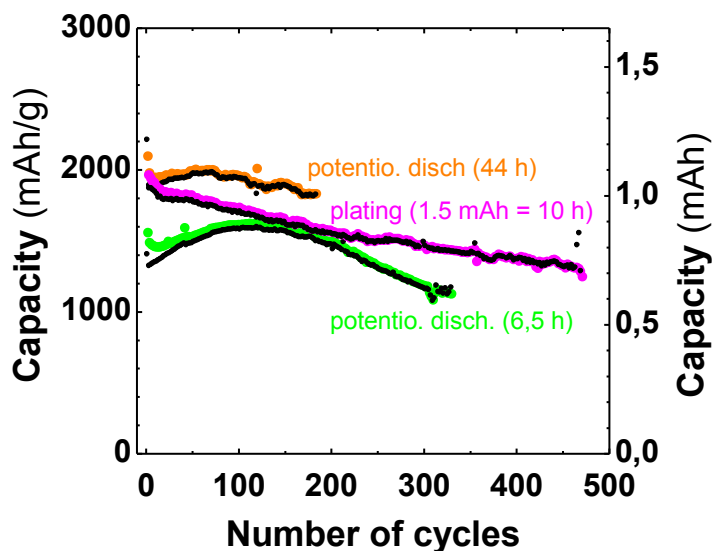


Figure 110: Capacity Retention plot of some Si|SiO₂/Csp/CMC [1:1:1]// LP30 + 10% FEC // Li half-cells treated with various technics. Colored dots = discharge capacity, small black dots = charge capacity.

Annex 5 (Chapter 4 - II.3): The beautiful freak show.

We were able to reach more than 800 cycles using a Si|SiO₂/Csp/CMC [1:1:1] electrode with a very low loading (0.14 mg of Si). This is a beautiful result in term of cycling retention but it is nonetheless totally impractical since the surface capacity is only 0.34 mAh/cm².

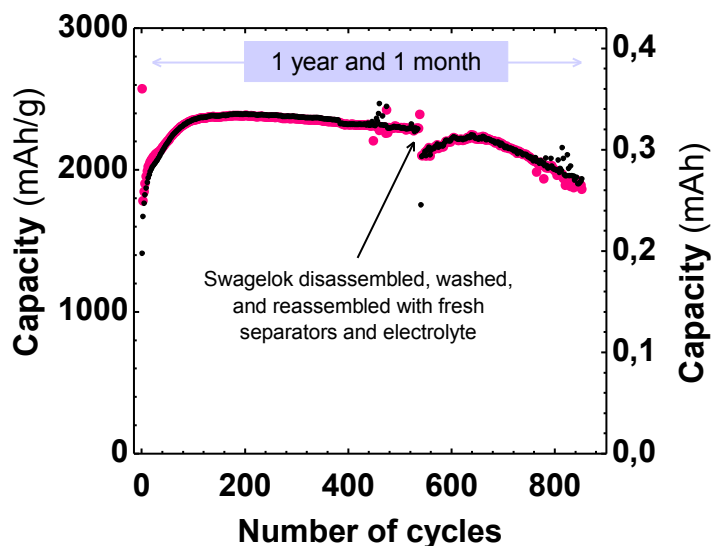


Figure 111: Capacity Retention plot of a Si|SiO₂/Csp/CMC [1:1:1]// LP30 + 10% FEC // Li half-cells with a very low loading of Si (0.14 mg) treated with a plating sequence of 30 min. Colored dots = discharge capacity, small black dots = charge capacity.

Annex 6 (Chapter 4 - II.1): Calculation of the Q error during a potentiostatic discharge.

The cycler's noise was determined by zooming the data so as to better visualize the noise (Figure 112b). By doing so, we note that our data points were falling in a narrow range of 140 nA, hence setting the accuracy in terms of current. The error implied by such noise equals to 6.2 μAh (44 [h] * 0.14 [μA]), which represents 0.4 % of the total charge (Q = 1.44 mAh) involved during the 44 h potentiostatic discharge.

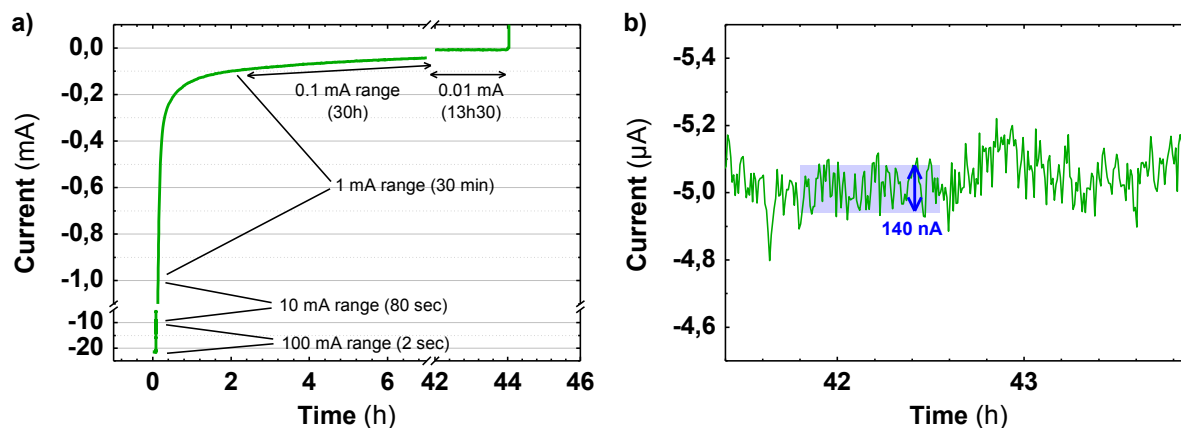


Figure 112: Current-Time profile of a 44 h potentiostatic discharge of a Si/Csp/CMC // LP30+FEC//Li half-cell. The caption in (a) indicate the I range selected to measure the current and the time it was used. (b) is a zoom of (a).

For sake of completion, we also checked the error due to the resolution of the potentiostat, which equals to 0.004 % of the I range set for the measurement. Owing to the low current value involved during the discharge ($< 100 \mu\text{A}$ for 30 h and $< 10 \mu\text{A}$ for 13 h out of 44 h) which enables very small I_{range} (Figure 112a), the error on the current was estimated to $0.157 \mu\text{Ah}$, which represents only 0.01 % of the total Q. This is negligible as compared to the error caused by the electrical noise.

Annex 7 (Chapter 4 - II.2.a): Effect of the FEC on treated Si electrodes.

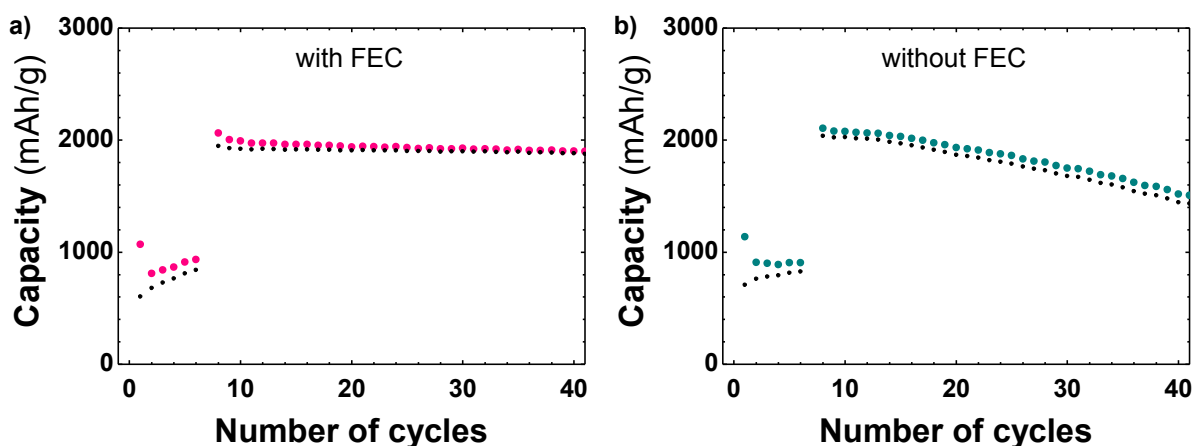


Figure 113: Capacity Retention plot of two Si/SiO₂/Csp/CMC[1:1:1] // Li half-cells using either LP30 + 10 % FEC (a) or LP30 (b) as electrolytes. Colored dots = discharge capacity, small black dots = charge capacity.

Annex 8 (Chapter 4 - II.3): Electrochemical performances of a SiO₂/Csp/CMC [2:1:1] as function of the current density.

It is possible to activate pure SiO₂ without pretreatments, but by decreasing the C-rate. At C/50 for instance, the potential of the negative electrode is > 0.1 V (potential at which the SiO₂ reduction may happen) for more than 10 h per cycle, which is enough to activate all the capacity in 50 cycles.

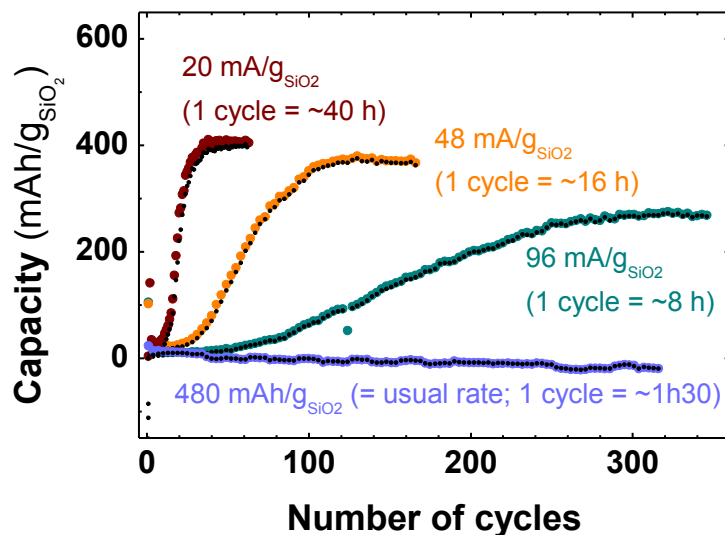


Figure 114: Capacity Retention of some SiO₂/Csp/CMC [1:1:1] // LP30 + 10% FEC // Li half-cells as function of the current density. The capacity associated to the Csp was subtracted from other cell capacities. Color dots = discharge, small black dots = charge.

Annex 9 (Chapter 4 - III.1.a): Electrochemical performances of a Si|SiO₂/Csp/CMC [2:1:1] electrode treated with a 20 h plating sequence.

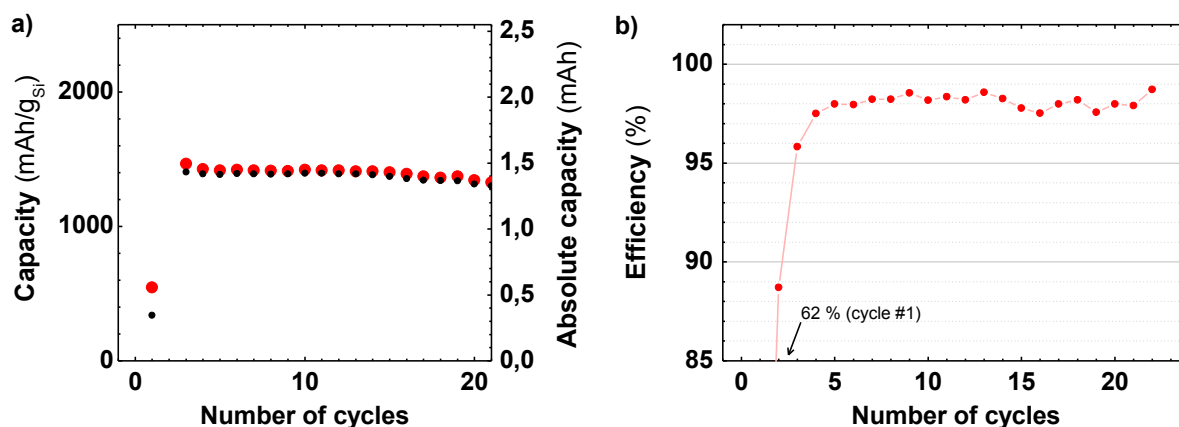


Figure 115: Capacity retention (a) and Coulombic efficiency (b) of a Si|SiO₂/Csp/CMC[2:1:1]//LP30 + 10 % FEC//Li half-cell treated with a 20 h plating sequence. In (a), colored dots = discharge capacity, small black dots = charge capacity.

Annex 10 (Chapter 4 - III.2.c): Plating sequence in various solvents.

When the plating sequence is performed in DME and TEGDME, there is no stripping plateau in the following charge, hence indicating that no plating actually occurs during the plating sequence (or if it does, the plated Li instantaneously reacts with the solvent). Thus, the plateau at -0.03 V corresponds to the solvent reduction, as confirmed by the brownish color of the separator in post-mortem analysis.

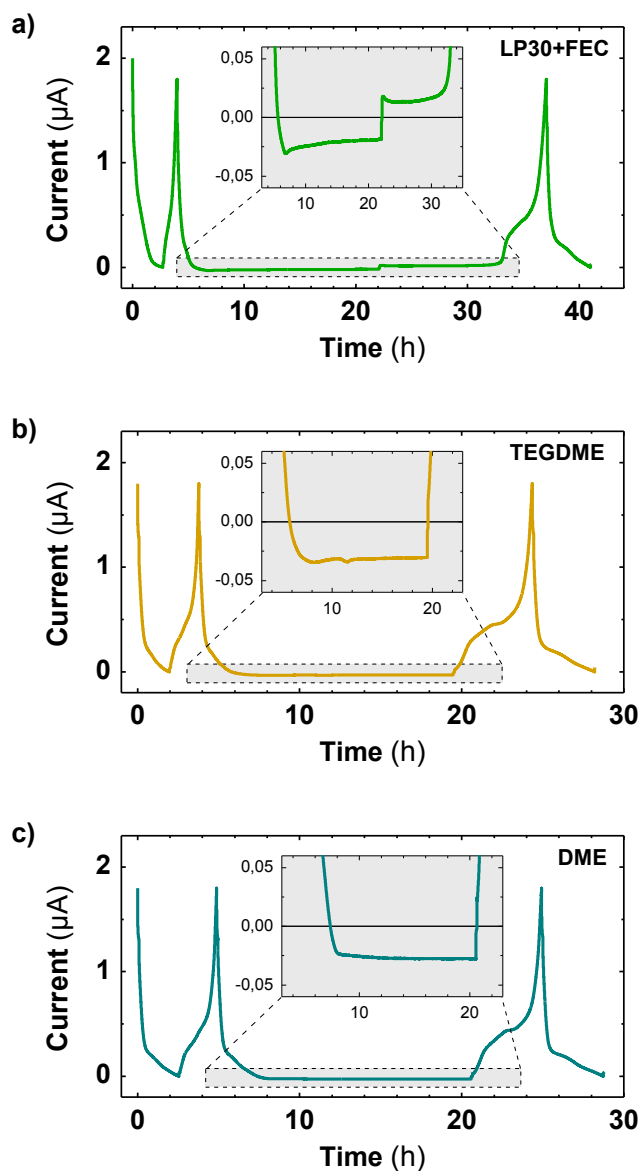


Figure 116: Potential-Time profiles of a some Si|SiO₂/Csp/CMC [1:1:1] // Li half-cells treated by a plating sequence of ~ 15 h in various electrolytes: LP30 + 10 % FEC (a), 0.5 M LiTFSI in TEGDME (b), and 0.5 M LiTFSI in DME (c).

Annex 11 (Chapter 4 - III.3.d): $\text{Li}_x\text{Si}-\text{O}_2$ cell in TEGDME with a capacity limited to 300 mAh/g

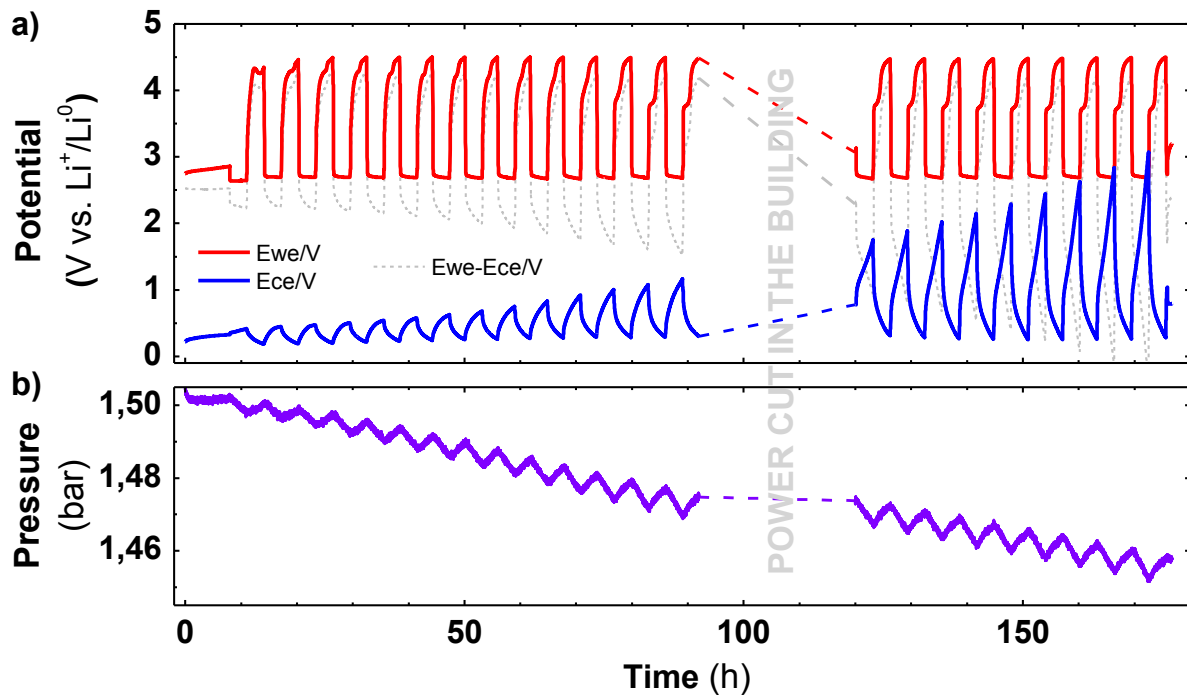


Figure 117: Potential-Time (a) and Pressure-Time (b) profiles of a $\text{Li}_x\text{Si} // 0.5 \text{ M LiTFSI in TEGDME} // \text{Csp} // \text{O}_2$ cell cycled at a current of $50 \mu\text{A}/\text{g}_{\text{carbon}}$ with a capacity limited to $300 \text{ mAh}/\text{g}_{\text{carbon}}$ (0.09 mAh). The Li_xSi electrode was prepared by galvanostatic discharge (C/2) stopped at 0 V, enabling a capacity of 0.89 mAh . Note that the cell was paused for 28 h due to a power cut in the building after 92 h of cycling.

Abstract

Supplying the world energy demand while reducing the greenhouse gases emissions is one of the biggest challenges of the 21st century; this requires the development of efficient energy storage devices enabling the utilization of renewable energies. Among them, Lithium-Air batteries are very attractive due to their high theoretical energy density – 10 times that of the current Li-ion batteries – but their development is hindered by the complexity of the chemistry at play.

In order to understand such chemistry, we designed a new electrochemical test cell that integrates a pressure sensor, thereby enabling an accurate *in operando* monitoring of the pressure changes during charge/discharge with high reproducibility and sensitivity. Its use is demonstrated by quantifying the parasitic reactions in Li-O₂ cells for various electrolytes frequently encountered in the literature. Through this comparative study, we are able to observe the phenomena currently limiting the performances of Li-O₂ batteries after a long cycling (> 1000 h), such as parasitic reactions and the instability of the Li anode.

To address the later issue, Li was replaced by a prelithiated silicon electrode made of Si particles oxidized in surface. We demonstrated the feasibility of enhancing both their capacity and cycle life *via* a pre-formatting treatment that triggers the reduction of their SiO₂ coating by liberating pure Si metal. The full Li_xSi-O₂ cells using such treated electrodes exhibit performances competing with the best analogous systems reported in the literature (> 30 cycles; more than 400 h of cycling), but the development of practical prototypes still requires to improve the cycle-life.

Résumé

Face aux défis du XXI^{ème} siècle concernant l'approvisionnement mondial en énergie et le réchauffement climatique, il est capital de développer des systèmes de stockage d'énergie efficaces et compétitifs. Parmi eux, la technologie Lithium-Air fait l'objet de nombreuses recherches car elle présente une densité d'énergie théorique dix fois supérieure à celle des batteries Li-ion actuellement utilisées, mais la complexité des réactions chimiques mises en jeu la cantonne au stade de la recherche.

Afin d'étudier de manière fiable et reproductible les batteries Li-Air, une nouvelle cellule de test électrochimique intégrant un capteur de pression a été développée. Elle permet d'estimer la quantité de réactions parasites associées à une configuration de batterie lors du cyclage à court et long terme (> 1000 h). Une étude comparative des différents électrolytes les plus utilisés a été réalisée, révélant la différence de comportement entre ces différentes espèces ainsi que l'instabilité de l'anode composée de lithium métallique.

Nous avons donc abordé le remplacement de l'anode de lithium par une électrode de silicium pré-lithié. En étudiant l'influence de différentes techniques de pré-lithiation sur des électrodes contenant des particules de Si oxydées en surface, un phénomène de réduction de SiO₂ en Si a été mis en évidence, apportant ainsi un gain substantiel en capacité. Les électrodes « activées » ont ensuite été utilisées en tant qu'anode dans les cellules complètes Li_xSi-O₂. Après optimisation, la durée de vie obtenue est supérieure à 400 h (> 30 cycles), ce qui est comparable à la littérature actuelle mais toutefois limité par la présence de réactions parasites.